

Technische Universität München

Lehrstuhl für Entwicklungsgenetik

Functional characterization of glutathione peroxidase 8 (GPX8)

Katalin Judit Buday

Vollständiger Abdruck der von der Fakultät Wissenschaftszentrum Weihenstephan für Ernährung, Landnutzung und Umwelt der Technischen Universität München zu Erlangung des akademischen Grades eines

Doktors der Naturwissenschaften (Dr. rer. nat.)

genehmigten Dissertation

Vorsitzende: Prof. Dr. Aphrodite Kapurniotu

Prüfer der Dissertation:

1. Prof. Dr. Wolfgang Wurst
2. Prof. Dr. Jan Riemer

Die Dissertation wurde am 13.05.2019 bei der Technischen Universität München eingereicht und durch die Fakultät Wissenschaftszentrum Weihenstephan für Ernährung, Landnutzung und Umwelt am 03.11.2019 angenommen.

Technische Universität München

Chair of Developmental Genetics

Functional characterization of glutathione peroxidase 8 (GPX8)

Katalin Judit Buday

Complete copy of the dissertation approved by the degree-awarding institution of Fakultät Wissenschaftszentrum Weihenstephan für Ernährung, Landnutzung und Umwelt of the Technische Universität München in partial fulfillment of the requirements for the degree of

Doktor rer.nat.

Chair: Prof. Dr. Aphrodite Kapurniotu

Dissertation examiners:

1. Prof. Dr. Wolfgang Wurst
2. Prof. Dr. Jan Riemer

The dissertation was submitted to the Technische Universität München on 13.05.2019 and accepted by the degree-awarding institution of Fakultät Wissenschaftszentrum Weihenstephan für Ernährung, Landnutzung und Umwelt on 03.11.2019.

TABLE OF CONTENTS

TABLE OF CONTENTS	I
SUMMARY.....	V
ZUSAMMENFASSUNG.....	VII
ABBREVIATIONS	IX
1. INTRODUCTION	1
1.1. Endoplasmic reticulum.....	1
1.1.1. Endoplasmic reticulum structure and function	1
1.1.2. Introduction to ER-stress and unfolded protein response (UPR)	2
1.1.3. Cellular processes for protein degradation upon ER-stress	5
1.1.3.1. Endoplasmic reticulum associated degradation (ERAD).....	5
1.1.3.2. Autophagy.....	6
1.2. Glutathione peroxidases (GPXs).....	8
1.2.1. GPX enzyme family is an essential antioxidant system within the cell	8
1.2.2. GPX4 and GPX7, the closest homologues to GPX8	8
1.2.3. Functions and knockout models of other glutathione peroxidases (GPX1-3, 5, 6) .	10
1.2.4. Monomeric glutathione peroxidase 8	11
1.3. Lipid metabolism	14
1.3.1. Relevance of fatty acid composition in membrane phospholipids	14
1.3.2. UPR, not only proteins but also lipids.....	15
1.4. Mitochondria associated membrane (MAM)	17
1.4.1. Function of MAM.....	17
1.4.2. Lipid synthesis and Ca ²⁺ trafficking at MAM site	18
1.5. Genome editing by CRISPR Cas9	20
2. MATERIALS.....	24
2.1. Equipment.....	24
2.2. Chemicals	25
2.3. Disposables and Kits	28
2.4. Enzymes	29
2.5. Antibodies.....	30
2.6. Cell lines.....	31
2.7. Mouse line	31
2.8. Oligonucleotides.....	32

Oligos for Gibson cloning	32
2.9. Bacteria.....	33
2.10. Cloning vectors.....	33
2.11. Software.....	36
3. METHODS.....	37
3.1. Cell culture-related methods	37
3.1.1. Murine embryonic fibroblasts	37
3.1.2. Determination of cell number	37
3.1.3. Cryopreservation and thawing cells	38
3.1.4. Cell viability assay	38
3.1.5. CRISPR/Cas9-mediated KO of individual genes	39
3.1.6. Immunofluorescence staining	39
3.1.7. Assessment of lipid peroxidation.....	40
3.1.8. Determination of intracellular Ca ²⁺ level	40
3.2. Nucleic acid-related methods	41
3.2.1. Phenol-chloroform extraction of genomic DNA from mouse ear punches and MEFs	41
3.2.2. Purification of bacterial plasmid DNA.....	41
3.2.3. Ligation of DNA fragments by Gibson cloning	41
3.2.4. (PCR) protocol for mouse genotyping	42
3.2.5. Restriction digestion	44
3.2.6. Agarose gel electrophoresis	44
3.2.7. Extraction of DNA fragment from agarose gels.....	44
3.2.8. Amplification of DNA fragments for cloning.....	44
3.2.9. Cloning of new vectors	45
3.3. Methods of gene transfer	46
3.3.1. Transformation of chemically competent bacteria	46
3.3.2. Lipofection	46
3.3.3. Lentivirus-mediated transfection	47
3.4. RNA-related methods	48
3.4.1. RNA isolation	48
3.4.2. cDNA synthesis	48
3.4.3. Microarray analysis.....	48
3.5. Protein-related methods	49
3.5.1. Protein purification from cells and tissues	49

3.5.2.	Sodium dodecyl sulfate polyacrylamide gel electrophoresis (SDS-PAGE)	49
3.5.3.	Western blot analysis	50
3.5.4.	Silver staining of SDS Gel	51
3.5.5.	Tandem affinity purification	51
3.5.6.	Mass spectrometry	52
3.6.	Histology	52
3.6.1.	Organ fixation	52
3.6.2.	Paraffin sections	53
3.6.3.	Cryosection	53
3.6.4.	H&E staining	53
3.6.5.	Immunohistochemical staining.....	54
3.6.6.	Oil Red staining	55
3.6.7.	Transmission electron microscopy (TEM).....	55
3.7.	Animal husbandry	56
3.7.1.	Animal facilities.....	56
3.7.2.	Establishment of new genetically modified mouse line	56
3.7.3.	High Fat Diet	56
3.7.4.	Whole body composition analysis on animals.....	57
4.	RESULTS	59
4.1.	Generation of monoclonal antibodies against GPX8	59
4.2.	GPX8 degrades upon ER stress induced by SERCA inhibitor	61
4.3.	Investigation of the degradation process of GPX8.....	63
4.3.1.	GPX8 has a dynamic turnover and the cytosolic lysine is crucial for the stability of the protein upon ER stress	63
4.4.	Generation and characterisation GPX8 KO in MEFs.....	67
4.4.1.	Generation of GPX8 KO in MEFs based on CRISPR/Cas9 technology	67
4.4.2.	Transmission electron microscopy analysis of CRISPR targeted <i>GPX8</i> knockout MEFs.....	70
4.4.3.	Absence of GPX8 sensitizes MEFs against saturated fatty acid-induced cell death	72
4.5.	GPX8 response to ER stress by SERCA inhibition	75
4.5.1.	SERCA inhibitors lead to GPX8 degradation, while KO of GPX8 does not influence ER stress response	75
4.5.2.	Determination of Ca ²⁺ level in <i>GPX8</i> WT and KO MEFs using Fura-2 based Ca ²⁺ sensors	77
4.5.3.	SERCA inhibition leads to subcellular translocalisation of GPX8	78
4.6.	Investigation of transcriptional regulation of <i>Gpx8</i>	81

4.6.1.	<i>In silico</i> promoter analysis	81
4.6.2.	Transcriptional analysis of GPX8 KO and WT mouse embryonic fibroblasts.....	83
4.7.	Identification of novel interaction partners of GPX8	86
4.7.1.	Yeast two hybrid	86
4.7.2.	Identification of GPX8 interaction partners.....	89
4.8.	Generation and characterisation of a <i>Gpx8</i>^{-/-} mouse line.....	94
4.8.1.	Generation of <i>Gpx8</i> ^{-/-} mouse line using CRISPR/Cas9.....	94
4.8.2.	Generation of MEFs from <i>Gpx8</i> ^{-/-} and <i>Gpx8</i> ^{wt/wt} mice.....	97
4.8.3.	MUFA and PUFA prevent palmitic acid and SCD1 inhibitor induced cell death in <i>Gpx8</i> ^{-/-} MEFs.....	99
4.8.4.	Knockout of GPX8 decreases body weight gain on high fat diet mice	100
4.8.5.	Structural analysis of <i>Gpx8</i> ^{wt/wt} and <i>Gpx8</i> ^{-/-} liver of HFD fed animals	104
4.8.6.	Transmission electron microscopy indicates aberrant mitochondria in <i>Gpx8</i> ^{-/-} animals.....	105
5.	DISCUSSION.....	108
5.1.	Monoclonal antibody production	108
5.2.	GPX8 stability upon ER stress.....	109
5.3.	Characterization of CRISPR targeted GPX8 knockout in MEFs.....	113
5.4.	Interaction partners and promoter analysis.....	118
5.5.	Analyzation of <i>Gpx8</i> ^{-/-} mouse line	121
6.	OUTLOOK	124
7.	REFERENCES	125
8.	APPENDIX.....	141
9.	CURRICULUM VITAE	143
10.	ACKNOWLEDGEMENT.....	146
11.	AFFIDAVIT	148

SUMMARY

Glutathione peroxidase 8 (GPX8) is one out of eight members of enzyme family of mammalian glutathione peroxidases, whereby GPX8 is the last identified member. Consequently, still little is known about the cellular functions of GPX8 and virtually no data is available concerning the *in vivo* relevance of this protein. Glutathione peroxidases contain either selenocysteine (Sec) or cysteine (Cys) in their active site, and are known to reduce hydrogen peroxides or organic peroxides to water or to their corresponding alcohols, respectively, at the expense of glutathione (GSH). Besides GSH GPX8 may also accept electrons from protein thiols like GPX4. Although GPX8 is structurally related to GPX7 and the ferroptosis regulator GPX4, GPX8 contains cysteine (Cys) in its catalytic center and has low glutathione peroxidase activity unlike GPX4. Also, while GPX4 localizes in the cytosol, mitochondria and nucleus of somatic cells, GPX8 is a transmembrane protein of the endoplasmic reticulum (ER) with a short N-terminal tail in the cytosol, followed by a single transmembrane domain and the rest of the protein including the catalytic center residing in the ER lumen. Based on *in vitro* studies, GPX8 was considered to act as a protein disulfide isomerase (PDI) oxidizing and thus reactivating enzyme using ER-oxidoreductin 1 (ERO1) derived H₂O₂, thereby contributing to oxidative protein folding in the ER. However, subsequent studies using INS-1E β-cells failed to confirm this assumption. In addition, GPX8 expression is under the transcriptional control of hypoxia inducible factor 2α (HIF2α), is enriched at MAM sites and was shown to regulate Ca²⁺ homeostasis in the ER.

To unravel yet-unrecognized GPX8 functions, I generated a series of novel tools including cell lines and mice deficient and proficient for GPX8. I show here that GPX8 is dynamically regulated in response to ER stress and that one of its cytosolic lysines (K10) plays a major role in the degradation process. Additionally, GPX8 knockout (KO) mouse embryonic fibroblasts emerged to be significantly more sensitive to palmitic acid-induced cell death than control cells, which could be exacerbated in the presence of a stearoyl-CoA-desaturase 1 (SCD1)-specific inhibitor. Interestingly, cell death inhibitors of known cell death pathways failed to rescue palmitic acid induced cell toxicity, while oleic acid and unsaturated fatty acids such as γ-linolenic acid and arachidonic acid prevented GPX8 KO cells from this form of cell death. Feeding GPX8 KO mice a 45% high fat diet for 20 weeks revealed that *Gpx8*^{-/-} males exhibited a significantly lower body weight and body fat mass

than *Gpx8*^{wt/wt} controls as determined by EchoMRI. Transmission electron microscopy analysis revealed aberrant cristae formation in the mitochondria of the heart, liver, brown adipose and white adipose tissues of *Gpx8*^{-/-} animals, suggesting an important role for GPX8 in mitochondrial homeostasis. The data presented here suggests that GPX8 is an important regulator of Ca²⁺ homeostasis and fatty acid metabolism at the mitochondrial associated membrane (MAM) site thereby contributing to the crosstalk between both organelles. Conclusively, my work lays the foundation for future studies that will address the underlying mechanisms of cellular Ca²⁺ signaling, fatty acid metabolism and the role of GPX8 in lipotoxicity.

ZUSAMMENFASSUNG

Die Glutathionperoxidase 8 (GPX8) zählt zur Enzymfamilie der Glutathionperoxidasen. Bisher wurden in Säugetieren acht Mitglieder dieser Familie beschrieben, wobei die GPX8 das zuletzt beschriebene Protein ist. Folglich ist über die Funktion, wie auch die *in vivo* Relevanz dieser Glutathionperoxidase, noch sehr wenig bekannt. Im katalytischen Zentrum tragen Glutathionperoxidasen entweder ein Selenocystein oder ein Cystein, wodurch die Reduktion von Wasserstoffperoxiden zu Wasser oder von organischen Peroxiden zu ihren entsprechenden Alkoholen katalysiert wird. Für diese Reaktionen wird in der Regel reduziertes Glutathion (GSH) benötigt, allerdings können die GPX8 und die ihr am nächsten homologe Proteine GPX4 und GPX7 unter GSH Mangel thiolhaltige Moleküle sowie Proteinthiole als Elektronendonoren nutzen. Obwohl die GPX8 das nächste Homolog zur GPX4 ist, welches als wichtigster Regulator der Ferroptose fungiert, hat die GPX8 Cystein im aktiven Zentrum und weist eine niedrige Glutathionperoxidaseaktivität auf. Im Gegensatz zur GPX4, welches im Zytosol, den Mitochondrien und im Zellkern lokalisiert ist, ist die GPX8 ein Transmembranprotein des Endoplasmatischen Retikulums (ER). Die GPX8 setzt sich aus einer kurzen N-terminalen zytosolischen Domäne, einer Transmembrandomäne und dem restlichen Teil der GPX8 inklusive der katalytischen Domäne zusammen, der im Endoplasmatischen Retikulum lokalisiert ist. Basierend auf vorherigen *in vitro* Studien, wurde die GPX8 als ein Enzym beschrieben, welches Protein Disulfid Isomerase (PDI) reoxidiert und somit reaktiviert und dabei gleichzeitig den von ER-oxidoreductin 1 (ERO1) erzeugten Wasserstoffperoxid reduziert, was zur korrekten oxidativen Faltung der Proteine im ER führt. Diese ursprüngliche Hypothese konnten jedoch durch Studien mit INS-1E β -Zellen nicht bestätigt werden. Zudem wurde gezeigt, dass die Expression der GPX8 durch Hypoxia Inducible Factor 2 α (HIF2 α) reguliert wird, und dass die GPX8 in der Mitochondrien-assoziierten Membran (MAM) angereichert ist, wo es die Ca²⁺ Homöostase reguliert.

Um die Funktion der GPX8 aufzuschlüsseln, wurde in dieser Arbeit eine Reihe von neuen Zell-, wie auch Mausmodellen entwickelt, bei denen GPX8 entweder genetisch inaktiviert oder überexprimiert wurde. Meine Daten zeigen, dass die GPX8 bei ausgelöstem ER Stress sehr schnell abgebaut wird und dass das zytosolische Lysin K10 für die Degradation

verantwortlich ist. Darüber hinaus konnte ich zeigen, dass die GPX8 KO MEFs eine ausgesprochene Sensitivität gegenüber Palmitinsäure-induziertem Zelltod zeigen, was durch Stearoyl-CoA Desaturase1 Inhibitor noch verstärkt werden konnte. Interessanterweise, konnte dieser Zelltod mit keiner der bekannten Inhibitoren gegen gängige Zelltodmechanismen, wie zum Beispiel Apoptose, Necroptose oder Ferroptose, verhindert werden. Im Gegensatz dazu, konnte der Palmitinsäure-induzierte Zelltod durch ungesättigte Fettsäuren, wie Ölsäure, γ -Linolensäure oder Arachidonsäure, vollständig verhindert werden. Mittels EchoMRI Analyse konnte ich zudem zeigen erste Daten liefern, dass *Gpx8*^{-/-} Mäuse bei Fütterung mit hohem Fettgehalt ein geringeres Gewicht, wie auch eine verringerte Gewichtszunahme im Vergleich mit den Wildtyp-Kontrolltieren aufwiesen. Ultrastrukturanalysen ergaben von diversen Geweben zeigten, v.a. im Herz, Leber, braunen und weiße Adipozyten eine abnormale Bildung von Cristae in den Mitochondrien von GPX8 knockout Tieren. Diese Daten deuten klar darauf hin, dass die GPX8 eine wesentliche Rolle in der Mitochondrien Homöostase spielt und als wichtiger Regulator der Ca²⁺ Homöostase, sowie des Fettsäuremetabolismus fungiert, wodurch es einen wichtigen Beitrag zur Kommunikation beider Organellen leistet. Mit dieser Arbeit wurde somit der Grundstein gelegt, wo in zukünftigen Studien die zugrundeliegenden, molekularen Mechanismen der GPX8 im Ca²⁺ Signaling, im Fettsäurestoffwechsel und in der Lipotoxizität untersucht werden können.

ABBREVIATIONS

°C	degree Celsius
μL	microliter
μM	micromolar
μm	micrometer
A	ampere
AB	adddback
ACAT	acyl-CoA cholesterol acyltransferase
ACSL4	long-chain fatty acyl-CoA synthetase-4
AGK2	2-Cyano-3-[5-(2,5-dichlorophenyl)-2-furanyl]-N-5-quinolinyl-2-propenamide
AGPAT	1-acylglycerol-3-phosphatase O-acyltransferase
Akt	RAC-alpha serine/threonine-protein kinase
ALS	amyotrophic lateral sclerosis
AMFR	E3 ubiquitin-protein ligase AMFR
AMP	adenosine monophosphate
AMPK	AMP-activated protein kinase
Arg (R)	arginine
ASK1	apoptosis signal regulating kinase 1
Asp (D)	aspartic acid
ATF6	activating transcription factor 6
Atg	autophagy-related protein
ATP	adenosine triphosphate
Atp1b1	sodium/potassium-transporting ATPase subunit beta-1
BAT	brown adipose tissue
BHQ	2,5-Di-t-butyl-1,4-benzohydroquinone
bp	base pair
Ca ²⁺	calcium
Cas	CRISPR-associated systems
CD4	cluster of differentiation 4
cDNA	complementary DNA
CHOP	CCAAT/Enhancer-Binding Protein Homologous Protein

CL	cardiolipin
CN-MAL	cytogenetically normal acute myeloid leukemia
CPA	cyclopiazonic acid
CPT	carnitine palmitoyltransferase
CRISPR	clustered regularly interspaced short palindromic repeats
CRKO	CRISPR knockout
crRNA	CRISPR RNA
Csf	macrophage colony-stimulating factor
Cys (C)	cysteine
Daam	disheveled-associated activator of morphogenesis
DAPI	4',6-diamidino-2-phenylindole
DBD	DNA binding domain
DGAT	diacylglycerol O-acyltransferase
dH ₂ O	distilled water
DHA	dehydroascorbic acid
DMEM	Dulbecco's Modified Eagle Medium
DMSO	dimethyl sulfoxide
DNA	deoxyribonucleic acid
dNTP	nucleoside triphosphate
DPBS	Dulbecco's Phosphate-Buffered Saline
DSB	double strand break
DTT	dithiothreitol
Dysf	dysferlin
EDEM	ER degradation enhancing α -mannosidase-like protein 1
EDTA	ethylenediaminetetraacetic acid
eif2 α	eukaryotic translation initiation factor 2 α
ER	endoplasmic reticulum
ERAD	endoplasmic reticulum associated degradation
ERK	extracellular signal-regulated kinase
ERO1	ER oxidoreductin 1
ERSE	ER stress response element
EtOH	ethanol
FACS	fluorescence-activated cell sorter
FAS	fatty acid synthase

FCS	fetal calf serum
FGF	fibroblast grow factor
g	gravitational force/ gram
GCL	glutamate cysteine ligase
GFP	green fluorescent protein
GPAT	glycerol phosphate acyl-CoA transferase
GPX	glutathione peroxidase
GRP75	glucose-regulated protein 75
GRP78	glucose-regulated protein 78
GSH	glutathione (reduced)
GSSG	glutathione (oxidized)
h	hours
H ₂ O ₂	hydrogen peroxide
HDR	homology-directed repair
HEK	human embryonic kidney
HFD	high fat diet
hGPX8	human GPX8
HIF	hypoxia-inducible factor
HIS3	imidazoleglycerol-phosphate dehydratase
HIV	human immunodeficiency virus
HRD	E3 ubiquitin-protein ligase synoviolin
HRE	HIF response element
Ifit-1	interferon-induced protein with tetratricopeptide repeats 1
IL-6	interleukin 6
IMM	inner mitochondrial membrane
IMS	intermembrane space
INSIG	insulin induced gene
IP3R	inositol phosphate-3-receptor
Ipo-8	importin-8
IRE1	inositol requiring enzyme 1
kDa	kilo Dalton
KO	knockout
LAMP2a	lysosome-associated membrane glycoprotein 2
LC3	microtubule-associated protein 1A/1B-light chain 3

LOOH	lipid hydroperoxide
LPCAT	lysophosphatidylcholine acyltransferase
LXR	oxysterols receptor LXR
Lys (K)	lysine
mAB	monoclonal antibody
MAM	mitochondria associated membrane
MARCH6	E3 ubiquitin-protein ligase MARCH6
MCU	mitochondrial calcium uniporter
MEF	mouse embryonic fibroblast
MeOH	methanol
Met (M)	methionine
MgCl ₂	magnesium chloride
mGPX8	mouse GPX8
min	minute
ml	milliliter
mM	millimolar
mRNA	messenger RNA
mTOR	mammalian target of rapamycin
MUFA	monounsaturated fatty acid
n	sample size
NaCl	sodium chloride
NaOH	sodium hydroxide
NE	nuclear envelope
neo	neomycin
ng	nanogram
NHEJ	non-homologous end-joining
nm	nanometer
nM	nanomolar
NMD	nonsense mediated decay
NOX4	NADPH oxidase 4
NPGPX	non-selenocysteine containing phospholipid hydroperoxide glutathione peroxidase
NS3	non-structural protein
OMM	outer mitochondria membrane

Orai	calcium release-activated calcium channel protein
Oxa1l	mitochondrial inner membrane protein OXA1L
PAM	protospacer adjacent motif
PBS	predicted biological score
PC	phosphatidylcholine
PCA	principal component analysis
Pcdh	protocadherin
PCR	polymerase chain reaction
PDI	protein disulfide isomerase
PE	phosphatidylethanolamine
PEMT	phosphatidylethanolamine N-methyltransferase
PERK	protein kinase R (PKR)-like endoplasmic reticulum kinase
PFA	paraformaldehyde
PG	phosphatidylglycerol
Phe (F)	phenylalanine
PI	phosphatidylinositol
PI3K	phosphatidylinositol 3-kinase
PI4Kb	Phosphatidylinositol 4-kinase beta
PLC	phospholipase C
PLOOH	phospholipid hydroperoxide
PPAR γ	peroxisome proliferator-activated receptor gamma
PRX4	peroxiredoxin 4
PSS	phosphatidylserine synthase
PTEN	phosphatase and tensin homolog
PUFA	polyunsaturated fatty acid
Puro	puromycin N-acetyl-transferase
RER	rough endoplasmic reticulum
RFP	red fluorescent protein
RIN	RNA integrity number
RNA	ribonucleic acid
RNF5	E3 ubiquitin-protein ligase RNF5
ROS	reactive oxygen species
rpm	revolutions per minute
RSL3	Ras-selective lethal 3

RXR	retinoic acid receptor RXR
RYR	ryanodine receptor
s.d.	standard deviation
S1P (MBTPS1)	membrane-bound transcription factor site-1 protease
S2P (MBTPS2)	membrane-bound transcription factor site-2 protease
SCAP	SREBP cleavage activating protein
SCD	stearoyl-CoA-desaturase
SDS	sodium dodecyl sulfate
sec	second
Sec (U)	selenocysteine
SEL1L	protein sel-1 homolog 1
SER	smooth endoplasmic reticulum
Ser (S)	serine
SERCA	sarco/endoplasmic reticulum Ca ²⁺ -ATPase
Sfn	14-3-3 protein sigma
sgRNA	single guide RNA
siRNA	small interfering RNA
Slc24a3	sodium/potassium/calcium exchanger 3
SOCE	store operated Ca ²⁺ entry
SRE	sterol regulatory element
SREBP	sterol regulatory element binding protein
ssRNA	single strand RNA
ST18	suppression of tumorigenicity
STAT	signal transducer and activator of transcription
SYVN	E3 ubiquitin-protein ligase synoviolin
TAD	transactivation domain
TAG	triacylglycerol
TAL	transcription activator-like
TALEN	TAL effector nucleases
TAP	antigen peptide transporter
Tapbp	tapasin
TCA	tricarboxylic acid cycle
TG	thapsigargin
Thr (T)	threonine

TMD	transmembrane domain
tracrRNA	trans-activating crRNA
tRNA	transfer RNA
UPR	unfolded protein response
UV	ultraviolet
V	volt
VDAC1	voltage dependent anion channel 1
VKOR	vitamin K epoxide reductase
VLCAD	very long chain acyl-CoA dehydrogenase
Vsp35	vacuolar sorting protein 35
w/v	weight/volume
WAT	white adipose tissue
WT	wild type
XBP1	X-box binding protein 1
Y2H	yeast two hybrid
YFP	yellow fluorescent protein
ZFN	zinc-finger nucleases

1. INTRODUCTION

1.1. Endoplasmic reticulum

1.1.1. Endoplasmic reticulum structure and function

The endoplasmic reticulum (ER) is a continuous membrane system found in eukaryotic cells, which consists of tubules, vesicles and cisterns. It is closely associated with several intracellular organelles and plasma membrane thereby promoting signal transmission [1, 2]. Based on function and morphology, two different forms of the ER can be discriminated: the ribosome-studded rough endoplasmic reticulum (RER), and the smooth endoplasmic reticulum (SER), which is devoid of ribosomes. Remarkably, in some cases the nuclear envelope (NE) is also mentioned as a form of ER due to the close association and continuity of the two organelles [3]. Oxidative protein folding, posttranslational modifications, protein quality control and biosynthesis of secretory and membrane proteins take place in the RER, while the SER is important for desaturation and elongation of fatty acids, synthesis of phospholipids and steroid hormones and also for calcium homeostasis. The proportion of RER and SER is dependent on cell type. Cells producing large amount of proteins for secretory pathways, such as β -cells or plasma cells, are rich in RER, while other cells, like hepatocytes contain more SER for detoxification reactions and lipid biosynthesis.

The maintenance of an oxidative environment in the ER is required for proper oxidative protein folding. Nevertheless, in this process reactive oxygen species (ROS) are generated as byproducts, which contribute to approximately 25% of ROS produced in a cell [4]. Protein disulfide isomerase (PDI) is an enzyme family whose members catalyze the formation, reduction and isomerization of disulfide bonds in substrate proteins [5]. While promoting disulfide bond formation in the substrate protein, PDI itself becomes reduced, and these electrons are taken by ER-membrane associated oxidoreductin (ERO1). ERO1 is a flavoprotein, which transfers the electrons to O_2 , thereby generating H_2O_2 . Notably, knockout of $ERO1\alpha$ and $ERO1\beta$ does not lead to a severe phenotype in mice [6], suggesting the existence of possible alternative PDI oxidizing systems. In this respect Peroxiredoxin 4 (PRX4), VKOR (Vitamine-K epoxy reductase), and dehydroascorbate (DHA) have been considered as oxidizing agents [7], although the efficiency of DHA and PRX4 for PDI

oxidation is rather low and the affinity of VKOR is higher only for membrane-bound PDIs [8]. This led to the belief that there might be other, more efficient systems in cells that serve as professional PDI oxidizing devices. In fact, the ER-resident glutathione peroxidases 7 (GPX7) and 8 (GPX8) have both been regarded as enzymes that efficiently oxidize PDI, and thereby contribute to its catalytic activity (see also below). Incorrectly formed disulfide bonds are reduced by glutathione (GSH), which, in turn, becomes oxidized (GSSG), and increases the relative level of GSSG in the ER. Unlike in the cytosol, where reduced GSH is highly abundant (GSH/GSSG molar ratio of $\sim 50,000/1$ [9]), the ratio of GSH/GSSG in the ER is close to equal, thus favoring the process of oxidative protein folding [10]. In addition, not only ERO1 but also the transmembrane complex NADPH oxidase 4 (NOX4) contributes to the production of substantial amounts of H_2O_2 in the ER [11].

1.1.2. Introduction to ER-stress and unfolded protein response (UPR)

ROS, generated by ERO1 and other sources, might be harmful in excess by inducing oxidative stress and damage to cell constituents, while at physiological concentrations they are kept in check by cellular antioxidant systems and have a crucial role in redox signaling. The oxidative protein folding capacity is dependent on many factors, such as redox environment, calcium ion (Ca^{2+}) concentration in the ER, glycosylation capacity, and energy storage and inflammation [12-14]. Alterations in any of these factors can interrupt proper oxidative folding capacity, leading to accumulation of unfolded proteins in the ER, which in turn finally initiates unfolded protein response (UPR), an adaptive mechanism for aberrant conditions [15]. UPR aims to resolve ER stress by activation of different parallel signaling pathways, which consist of numerous enzymes and transcription factors. The signal for their activation originates from three transmembrane proteins in the ER that can sense the accumulation of unfolded proteins: inositol-requiring kinase 1 (IRE1,) activating transcription factor 6 (ATF6) and protein kinase RNA-like endoplasmic reticulum kinase (PERK). Under stress-free conditions a chaperone, immunoglobulin heavy chain binding

protein (GRP78/BIP), retains these sensors in an inactive state by association with their luminal domains (Fig. 1).

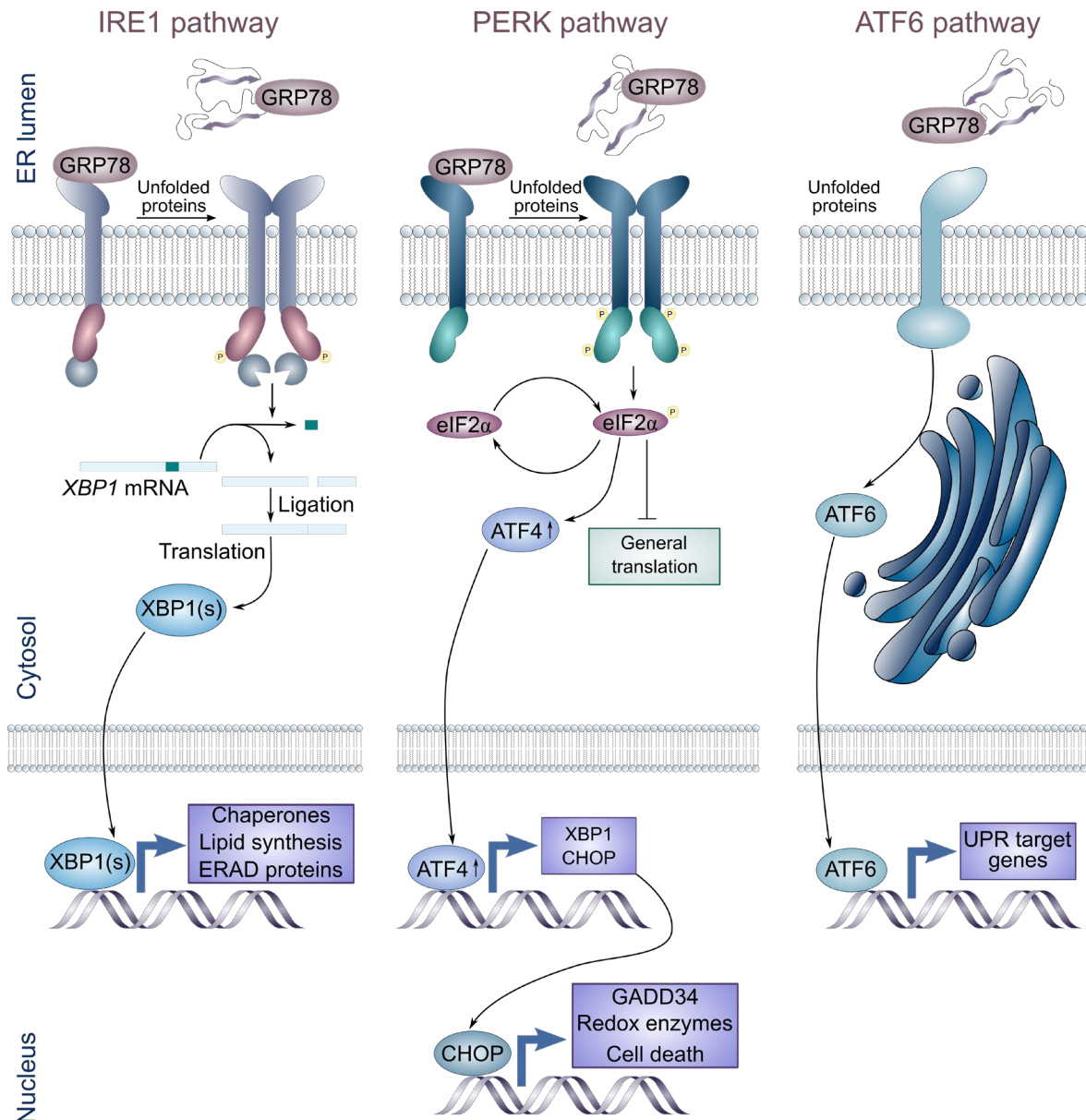


Figure 1 Signaling pathways in unfolded protein response (UPR)

The scheme depicts the three signaling pathways that are activated in response to accumulation of unfolded proteins in the ER. Under basal conditions, IRE1, PERK and ATF6 are associated with GRP78 thereby the transmembrane proteins are in their inactive form. However, when unfolded proteins accumulate, GRP78 has higher affinity to bind to the hydrophobic surfaces of unfolded proteins, therefore it dissociates from IRE1, PERK and ATF6. On release from GRP78, IRE1 and PERK undergo dimerization and auto-phosphorylation, whereas ATF6 migrates to the Golgi

apparatus. Activated IRE1 splices the mRNA of XBP1, which results in a frameshift in the coding sequence of XBP1. However, after translation, spliced XBP1 becomes an active transcription factor of genes that are involved in lipid biosynthesis, ERAD and protein folding. In parallel, activated PERK phosphorylates eif2 α , which leads to the inhibition of general translation. While under these conditions translation of ATF4 is increased, it induces gene expression of XBP1 and CHOP. Subsequently, CHOP is responsible for the expression of redox enzymes and if the stress is sustained, it induces cell death. Finally, ATF6 undergoes proteolytic cleavage in the Golgi apparatus, by which the soluble domain is released, thereby activating the expression of genes involved in UPR. Figure adjusted from [16].

IRE1 possesses endoribonuclease activity and contains a Ser/Thr kinase domain in its cytosolic part [17, 18]. Following the accumulation of unfolded proteins, GRP78 dissociates from IRE1 as it has a higher affinity to bind to the hydrophobic surfaces of unfolded proteins. GRP78 dissociation leads to auto-phosphorylation and homo-dimerization of IRE1, which results in the activation of its cytosolic Ser/Thr kinase and endoribonuclease activity. IRE1 through its endoribonuclease domain splices 26 nucleic acids in the *X-box-binding protein 1 (XBP1)* mRNA, resulting in a frame shift in its coding sequence, thereby leading to the translation of a 40 kDa isoform instead of 33 kDa. These events activate transcription factors that are involved in UPR and ER-associated degradation (ERAD) response in order to adapt to the ER folding capacity [19].

Similar to IRE1, PERK becomes active via homodimerization and autophosphorylation after being released from GRP78. It also possesses a Ser/Thr protein kinase activity that is able to phosphorylate eukaryotic translational initiation factor 2 (eIF2 α) on the α subunit at Ser51 following GRP78 release. This phosphorylation interrupts the interaction between eIF2 α and methionyl-transfer Ribonucleic Acid (Met-tRNA), therefore inhibiting the general protein synthesis. Importantly, the translation of activating transcription factor 4 (ATF4) is favored only under these conditions, which is responsible for the expression of various genes involved in UPR and ER-stress mediated apoptosis, including CCAAT-enhancer-binding protein homologous protein (CHOP). Indeed, CHOP only becomes stable upon strong and prolonged activation of PERK [20].

ATF6 is a type II transmembrane protein, which contains a Golgi-localization signal. However, under homeostatic conditions GRP78 binds to ATF6 and conceals the Golgi-localization signal whereby ATF6 is retained in the ER membrane. Nevertheless, upon ER-stress on release from GRP78, ATF6 translocates to the Golgi apparatus. In the Golgi, the transcription factor domain of ATF6 is activated via regulated proteolysis by site 1 protease (S1P) and site 2 protease (S2P) [21]. Activated ATF6 migrates to the nucleus and binds to both the CCAAT-enhancer-binding protein (C/EBPs) and the ER-stress response element 1 (ERSE), thereby contributing to the expression of genes that repress ER-stress such as GRP78, XBP1 and genes involved in ERAD [19].

The goal of the UPR is to decrease general protein synthesis and eliminate unfolded/misfolded proteins either by their refolding or by degradation. In case of sustained ER stress, UPR triggers apoptosis.

1.1.3. Cellular processes for protein degradation upon ER-stress

1.1.3.1. Endoplasmic reticulum associated degradation (ERAD)

One of the most critical processes in response to ER-stress is the targeting of misfolded proteins for subsequent degradation. There are different possibilities to eliminate harmful unfolded or misfolded proteins. In eukaryotic cells ERAD is one way to recycle unwanted or defective proteins to regulate cellular homeostasis. The challenge of this quality control mechanism is to recognize insufficient proteins and transport them into cytosol for ubiquitination and proteasomal degradation. In addition, growing evidence indicates that not only defective proteins are processed by ERAD, but also proteins that are considered to be folded thereby favoring the regulation of their cellular level [22]. ERAD substrates are recognized by ER chaperones due to their inappropriate maturation tags; for instance incorrect N-glycosylation or exposure of hydrophobic patches [23-25]. Many chaperones have been shown to participate in recognition processes including GRP78, calnexin/calreticulin or ER degradation enhancing α -mannosidase-like protein 1 (EDEM1). These proteins not only contribute to the recognition of defective proteins, but also to the

delivery to the retrotranslocation channel [26-29]. Notably, before a protein is removed from the ER, all disulfide bonds have to be reduced by PDIs [30].

One of the best characterized E3 ubiquitin ligase is the ER resident SEL1L-HRD1 complex [31-33]. HRD1 contains six transmembrane domains that form the retrotranslocation channel and promote the transport of targeted proteins from the ER into the cytosol. Additionally, the cytosolic tail of HRD1 is required for the ubiquitination of substrate proteins as they enter the cytosol, thereby increasing their solubility and preventing their aggregation [34]. Ubiquitin is a 76 amino acid length peptide, serving as a signal for proteasomal recognition to advance the degradation of specified proteins [35]. Above all, *in vivo* studies proved that knockout of HRD1 and SEL1L lead to embryonic death in mice, indicating the significant relevance of ERAD proteins [36, 37].

1.1.3.2. Autophagy

Moreover, UPR can trigger lysosomal degradation via autophagy, which is an alternative possibility to eliminate defective proteins [38-40]. It is an evolutionary conserved pathway from yeast to mammalian cells [41]. Autophagy was originally described as a programmed cell death. However, based on further evidence, it is now well accepted that although cells can exhibit increased autophagic vacuolization upon activation of their cell death, this is not the mechanism by which cells actually die [42]. In fact, autophagy is essential for constitutive turnover of damaged organelles, proteins, lipids and other (macro)molecules, therefore promoting cell survival rather than cell death [43].

So far, three types of autophagy have been described, which are discriminated by their unique molecular features: (1) macroautophagy, (2) microautophagy and (3) chaperone-mediated autophagy. As its name suggests, chaperon mediated autophagy relies on chaperons that recognize specific substrates and transport them to the lysosome. With the assistance of lysosome-associated membrane protein 2a (LAMP2a), the substrates enter into the lumen of the lysosome where their disassembly and degradation take place [44]. In contrast, microautophagy is mediated by lysosome membrane, which isolate engaged substrates in the cytosol for subsequent degradation [45]. Finally, macroautophagy (later on autophagy) is an essential process for the clearance of protein aggregates and

organelles [46]. Mammalian target of rapamycin (mTOR) was considered as the key regulator of autophagy, although recent evidence indicates that it can be activated not only in an mTOR dependent, but also in an mTOR independent manner. Physiological perturbations, such as nutrient deprivation, hypoxia, ER stress, or infection induce phagophore formation, which likely originate from the ER-, or mitochondria membrane, mitochondria-associated membrane (MAM) or plasma membrane [47-50]. Upon phagophore elongation, substrate molecules or organelles are selectively isolated. Finally, by enclosing phagophore, a double membrane vesicle (autophagosome) is formed which is then loaded with molecules that are targeted for subsequent degradation. Eventually, autophagosome fuse either directly with the lysosome or with the late endosome forming amphisomes [51] which are engaged to subsequently fuse with lysosome. Finally, in the lysosome numerous low pH active enzymes promote the degradation of the content of amphisome or autophagosome [52].

One of the key regulators of phagophore formation, maturation and of the fusion of autophagosome with lysosome is the well-characterized microtubule-associated protein 1 light chain 3 (LC3) or autophagy-related protein 8 (Atg8). Upon activation of autophagy, LC3 is cleaved by autophagy-related protein 7 (Atg7), thereby forming LC3-I which subsequently conjugates with phosphatidylethanolamine (PE) in the phagophore membrane. The conjugation of LC3-I with PE results in the formation of LC3-II, which is commonly used as a marker of the steady state level of autophagosomes. LC3-II is either associated with the inner or outer leaflet of the autophagosome membrane. Therefore, LC3-II is degraded within the autolysosome or dissociated from PE and recycled, respectively [53].

ER stress is closely related to autophagy since PERK facilitates ATF4 and CHOP dependent upregulation of LC3, and other autophagy related proteins such as Atg5, Atg7 or Atg3, Atg10, beclin 1, p62 [54, 55]. Beside these, IRE1 can induce phosphorylation of apoptosis signal regulating kinase 1 (ASK1), resulting in phosphatidylinositol 3-kinase (PI3K) and beclin 1 activation, which triggers autophagy [56, 57]. Finally, it has been also shown that ER stress can promote autophagy by inhibiting mTOR activity [58]. Consequently, dysregulation of protein degradation through the ERAD pathway or autophagy causes

accumulation of unwanted molecules, which are considered to contribute to several diseases including amyotrophic lateral sclerosis (ALS), Alzheimer's disease, Huntington disease, diabetes, metabolic syndrome and cancer [59].

1.2. Glutathione peroxidases (GPXs)

1.2.1. GPX enzyme family is an essential antioxidant system within the cell

Glutathione peroxidases (GPXs) belong to a phylogenetically related enzyme family, that are considered to be essential in the reduction of H₂O₂ and fatty acid hydroperoxides to water and to their corresponding alcohols, respectively. Those reactive molecules are important in signaling pathways via regulation of growth, proliferation and differentiation, but are harmful in excess [60-63]. So far 8 members of this enzyme family have been identified, of which GPX1-4 (and GPX6 in human) are selenocysteine (Sec) containing enzymes, whereas GPX5 (GPX6 in rodent) and GPX7-8 are cysteine containing isoforms [64]. GPX1-3,5 and 6 form homooligomers, whereas GPX4, GPX7 and GPX8 have been described as monomers, due to the lack of an oligomerization interface [65]. Moreover, GPX4,7-8 are considered to be evolutionary closely related. GPX1-4 and 6 preferentially use GSH as an electron donor, although GPX4 efficiently accepts electrons from other low molecular thiols and protein thiols if GSH concentrations are limited (Fig. 2), as physiologically evident in late sperm cells [66]. In order to elucidate the *in vivo* role of GPXs, knockout studies have been performed in mice for most members of this family of enzymes. These studies point to the unique relevance of GPX4 in early embryogenesis [67], although knockout mouse models for *Gpx6* and *Gpx8* have not been published yet.

1.2.2. GPX4 and GPX7, the closest homologues to GPX8

Whole body deletion of *Gpx4* in mice leads to embryonic lethality at the gastrulation stage (E 7.5) [67]. It is similar to the phenotype of glutamate cysteine ligase (GCL) knockout mice [68], suggesting that GPX4 might be one of the limiting GSH utilizing enzymes. There are three different isoforms expressed of GPX4: cytosolic, mitochondrial and nuclear, although only the cytosolic form is essential for development according to the *in vivo* knockout

mouse models. This is consistent with their specific expression patterns, since most of the somatic cells express the cytosolic form. Additionally, almost exclusively sperm cells express the mitochondrial and nuclear isoforms of GPX4.

Nevertheless, the constitutive knockout of the nuclear and mitochondrial isoforms leads to perturbed sperm chromatin condensation [69] and male infertility, respectively. Additionally, tissue specific knockout mouse models have been established and have indicated the crucial role of GPX4 for in various neuronal subpopulations [70-73], photoreceptor cells [74], skin development [75], endothelial cells [76], T cell mediated immunity [77], hematopoiesis [78] and liver protection [79]. Subsequent studies further demonstrated that GPX4 is the key regulator of a recently discovered cell death form, called ferroptosis [80], which is defined by the accumulation of lipid hydroperoxides in an iron dependent manner.

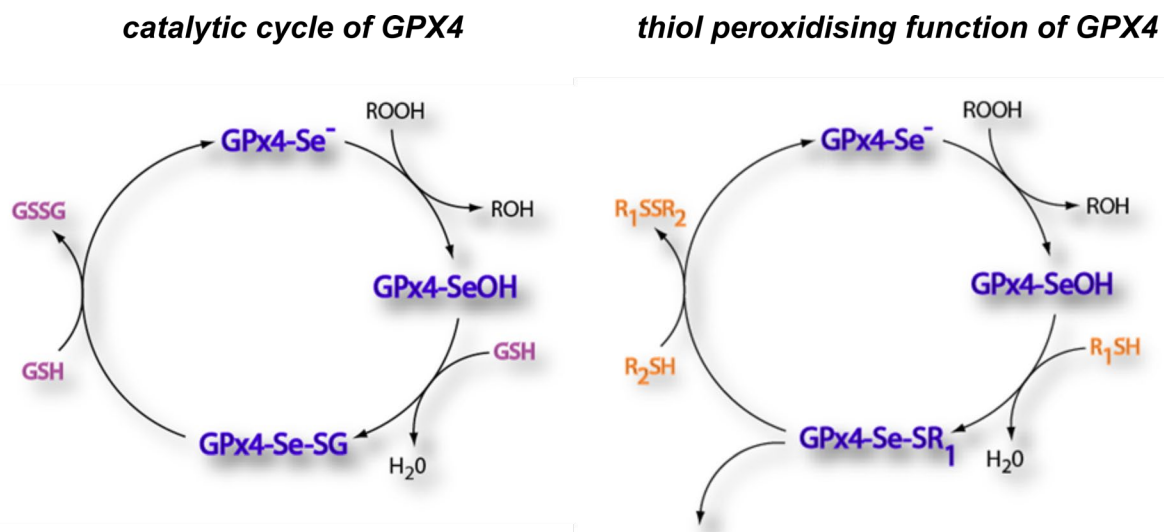


Figure 2 Catalytic cycle of glutathione peroxidase 4 (GPX4)

GPX4 detoxifies H_2O_2 or organic peroxide- specifically phospholipid hydroperoxide- to water and the corresponding alcohols, respectively. In this reaction the Sec in active site is oxidized to selenic acid which subsequently reacts with glutathione (GSH) thereby forming a mixed selenadisulfide bond (left). To complete the cycle, a second GSH molecule reduces Sec of GPX4 and in turn, oxidized diglutathione (GSSG) is released. However, when GSH is limiting, GPX4 is able to use protein thiols as electron donors (right). In this reaction, GPX4 forms an intermolecular disulfide bond and by using a second protein thiol, this reaction mediated by GPX4 introduces an intramolecular disulfide bond in the substrate protein. Figure adopted from [81].

GPX7 is an ER resident protein, showing a high degree of sequence homology to GPX8. Based on *in vitro* studies, GPX7 was initially reported as a non-selenocysteine containing phospholipid hydroperoxide glutathione peroxidase (NPGPX) [82], which is capable of reoxidizing PDI and reducing H₂O₂ [83]. In parallel, the first knockout mouse model indicated that depletion of GPX7 *in vivo* leads to systemic oxidative stress, increased tumorigenesis, adipocyte hypertrophy and reduced life span [84, 85]. Moreover, GPX7 was shown to covalently bind to GRP78, thereby promoting its chaperone activity, hence loss of GPX7 results in accumulation of unfolded proteins due to the decreased activity of GRP78 [84]. In addition, depletion of GPX7 induces preadipocyte differentiation to adipocyte, thus increasing body fat mass in mice [85]. Consequently, these studies hint to the importance of monomeric GPX4 and GPX7 in cell and tissue protection.

1.2.3. Functions and knockout models of other glutathione peroxidases (GPX1-3, 5, 6)

GPX1 was the first described member of the glutathione peroxidase family, with a cytosolic and mitochondrial localization [86, 87]. It is highly abundant in the liver and kidney where it contributes to cellular defense against oxidative stress. Knockout studies demonstrated that the lack of the protein is compatible with life [88, 89], however *Gpx1*^{-/-} animals exhibit morphological aberrations in cardiac mitochondria and myocytes [90]. In addition, acute oxidative stress leads to the death of *Gpx1*^{-/-} mice, which can be prevented by selenium supplementation. This indicates that GPX1 has indeed an important antioxidant function [91].

GPX2 is closely related to GPX1 with a high expression level in gastrointestinal tract and liver [92]. *Gpx2*^{-/-} mice develop normally [93], although the protein enzyme was considered to be relevant for inflammation and cancer development [94-97].

GPX3 has been characterized as an extracellular protein, which enters the ER for posttranslational modification, but due to the lack of ER retention signal, it is secreted into the blood stream. GPX3 is one of the most abundant selenoproteins in plasma. Beside this, it is also present in other body fluids, kidney and adipocytes, where its expression level

increases during adipogenesis [98-101]. Additionally, recent studies argue for the involvement of GPX3 in cancer pathogenesis [102-104].

GPX5 is a selenium independent glutathione peroxidase, which is mainly expressed in epididymis [105]. It is the closest homolog to GPX3. Along with GPX3 it constitutes for more than 95% of GPXs present in epididymis. *Gpx5* knockout mice did not exhibit any obvious phenotype. Despite its fundamental role in detoxification of hydroperoxides and maintaining DNA integrity in sperm, the fertility of young males were not affected by the genetic abrogation of GPX5 [106].

GPX6 is a selenoprotein in humans, whereas in other species it contains Cys in the active site [107]. It has not been expressed and purified yet, therefore there is no data available according its substrate specificity. Moreover, the knowledge about its *in vivo* and *in vitro* function is also very limited, due to the lack of cellular and knockout animal studies.

1.2.4. Monomeric glutathione peroxidase 8

GPX8 is the latest identified member of GPX family which was first recognized in an *in silico* analysis. As mentioned above, it is a CysGPX with high degree of sequence homology to GPX4 and GPX7 (Fig. 3). Due to the absence of an oligomerization domain, these more closely related GPX are considered to be present as monomers. The 209 amino acid long protein was shown to be anchored to the ER-membrane via a single transmembrane domain. The N-terminus of GPX8 contains a short cytosolic stretch of 18 amino acids, which is followed by a single transmembrane domain while the rest of the protein faces the ER lumen [83]. Additionally, instead of KDEL an unusual KEDL ER retrieval signal is found at the C-terminal part of the protein. GPX8 contains four cysteines, of which one localizes in the cytosol (C₁₁), one in the transmembrane region (C₂₈) and two in the ER lumen (C₇₉, C₁₀₈). C₇₉ is the conserved catalytic residue among GPXs, required for its putative peroxidase activity [83, 108].

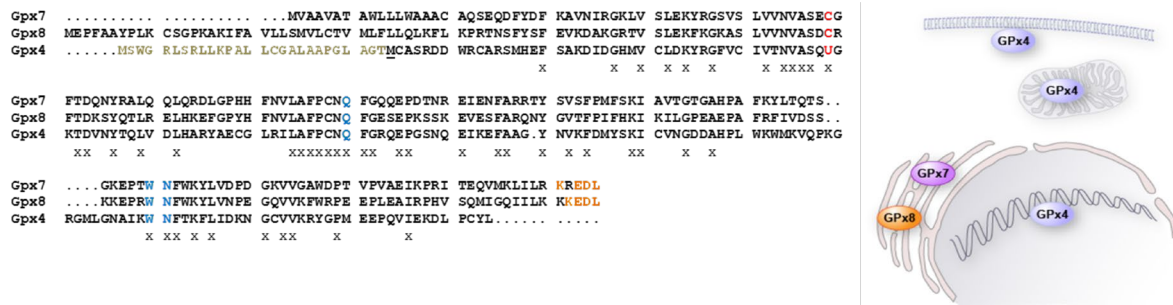


Figure 3 Sequence homology and subcellular localization of GPX4, GPX7 and GPX8

Sequence alignment of mouse GPX4, GPX7 and GPX8 shows a relatively high degree of homology in their primary structure (left). The Cys (C) of GPX8 and GPX7 and Sec (U) of GPX4 in active site are highlighted with red, while oranges indicate the KEDL and KREDL ER-retention signals of GPX8 and GPX7, respectively. On the right, the subcellular localization of GPX4, GPX7 and GPX8 is shown. While GPX4 comes in three flavors, a cytosolic, a mitochondrial and a nuclear isoform, GPX7 and GPX8 have been considered as ER resident proteins. GPX7 is present in the ER lumen, while GPX8 contains a short cytosolic loop, a single transmembrane domain, and the catalytic site of the protein facing the ER lumen. Figure kindly provided by Dr. Marcus Conrad (unpublished).

Interestingly, the cytosolic domain of GPX8 is targeted by Hepatitis C Virus (HCV), since GPX8 is cleaved at C₁₁ by virus protease NS3-4A [109]. Notably, overexpression and knockdown studies suggest that GPX8 contributes to viral particle production, presumably via its C₇₉ catalytic activity [109]. The first *in vitro* and *in situ* studies proposed that GPX8 has a low GSH peroxidase activity pursuant to the absence of GSH interface, however it reacts more efficiently with PDI [83]. Based on crystal structure analysis of the luminal part of human GPX8 it was found that the protein harbors a thioredoxin fold ($\beta\beta\beta\alpha\beta\alpha\beta\beta\alpha$), which is typical for other GPX family members [110]. Moreover, ERO1 α was shown to interact with the soluble domain of human GPX8, reflecting its possible involvement in oxidative protein folding [83]. In parallel, Appenzeller-Herzog and co-workers implicated the role of GPX8 in the detoxification of H₂O₂ produced by deregulated ERO1, which further promotes the idea of its contribution to protein folding. The same group also demonstrated that loss of GPX8 induces ER stress and cell death due to H₂O₂ leakage from the ER into the

cytosol [111].

Apart from that, *in vitro* studies were performed on HeLa cells, which implicated that GPX8 mRNA level as well as protein level are enhanced upon hypoxia-inducible factor (HIF) stabilization. Consequently, mutation in the HIF response element (HRE) in the *GPX8* promoter resulted in decreased expression of the protein despite HIF stabilization. In addition, it was also reported that HIF α binds to HRE1 as well as to HRE2 in the promoter region of *GPX8*, however the binding affinity to HRE1 was higher. Silencing of HIF2 α but not HIF1 α abrogated GPX8 expression after treating cells with a HIF stabilizing agent. Finally, knockdown of GPX8 was found to strongly enhance fibroblast growth factor (FGF) induced extracellular signal-regulated kinase 1/2 (ERK1/2) phosphorylation and insulin signaling which is a hallmark for increased proliferation in the absence of GPX8 [65]. However, there is no direct evidence for the exact mechanism by which GPX8 regulates FGF and insulin signaling, but based on previous studies it can be hypothesized that it occurs via an increase in the H₂O₂ flux arising from the ER, and the known effects of H₂O₂ on transient oxidation and inactivation of phosphatases [65, 112]. Interestingly, similar findings were demonstrated for *Gpx1*^{-/-} mice as *Gpx1*^{-/-} animals exhibited higher insulin sensitivity and increased resistance to high fat diet-induced obesity, mediated through increased phosphatase and tensin homolog (PTEN) oxidation and elevated phosphoinositide 3-kinase (PI3K)/Akt signaling [113].

Recently, it has been reported that GPX8 is involved in Ca²⁺ homeostasis. This finding is based on an *in vitro* experiment conducted on HeLa cells, where Sitia and co-workers demonstrated that GPX8 is enriched in the mitochondria associated membrane (MAM) and the overexpression of the protein leads to decreased ER Ca²⁺ level, as well as lower histamine-induced Ca²⁺ release from the ER to mitochondria and cytosol. The Ca²⁺ level in the ER is balanced by the uptake via sarco/endoplasmic reticulum Ca²⁺ ATP-ase (SERCA) and by the leakage via inositol phosphate-3-receptor (IP3R) and the ryanodine receptor (RYR). It was also demonstrated that GPX8 regulates SERCA2b activity as well as the passive release via IP3R. Additionally, further experiments proved that the transmembrane domain (TMD) of GPX8 plays a crucial role in the regulation of Ca²⁺ signaling, while its peroxidatic

cysteine (C₇₉) is also required for this purpose [114].

In parallel, Mehmeti and co-workers more recently implicated that GPX8 and GPX7 contribute to the prevention against palmitate induced lipotoxicity in insulin secreting INS-1E cells. It has been suggested that palmitate leads to accumulation of H₂O₂, which resulted in subsequent cell death. Stable expression of GPX8 and GPX7 decreased H₂O₂ levels and lowered the expression of ER stress markers in response to palmitate supplementation, thereby increasing cell viability. In addition, GPX8 and GPX7 have been shown to increase glucose stimulated insulin secretion in INS-E1 cells, albeit they did not enhance PDI oxidizing capacity. These results suggest that the folding of insulin does not depend on the expression of these ER resident GPXs in INS-E1 insulin secreting β -cell line [115].

1.3. Lipid metabolism

1.3.1. Relevance of fatty acid composition in membrane phospholipids

Lipid metabolism plays a crucial role in cellular signaling by regulating energy homeostasis, proliferation, membrane composition, fluidity and even cell death. The balance between lipid degradation (lipolysis or lipophagy) and biosynthesis (lipogenesis) is regulated via multiple parallel mechanisms. In excess of free fatty acids, cells store the majority of these fatty acids as triacylglycerol (TAG) along with cholesterol and sterol esters in lipid droplets, which are surrounded by a phospholipid monolayer. This spatial isolation is necessary to prevent the direct contact between the hydrophilic cytosol milieu and the hydrophobic fatty acids. In addition, lipid droplets also isolate potentially toxic lipids in order to prevent lipotoxicity, which could result in cell death. However, fatty acids are not only stored as energy sources in lipid droplets but are also integrated into membrane phospholipids, indicating that these molecules are critical for signaling [116].

ER houses numerous enzymes that are essential for lipid biosynthesis, including synthesis of phosphatidylcholine (PC), phosphatidylethanolamine (PE), phosphatidylinositol (PI), cholesterol and TAG. Consequently, ER membranes are enriched in PC and PE, however their sphingolipid and cholesterol content is limited. Although these lipids are synthesized

in the ER, they are not only incorporated directly into the ER membrane but are also distributed to other organelles via contact sites or secretory pathway vesicles [3]. To facilitate the transfer of these products, some reaction of lipid biosynthesis takes place at the organelle contact site, close to their target destination [117]. Supporting this evidence, several studies have reported that, for instance, phosphatidylserine synthase 1 and 2 (PSS1, PSS2), the rate limiting enzymes for phosphatidylserine synthesis and diacylglycerol O-acyltransferase 2 (DGAT2), are enriched in MAM site [118, 119].

Importantly, more recently, attention has focused on the lipid composition of the ER membrane, which influences the activity of enzymes required for lipid biosynthesis. This might be a feedback mechanism how the cells sense and regulate their lipid content to adapt various conditions [120-124]. Nevertheless, it has been previously reported that the lipid composition in the ER membrane influences Ca^{2+} levels in the ER lumen. Preliminary work by Fu *et al.* demonstrated that high fat diet (HFD) in animals results in increased level of monounsaturated fatty acid in ER membrane, than those that were having control chow diet. In addition, HFD promoted the biosynthesis of PC, consequently increasing the ratio of PC/PE. This alteration in ER membrane lipid composition lowered Ca^{2+} levels in the ER lumen by inhibiting SERCA activity, which in turn resulted in increased ER stress in obese mice. More importantly, reversing the ratio between PC/PE via suppression of phosphatidylethanolamine N-methyltransferase (PEMT), the enzyme which converts PE to PC, significantly improved Ca^{2+} transport activity of liver microsomes [125]. In line with this, Bi *et al.* reported that in *Drosophila* fat cells SERCA is essential for lipid storage through the interaction with a lipid related protein, called Seipin [126]. This further points out the crucial role of Ca^{2+} homeostasis in lipid metabolism.

1.3.2. UPR, not only proteins but also lipids

As discussed above, UPR maintains ER homeostasis in case of accumulation of unfolded proteins. Nonetheless, ER stress sensors IRE1, PERK and ATF6 not only facilitate suppression of misfolded protein induced stress but also significantly affect lipid metabolism. Indeed, UPR activation results in the extension of the ER volume to promote

stress attenuation, which requires increased production of membrane lipids [127]. The ER proliferation is regulated by *Xbp1* [128-130] via transcription of enzymes, which are crucial for PC and PE biosynthesis, such as members of the Lipin protein family and 1-acylglycerol-3-phosphatase O-acyltransferase (AGPAT) [130, 131]. Similarly, ATF6 can directly induce expression of genes involved in lipid biogenesis [132], and also target IRE1 and XBP1 transcription under ER overload, which further increases the rate of lipid synthesis [133, 134]. Recent studies indicate that UPR sensors can be directly activated by the excess of saturated fatty acid in the ER membrane as well as by alterations of sterol concentrations [135-137]. More importantly, PERK and IRE1 are able to sense alterations of membrane lipids composition and induce downstream events in UPR signaling even if their luminal region is missing which is responsible for the recognition of misfolded proteins [138]. Above all, these findings point towards a strong relation between membrane fatty acid composition and ER stress.

The mechanism of fatty acid desaturation has to be carefully controlled to prevent ER stress and cell death. Consequently, the proteins that are involved in this pathway are highly conserved from prokaryotes to eukaryotes. In mammalian cells, the enzymes that are involved in fatty acid desaturation are regulated by sterol regulatory element binding protein (SREBP). In the presence of sterol, SREBP forms a complex with SREBP cleavage activating protein (SCAP), which is retained in the ER via the interaction with insulin induced gene 1 or 2 (INSIG1, INSIG2). However, in the absence of sterol, SCAP undergoes conformational changes, which result in the dissociation of SREBP-SCAP complex from INSIG1/INSIG2. Subsequently, the complex is transported to the Golgi apparatus and processed by proteolytic cleavage. In turn, the soluble domain of the complex is released and migrates to the nucleus, where it binds to sterol regulatory element motifs (SRE) in the DNA and induces expression of genes that are required for fatty acid and cholesterol synthesis and uptake [139].

Stearoyl-CoA-desaturase 1 (SCD1), a key enzyme involved in the production of monounsaturated fatty acids (MUFA), has been shown to be a fundamental player in regulating fatty acid composition in membrane phospholipids. SCD1 is indeed a well-characterized enzyme, localized in the ER membrane, which converts palmitic acid (C16:0)

and stearic acid (C18:0) to palmitoleic acid (C16:1) and oleic acid (C18:1), respectively. More importantly, it was reported that knockdown of SCD1 induces UPR in HeLa cells which is enhanced by the supplementation of palmitic acid, or by knockdown of lysophosphatidylcholine acyltransferase 3 (LPCAT3), an enzyme required for the incorporation of polyunsaturated fatty acids (PUFA) into phosphatidylcholine. In addition, it was also shown that oleic acid and several PUFAs were able to attenuate ER stress, induced by SCD1 knockdown [136]. *In vivo* studies conducted on mice indicated that *Scd1* knockout leads to decreased body weight and body fat mass. Additionally, *Scd1*^{-/-} animals exhibited increased oxygen consumption, insulin sensitivity and higher expression level of genes that are involved in fatty acid oxidation, such as carnitine palmitoyltransferase-1 (CPT-1), a very long chain acyl-CoA dehydrogenase (VLCAD), while expression of fatty acid synthase (FAS) and glycerol phosphate acyl-CoA transferase (GPAT), genes are involved in lipogenesis, were decreased. Furthermore, *Scd1*^{-/-} animals displayed increased levels of C16:0 and C18:0, whereas, as expected the contents of C16:1 and C18:1 were reduced [140].

1.4. Mitochondria associated membrane (MAM)

1.4.1. Function of MAM

Physical associations between intracellular organelles are important to promote signaling pathways and molecular transport. The mitochondria associated (ER-) membrane (MAM) is a reversible tethering site between the ER and mitochondria which is about 10-30 nm wide [141] and consists of several defined lipids and membrane bounded proteins. The distance between the ER and mitochondria membrane depends on whether the contact sites are formed with the SER or with the RER. In case of SER, the MAM site is about 9-16 nm, while if RER creates a contact site with the mitochondria, this distance can increase up to 19-30 nm [142, 143]. The association of ER and mitochondria serves as a platform for regulating a wide range of cellular processes, such as lipid synthesis, Ca²⁺ trafficking, autophagy and cell death. Consequently, impaired functions of MAM are related to different pathophysiological conditions such as Alzheimer's disease (AD) [144], Parkinson's

disease (PD) [145], Fronto-temporal dementia (FTD), Wolfram syndromes (WS1/WS2) [146], metabolic diseases [147], lysosomal storage diseases [148] amyotrophic lateral sclerosis (ALS) and aging [141]. In order to investigate MAM's function, several studies have been performed to identify proteins present at the ER mitochondria contact site. In a recent study, Poston *et al.* identified 1212 proteins as candidates in MAM fraction, which were divided into three groups: (1) MAM-resident proteins, those are only present at the MAM but not in the ER nor in the mitochondria, (2) MAM enriched proteins are present in other organelles as well, but they are enhanced in the MAM, and (3) MAM associated proteins those temporarily localize in MAM [149]. The results of mass spectrometry analysis of mouse brains implicated that the MAM site plays a crucial role in Ca²⁺ signaling, cellular survival, and that it is responsible for numerous neurological diseases.

1.4.2. Lipid synthesis and Ca²⁺ trafficking at MAM site

Lately MAM has become an important topic as it was revealed to be involved in several diseases. Despite scientists giving more and more attention to its relevance, still very little is known about all signaling pathways that are transmitted between the ER and mitochondria through their contact sites. Besides the ER, mitochondria are also involved in the synthesis of numerous lipids like PE, phosphatidylglycerol (PG) and cardiolipin (CL), which are required for cristae formation [150]. However, other lipids like phosphatidylserine (PS), phosphatidylinositol (PI), sterols and PC have to be transported into the mitochondria. Those lipids mostly originates from the ER, therefore their transport requires the assembly of transporter protein complexes at ER-mitochondria contact site. Not only transport of lipids takes place at MAM but as discussed above (see 1.3.1.), several enzymes involved in lipid biosynthesis are enriched here, including acyl-CoA cholesterol acyltransferase (ACAT), diacylglycerol acyltransferase (DGAT) [151, 152], phosphatidylserine synthase (PS) [119], phosphatidylethanolamine-N-methyltransferase 2 [153], and long-chain fatty acyl-CoA synthetase-4 (ACSL4) [154]. The significance of MAM in lipid metabolism is also supported with the finding that lipid droplets in hepatoma cells are localized in close proximity to ER and also to mitochondria [155].

Lipid biosynthesis is closely related to Ca^{2+} signaling, therefore MAM is an important platform for Ca^{2+} trafficking as well. The ER/SR (sarcoplasmic reticulum) are the major reservoir for Ca^{2+} and its concentration in these organelles has to be maintained upon various signaling. Indeed, in the ER several proteins are present which take care of the precise regulation of Ca^{2+} level via its uptake and release. As discussed above (1.2.3), in the ER membrane the most important active transporter responsible for Ca^{2+} uptake is the SERCA, whereas RYR and IP3R release Ca^{2+} if the concentration increases. RYR is mainly present in muscle and some neuron cells, while IP3R is ubiquitously expressed. IP3R opens only upon binding of the second messenger, IP3 at the N-terminal [156], however elevated Ca^{2+} level in the ER lumen increases the sensitivity of IP3R to IP3 [157, 158]. In addition, in the lumen of ER/SR Ca^{2+} is buffered by chaperones such as calreticulin, GRP78 and PDI. These proteins, beside binding Ca^{2+} , are also able to regulate the activity of Ca^{2+} pumps and release channels [159, 160]. Under specific conditions Ca^{2+} in the ER is released into the cytosol as well as towards mitochondria. At the ER mitochondria contact site, IP3R and voltage dependent anion channel 1 (VDAC1) in the outer mitochondria membrane (OMM) are in close proximity, where they are tethered by glucose-regulated protein 75 (GRP75), forming a molecular bridge between the two proteins that facilitate the transmission of Ca^{2+} signals [161]. Although Ca^{2+} can pass through the OMM without transporters as well, the inner mitochondria membrane is impermeable, even for protons. Therefore, the mitochondrial calcium uniporter (MCU), a transmembrane protein in the inner mitochondrial membrane (IMM), is necessary to assist the uptake of Ca^{2+} from the intermembrane space (IMS) to the matrix of mitochondria [162].

Ca^{2+} signaling between the ER and mitochondria affects the activity of several enzymes involved in ATP production, lipid biosynthesis and cell survival. Prolonged elevated Ca^{2+} concentration in the mitochondria, however induces apoptosis by opening the mitochondrial permeability transition pore (PTP), consequently inducing cytochrome c release, a critical event in apoptotic cell death mechanisms [163]. Due to the multiple roles of Ca^{2+} in cellular signaling pathways, alterations in Ca^{2+} homeostasis are considered to be related to various diseases including diabetes [164], vascular and cardiovascular diseases [165-168], neurodegeneration [169-171], viral infections [172, 173], lung diseases [174, 175], non-alcoholic fatty liver disease [176], and cancer [177].

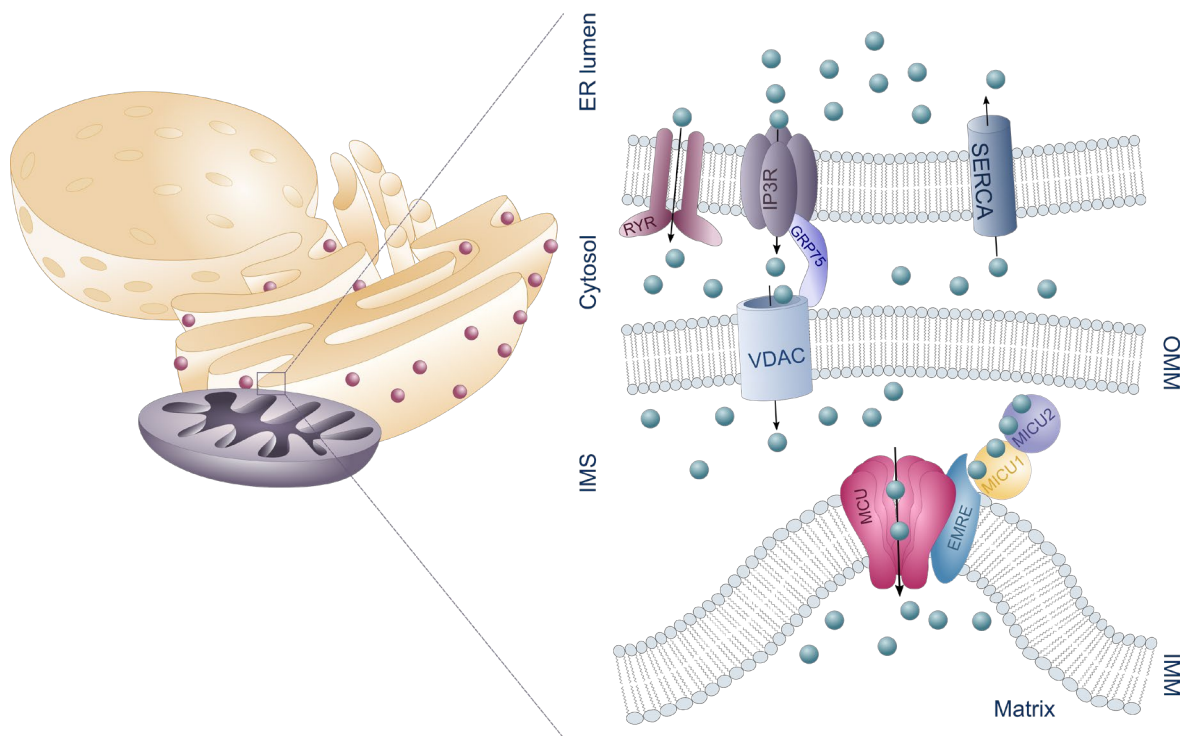


Figure 4 Ca^{2+} trafficking at the mitochondria associated membrane (MAM) site

The MAM serves as a platform for signaling between mitochondria and ER. Ca^{2+} signaling through this organelle contact site is crucial for several intracellular processes including ATP synthesis, tricarboxylic acid (TCA) cycle, and cell death. Since ER is the major Ca^{2+} store in the cell, the sarco/endoplasmic reticulum Ca^{2+} -ATPase (SERCA) has to constantly pump Ca^{2+} into the ER lumen even against a strong Ca^{2+} gradient, which requires a large amount of energy. In parallel, inositol 1,4,5-triphosphate receptor (IP3R) and ryanodine receptor (RYR) release Ca^{2+} into the cytosol and mitochondria. IP3R is tethered to voltage dependent anion channel (VDAC) via glucose-regulated protein 75 (GRP75) thereby favoring a rapid Ca^{2+} uptake into the intermembrane space (IMS) of mitochondria. In the inner mitochondrial membrane the mitochondrial Ca^{2+} uniporter (MCU) forms a complex with several proteins to promote Ca^{2+} uptake from the IMS into the matrix of the mitochondria. Figure adjusted from [178].

1.5. Genome editing by CRISPR Cas9

Clustered regularly interspaced short palindromic repeats (CRISPR)/CRISPR-associated systems (Cas) was proved to belong to bacterial and archaeal adaptive immune systems. It provides protection for the organism against viruses and plasmids [179-181]. The CRISPR locus in bacterial genomic DNA consists of palindromic repeats interspaced by similarly

sized variable fragments (spacers), an AT rich promoter region located upstream of the operon of several Cas proteins, and a small trans-activating crRNA (tracrRNA) coding region [182]. It was found that the spacer DNA sequences originate from viral invaders, which previously infected the host organism. In the adaptive step of CRISPR/Cas mediated immunity ~30 nucleotides of the invasive DNA are incorporated into the bacterial genome at the proximal end of CRISPR array (Fig. 5). The acquisition of new spacers requires the presence of 2-5 nucleotide length protospacer adjacent motif (PAM) in the foreign DNA, which is recognized by Cas9 [183]. Subsequently, Cas9 promotes the association of DNA sequence and CAS1/2 complex allowing the insertion of the spacer sequence directly after the promoter leader sequence [184-187].

The adaptation step is followed by the expression phase in which the transcription of spacer sequences occurs and precursor RNA (pre-crRNA) is produced. This transcription product undergoes enzymatic modification in order to generate mature crRNA, which is suitable to form complex with Cas9 and tracrRNA [188]. Subsequently, this complex is able to bind complementary sequences of viral or plasmid DNA and introduce double strand break (DSB) in the presence of the PAM sequence [189].

Previously, different technologies have been used for manipulating DNA, but these methods mostly relied on site-specific recognition of DNA by small molecules, oligonucleotides and self-splicing introns. More recently, DNA-recognition proteins have been identified, such as zinc-finger nucleases (ZFNs) and TAL effector nucleases (TALENs) which were the predecessors of RNA-programmable CRISPR/Cas technology [190, 191]. Researchers have been used this approach to perform studies, based on genome editing in a programmable manner. CRISPR/Cas allows targeted mutagenesis in eukaryotic cells, by lentiviral or retroviral transfection of Cas9 and single guide RNA (sgRNA), which is the product of the fusion of crRNA and tracrRNA. This genome editing has already been applied for plants, fungi, bacteria, mice and even humans [192]. However, using this approach on humans is ethically questionable [193]. CRISPR/Cas, as well as other genome editing tools, rely on the DNA repair mechanism of the cell.

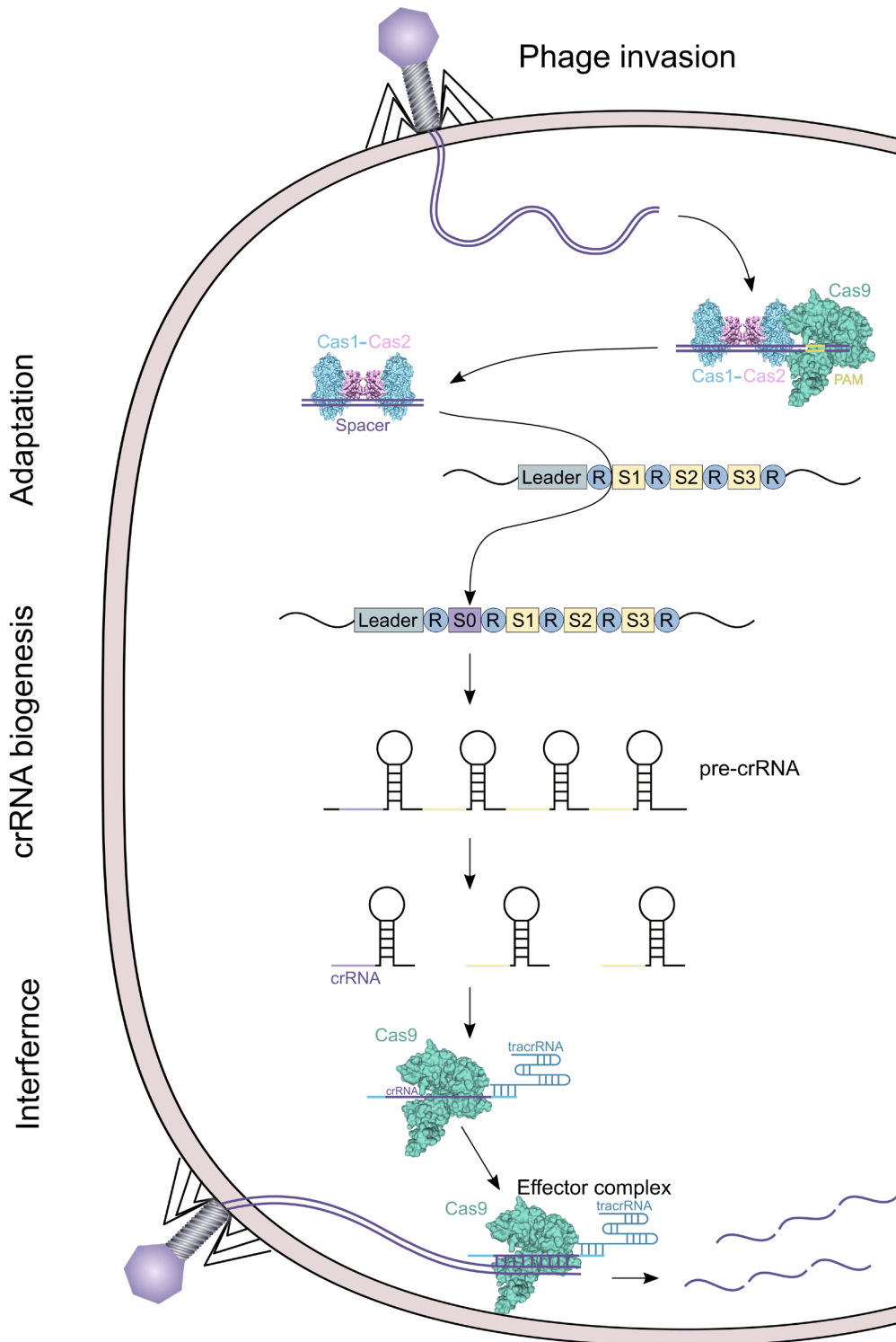


Figure 5 CRISPR-Cas system in prokaryotes

The adaptive immune system of prokaryotes consists of three steps. In the first step, in response to phage invasion, an adaptive phase takes place in which the new spacer sequence is selected and acquired. Cas9 recognizes the protospacer adjacent motif (PAM) in foreign DNA, whereas the complex of Cas1 and Cas2 promotes the integration of the spacer sequence into the CRISPR array. In the second phase, the precrRNA is synthesized which is further processed to generate crRNA. Therefore, upon another phage invasion, this crRNA along with Cas9 and tracrRNA are used to

target and introduce double strand breaks (DSB) in the phage DNA (interference phase). Figure adjusted from [194].

For this purpose, one possibility is the homology-directed repair (HDR), which requires the presence of an exogenous DNA template to promote DNA repair. The other option is the non-homologous end-joining (NHEJ) in which, due to the lack of proofreading, insertion and/or deletion can occur [195].

Targeting the gene of interest can be either for knockout or for loss of function mutation studies. DSB results in a frameshift mutation, which introduces pre-mature stop codons or nonsense mediated decay (NMD) of the transcript. As the deletion occurs on individual alleles, using the CRISPR/Cas tool, heterozygous or bi-allelic modifications can be performed in diploid cells [196, 197]. In addition, this approach has been successfully used for generating knockout/knockin animals by injecting Cas9 protein along with sgRNA into a single cell embryo [198-200].

2. MATERIALS

2.1. Equipment

Equipment	Company
2100 Bioanalyzer	Agilent
Axiovert 40 CFL Microscope	Zeiss, Jena, Germany
AxioCam MRc	Zeiss, Jena, Germany
BD FACSAria II	BD Biosciences
BD FACSCANTO II	BD Biosciences
Biological safety cabinet	Telstar
CB150 CO2 Incubator	Binder, Tuttlingen, Germany
Centrifuge 5424R	Eppendorf, Hamburg, Germany
ChemiDoc Imaging system™	Bio-Rad, Munich, Germany
Consort EV series power supplies	Sigma-Aldrich GmbH, Taufkirchen, Germany
DNA Engine Tetrad®2	MJ Research
EchoMRI	Zinsser Analytic GmbH
FACS Canto II	BD GmbH, Heidelberg, Germany
FVL-2400N Combi-Spin, Mini-Centrifuge/Vortex	BioSan, Medical-Biological Research and Technologies
Hei-Standard Magnetic Stirrer	Heidolph Instruments GmbH & CO. KG
Hemocytometer (Neubauer chamber)	Marienfeld, Lauda Königshofen, Germany
Inverse Labmicroscope Leica DM IL LED	Leica, Wetzlar, Germany
Kryostat Microm HM 560	Thermo Scientific, Bonn, Germany
Leica EG1160 Embedding Center, Dispenser + hot Plate	Leica, Wetzlar, Germany
Milli-Q® Integral Water Purification System	Merck-Millipore, Darmstadt, Germany
Mini-PROTEAN® Tetra electrophoresis chamber	Bio-Rad, Munich, Germany
Mr. Frosty™ freezing container	Thermo Fisher, Bonn, Germany
NanoDrop 1000 Spectrophotometer	Thermo Fisher, Bonn, Germany
New Brunswick™ Innova® 42/42R Incubation shaker	Eppendorf, Hamburg, Germany
Olympus confocal microscope IX81	Olympus, Münster, Germany
Roller 10 D	IKA Labortechnik, Staufen, Germany
Rotary Microtom Mikrom HM355S	Thermo Fisher, Bonn, Germany
Rotospin - Test Tube Rotator	Labinco, Manufacturing in the Netherlands
Rührwerk Eurostar RW16	IKA Labortechnik, Staufen, Germany
Sharp-R-941-BK-W-Inverter-Microwave	Sharp
Sonification device Q125	Qsonica
SpectraMax M5 Microplate Reader	Molecular Device GmbH, Biberach, Germany

Thermomixer® C	Eppendorf, Hamburg, Germany
Trans-Blot Turbo Transfer System™	Bio-Rad, Munich, Germany
Vortex Genie 2	Scientific Industries, Bohemia, USA
Waterbath VWB 12	VWR, Radnor, USA

2.2. Chemicals

Chemical	Company	Catalog-No
(R) MG132 5 mg	Cayman Chemical, USA	13697
1,4 Dithiothreitol (DTT)	Sigma-Aldrich GmbH, Taufkirchen, Germany	D0632
2,5-Di-t-butyl-1,4- benzohydroquinone (BHQ)	Selleckchem	S3628
2-mercaptoethanol	Sigma-Aldrich GmbH, Taufkirchen, Germany	M6250
Acetic acid	Merck KGaA, Darmstadt, Germany	1000632500
Agarose	Invitrogen, Karlsruhe, Germany	15510-027
AGK2	Merck-Millipore, Darmstadt, Germany	566324
α -Linolenic Acid	Cayman Chemical, USA	90210
Ampicillin	Sigma-Aldrich GmbH, Taufkirchen, Germany	A9518
Anti-FLAG(R) M2 Magnetic beads	Sigma-Aldrich GmbH, Taufkirchen, Germany	M8823
AquaBluer® Cell Viability Assay solution	MultiTarget Pharmaceuticals LLC, Salt Lake City, USA	6015
Arachidonic Acid	Sigma-Aldrich GmbH, Taufkirchen, Germany	A9673
Auranofin	Sigma-Aldrich GmbH, Taufkirchen, Germany	A6733
Blasticidin S hydrochloride	Sigma-Aldrich GmbH, Taufkirchen, Germany	15205
BODIPY 493/503	Life Technologies, Karlsruhe, Germany	D-3922
BODIPY 581/591 C11	Life Technologies, Karlsruhe, Germany	D3861
Bovine Serum Albumin Fraction V	Carl Roth GmbH & Co, Karlsruhe, Germany	0163.2
Bovine Serum Albumin, fatty acid free	Sigma-Aldrich GmbH, Taufkirchen, Germany	A8806-5G
Bromophenol Blue	Sigma-Aldrich GmbH, Taufkirchen, Germany	B0126
Chloroquine diphosphate salt	Sigma-Aldrich GmbH, Taufkirchen, Germany	C6628

MATERIALS

cOmplete™ Protease Inhibitor Cocktail	Sigma-Aldrich GmbH, Taufkirchen, Germany	4693116001
Cyclopiazonic acid from <i>Penicillium cyclopium</i>	Sigma-Aldrich GmbH, Taufkirchen, Germany	C1530
Desthiobiotin elution buffer	IBA Lifesciences, Göttingen, Germany	2-1000-025
Dimethyl sulfoxide (DMSO)	Sigma-Aldrich GmbH, Taufkirchen, Germany	D2650
DMEM	Thermo Fisher, Bonn, Germany	21969-035
DNA loading dye (6 x)	Thermo Fisher, Bonn, Germany	R0611
Doxycycline hyclate	Sigma-Aldrich GmbH, Taufkirchen, Germany	D9891
Dynabeads M-280 Strepavidin	Invitrogen, Karlsruhe, Germany	112-05D
Emetine	Sigma-Aldrich GmbH, Taufkirchen, Germany	E2375
Eosin solution	Carl Roth GmbH & Co, Karlsruhe, Germany	X883.1
Erastin	Merck-Millipore, Darmstadt, Germany	329600
Ethanol	Merck KGaA, Darmstadt, Germany	1.00983.2500
Ethylendiamintetraacetatic acid (EDTA)	Sigma-Aldrich GmbH, Taufkirchen, Germany	E9884
Fetal Calf Serum (FCS) LOT41Q6942K	Thermo Fisher, Bonn, Germany	10270
Anti-FLAG M2 Affinity Gel	Sigma-Aldrich GmbH, Taufkirchen, Germany	A-2220
FLAG peptide	Sigma-Aldrich GmbH, Taufkirchen, Germany	F3290
Glutaraldehyde (2.5%)	Science Services, Munich, Germany	15960
Glycerol	Sigma-Aldrich GmbH, Taufkirchen, Germany	G5516
Goat serum	Cell Signaling Technologies, Danvers, USA	5425
Hydrogen peroxide	Carl Roth GmbH & Co, Karlsruhe, Germany	8070.2
Hemalaun solution acid acc. to Mayer	Carl Roth GmbH & Co, Karlsruhe, Germany	T865.2
L-Glutamine	Invitrogen, Karlsruhe, Germany	25030
Linoleic	Cayman Chemical, USA	90150
Linolenic acid	Sigma-Aldrich GmbH, Taufkirchen, Germany	L2376
Lipoxstatin-1	Sigma-Aldrich GmbH, Taufkirchen, Germany	SML1414
Magnesium sulfate (MgSO4)	Sigma-Aldrich GmbH, Taufkirchen, Germany	M7774
Methanol	Sigma-Aldrich GmbH, Taufkirchen, Germany	322415
MiTMAb	Abcam, Cambridge, USA	120466

MATERIALS

Necrostatin-1	Enzo Life Sciences GmbH, Lörrach, Germany	BML-AP309-0020
N-ethylmaleimide	Sigma-Aldrich GmbH, Taufkirchen, Germany	E3876
Nonidet-P40 (NP-40)	Fluka Chemie GmbH, Buchs, Switzerland	W401404
NOX inhibitor	Cayman Chemical, USA	17764
OcTMAB	Abcam, Cambridge, USA	120467
Oil Red O	Sigma-Aldrich GmbH, Taufkirchen, Germany	O0625
Oleic acid	Cayman Chemical, USA	90260
Opti-MEM®	Life Technologies, Karlsruhe, Germany	11058021
Pageruler Prestained,Protein Ladder	Thermo Fisher, Bonn, Germany	26616
Paraffin wax	Polysciences, Warminster, USA	19652
Paraformaldehyde (PFA)	Carl Roth GmbH & Co, Karlsruhe, Germany	0335.3
Dubeccos Phosphate Buffered Saline (DPBS)	Life Technologies, Karlsruhe, Germany	14190094
Penicillin/Streptomycin	Invitrogen, Karlsruhe, Germany	15140-122
PhosSTOP™	Sigma-Aldrich GmbH, Taufkirchen, Germany	4906845001
Potassium chloride	Sigma-Aldrich GmbH, Taufkirchen, Germany	4504
Pro-myristic	Abcam, Cambridge, USA	120476
propylene glycol	Sigma-Aldrich GmbH, Taufkirchen, Germany	398039
proteinase K	Carl Roth GmbH & Co, Karlsruhe, Germany	7528.1
Puromycine dihydrochloride	Sigma-Aldrich GmbH, Taufkirchen, Germany	P7255
Rapamycin	Sigma-Aldrich GmbH, Taufkirchen, Germany	r8781
RNaseZap	Sigma-Aldrich GmbH, Taufkirchen, Germany	R2020
SCD1 inhibitor	Abcam, Cambridge, USA	142089
Seahorse XF Palmitate-BSA FAO Substrate	Agilent, Santa Clara, USA	102720-100
Skim Milk Powder	Sigma-Aldrich GmbH, Taufkirchen, Germany	70166
S.O.C. Medium	Thermo Fisher, Bonn, Germany	15544034
Sodium acetate	Sigma-Aldrich GmbH, Taufkirchen, Germany	S8750
Sodium chloride (NaCl)	Sigma-Aldrich GmbH, Taufkirchen, Germany	9888
Sodium dodecyl sulfate (SDS)	Carl Roth GmbH & Co, Karlsruhe, Germany	2326.2
Sodium hydroxide (NaOH)	Carl Roth GmbH & Co, Karlsruhe, Germany	6771.1

Sodium pyrophosphate	Sigma-Aldrich GmbH, Taufkirchen, Germany	S6422
Strep-Tactin® Superflow® 50% suspension	IBA Lifesciences, Göttingen, Germany	2-1206-010
SYBR® Safe DNA stain	Thermo Fisher, Bonn, Germany	S33102
Thapsigargin	Enzo Life Sciences GmbH, Lörrach, Germany	BML-PE180-0001
Tris(2-carboxyethyl)phosphine hydrochloride	Sigma-Aldrich GmbH, Taufkirchen, Germany	C4706-2G
Triton X-100	Sigma-Aldrich GmbH, Taufkirchen, Germany	X100
Trypsin-EDTA	Invitrogen, Karlsruhe, Germany	25300
Tunicamycin	Enzo Life Sciences GmbH, Lörrach, Germany	BML-CC104-0010
Tween20	Sigma-Aldrich GmbH, Taufkirchen, Germany	P5927
VECTASHIELD® HardSet™ Mounting Medium with DAPI	Enzo Life Sciences GmbH, Lörrach, Germany	VC-H-1200-L010
X-TremeGene™ HP DNA Transfection Reagent	Roche Diagnostics, Mannheim, Germany	6366236001
Xylool Roticlear®	Carl Roth GmbH & Co, Karlsruhe, Germany	A538.1
Z-VAD-FMK	Enzo Life Sciences GmbH, Lörrach, Germany	ALX-260-020-M001
γ-Linolenic Acid	Cayman Chemical, USA	90220

(1*S*,3*R*)-RSL3 was kindly provided by Prof. Dr. Derek Pratt, Ottawa University, Ottawa, Canada

2.3. Disposables and Kits

Disposables and Kits	Company	Catalog-No
12 % Mini-PROTEAN® TGX Stain-Free™ Precast Gels	Bio-Rad, Munich, Germany	456-8043
4–20% Mini-PROTEAN® TGX™ Precast Protein Gels	Bio-Rad, Munich, Germany	4561094
Clarity Western ECL Substrate	Bio-Rad, Munich, Germany	1705061
Corning® cell strainer	Sigma-Aldrich GmbH, Taufkirchen, Germany	CLS431750-50EA
Gibson Assembly® Cloning Kit	New England Biolabs	E5510S
Illumina® TotalPrep™ RNA Amplification Kit	Thermo Fisher, Bonn, Germany	AMIL1791
iScript™ cDNA Synthesis Kit	Bio-Rad, Munich, Germany	1708891
Millex-GP 33mm PES .22µm Sterile 50/pk	Merck-Millipore, Darmstadt, Germany	SLGP033RS

Millex-HP Syringe Filter Unit, 0.45 µm	Merck-Millipore, Darmstadt, Germany	SLHP033RS
MouseRef-8 v2.0 Expression BeadChip	Illumina	BD-202-0202
Nunc® CryoTubes®	Thermo Fisher, Bonn, Germany	V7634-500EA
Peroxidase Substrate Kit (DAB)	Vector Laboratories	Sh-4100
Pierce Silver Stain for Mass Spectrometry	Thermo Fisher, Bonn, Germany	24600
Pierce™ BCA Protein Assay Kit	Thermo Fisher, Bonn, Germany	23225
Pierce™ Protein Concentrators PES, 3K MWCO	Thermo Fisher, Bonn, Germany	88512
Plasmid Maxi Kit	Qiagen, Hilden, Germany	12163
QIAprep Spin Miniprep Kit	Qiagen, Hilden, Germany	27104
RNA 6000 Nano Kit	Agilent, Santa Clara, USA	5067-1511
RNase-Free DNase Set	Qiagen, Hilden, Germany	79254
RNeasy Mini Kit	Qiagen, Hilden, Germany	74104
Roti®-Histokitt	Carl Roth GmbH & Co, Karlsruhe, Germany	6638.1
Trans-Blot® Turbo™ Transfer Pack	Bio-Rad, Munich, Germany	170-4156
Vectastain ABC HRP Kit	Vector Laboratories	PK-4000
Wizard® SV Gel and PCR Clean-Up System	Promega, Mannheim, Germany	A9282
Disposable Vinyl Specimen Molds	Weckert Labortechnik, Kitzingen, Germany	4557
GeneRuler 1 Kb Plus DNA Ladder	Fermentas Life Science, Bonn, Germany	SM1331
Parafilm M®	Pechiney Plastic Packaging Company	PM996
PageRuler prestained protein ladder	Thermo Fisher, Bonn, Germany	26616
Tissue Tek® Compound Embedding Medium	Weckert Labortechnik, Kitzingen, Germany	4583
MitoTracker™ Red CMXRos	Thermo Fisher, Bonn, Germany	M7512
CellLight™ Golgi-RFP, BacMam 2.0	Thermo Fisher, Bonn, Germany	C10593
Lyso-tracker	Thermo Fisher, Bonn, Germany	L12492

2.4. Enzymes

Enzyme	Company	Catalog-No
Taq DNA Polymerase	Invitrogen, Karlsruhe, Germany	18038-026
Herculase II Fusion DNA Polymerase	Agilent, Santa Clara, USA	600677
T4 DNA Ligase	New England Biolabs	M0202S
Proteinase K	Carl Roth GmbH & Co, Karlsruhe, Germany	7528.1
Restriction Endonucleases	New England Biolabs	various

2.5. Antibodies

Primary	Species	Dilution	Company	Catalog-No
GRP78	rabbit	1:1000	Cell Signaling Technologies, Danvers, USA	3177
PERK	rabbit	1:1000	Cell Signaling Technologies, Danvers, USA	3192
pPERK	rabbit	1:1000	Cell Signaling Technologies, Danvers, USA	3179
β -actin	mouse	1:10000	Sigma-Aldrich GmbH, Taufkirchen, Germany	A5441
LC-3	rabbit	1:1000	Cell Signaling Technologies, Danvers, USA	12741
GFP	chicken	1:1000	Aves	gfp-1020
GAPDH				
Flag	mouse	1:1000	Sigma-Aldrich GmbH, Taufkirchen, Germany	F3165
PDI	rabbit	1:1000	Cell Signaling Technologies, Danvers, USA	3501
Ubiquilin1	rabbit	1:1000	Novus	NB120- 3341
Ubiquilin 2	mouse	1:1000	Abnova GmbH	H00029978- M03
Ubiquilin 4	rabbit	1:1000	Abnova GmbH	PAB16793
ST18	rabbit	1:1000	OriGene Technologies, Inc.	TA334234
mGPX8 (10F10)	rat	1:10	Dr. Elisabeth Kremmer, Helmholtz Zentrum München, Germany	
mGPX8 (2F4)	rat	1:10	Dr. Elisabeth Kremmer, Helmholtz Zentrum München, Germany	
mGPX8 (24F3)	rat	1:10	Dr. Elisabeth Kremmer, Helmholtz Zentrum München, Germany	
hGPX8 (29H3)	rat	1:10	Dr. Regina Feederle, Helmholtz Zentrum München, Germany	
hGPX8 (24H5)	rat	1:10	Dr. Regina Feederle, Helmholtz Zentrum München, Germany	
hGPX8 (30A4)	rat	1:10	Dr. Regina Feederle, Helmholtz Zentrum München, Germany	
Secondary	Species	Dilution	Company	Catalog-No
α -rabbit-bio	goat	1:250	Vector Laboratories Inc., Burlingame, USA	BA-1000
Alexa Fluor 488 α - rabbit	donkey	1:250	Life Technologies, Karlsruhe, Germany	A21206
Alexa-fluor 594 α - mouse	donkey	1:250	Life Technologies, Karlsruhe, Germany	A11058
α -mouse-bio	goat	1:250	Vector Laboratories Inc., Burlingame, USA	BA-9200

α -rabbit-HRP	goat	1:5000	Santa Cruz Biotechnologies, Heidelberg, Germany	SC-2030
α -mouse-HRP	goat	1:5000	Santa Cruz Biotechnologies, Heidelberg, Germany	SC-2031
α -rat-HRP	goat	1:5000	Dianova GmbH, Hamburg, Germany	90553
α -chicken-HRP	goat	1:5000	Abcam, Cambridge, USA	ab97135

2.6. Cell lines

Mouse embryonic fibroblasts (MEFs):

MEFs were isolated from mouse embryos as described later (see 2.12.1). *Gpx8*^{wt/wt} or *Gpx8*^{-/-} mice were mated to generate cell lines with different genotypes. *Gpx8*^{-/-} mice carry a CRISPR mediated deletion of 16 bp in the critical exon 2 of *Gpx8*, which results in a frameshift mutation, consequently the gene product is destroyed.

Human Embryonic Kidney (HEK293T):

Human embryonic kidney (HEK) 293T cells were purchased from ATCC (ATCC® CRL-3216™) and used as packaging cell line for virus production.

2.7. Mouse line

Gpx8^{-/-} CRKO:

The *Gpx8*^{-/-} CRKO mouse line was generated with the help of Dr. Florian Giesert (HMGU). The second exon of *Gpx8* was targeted by CRISPR Cas9 to induce deletion and consequently the frameshift in the coding sequence of the gene. Due to the frameshift, protein synthesis of GPX8 is interrupted by the altered coding sequences and a premature stop codon. Therefore, mice that carry the deletion in exon 2 are systemically knockout for of GPX8. In order to introduce the deletion in C57BL/6N mice, Cas9 mRNA and guide RNA were injected into single cell embryos. After the offspring was born, they were genotyped and the mouse carrying the deletion was mated with C57BL/6N *Gpx8*^{wt/wt} animals to maintain the modified allele and generate *Gpx8*^{-/-} homozygous mice.

2.8. Oligonucleotides

Oligos for Gibson cloning

Oligo label	Sequence
mGpx8 Gibs forw	GAATCAAGCTTATCGATACCGTCGACGGATCCTTCGAAATGGAGCCTTTCGCTGCCTAC
mGpx8 Gibs rev	GAGGGCCCCGGGCGGCCGCTACGTAACCGGTCTCGAGTCATAGATCCTCTTTCTTTTAA G
hGpx8 Gibs forw	GAATCAAGCTTATCGATACCGTCGACGGATCCTTCGAAATGGAGCCTTTCGAGCTTAC
hGpx8 Gibs rev	GAGGGCCCCGGGCGGCCGCTACGTAACCGGTCTCGAGTCATAGATCCTCTTTCTTTTAA TG
Gpx8-YFP Gibs forw	CCGGTCAATCAAGCTTATCGATACCGTCGACGGATCCTTATGGAGCCTTTCGCTGCCTA C
Gpx8-YFP Gibs rev	ATTGCTCGGAGGGCCCCGGGCGGCCGCTACGTAACCGGTCTCATAGATCCTCTTTCTTGT ACAGCTCGTC
Gpx8 rev for fusion	CTCCTCGCCCTTGCTCACCTTTTTAAGAATAATTTG
YFP forw for fusion	CAAATTATTCTTAAAAAGGTGAGCAAGGGCGAGGAG
YFP-mock Gibs forw	CCGGTCAATCAAGCTTATCGATACCGTCGACGGATCCTTATGGTGAGCAAGGGCGAG GAGCTG
YFP-mock Gibs rev	ATTGCTCGGAGGGCCCCGGGCGGCCGCTACGTAACCGGTCTTACTTGTACAGCTCGTCC ATGCCGAGAGTG
Gpx8 FST C11S rev	TTGCTTTGGGCCCCGGAACCTTTTTAATGGGTAGGCAGCGAA
Gpx8 FST C11S forw	TTCGCTGCCTACCCATTAATAAGTTCCGGGCCCAAAGCAA
Gpx8 FST C28S rev	GAGAAAAAGCATCACGGTGCTCAGAACCATAGAGAGCAA
Gpx8 FST C28S forw	TTGCTCTATGGTTCTGAGCACCGTGATGCTTTTTCTC
Gpx8 FST C79S rev	CTTGCTGTGAAGCGGGAGTCACTAGCCAC
Gpx8 FST C28S forw	GTGGCTAGTGACTCCCCTTACAGACAAG
Gpx8 FST C79S rev	CTCCGATTCTCCAACTGATTGCTCGGAAAAGCCAGGAC
Gpx8 FST C108S forw	GTCCTGGCTTTCCGAGCAATCAGTTTGGAGAATCGGAG
Gpx8 K10R forw	GCTGCCTACCCATTAAGATGTTCCGGGCCCAA
Gpx8 K10R rev	TTTGGGCCCGAACATCTTAATGGGTAGGCAGC
Gpx8 K38R forw	TTTCTCTCAGTTAAGATTCCTGAAGCCGAGA
Gpx8 K38R rev	TCTCGGCTCAGGAATCTTAAGTGAAGGAGAAA
Gpx8 K141R forw	ATCTCCACAAGATTAGGATTTAGGGCCGGAA
Gpx8 K141R rev	TTCCGGCCCTAAAATCCTAATCTTGTGGAAGAT
Gpx8 K10/15R forw	TGTTCCGGGCCCAGAGCAAAGATATTT
Gpx8 K10/15R rev	AAATATCTTTGCTCTGGGCCCGGAACA
Gpx8 K10/17R forw	GGGCCCAAAGCAAGAATATTTGCAGTT
Gpx8 K10/17R rev	AACTGCAAATATTCTTGCTTTGGGCC
Gpx8 K10/15/17R forw	TGTTCCGGGCCCAGAGCAAGAATATTTGCAGTT
Gpx8 K10/15/17R rev	AACTGCAAATATTCTTGCTCTGGGCCCGGAACA
Gpx8 K15R forw (c)	GTTCCGGGCCCAGAGCAAAGATATTTG
Gpx8 K15R rev (b)	CAAATATCTTTGCTCTGGGCCCGGAAC
Gpx8 K17R forw	TCCGGGCCCAAAGCAAGGATATTTGCAGTTTTG
Gpx8 K17R rev	CAAACTGCAAATATCCTTGCTTTGGGCCCGGA

Oligos for sequencing

Oligo label	Sequence
seq primer MEF CRISPR G1 forw	ATGGAGCCTTTCGCTGCCTACCCA
seq primer MEF CRISPR G1 rev	AGCGGGTCTCAAAGCATCTCCTAG
seq primer MEF CRISPR G2 forw	CTAAAAATATGGAATCTATCAGA
seq primer MEF CRISPR G2 rev	GAGAAGAATGAACAACATTGAGGC
seq primer MEF CRISPR G1+G2 forw	CTCTATGGTTCTGTGCACCGTGATGC
seq primer MEF CRISPR G1+G2 rev	GACTTGGGCTCCGATTCTCCAAACTGA

Oligos for mouse genotyping

Oligo label	Sequence
Mouse genotyping Gpx8 exon2 forw	GCTTCCTGGTTGTAACGTG
Mouse genotyping Gpx8 exon2 rev	CAACAATAAATCTAACGCAGGTC

Oligos for CRISPR/Cas9 genome editing

Oligo label	Sequence
Gpx8 CRISPR G1 for	CACCGAGCTGTTGGTTCTCGGCTTCGT
Gpx8 CRISPR G1 rev	TAAAACGAAGCCGAGAACCAACAGCTC
Gpx8 CRISPR G2 for	CACCGCCCTATCACTTCAACGTCCGT
Gpx8 CRISPR G2 rev	TAAAACGGACGTTGAAGTGATAGGGC

2.9. Bacteria

DH5 α *E.coli* F- endA1 glnV44 thi-1 recA1 relA1 gyrA96 deoR nupG Φ 80dlacZ Δ M15 Δ (lacZYA-argF)U169, hsdR17(rK- mK+), λ -

2.10. Cloning vectors**442-PL1-IRES-PURO:**

The replication incompetent lentiviral vector 442-PL1-IRES-puro (Fig. 6) was a kind gift from Prof. Tim Schröder (ETH Zurich). The vector served as a backbone for cloning of mouse *Gpx8* cDNA with different modifications.

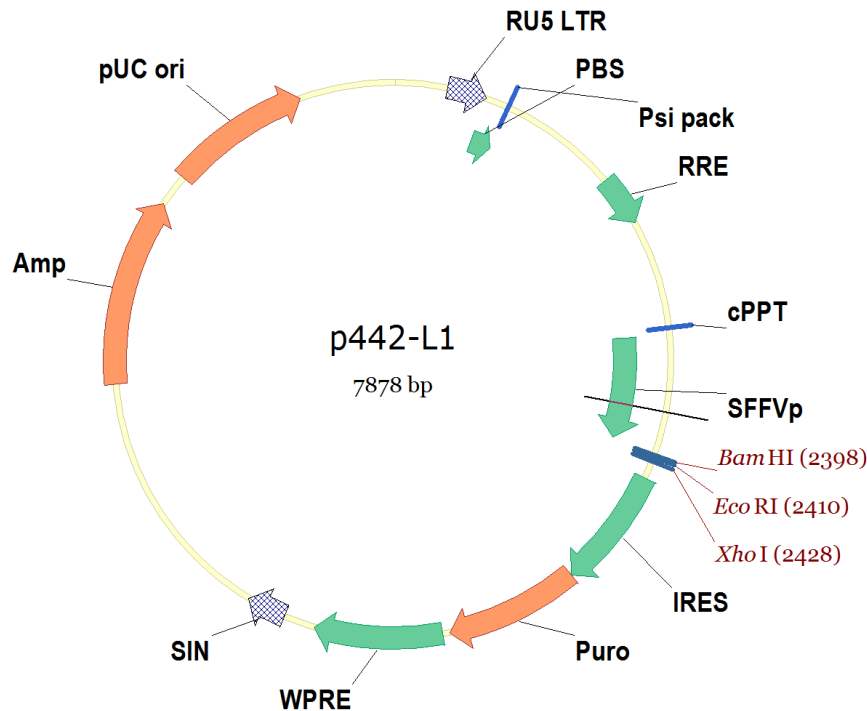


Figure 6 Map of the lentiviral expression plasmid 442-PL1 IRES puro

442-PL1 transfer vector was generated by modifications of the human immunodeficiency virus (HIV) lentiviral vector. Due to this modifications, the 442-PL1 vector consists of a reduced viral genome, lacking the required coding sequence for infection and integration of the virus. The expression of target cDNA is regulated by spleen foci forming virus promotor (SFFVp). Abbreviations: internal ribosome entry site (IRES), puromycin N-acetyl-transferase (puro), primer binding site (PBS), central poly-purine tract (cPPT), woodchuck hepatitis virus posttranscriptional regulatory element (WPRE), rev responsive element (RRE), self-inactivating 3'LTR (SIN), retroviral packaging element (Psi pack), ampicillin resistance gene beta-lactamase (Amp), origin of replication (pUC ori), and R and U region from HIV (RU5 LTR). Restriction site used for cloning are indicated by XhoI, BamHI and EcoRI.

pRSGT16-U6Tet-CMV-TetRep-2A-tagRFP-2A-Puro:

The map of pRSGT16-U6Tet-CMV-TetRep-2A-tagRFP-2A-Puro is shown in Fig. 7. pRSGT16-U6Tet-CMV-TetRep-2A-tagRFP-2A-Puro was used as a doxycycline-inducible sgRNA expressing plasmid in LentiCas9-Blast transduced target cells. The vector was purchased from Collecta.

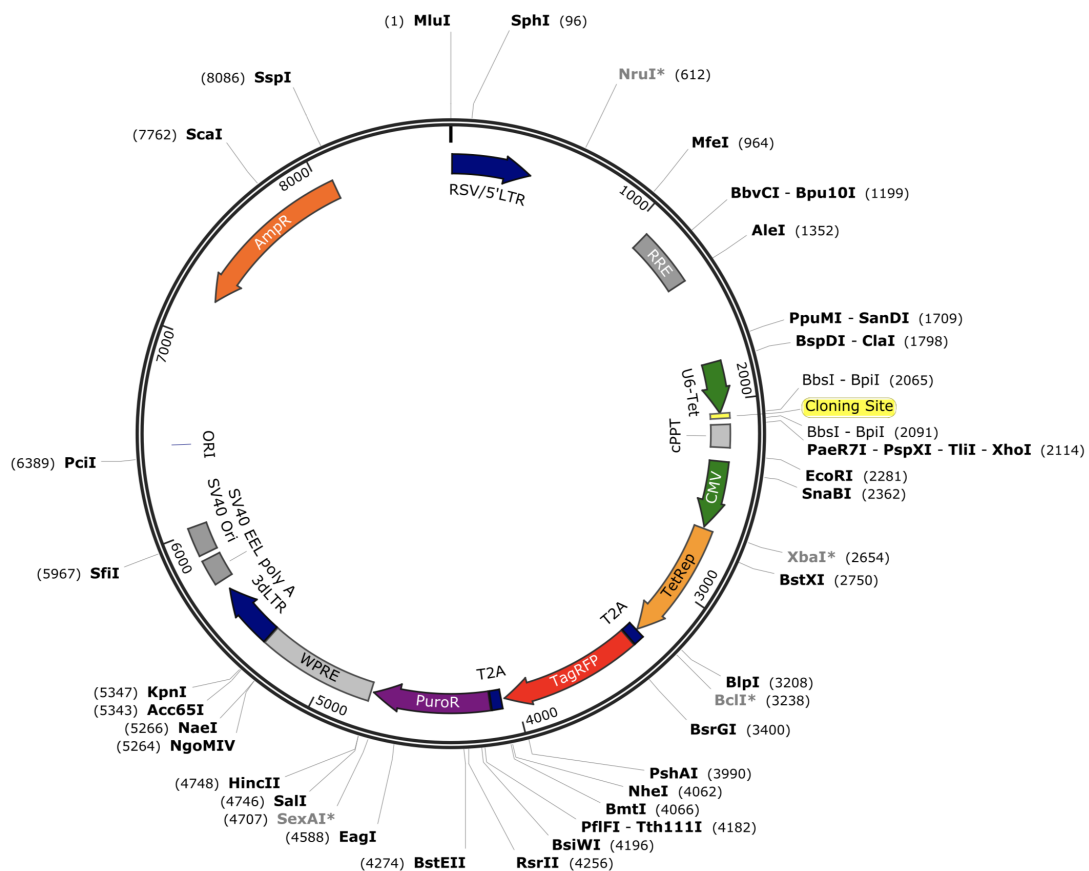


Figure 7 The pRSGT16-U6Tet-sh-CMV-TetRep-2A-TagRFP-2A-Puro vector is a human immunodeficiency virus (HIV) lentiviral-based vector which was purchased from Collecta. The vector has a doxycycline-inducible U6-Tet promoter to express sgRNA constructs. Abbreviations: ampicillin resistance gene (AmpR), (RSV/LTR), rev responsive element (RRE), tetracycline inducible U6 promoter (U6-Tet), central poly-purine tract (cPPT), cytomegalovirus promoter (CMV), Tet repressor proteins (TetRep), red fluorescent protein (TagRFP), puromycin resistance gene (PuroR), woodchuck hepatitis virus posttranscriptional regulatory element (WPRE), origin of replication (SV40 Ori).

pEcoEnv-IRES-puro, pMDLg/pRRE, pRSV-Rev:

The third generation packaging system consists of three vectors, pEcoEnv-IRES-puro, pMDLg/pRRE, pRSV-Rev, which were co-transfected with the corresponding plasmid to generate virus particles and transfect targeted cells (see 3.3.).

2.11. Software

Software	Supplier
FlowJo	FlowJo LLC, Ashland, USA
GraphPad Prism 7.0	GraphPad Software Inc., USA
Image Lab	Bio-Rad, Munich, Germany
iTEM Software	Olympus Soft Imaging Solutions, Münster, Germany
ImageJ	Free Software
Fintch TV	Free Software
Vector NTI	Thermo Fisher, Bonn, Germany
EndNote X8	Clarivate Analytics, Philadelphia, USA
Inkscape 0.92.4	Free Software

3. METHODS

3.1. Cell culture-related methods

3.1.1. Murine embryonic fibroblasts

Gpx8^{wt/wt} and *Gpx8*^{-/-} mice were mated separately and the females were checked every day for vaginal mucous plug. Between 13-14 days after the plug test was positive (embryonic development day 13.5-14.5), the pregnant females were euthanized by cervical dislocation. Subsequently the uterus was removed and transferred into a Dulbecco's Phosphate-Buffered Saline (DPBS) containing Petri dish. The embryos were separated by dissecting the uterus, washed in DPBS to remove blood and dissected under sterile conditions. The head and the red tissues (liver and heart) were removed from the embryos. The remaining of the embryos was separately transferred into new 10 cm cell culture dishes and the bodies were minced with a scalpel. Trypsin (0.05% trypsin-EDTA) was added to each tissue and incubated for 10 min at 37 °C. After incubation, the cells were homogenized by pipetting, and centrifuged at 400 x g for 5 min. The supernatant was removed, the cell pellet was resuspended in DMEM and the cells were transferred into 10 cell culture plates. The isolated primary cells were cultured at 3% O₂, 5% CO₂ at 37°C in standard DMEM. After reaching passage 20, primary MEFs are considered to be immortalized, therefore the culturing conditions were changed to 20% O₂, 5% CO₂ and 37°C. In order to reach this immortalized state, cells were split 1:2 once they reached almost confluency. The immortalized cells were used for further experiments.

Standard DMEM: DMEM, 10% FCS, 100 µg/mL streptomycin, 100 U/mL penicillin, 2 mM L-glutamine

3.1.2. Determination of cell number

To determine cell number, adherent cells were washed with DPBS and removed from cell culture dish by adding trypsin and incubating for 5 min at 37 °C. The cell suspension was homogenized by pipetting and diluted in 10 mL of standard DMEM. 10 µL of the suspension was used to determine cell number using Neubauer chamber.

3.1.3. Cryopreservation and thawing cells

Cryopreservation allows cells to be stored for years in liquid nitrogen. For cryopreservation cells were collected from 80% confluent 10 cm cell culture dish by adding trypsin. Then, the cells were transferred in a 10 mL standard DMEM containing falcon tube and centrifuged at 400 x g for 5 min at room temperature. After removing the supernatant, the cell pellet was resuspended in 4 mL freezing medium which contained standard DMEM, 50-90% FCS and 10% DMSO and aliquoted into cryogenic vials (1 mL for each tube). The vials were placed into a freezing container and stored overnight at -80°C. The next day, the cells were transferred to nitrogen tank for long term storage.

The thawing procedure of cryopreserved cell has to be performed rapidly in order to decrease the exposure of damaging ice crystals. Therefore, the cryovials were placed into a water bath at 37°C and after the cells were thawed, the suspension was transferred into a falcon tube, containing 10 mL of pre-warmed standard DMEM. To remove DMSO, the cells were centrifuged at 400 x g for 5 min at room temperature. After the centrifugation the supernatant was removed, the cells were resuspended in 10 mL of standard DMEM and finally plated into a 10 cm cell culture dish.

Standard DMEM: DMEM, 10% FCS, 100 µg/mL streptomycin, 100 U/mL penicillin, 2 mM L-glutamine

3.1.4. Cell viability assay

Determination of cell viability was performed using the AquaBluer method. This assay is based on the measurement of cellular activity in response to different cytotoxic compounds. The compound reflects the activity of the complex I and complex II of the mitochondrial electron transport chain. Active mitochondria reduce AquaBluer, and the reduced compound has an altered fluorescent emission on a different wavelength. For the assay, cells were plated into a 96-well plate (2000 cells/well) and incubated overnight. The next day, the treatment was conducted with different compounds including thapsigargin (TG), tunicamycin, dithiothreitol (DTT), 2,5-Di-t-butyl-1,4-benzohydroquinone (BHQ), cyclopiazonic acid (CPA), RSL3, erastin, rapamycin, chloroquine, AGK-2, dynamin inhibitors (MiTMAB, OctMAB, Pro-Myristic acid), stearoyl-CoA-desaturase 1 (SCD1) inhibitor, NADPH oxidase 1 and 4 (NOX1 and 4) inhibitor. 24 hours after the treatment the medium was

removed, AquaBluer was diluted (1:100) in standard DMEM and 100 μ L was added to each well. The cells were then incubated with the compound for 6-8 hours at 37°C in the cell culture incubator and the fluorescence emission was measured at 562 nm using the SpectraMax microplate reader (Molecular Device GmbH).

3.1.5. CRISPR/Cas9-mediated KO of individual genes

To knockout *Gpx8* by CRISPR/Cas9 in cultured cells, the critical exon (exon 2) was targeted by single guide RNAs (sgRNA), which were designed by an online tool (<http://www.crisprscan.org/>). The guides were cloned into the doxycycline inducible pRSGT16-U6Tet-CMV-TetRep-2A-tagRFP-2A-Puro lentiviral vector. First, MEFs were transfected with lentiviral particle coding Cas9 and a blasticidin resistance gene, and the positive cells were selected by supplementing the standard DMEM with 10 μ g/mL blasticidin for two weeks. For generating stable cell line carrying the sgRNA expressing vector, virus was produced as described later (see 3.3.3.). Subsequently, MEFs with viral expression of Cas9 were used for the second transduction with pRSGT16-U6Tet-CMV-TetRep-2A-tagRFP-2A-Puro vector carrying CRISPR sgRNA. Two days after transfection, puromycin selection was performed using 2.5 μ g/mL puromycin for 3 days to remove the non-transfected cells. Thereafter, the resistant cells were seeded at very low density for single cell cloning (30 cells/96 well plate), and doxycycline (50 μ g/mL) was added to the medium to induce the expression of guide RNA. The expanded clones were genotyped and sequenced for the purpose of validation the presence or the absence of deletion in the specific locus. Finally, immunoblot analysis was performed to evaluate the protein level that had been transcribed from the targeted gene in the single cell clones.

3.1.6. Immunofluorescence staining

Sterile glass coverslips were placed into a 12 well cell culture dish and coated with poly-L-lysine. 20000 cells/well were seeded onto the wells and incubated overnight. The following day if necessary, the cells were treated for a given time. Subsequently, the medium was aspirated, the cells were washed two times with DPBS and then they were fixed with 4% PFA for 15 min. The fixing solution was removed, and the cells were washed again with DPBS 3 times for 5 min each. If antibody staining was conducted, the cells were blocked with goat serum for 1 hour, at room temperature. The blocking solution was aspirated, the

cells were rinsed with TBS-T and the corresponding primary antibody was diluted according to the manufacturer's protocol. Thereafter, the diluted antibody was added to the cells and incubated overnight at 4 °C. The next day, the coverslips were washed with TBS-T and the secondary antibody was diluted and added to the cells for 2 hours. After the secondary antibody was removed, the cells were washed 3 times in TBS-T. Finally, the cells were mounted on slides using VECTASHIELD® Hardset Antifade Mounting Medium with DAPI. The slides were stored at 4 °C until the pictures were taken using Olympus Confocal microscope IX81 (Olympus, Münster, Germany).

In case of using fluorescence organelle trackers for live cell imaging, cells were incubated with the specified organelle tracker according to the manufacturer's protocol, then post-fixed with 4% PFA and mounted as described before.

3.1.7. Assessment of lipid peroxidation

For determining lipid peroxidation, 1×10^5 cells were seeded onto a 6-well plate and incubated overnight under standard conditions. On the following day, the cells were treated for 3 hours with either thapsigargin or RSL3 with or without liproxtatin-1. Subsequently, the cells were incubated with C11-BODIPY (581/591) (1 μ M) for 15 min at 37 °C. After the incubation, the cells were harvested by trypsinisation, washed with DPBS and resuspended in 500 μ L ice-cold DPBS. Using a cell strainer, cells were transferred into FACS tubes and the samples were placed on ice and protected from light during the measurement. Lipid peroxidation was assessed by detecting fluorescence change of BODIPY (C581/591) at 488 nm using BD FACS Canto II flow cytometer. The analysis of data was performed using FlowJo Software.

3.1.8. Determination of intracellular Ca²⁺ level

All experiments concerning the intracellular Ca²⁺ measurement analysis were performed by the group of Prof. Dr. Ivan Bogeski (Göttingen University, Germany).

3.2. Nucleic acid-related methods

3.2.1. Phenol-chloroform extraction of genomic DNA from mouse ear punches and MEFs

Adherent cells were trypsinized and the cell pellet was used to isolate genomic DNA. Ear punches from mice or cell pellets from MEFs were lysed overnight in 300 μ L of lysis buffer containing 50 μ g/mL proteinase K in a thermo shaker at 55 $^{\circ}$ C and 750 rpm. The following day, the protein and lipid content were removed by adding 300 μ L of phenol/chloroform/isoamylalcohol (pH 7.9). The samples were mixed thoroughly, then centrifuged for 6 min at 18,400 x g at room temperature. Due to the centrifugation, two phases are separated, where the negatively charged DNA is solved in the aqueous phase (upper phase) and the proteins, lipids are contained in the organic phase (lower phase). After centrifugation, 200 μ L of the upper phase was transferred into an Eppendorf tube containing 500 μ L 75 mM NaCl dissolved in 100% ethanol. The precipitated DNA was separated by centrifugation at 18,400 x g for 20 min at 4 $^{\circ}$ C. The supernatant was removed, the pellet was washed with 70% ethanol and centrifuged under the same conditions as in the previous step. Finally, the supernatant was removed, the pellet was dried for 2 hours at room temperature and was then dissolved in 100 μ L MilliQ water.

Lysis buffer: 10 mM Tris (pH 7.6), 10 mM EDTA, 0.5 % SDS, 10 mM NaCl, 300 μ g/mL proteinase K

Proteinase K: 50 mM Tris (pH 7.6), 5 mM EDTA (pH 8), 10 mg/mL proteinase K

3.2.2. Purification of bacterial plasmid DNA

Isolation of plasmid DNA from bacterial cells is a crucial step in cloning workflow. First, the LB medium was supplemented with the corresponding antibiotic, then single bacterial colonies were inoculated to prepare Miniprep (2 mL of LB medium) or Maxiprep (200 mL of LB medium) and incubated overnight at 37 $^{\circ}$ C under constant shaking. The next day, the plasmid DNA was purified from bacterial cells using QIAGEN[®] Plasmid Mini or Maxi Kits by following the manufacturer's protocol. The quantity and quality of isolated DNA were assessed using NanoDrop 1000 Spectrophotometer.

3.2.3. Ligation of DNA fragments by Gibson cloning

Gibson assembly is used to ligate two or more overlapping DNA fragments with blunt ends simultaneously. In order to effectively join the fragments, they have to contain at least a

15-80 bp overlapping sequence on the both 5' and 3' sides. The vector DNA was linearized by digestion with restriction enzymes which were specific to the targeted DNA sequence. The overlaps of the inserts were achieved by designing specific primers for the PCR amplification of DNA. Herculase II Fusion polymerase was used for the PCR reaction in a 50 μ L reaction mix in the presence of 4 % DMSO, 0.2 mM dNTP, 0.5 μ M of the individual reverse and forward primer, 2 μ L of DNA template and 5 x reaction mix (see Table 1). The digested vector DNA and the PCR product were separated by agarose gel electrophoresis, and both sample DNAs were isolated from agarose gel by applying Wizard[®] SV Gel and PCR Clean Up System (Promega). For the ligation of the vector and insert, Gibson Assembly[®] Master Mix (NEB) was used in a total volume of 20 μ L. For the procedure, 50 ng of vector DNA was used in the 3-fold molar excess of insert DNA. The reaction mix was incubated at 50°C for 60 min and 2 μ L of the ligation mix was applied for the transformation of bacteria.

3.2.4. (PCR) protocol for mouse genotyping

This method was developed to detect alterations in mouse genome by PCR. The primers were designed for the critical exon of *Gpx8*, which was targeted by CRISPR/Cas9. In order to be able to distinguish the 16 bp difference between WT and KO alleles, the reverse and forward primers were designed to bind in a close proximity upstream and downstream to the CRISPR/Cas9 cleavage site.

Therefore, the PCR of *Gpx8*^{wt/wt} mouse DNA resulted in a 262 bp product while the amplification of *Gpx8*^{-/-} mouse DNA generated a 246 bp product. 25 μ L of the PCR reaction was set using 2 μ L DNA, isolated from either the ear clip or the tail (see 3.2.1.), 0.2 mM dNTP, 1.5 mM MgCl₂, 2,5 μ L 10 X Master Mix, 0.5 μ M of each primer and 0.3 μ L Taq polymerase (Table 1). The reaction mix was placed into a MJ Research Dyad Dual 96-well PCR machine and the program was allowed to run for 35 x cycles (see Table 2). Finally, the PCR product was separated in 2.5 % agarose gel, and the DNA was visualized by ChemiDoc[™] UV transilluminator.

PCR Master Mix (<i>Taq</i> DNA polymerase)	
Forward primer (10 μ M)	1.3 μ L
Reverse primer (10 μ M)	1.3 μ L
10X PCR Buffer (200 mM Tris-HCl pH 8.4, 500 mM KCl)	2.5 μ L
MgCl ₂ (50 mM)	0.75 μ L
Deoxyribonucleotide triphosphate (dNTP)	0.5 μ L
<i>Taq</i> DNA Polymerase (5U/ μ L)	0.3 μ L
dH ₂ O	16.35 μ L
Sample DNA	2 μ L
Total volume	25 μ L

PCR Master Mix (<i>Herculase II Fusion</i> DNA polymerase)	
Forward primer (10 μ M)	2.6 μ L
Reverse primer (10 μ M)	2.6 μ L
5x <i>Herculase II</i> Reaction Buffer	10 μ L
Dimethyl sulfoxide (DMSO)	2 μ L
Deoxyribonucleotide triphosphate (dNTP)	1.25 μ L
<i>Herculase II Fusion</i> DNA polymerase	0.5 μ L
dH ₂ O	28.55 μ L
Sample DNA	3 μ L
Total volume	50 μ L

Table 1 Standard protocol for PCR Master Mix for *Taq* DNA polymerase and *Herculase II Fusion* DNA polymerase

Standard program for polymerase chain reaction (PCR)			
Nr. of cycle		Temperature	Time
1 x	denaturation	95 °C	5 min
35 x	denaturation	95 °C	30-60 sec
	annealing	T _m of primers -5 °C	30-60 sec (depending on the size of primer)
	elongation	72 °C	<i>Taq</i> 1 min/0.5 kb, <i>Herc</i> 1 min/1 kb
1 x	extention	72 °C	5 min
1 x	cooling	4 °C	until required

Table 2 Standard protocol for DNA amplification by PCR reaction

3.2.5. Restriction digestion

This step of cloning workflow is important to create compatible ends of the vector for the ligation. Restriction enzymes were purchased from New England Biolabs GmbH and were applied to digest vector DNA. 50 μ L of reaction mix was prepared following the manufacturer's protocol. The linearized DNA was separated in 0.8% agarose gel and isolated using Wizard® SV Gel and PCR Clean Up System (Promega). The concentration of DNA was measured by NanoDrop 1000 Spectrophotometer.

3.2.6. Agarose gel electrophoresis

Agarose gel electrophoresis is the most common method used to separate DNA fragments according to their charge, which correlates with their size. Depending on the size of DNA fragments, 0.8-2.5 w/v % agarose gel was prepared using 1 x TAE buffer and supplemented with SYBR® Safe dye in a 1:10000 dilution ratio. The gel was placed into a running chamber filled with 1 x TAE buffer and allowed to solidify. The DNA samples were mixed with 6 x loading dye (Thermo Fisher) and loaded into the pockets of the gel. To separate the DNA fragments, 100-120 V was applied for 45-180 min depending on the DNA fragment sizes. For visualization of the separated DNA fragments, ChemiDoc™ UV transilluminator was applied.

TAE buffer (10 x): 200 mM Tris, 100 mM sodium acetate, 6 mM EDTA (pH:7.5)

3.2.7. Extraction of DNA fragment from agarose gels

After separation of DNA fragments in agarose gels, the required fragments were isolated using a scalpel and the DNA was purified by applying Wizard® SV Gel and PCR Clean Up System (Promega) according to the manufacturer's protocol. The DNA content was quantified by NanoDrop 1000 Spectrophotometer.

3.2.8. Amplification of DNA fragments for cloning

PCR allows the *in vitro* amplification and addition of overlapping sequences of the insert DNA before ligation into the vector. The PCR reaction mix was prepared in 50 μ L final volume containing Herculase II Fusion polymerase, 0.5 μ M of both forward and reverse primer, 200 μ M dNTPs, 100 nM of DNA template and 8 % DMSO. The following program

was set up on the PCR machine (see Table 2). The PCR products were separated by agarose gel electrophoresis and purified (see 3.2.6., 3.2.7.)

3.2.9. Cloning of new vectors

Cloning of lentiviral sgRNA plasmids (pRSGT16-U6Tet-CMV-TetRep-2A-tagRFP-2A-Puro)

The pRSGT16-U6Tet-CMV-TetRep-2A-tagRFP-2A-Puro cloning and expression vector was obtained from Collecta. The third generation human immunodeficiency virus (HIV)-based lentiviral vector was linearized and used to generate stable sgRNA expressing cells. The vector has an inducible U6-Tet promoter responsible for the controllable expression of sgRNAs. Online tool (<http://crispor.tefor.net/>) was used to design and optimize CRISPR guides. The suggested oligos were ordered in lyophilized form and dissolved in nuclease-free dH₂O to reach the final concentration of 100 µM. In order to clone the oligos in the linearized vector, sense and antisense oligos were used in equal amounts (1 µM), diluted in 1 x TE buffer to give a final volume of 100 µL, and incubated at 100 °C for 5 min. The annealed oligos were allowed to cool down and then ligated in the pRSGT16-U6Tet-CMV-TetRep-2A-tagRFP-2A-Puro vector. For the ligation, 50 ng of the vector was mixed with 4 µL of prepared oligos, 1 µL of T4 DNA ligase (New England Biolabs) with the corresponding ligation buffer (New England Biolabs) and then incubated overnight at 4°C.

TE buffer: 10 mM Tris (pH 7.6), 1 mM EDTA (pH 8)

Sense oligo: CACCN₂₀GT

Antisense oligo: TAAAACN₂₀(C)

Cloning into 442-PL1-IRES-PURO/NEO/Blast/Venus viral expressing vector:

The third generation lentiviral vector 442-PL1-IRES-puro (a kind gift from Prof. Dr. Timm Schröder, ETH Zurich) was used to express different recombinant proteins, including GPX8 WT, GPX8-STREP(2x)/FLAG-KEDL WT, each single cysteine mutant and all cysteine mutant of GPX8, as well as GPX8 WT-YFP and GPX8 lysine mutants. First, the vector was digested with *Bst*BI and *Xho*I (see 3.2.5.) and purified by gel extraction. PCR was performed to generate different constructs (fusion, point mutation) for the insertion. The primers (see 2.8.) were designed to allow Gibson cloning, which was used to ligate the insert and

vector backbone. After virus production (see 3.3.3.), the transfected cells were selected by using corresponding antibiotics and used for further experiments or frozen for long term storage (see 3.1.3).

3.3. Methods of gene transfer

3.3.1. Transformation of chemically competent bacteria

For the transformation procedure, the *DH5 α* *E.coli* strain was used. The competent bacterial cells were taken out from -80 °C and allowed to thaw on ice for 30 min. Meanwhile, LB agar plates containing the corresponding antibiotics for selection were removed from storage (4 °C) and warmed up to room temperature. 10-50 ng of the plasmid DNA was added to the cells, which were then gently mixed by flicking. In the following step, the cells were incubated on ice for 5 min and the plasmid DNA was introduced into the bacterial cells by applying heat shock at 42°C for 30 sec. Next, the cells were placed on ice for 2 min before 500 μ L of S.O.C. medium (without antibiotics) was added to the suspension. Then, the bacterial cells were allowed to recover by incubation at 37 °C for 1 hour under constant shaking. Subsequently, 100 μ L of the cell suspension was seeded on LB agar plate, which was then incubated overnight at 37°C.

LB Agar: 20 mM MgSO₄, 10 mM KCl, 1 % (w/v) Trypton, 0.5 % (w/v) bacto yeast extract, 0.5 % (w/v) NaCl, 1.2 % bacto agar

3.3.2. Lipofection

The lipid-mediated DNA transfection procedure is a very effective method for introducing plasmid DNA into eukaryotic cells. To this end, 50,000 cells/ well were seeded into 6-well plate and incubated overnight to allow them to attach. On the following day, 200 μ L serum free standard DMEM medium or OPTIMEM (Gibco) was mixed with 2 μ g plasmid DNA and 6 μ L X-tremeGENE HP DNA (1 μ g DNA/ 3 μ L X-tremeGENE HP DNA). The transfection complex was vortexed for 30 sec and incubated for 15 min at room temperature. The medium of targeted cells was supplemented with the transfection mix and incubated for 48-72 hours, which is required to detect the expression of transgene.

3.3.3. Lentivirus-mediated transfection

This method is commonly used for efficient gene delivery in cell types, which are not susceptible to lipid-mediated transfection. HEK293T cells were employed as a packaging cell line. To this end, cells were seeded on a 10 cm cell culture dish and allowed to attach and grow overnight. The following day, HEK293T cells reached 70% confluence and the lipofection was performed (see 3.3.2) with the third generation lentiviral vectors that carried the transgene along with the third generation packaging system which consists of three plasmids the pEcoEnv-IRES-puro envelope plasmid and the two packaging plasmids, pMDLg/pRRE (encoding GAG and Pol) and pRSV-Rev (encoding Rev). The molar ratio of the vectors and insert remained constant (see Table 3.). Two days after the lipofection, the target cells were seeded into 6 well plate (50,000 cells/well) and allowed to attach overnight. The next day, the virus particles were collected from the medium of HEK293T cells by transferring the medium into a 15 mL falcon. In order to remove dead cells, the medium was centrifuged at 400 x g for 5 min and the supernatant was filtered using a 45 μ m low protein binding sterile filter (Millex). Finally, the medium was removed from the target cells and replaced with a fresh medium mixed with an infectious medium in a 1:1 ratio. The selection with the corresponding antibiotics was started 48 hours after transfection.

Name of plasmid	Molar ratio	Amount of DNA (μ g)
pEcoEnv-IRES-puro	2	0.91
pRSV-Rev	5	2.27
pMDLg/pRRE	10	4.55
Lentivirus carrying the gene of interest	5	2.27

Table 3 Virus production was performed using HEK293T cells. The table demonstrates the molar ratio and amount of applied DNA (μ g) of different plasmids.

3.4. RNA-related methods

3.4.1. RNA isolation

Due to the high activity of RNases, it is necessary to clean all equipment used for the isolation thoroughly with RNaseZAP (Sigma) to prevent possible damage of the samples during the purification procedure. Total RNA was purified from cells or tissues by applying the RNeasy Mini Kit (Qiagen) according to manufacturer's protocol. In the case of mouse tissues, according to the protocol, 10 mg of each tissue was collected. If RNA was isolated from cells, 1×10^6 cells were first plated on a 10 cm cell culture dish. On the following day, the medium was aspirated and the cells were washed 2 times with ice-cold DPBS (Gibco) and harvested by adding 350 μ L RLT Buffer. For animal tissues, 350-600 μ L RLT Buffer was applied depending on the sample size. The isolated RNA was stored at -80°C until required for further applications.

3.4.2. cDNA synthesis

The concentration and quality of purified RNA were determined by NanoDrop spectrophotometer. For cDNA synthesis, 2 μ g of RNA template was applied using the Reverse Transcription System Kit (Promga), according to manufacturer's description.

3.4.3. Microarray analysis

The isolated RNA (see 3.4.1) was diluted to a final concentration of 100 ng/ μ L in RNase free water. Agilent 2100 Bioanalyzer was used to assess RNA quality and samples with an RNA integrity number (RIN) over 7 were used for microarray analysis. Total RNA was amplified using the GeneChip® WT PLUS Reagent Kit and the synthesized cDNA was hybridized on Mouse Clariom S arrays (Affymetrix, Santa Clara, US). Staining and scanning (GeneChip Scanner 3000 7G) were performed according to the Affymetrix protocol. Expression console (v.1.4.1.46, Affymetrix) was used for quality control and to obtain annotated normalized RMA gene-level data. Statistical analyses were performed in R (Version 3.3.1.). The RNA amplification, hybridization and statistics were done by Dr. Martin Irmeler (HMGU).

3.5. Protein-related methods

3.5.1. Protein purification from cells and tissues

With this method, samples were prepared for immunoblot analysis. First, the lysis buffer was supplemented with a protease and a phosphatase inhibitor (Roche). Afterwards, cell culture dishes were placed on ice, the medium was aspirated and the cells were washed 2 times with ice-cold PBS. According to the size of cell culture dish, 100-500 μ L LCW lysis buffer was used to lyse the cells with a cell scraper. The cell suspension was transferred into a 1,5 mL microcentrifuge tube and incubated on ice for 30 min.

For organs, the freshly dissected mouse tissues were placed immediately into liquid nitrogen to snap freeze and stored at -80 °C for long term until required for further processing. For protein extraction, 300-1000 μ L of LCW lysis buffer was added to each tissue, depending on size. The tissues were homogenized with an electric homogenizer (Eurostar RW16, IKA- Labortechnik) and the suspension was incubated on ice for 30 min. After incubation, the cell or tissue suspension was centrifuged at 4 °C 18,400 x g for 30 min. The supernatant was removed, placed into a new microcentrifuge tube and stored at -20 °C until required. 25 μ L aliquots each containing 25 μ g protein were prepared for Western Blot analysis. This was performed by measuring the concentration of the protein lysate using Pierce BCA Protein Assay Kit (Thermo Scientific) as described in the manufacturer's instructions. Finally, 5 μ L of 6 x loading buffer was added and the aliquots were immediately used for Western Blot or were stored at -20 °C.

LCW lysis buffer: 0.5% Triton X-100, 0.5% SDS, 150 mM NaCl, 20 mM Tris, 10 mM EDTA, 30 mM Sodium-pyrophosphate

6x loading buffer: 375 mM Tris, 9% SDS, 9% β -mercaptoethanol, 50% glycerol, 0.03% bromophenol blue

3.5.2. Sodium dodecyl sulfate polyacrylamide gel electrophoresis (SDS-PAGE)

For SDS-PAGE, 12% or gradient (4%-16%) precast SDS Mini-PROTEAN® TGX™ Stain-Free Protein Gels (Bio-Rad) were applied. Before loading, the protein samples were incubated at 95 °C for 7 min, spinned down with a table centrifuge and directly loaded into the acrylamide gel. The western blot chamber was filled with 1 x running buffer and the protein

samples along with protein ladder (Prestained Protein Page Ruler) were allowed to migrate at 80 V for 2-3 hours depending on the size of proteins to be separated. After separation, the gel was removed from the apparatus and aligned on a polyvinylidene difluoride membrane (Trans-Blot® Turbo™ PVDF, BioRad).

Running buffer (10 x): 1% SDS, 250 mM Tris, 2.5 M glycine

3.5.3. Western blot analysis

The transfer was performed by using semi-dry Trans-Blot® Turbo™ Transfer System (Bio-Rad). To provide equable contact between the layers, blot roller was applied to remove any air bubbles from the assembled transfer pack. Either the standard program (30 min, 25 V, 1 A) or the mixed molecular weight program (7 min, 25 V, 2.5 A) was set according to the size of proteins to be detected. Subsequently, the blotting sandwich was disassembled and the membranes were placed into a 50 mL falcon and washed with TBS-T before blocking was started. Different blocking solutions were used according to the antibody requirement, and the membranes were incubated for 1 hour at room temperature under constant rolling on a rolling plate (Roller 10 D, IKA Labortechnik). Meanwhile, the antibody was diluted in blocking solution and kept on ice until the blocking was completed. Afterwards, the blocking solution was replaced with a diluted antibody and the membranes were incubated overnight at 4 °C under rolling conditions. The following day, the antibody was discarded and the membranes were washed 3 times for 5-10 min with TBS-T before the incubation with the HRP conjugated secondary antibody was started. The secondary antibody was also diluted in the blocking solution as recommended by the manufacture's protocol. After 1.5 hours incubation, the secondary antibody was removed and the blots were washed 3 times with TBS-T for 5-10 min. For signal development, the membrane was placed in a transparent plastic wrap and Clarity™ Western ECL Blotting Substrate (Bio-Rad) was added on the top of the membrane. The excess reagent was removed and the blot was placed into the ChemiDoc™ Imaging system (Bio-Rad) for visualization. If required, the membrane was reused to detect different proteins. In that case, after developing the antibody was removed by incubating the membrane with 0.5 M NaOH for 7 min. Subsequently, the blot was blocked and used for hybridization with another antibody. The protein quantification was performed with ImageLab software (Bio-Rad).

TBS (10 x): 1.5 M NaCl, 250 mM Tris, adjust pH to 7.4

TBS-T: 100 mL TBS (10 x), 900 mL dH₂O, 1 mL Tween (0.1%)

Blocking solution: 5 w/v % BSA or skim milk diluted in TBS-T

NaOH: 20 g NaOH, volume adjusted to 1000 mL (0.5 M)

3.5.4. Silver staining of SDS Gel

Silver staining is a very sensitive method for detecting proteins in acrylamide gel. This approach was performed using the Pierce[®] Silver Stain for Mass Spectrometry Kit from Thermo Scientific, according to manufacturer's instructions.

3.5.5. Tandem affinity purification

This technique was developed to study protein-protein interactions [201]. First, the protein of interest is fused to an additional tag, which allows purification. GPX8 was fused to a STREP (2x)/FLAG tag, which was placed at the C-terminal of the protein just before the KEDL ER retention signal. This helped to avoid localization changes of GPX8 in the presence of the tag. The construct was obtained from Addgene, cloned into 442-PL1-IRES-PURO (see 3.2.9.), and then virus production was performed (see 3.3.3). MEFs were transfected with the virus and subsequently selected with puromycin (2 µg/ml) for getting stable expressing clones. For co-immunoprecipitation studies, the cells were seeded into a 15 cm cell culture dish, 5x for each cell line and condition. During the beginning of the isolation, the light was turned off because of the usage of a light sensitive compound in the lysis buffer. The cells were placed on ice, then the medium was aspirated and the cells were washed 2 times with ice-cold PBS. After PBS was completely removed, 1.5 mL lysis buffer was added and the cells were collected into microcentrifuge tubes using a scarper. The suspension was incubated on ice for 15 min and centrifuged at 9,391 x g, 4 °C for 10 min. During incubation and centrifugation, the beads were prepared. 25 µL biotinylated beads were divided into 1.5 mL microcentrifuge tubes (2 tubes for each condition), after which 500 µl washing buffer was added and the beads were spun down using a table centrifuge. The supernatant was removed and the washing step was repeated one more time. Subsequently, the supernatant of the cell lysates were sterile-filtered using a 0.22 µm filter (Millex), and then transferred into microcentrifuge tubes, which contained biotinylated

beads. The beads were incubated for 2 hours at 4 °C under constant rotation (45 rpm). After incubation, the beads were spun down for 30 sec at 20 x g and then washed 3 times with washing buffer. The protein was eluted from the beads using a 250 µL elution buffer and incubated for 3 min. The beads were separated by centrifugation and the supernatant was transferred into a sterile microcentrifuge tube and stored at -20 °C for long term.

TBS: 50 mM Tris-HCl, pH 7.4, 150 mM NaCl

Lysis buffer: sterile TBS, 5 % Nonidet-P40, protease inhibitor 1 x (Roche), 20 nM N-ethylmaleimide

Washing buffer: TBS (sterile), 5% Nonidet-P40, protease inhibitor 1 x (Roche)

Desthiobiotin Elution buffer (10 x): 1 M Tris-HCl, 1.5 M NaCl, 10 nM EDTA, 25 mM Desthiobiotin, pH 8.0

Desthiobiotin Elution buffer (1 x): dilute desthiobiotin elution buffer 10 x in sterile TBS

FLAG elution buffer: 200 µg/mL FLAG peptide, sterile TBS

3.5.6. Mass spectrometry

Protein samples were purified via tandem affinity purification as described before (see 3.5.5.) and subjected for mass spectrometry analysis. For each group, 3 samples were prepared and individually measured. The samples were further processed and analyzed by the Research Unit Protein Science (PROT) – Core Facility Proteomics, Helmholtz Zentrum München (Dr. Uli Ohmayer and Dr. Stefanie Hauck).

3.6. Histology

3.6.1. Organ fixation

The aim of fixation is to maintain cellular and subcellular structures and simultaneously to immobilize antigen. The dissected tissues were transferred immediately into ice-cold 4% PFA and incubated for 24 hours at 4 °C. On the following day, the organs were placed into 70% EtOH for at least 24 hours at 4°C. Subsequently, dehydration of tissue was performed by incubation in an ascending series of ethanol (80%, 95%, 100%) for 2 hours each. In order to remove all remaining water from the tissues, the samples were placed

into Xylool for 2 hours at room temperature under constant rocking. Finally, the organs were transferred into liquid paraffin, incubated overnight at 60 °C, and after incubation, embedded in paraffin in disposable vinyl specimen molds.

3.6.2. Paraffin sections

The prepared paraffin-embedded blocks (see 3.6.1.) were stored at room temperature until subsequent cutting. The tissues were cut with rotary microtome HM355S (Thermo Fischer) into 7 µm thick sections and transferred into a water bath (37 °C) to allow the unfolding of the slices. Subsequently, the sections were placed on a slide and dried at 37 °C for 24 hours. Finally, they were stored at room temperature until utilization for immunohistochemical staining.

3.6.3. Cryosection

The dissected tissues were washed with PBS. Disposable vinyl specimen molds were half filled with Tissue Tek® medium and placed on dry ice. After the medium was hardened, the tissues were transferred into the molds where they were fully filled with Tissue Tek® medium. Subsequently, the molds were incubated on dry ice until the medium was completely frozen and the organs were cut in 14-20 µm thick section with a cryostat (Microm HM 60). The thickness of slices was dependent on the type of the organ. Finally, the slides were stored at -80 °C until they were further processed.

3.6.4. H&E staining

H&E staining is the most widely applied method on tissue sections. Haematin is the oxidized form of haematoxylin which is the active compound in the staining solution. In aqueous alkaline conditions haematin is blue and less soluble, while in acidic alcoholic conditions it becomes red and more soluble. The compound binds to lysine residues of histone proteins, therefore it visualizes cell nuclei. The paraffin was removed from the embedded tissues by washing the slides 3 times in xylool for 5 min each. Subsequently, the rehydration was done by applying a descending series of ethanol (100%, 95%, 70%) 2 times for 10 min each. When cryosections were used, these steps were not necessary. In the following steps, the sections were placed into dH₂O and washed 2 times for 5 min before they were stained with haematoxylin for 7 min. The residual staining solution was removed

by transferring the slides into dH₂O for a few seconds before they were immediately placed into tap water containing chamber. The chamber was moved under the tap and the water was allowed to run slowly into the chamber for 10 min, helping the staining to turn blue due to the increase in pH. After one more washing step in dH₂O, the tissues were placed into 0.5% eosin Y staining solution with the supplementation of 100% acetic acid (1 drop acetic acid/100 mL eosin). The sections were removed after 3 min incubation which was followed by washing in dH₂O for 2 min. Finally, the tissues were dehydrated in increasing concentrations of ethanol (70%, 80%, 95%, 100%) for 2 min each. Afterwards, they were incubated in xylol for 5 min before they were mounted with Rothi-Histo Kit. The samples were analyzed at microscope Axioplan2 Imaging (Zeiss) and the pictures were taken by using the AxioCam MRc camera and the AxioVision software (both Zeiss).

3.6.5. Immunohistochemical staining

Immunohistochemistry allows the detection of proteins in sections using specific antibodies with a fluorescent or chromogenic readout. First, the paraffin was removed from the slides as described before (see 3.6.4.), then the tissues were rinsed with dH₂O 3 times for 5 min each. Afterwards, antigen unmasking was performed by transferring the sections into a boiling citrate buffer, incubated just below boiling temperature for 10 min, and then cooled for 30 more min at room temperature. In order to inhibit the endogenous peroxidase activity, the tissues were placed into a 3% H₂O₂-MeOH solution for 10 min and washed 3 times in dH₂O for 5 min each. Subsequently, the tissues were blocked in blocking solution for 1 hour at room temperature and then they were rinsed 3 times in TBS-T for 5 min. The antibody was diluted according to the manufacturer's protocol and added onto the tissue slices for overnight incubation at 4 °C. The following day, the primary antibody was removed and the slides were washed with TBS-T and incubated with the corresponding biotinylated secondary antibody. After 30 min incubation, the ABC reagent was added onto the tissue for 30 min and then the slides were washed in TBS-T. Finally, Diaminobenzidin (DAB)-reagent was used to develop the tissue slices. The incubation time of DAB depends on the antibody and type of organ, but generally 3-5 min of incubation was performed before the sections were immersed in dH₂O. If required, the slides were counterstained with haematoxylin (see 3.6.4.), and following dehydration, the sections were mounted as described before (see 3.6.4.).

Citrate Buffer: 10 mM sodium citrate, pH 6.0

TBST Buffer: 25 mM TRIS, 125 mM NaCl, 0.1% Tween-20, pH 7.6

Blocking Solution: TBS-T, 5% goat-serum

ABC-Reagent: Vectastain ABC HRP Kit (Vector Laboratories)

DAB-Reagent: Peroxidase Substrate Kit, DAB

3.6.6. Oil Red staining

Oil Red O is a fat-soluble dye, therefore this technique is used to detect lipids and neutral triglycerides in tissue sections or in cells. Freshly dissected tissues were taken for staining. The slides were removed from -80°C and allowed to air dry for 30 min at room temperature before they were fixed in ice-cold 4% PFA. The samples were dried again for another 30 min and then rinsed immediately in dH₂O. The tissues were allowed to dry at room temperature for 15 min before absolute propylene glycol was added onto the sections. Pre-warmed Oil Red O solution was used to stain the slides for 10 min at 60 °C. Subsequently, the tissues were differentiated in 85% propylene glycol for 5 min, then rinsed in dH₂O two times. Finally, the sections were counterstained with haematoxylin as described before (see 3.6.4.) and mounted with Rothi-Histo Kit.

Oil Red O: 0.5 g Oil Red O, 100 mL propylene glycol, heated up to 95 °C and filtered through 22 µm filter

3.6.7. Transmission electron microscopy (TEM)

2.5% electron microscopy grade glutaraldehyde (Science Services) were used to fix the freshly harvested cells or dissected tissue before post-fixation was performed in 2% aqueous osmium tetroxide. Next, the samples were dehydrated in a gradual series of ethanol (30-100%) and then placed into propylene oxide and embedded in Epon (Merck) and baked for 24 hours at 60 °C. Ultrathin sections were prepared and placed onto 200 mesh copper grids and then stained with uranyl acetate and lead citrate before transmission electron microscopy analysis (Zeiss Libra 120 Plus, Carl Zeiss NTS GmbH, Oberkochen, Germany). Pictures were taken using Slow Scan CCD-camera and iTEM software (Olympus Soft Imaging Solutions, Münster, Germany)

3.7. Animal husbandry

3.7.1. Animal facilities

Mice were kept and bred in the animal facility of Helmholtz Zentrum München which provide animal housing with a controlled environment including a constant supply of food and water, standard temperature ($22 \pm 2^\circ\text{C}$), humidity ($55 \pm 5\%$), and 12 hours light/dark cycle. 2-5 animals were grouped per cage which contained nesting material, housing in case of breeding and additional supplementation in specific cases if required. The offspring were weaned from the mother between 20-25 days after birth. In order to determine the genotype of the animals, the offspring received ear punches upon separation. All experiments performed on animals were in compliance with the German Animal Welfare Law and have been approved by the institutional committee on animal experimentation and the government of Upper Bavaria.

3.7.2. Establishment of new genetically modified mouse line

Zygotes at the pronuclear stage were removed from C57BL/6N mice and directly injected with Cas9 mRNA and sgRNA targeting the critical exon (exon 2) of *Gpx8*. The efficiency of the guide was previously tested in MEFs. Thereafter, the cells were implanted into a foster mother animal and 3 weeks later the offspring were genotyped to identify the animals, which carried the mutation at the respective locus. One positive female was obtained and backcrossed with a *Gpx8*^{wt/wt} C57BL/6N male to generate heterozygous animals, which were then used for another breeding to generate *GPX8*^{-/-} mice. The mouse line was expanded and the animals were used for further experiments in order to analyze the role of GPX8 *in vivo*.

3.7.3. High Fat Diet

In order to induce ER stress in animals, the mice were kept on 45% high fat diet (Research Diets: D12451) for 22 weeks (see Table 4). The body weight and food intake of the animals were controlled every week. At the endpoint of the experiment, the mice were sacrificed for organ withdrawal, serum analysis and body composition measurement.

3.7.4. Whole body composition analysis on animals

This procedure was performed using the EchoMRI™ device, which measures whole body fat, lean mass, free water and total water content. The animals were kept on a 45 % HFD for 22 weeks as described (see 3.7.3.) before being euthanized by cervical dislocation. Right after the body weight was measured, the animals were placed immediately into the MRI machine to analyze body composition. The data were converted into an Excel file and a statistical test was performed by GraphPad Prism.

Class description	Ingredient	Grams	Grams
Protein	Casein, Lactic, 30 Mesh		200.00 g
Protein	Cystine, L		3.00 g
Carbohydrate	Sucrose, Fine Granulated		176.80 g
Carbohydrate	Lodex 10		100.00 g
Carbohydrate	Starch, Corn		72.80 g
Fiber	Solka Floc, FCC200		50.00 g
Fat	Lard		177.50 g
Fat	Soybean Oil, USP		25.00 g
Mineral			50.00 g
	<i>Sucrose, Fine Granulated</i>	8.991 g	
	<i>Potassium Citrate, Monohydrate</i>	16.5 g	
	<i>Calcium Phosphate, Dibasic</i>	13 g	
	<i>Calcium Carbonate, Light, USP</i>	5.5 g	
	<i>Sodium Chloride</i>	2.59 g	
	<i>Magnesium Sulfate, Heptahydrate</i>	2.576 g	
	<i>Magnesium Oxide, Heavy, DC USP</i>	419 mg	
	<i>Ferric Citrate</i>	210 mg	
	<i>Manganese Carbonate Hydrate</i>	122.5 mg	
	<i>Zinc Carbonate</i>	56 mg	
	<i>Chromium Potassium Sulfate</i>	19.5 mg	
	<i>Copper Carbonate</i>	10.5 mg	
	<i>Ammonium Molybdate Tetrahydrate</i>	3 mg	
	<i>Sodium Fluoride</i>	2 mg	
	<i>Sodium Selenite</i>	0.5 mg	
	<i>Potassium Iodate</i>	0.5 mg	
	<i>Total Mineral:</i>	50 g	
Vitamin	Choline Bitartrate		2.00 g
Vitamin			1.00 g
	<i>Sucrose, Fine Granulated</i>	784.2 mg	
	<i>Vitamin E Acetate, 50%</i>	100 mg	
	<i>Niacin (a.k.a. B3)</i>	30 mg	
	<i>Biotin, 1%</i>	20 mg	
	<i>Pantothenic Acid, d, Calcium (a.k.a. B5)</i>	16 mg	
	<i>Vitamin D3, 100,000 IU/gm</i>	10 mg	
	<i>Vitamin B12, 0.1% Mannitol</i>	10 mg	
	<i>Vitamin A Acetate, 500,000 IU/gm</i>	8 mg	
	<i>Pyridoxine HCl (a.k.a. B6)</i>	7 mg	
	<i>Riboflavin (a.k.a. B2)</i>	6 mg	
	<i>Thiamine HCl (a.k.a. B1)</i>	6 mg	
	<i>Folic Acid</i>	2 mg	
	<i>Menadione Sodium Bisulfite</i>	0.8 mg	
	<i>Total Vitamine:</i>	1.00 g	
Dye	Dye, Red FD&C #40, Alum. Lake 35-42%		0.05 g
Total:			858.15 g

Table 4 Food composition of 45 % High fat diet

The table demonstrate the composition of high fat diet, which was applied to investigate diet-induced obesity in mice.

4. RESULTS

4.1. Generation of monoclonal antibodies against GPX8

Since at the beginning of the thesis there was no commercial monoclonal antibody (mAb) for mouse GPX8 (mGPX8) and human GPX8 (hGPX8) available, it was essential to produce these antibodies to allow the *in vitro* and *in vivo* analysis of the protein. Monoclonal mouse and human GPX8 antibodies were generated in collaboration with the antibody facility of Helmholtz Zentrum München (Elisabeth Kremmer and Andrew Flatley) using hybridoma technology. This method allows the production of rapidly expanding and high quality mAbs which can be used for several tools in molecular biology and even for therapeutics [202].

The first step of mAb generation is the selection of the peptide which can be used for the immunization of the targeted animal (Fig. 8A). In the case of mGPX8 mAb production, the rats were immunized with two distinct peptides (RFTDKSYQTLRELHKE and VDSSKKEPRWNFWK) separately, with both peptides being specific for certain regions of mGPX8. To produce hGPX8 mAb for the immunization step, the neighboring sequences of active cysteine of GPX8 (Cys79) were used (CNQFGESEPRPSKEV and CQLTDRNYLG), although it was calculated that these peptides have a low antigenicity index. Subsequently, the plasma cells from immunized rats were fused with immortal myeloma cells to generate cells possessing both parental properties, the antibody production and immortality. The fused cells were diluted in order to allow the formation of single clones and the secreted antibodies were collected with the supernatants. Finally, the antibodies were validated for antigen specificity in our laboratory by immunoblot blot analysis using protein lysate from MEFs with or without viral overexpression (o.e.) of either mGPX8 or hGPX8.

Interestingly, mGPX8 was not only detectable in MEFs with exogenous expression of the protein but also in wild type (parental) cells (Fig. 8B). Three appropriate clones which were selected and expanded from screening (10F10, 2F4, 24F3) were obviously the most efficient ones, therefore they were used for subsequent experiments. In addition, despite the previous prediction of low antigenicity index for the peptides used for hGPX8 mAb production, several very good quality hGPX8 mAbs were identified while testing the

supernatant of hybridoma cell clones (Fig. 8B). In total, 47 mouse and 37 human clones were tested and three clones of each mAb were expanded (Fig. 8C).

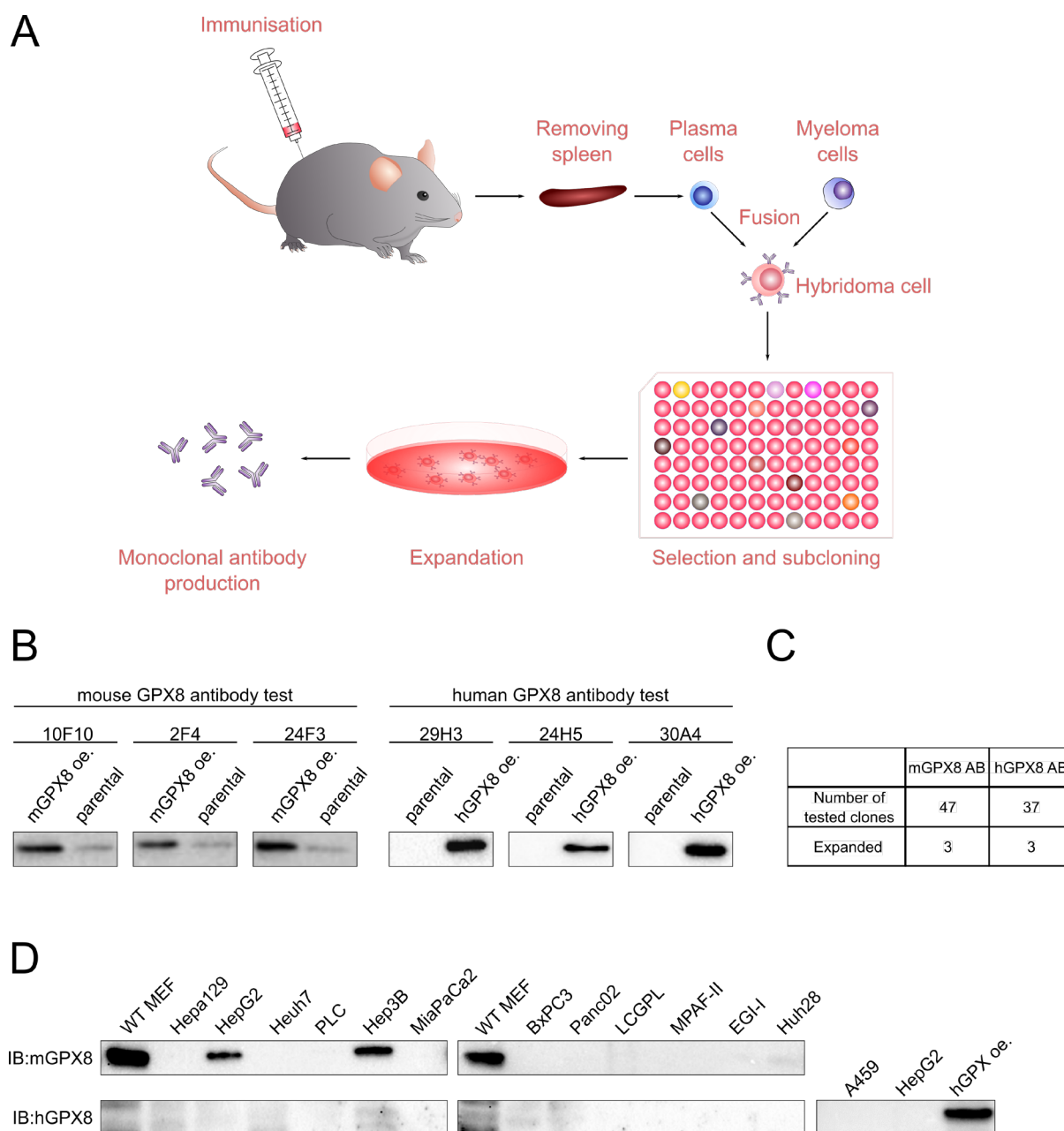


Figure 8 Generation of mouse and human GPX8 monoclonal antibodies

(A) Workflow showing the generation of monoclonal antibody by hybridoma technology. First, the immunization takes place of the animals by different peptides. Subsequently, the spleen is removed and immune cells are isolated from the organ. The isolated plasma cells are then fused to myeloma cells to generate hybridoma cells, which share both parental features, the antibody production and immortality. Next, subcloning and selection take place which allow the expansion of single clones, with identical genetic background. Each clone produces a different antibody with distinct specificity for the antigen. **(B)** Immunoblot analysis of mouse and human GPX8 antibody screening using

antibodies from different hybridoma subclones. For the mouse GPX8 antibody screening, mouse GPX8 overexpressing MEFs served as positive control, while for human antibody screening the same parental cell line was used with the viral expression of human GPX8. **(C)** The table shows the number of tested clones of which 3 mouse and 3 human clones were selected for further expansion and application. **(D)** Immunoblot analysis of different cancer cell lines using the newly established antibodies (10F10 for mouse and 29F3 for human GPX8).

The expanded antibodies were tested on various cancer cell lines by immunoblot analysis, but only the mGPX8 antibody detected the protein in two human cancer cell lines (HepG2 and Hep3B) (Fig. 8D). Additionally, the mGPX8 mAbs were tested for further applications including immunohistochemical (IHC) staining on paraffin and cyro-section of mouse tissues, or co-immunoprecipitation. Nevertheless, none of the three clones was suitable for these purposes, unfortunately (data not shown).

4.2. GPX8 degrades upon ER stress induced by SERCA inhibitor

To investigate whether GPX8 is involved in oxidative protein folding, drug induced ER-stress was studied in MEFs using different ER-stress inducing agents: (I) thapsigargin (TG), a well-known SERCA inhibitor, blocks the Ca^{2+} uptake of the ER and leads to the accumulation of unfolded proteins due to the perturbation of chaperon function [203, 204]; (II) tunicamycin, an inhibitor of the biosynthesis of glycoproteins [205, 206]; and dithiothreitol (DTT), a strong reducing agent [207].

For this purpose, MEFs with overexpression of mouse GPX8 (GPX8 oe.) and wild type (WT) MEFs were treated with the compounds in a concentration-dependent manner, and cell viability assays were conducted. Since previous findings indicated that GPX8 might promote oxidative protein folding, a protective effect of GPX8 was expected in GPX8 oe. MEFs. However, the results did not show any impact of GPX8 on cell death induced by ER stress triggering stimuli (Fig. 9A). Moreover, the cells were treated with the compounds in a time-dependent manner up to 12 hours and GPX8 levels were monitored every 3 hours by immunoblot analysis. While tunicamycin and dithiothreitol showed no effect on GPX8 protein level, initial results indicated that TG resulted in rapid GPX8 degradation within the first 3 hours (data not shown). Therefore, to investigate this phenomenon in more detail, the experiment was repeated and GPX8 levels were analysed every 2 hours (Fig. 9B). As it

has been previously discussed, ER stress activates UPR and induces expression of genes that increase folding capacity (1.1.2.).

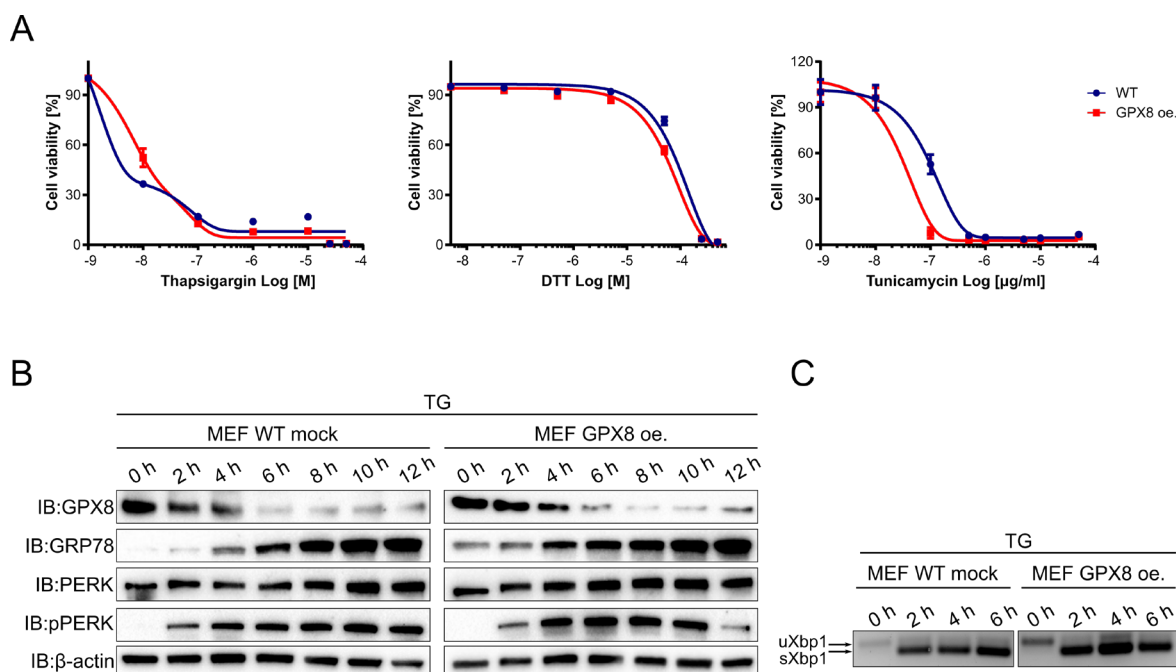


Figure 9 Thapsigargin induces GPX8 degradation

(A) Dose-dependent toxicity of various ER stress inducing agents. Cell viability was assessed 24 hours after the treatment using AquaBluer method. Data represents the mean \pm s.d. $n=3$ from a representative experiment. **(B)** Immunoblot analysis of mouse GPX8 and mock transfected MEFs which were treated with 20 nM thapsigargin (TG) in a time-dependent manner. The data indicates rapid degradation of GPX8 in the presence of SERCA inhibitor. In parallel, ER stress was induced, shown by enhanced GRP78 expression and PERK phosphorylation. **(C)** XBP1 splicing was determined upon thapsigargin treatment by PCR using primers that bind in a close proximity of IRE1 targeted region of Xbp1 mRNA. Splicing of Xbp1 mRNA resulting in a smaller PCR product in that the deletion of 26 nucleotide can be distinguished from the unspliced variant (Abbreviations: s.d.: standard deviation, n : sample size).

Accordingly, increased GPX8 protein level was expected in response to thapsigargin, although an unforeseen decrease was observed. Western blot analysis indicated remarkable and rapid degradation of GPX8 in the control cells (WT mock) as well as in the GPX8 oe. cells in response to thapsigargin treatment. In order to confirm the presence of ER stress and the activation of UPR following SERCA inhibition, the expression level of GRP78 and phosphorylation of PERK were analyzed by Western blot. Both stress markers exhibited increased levels, confirming the activation of the UPR signaling pathway. Since it

is well-known that UPR consists of three parallel pathways, *Xbp1* splicing was also investigated as a marker for IRE1 activation. To address this, mRNA was isolated from cells following the treatment with the aforementioned compound and PCR was performed using primers, which were designed in a close proximity upstream and downstream of the IRE1 targeted region in *Xbp1*. As illustrated in Fig. 9C, *Xbp1* splicing occurred within the first two hours after adding the inhibitor to the cells, similar to PERK phosphorylation. In conclusion, the data indicates that both UPR pathways were activated simultaneously.

4.3. Investigation of the degradation process of GPX8

4.3.1. GPX8 has a dynamic turnover and the cytosolic lysine is crucial for the stability of the protein upon ER stress

Based on the knowledge gathered from preliminary work, the next goal was to investigate the stability and half-life of GPX8. To address this, emetine dihydrochloro hydrate (later on emetine), which is a well-known inhibitor of protein synthesis in eukaryotes, was applied. Emetine binds to the 40S subunit of the ribosome [208], allowing it to be used for the investigation of the half-life of a protein of interest. GPX8 WT MEFs were treated with emetine simultaneously with thapsigargin in the presence or absence of the well-known proteasome inhibitor MG132 [209] in a time dependent manner. To monitor changes in the protein level of GPX8, immunoblot analysis was performed (Fig. 10A).

Thapsigargin led to GPX8 degradation as it was demonstrated before (see 4.2); however, emetine additionally enhanced the degradation of the protein. When comparing samples treated only with emetine, GPX8 level strongly decreased within the first 90 min, indicating a dynamic turnover (Fig. 10A). Moreover, Fig. 10A demonstrates that MG132 stabilized GPX8 level, however emetine supplementation attenuated this effect.

Since protein quality control consists of several complexes which contribute to the selection and transport of proteins that are targeted for subsequent degradation, siRNA silencing was performed. Individual subunits of different E3-ubiquitin ligase transmembrane complexes were targeted by siRNAs (two distinct siRNAs for each subunit) in order to identify which complex or complexes of the quality control machinery are required for the degradation of GPX8.

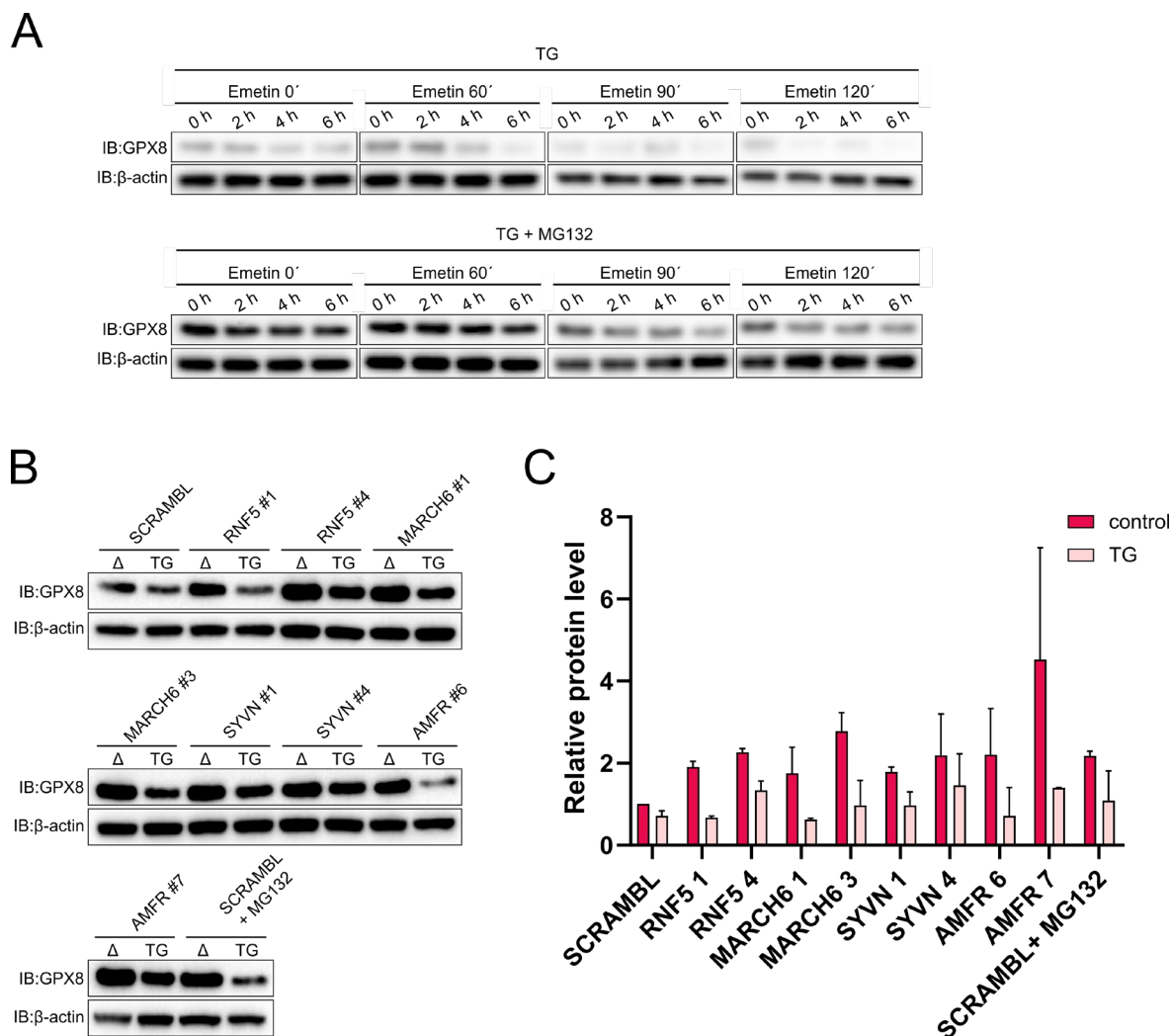


Figure 10 Silencing of E3 ubiquitin ligases stabilizes GPX8 under non-stressed conditions

(A) Immunoblot analysis of WT MEF treated with TG (20 nM) with or without MG132 (500 nM) and emetine (100 µg/ml) simultaneously in a time-dependent manner. The blot represents the stability of GPX8 upon translational inhibition in the presence or absence of SERCA inhibitor and proteasome inhibitor. MG132 increased the stability of GPX8, demonstrating the involvement of proteasome in the degradation process of GPX8 upon thapsigargin treatment. **(B)** Immunoblot analysis shows the stability of GPX8 using different siRNA for specific subunits of different ERAD quality control complexes. WT MEFs were incubated with siRNA for 48 hours and subsequently treated with thapsigargin (20 nM) for 6 hours to induce the degradation of GPX8. To inhibit proteasomal degradation, MG132 (500 nM) was used as positive control simultaneously with thapsigargin. **(C)** Quantitative densitometry analysis demonstrates the level of GPX8 under inhibition of different ERAD complexes.

WT MEFs were preincubated with different siRNAs for 48 hours and subsequently treated with thapsigargin. Control RNA (scramble) was used either with or without MG132. Indeed, all of the applied siRNAs for distinct complexes increased the basal level of GPX8, similar to MG132, just as seen in Fig. 10B. However, 6 hours of thapsigargin treatment resulted in

partial GPX8 degradation even in the presence of siRNAs. The strongest inhibitory effect under normal conditions was observed when siRNA was applied against AMFR, while when cells were treated with thapsigargin, RNF5 and SYVN siRNA exhibited the most robust effects on GPX8 stability.

The results of the siRNA experiment and the fact that MG132 could not completely block thapsigargin-induced GPX8 breakdown indicate the involvement of other protein degradation processes such as autophagy. This possibility was tested by treating cells with thapsigargin in the presence or absence of either MG132 or chloroquine, the latter a known autophagy inhibitor [210]. Interestingly, as Fig. 11A indicates, thapsigargin-induced GPX8 degradation was inhibited by using either aforementioned inhibitors. Nevertheless, it has been indicated that chloroquine displays other side effects besides inhibiting lysosomal degradation, including increasing pH of the lysosome and blocking enzymes responsible for hydrolysis [211, 212].

In order to gain deeper insight into the breakdown mechanism of GPX8, online prediction was performed in order to identify possible ubiquitination sites, which could be targeted by E3-ubiquitin ligases to facilitate the clearance of the protein. According to the tool, lysine (K) in position 10 (K10), 38 (K38) and 141 (K141) have been found to be most likely involved in this process (Fig. 11C). To address this probability, the predicted lysine were individually mutated using overlap PCR, cloned into lentiviral vector (442-PL1-Neo) and, following virus production, GPX8 knockout (GPX8 KO) MEFs were infected with the distinct viruses (production of GPX8 KO MEFs see 4.4.1.). Neomycin was used to select transfected cells, and finally protein stability was investigated by immunoblot blot after thapsigargin treatment. As expected, in the WT cells a strong decrease was observed in GPX8 level when SECRA was inhibited by the compound, while substitution of K10 to arginine (R) enhanced GPX8 stability (Fig. 11C).

Since ubiquitination machinery has been described as being present in the cytosol and the mutation of one of the cytosolic lysine increased stability of the protein, this cytosolic domain was further investigated. Since two additional lysine (K15 and 17) are located in the cytosolic loop of GPX8, the coding region of these amino acids were mutated simultaneously with K10. As described before, immunoblot analysis was performed after

thapsigargin treatment in order to investigate whether any of these additional mutations increase the effect of K10R on GPX8 stability. Interestingly, there was no further significant improvement in stabilization of GPX8 upon the additional mutations. Consequently, K10 seems to be the most important lysine of GPX8, which is possibly targeted by ubiquitination and proteasomal degradation upon thapsigargin treatment.

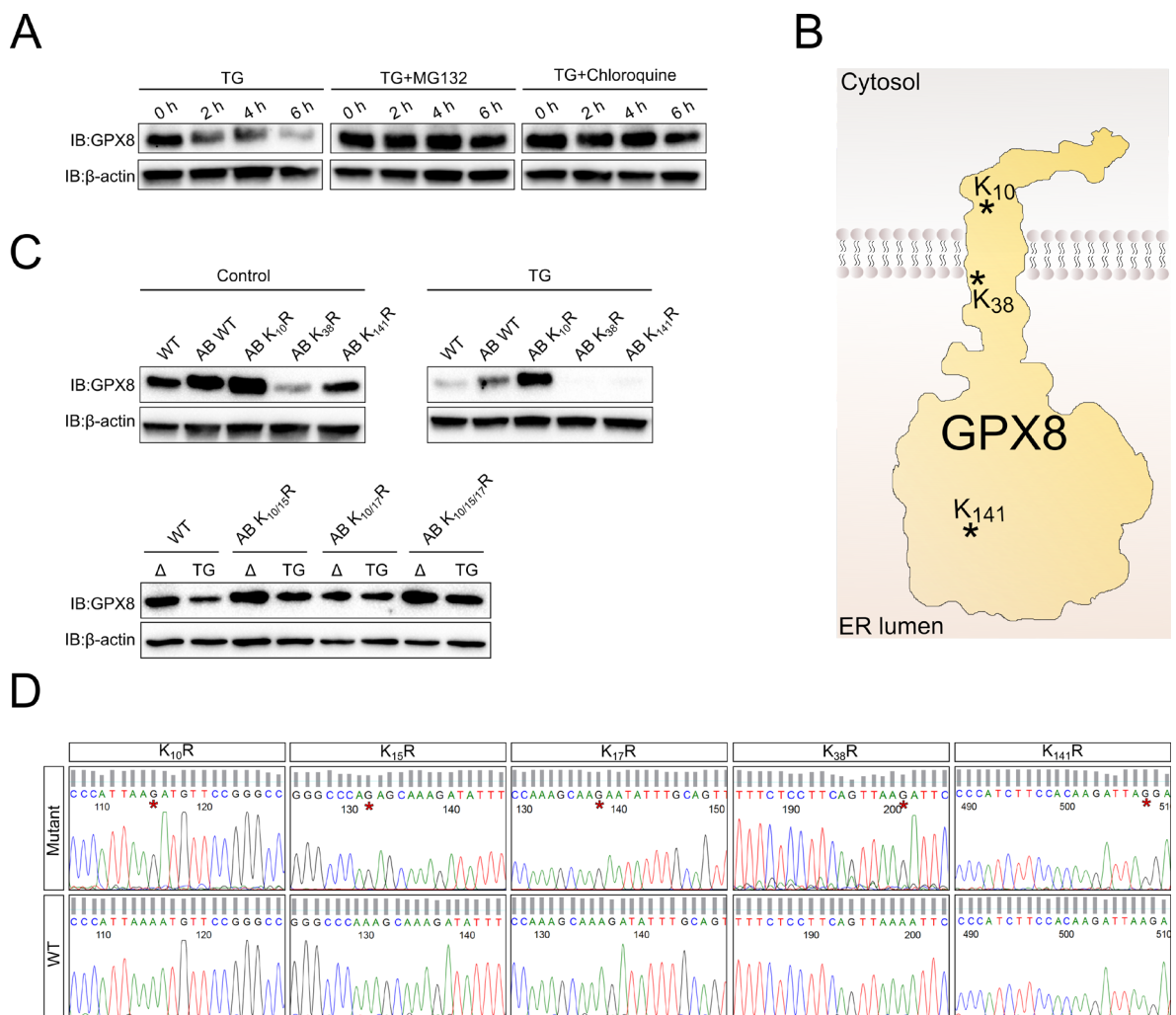


Figure 11 K10 is crucial in the regulation of the stability of GPX8 under TG induced ER-stress

(A) Immunoblot analysis of WT MEFs treated with TG in the presence or absence of either proteasome (MG132 500 nM) or autophagy (chloroquine 10 μM) inhibitor. (B) Scheme of localization of lysine in GPX8 which were predicted to be targeted by ubiquitination. (C) Immunoblot analysis of WT MEFs and GPX8 KO MEFs transfected with distinct lysine mutant of GPX8 (AB). All cell lines were challenged with 20 nM TG for 6 hours and analyzed by Western blot. The data demonstrates a decrease in GPX8 degradation upon TG treatment in the present of cytosolic lysine mutations. (D) Sequence analysis shows the individual mutations in the coding sequence of Gpx8. The modified nucleotides are marked with asterisks.

4.4. Generation and characterisation GPX8 KO in MEFs

4.4.1. Generation of GPX8 KO in MEFs based on CRISPR/Cas9 technology

In order to analyze the role of GPX8 *in vitro*, knockout cells were generated by CRISPR/Cas9 based technology. Initially, an online tool (<http://www.crisprscan.org/>) was used to design guides for the targeted region of GPX8 (Fig. 12A). Two guides were selected as they were considered to be the most effective ones and to have the least potential off target effects according to the tool. The selected guides were individually cloned into the pRSGT16-U6Tet-CMV-TetRep-2A-tagRFP-2A-Puro expression vector and, after virus production (3.3.3), Cas9 expressing MEFs were infected with the viruses (expressing either guide 1 or guide 2). The transfected cells were selected with puromycin (2 µg/ml) and the expression of sgRNA was induced by doxycycline (50 µg/ml). Single cell cloning was performed and the efficiency of the CRISPR/Cas9 based knockout was analyzed by Western blot. Unfortunately, using single guides only one clone was confirmed to be knockout for GPX8 (Cl2) (Fig. 12B). Sequence analysis confirmed the deletion in the second exon of *Gpx8*, but only one allele contained an “out frame deletion” of 10 bp while on the other allele an in-frame deletion of 6 bp was observed (Fig. 12C,D).

Thus, to improve the efficiency of this technology, the two guides were used simultaneously as described before. MEFs were transfected with the viruses, selected with puromycin (2 µg/ml) prior to doxycyclin (50 µg/ml) supplementation to induce the expression of sgRNAs. The cells were diluted to allow for single cell formation. DNA of single cell clones were isolated and used for validation of the knockout by genotyping PCR. The data demonstrates that several clones were modified by CRISPR/Cas9 (Cl1, Cl10, Cl15, Cl17, Cl28) (Fig. 12E), however, sequence analysis was only adequate for Cl28 (Fig. 12G) in which a 191 bp deletion on both allele was confirmed. Moreover, protein was isolated from the clones to perform immunoblot analysis to confirm the absence or presence of GPX8. Fig. 12F indicates that GPX8 was successfully deleted in clones Cl1, Cl10, Cl17 and Cl28.

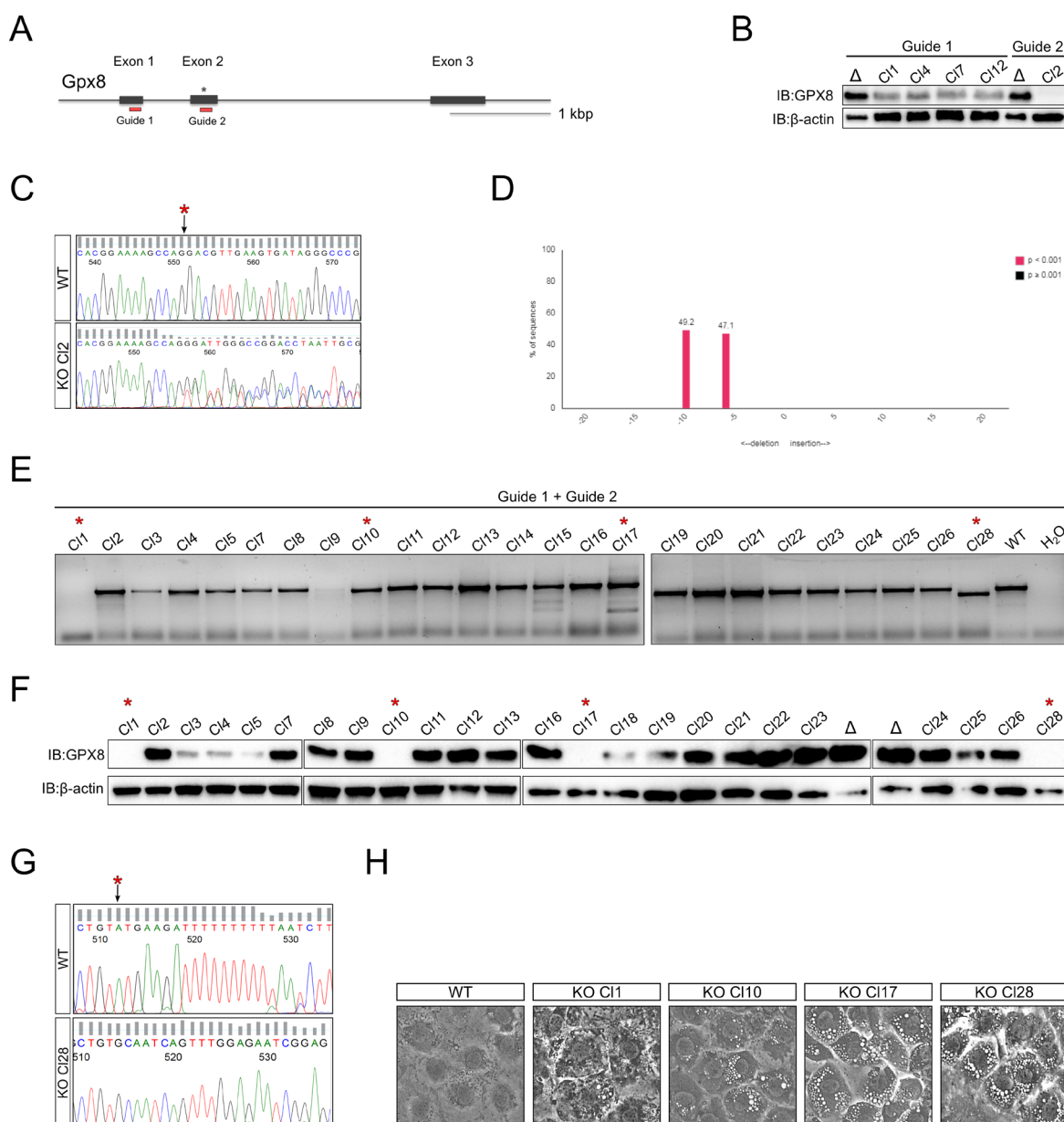


Figure 12 Generation of CRISPR/Cas9-mediated knockout of GPX8 in MEFs

(A) Shown is the wild type allele of mouse *Gpx8* consisting of 3 exons, located on chromosome 13. The second exon encodes the catalytically active cysteine which is marked with an asterisks. Using an online tool (<http://www.crisprscan.org/>), two guides were selected to introduce genetic alterations in the coding region of *Gpx8*. The binding sites of the guides are highlighted with red. (B) Immunoblot analysis of single cell clones targeted either with “Guide 1” or “Guide 2”. The data indicates the knockdown of GPX8 when “Guide 1” was used, while when “Guide 2” was applied, one clone (C12) was found to be knockout (KO). (C) Sequence analysis of the CRISPR/Cas9 targeted region of *Gpx8* using “Guide 2”. The sequence of WT and KO “C12” DNA was compared. The data shows the genetic alteration in the KO sequence, the cleavage site is marked with an asterisks. (D) An online tool (<https://tide.nki.nl/>) was used to distinguish the two different alleles and identify the length of each deletions. The tool identified a 10 bp deletion on one allele and a 6 bp deletion on the other allele in KO clone C12. (E) PCR analysis of several MEF clones targeted with “Guide 1” and “Guide 2” simultaneously. (F) Immunoblot analysis demonstrates the absence of GPX8 in numerous clones (C1, C10, C17, C28) when the two guides were used simultaneously. (G) Sequence analysis of KO C128 shows a 191 bp deletion on both alleles. The cleavage site is marked with an asterisks. (H)

Similar morphologic changes were observed in almost all GPX8 KO clones (Cl10, Cl17, Cl28) which was detected by bright-field microscopy. Upon high confluency, vesicles accumulated in the KO clones, which was not observed in the WT cells.

Interestingly, while keeping GPX8 KO MEF clones in culture, vesicle formation was detected when cultured at high cell confluency. To investigate these vesicles, different methods were applied. First, lipid droplet (LD) staining was performed using BODIPY 493/503 to analyze whether these structures are LD, although the staining was negative (Supplementary Fig. 1).

These vesicles exhibited a similar appearance like autophagosomes which were previously observed upon chloroquine treatment. Chloroquine is known to cause the accumulation of autophagosomes within the cells due to the aberrant lysosomal degradation.

To investigate whether GPX8 KO leads to arrested autophagic flux, immunoblot analysis was conducted using LC3 antibody, a well-known marker for autophagy. Under specific conditions, if autophagy is activated, LC3-I and subsequently LC3-II are generated, which is either converted back to LC3-I or digested within the lysosome. Therefore, the ratio between LC3-I and LC3-II level is balanced under proper conditions. Yet, in Gpx8 KO MEFs (Cl17, Cl28, Cl1, Cl10) under normal cell culture conditions, LC3-II was found to be remarkably accumulated compared to the level of control cells (Fig. 13A.). This indicates an activation of autophagy along with a possible impaired turnover by the lysosome.

Unlike GPX4, which is one of the closest homologues of GPX8, knockout of GPX8 was not lethal in MEFs. Therefore, the expression level of GPX4 and GPX7 were examined by Western blot analysis to address potential compensation by these proteins, which might promote cell survival. Indeed, neither GPX4 nor GPX7 exhibited altered expression levels in response to various GPX8 level, thus a compensatory mechanism of these proteins can be ruled out (Fig. 13B).

Moreover, as GPX4 is known to be the key enzyme in the detoxification of lipid peroxides, lipid peroxidation was determined in GPX8 KO MEFs using BODIPY 581/591. For this purpose, the cells were treated with RSL3 with or without liproxtatin-1. RSL3 served as a positive control since it is a well-known GPX4 inhibitor which accordingly induces the

accumulation of lipid peroxides [213], and liproxtatin-1, a drug that reduces oxidized lipids, as negative a control [214]. Nonetheless, knockout of GPX8 (CI28) did not result in increased lipid peroxidation compared to GPX8 WT MEFs, whether under non-stressed conditions or under RSL3 treatment.

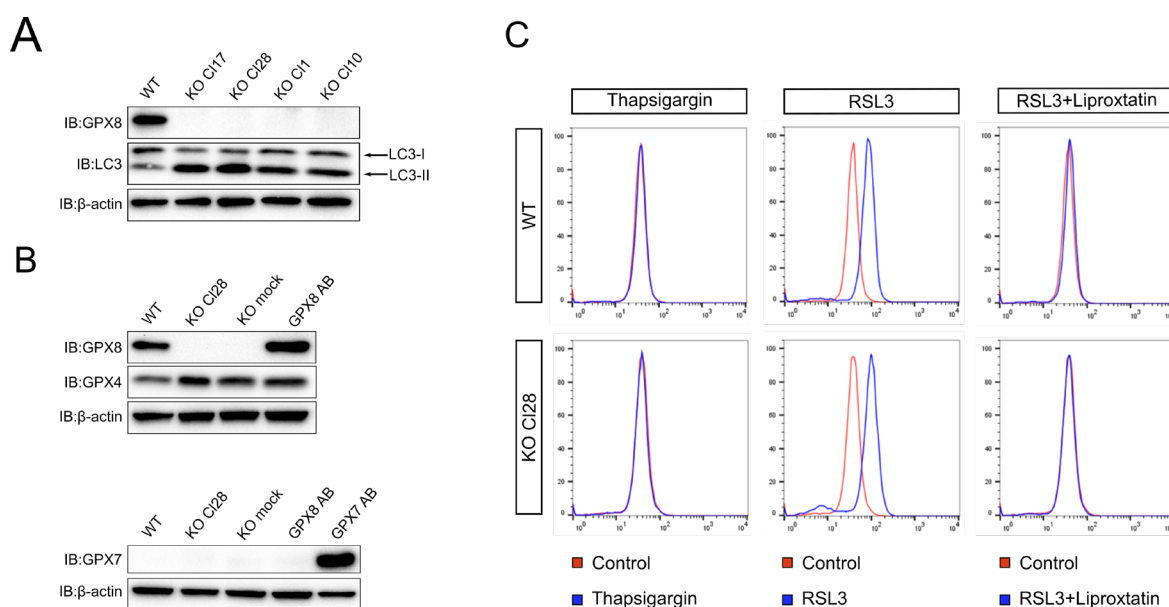


Figure 13 GPX8 KO MEFs exhibit accumulation of LC3-II

(A) Immunoblot analysis of GPX8 WT and GPX8 KO clones (KO CI17, KO CI28, KO CI1, KO CI10). The results indicate higher steady state level of LC3-II in GPX8 KO MEFs compared to control cells (WT). **(B)** Immunoblot analysis revealed no compensation of any of GPX8 homologue proteins in GPX8 KO MEFs. **(C)** Lipid peroxidation was determined using BODIPY 581/591 C11. Under control cell culture conditions or under treatment with either thapsigargin or RSL3, GPX8 KO MEFs did not exhibit higher levels of lipid hydroperoxides compared to GPX8 WT MEFs.

4.4.2. Transmission electron microscopy analysis of CRISPR targeted *GPX8* knockout MEFs

For a better understanding of the phenotypes that were observed in the GPX8 KO MEFs, ultrastructural analysis was performed using transmission electron microscopy (TEM). To investigate the aforementioned alteration in subcellular morphology upon high cell confluence, GPX8 WT and KO MEFs were examined under basal conditions as well as under glucose starvation.

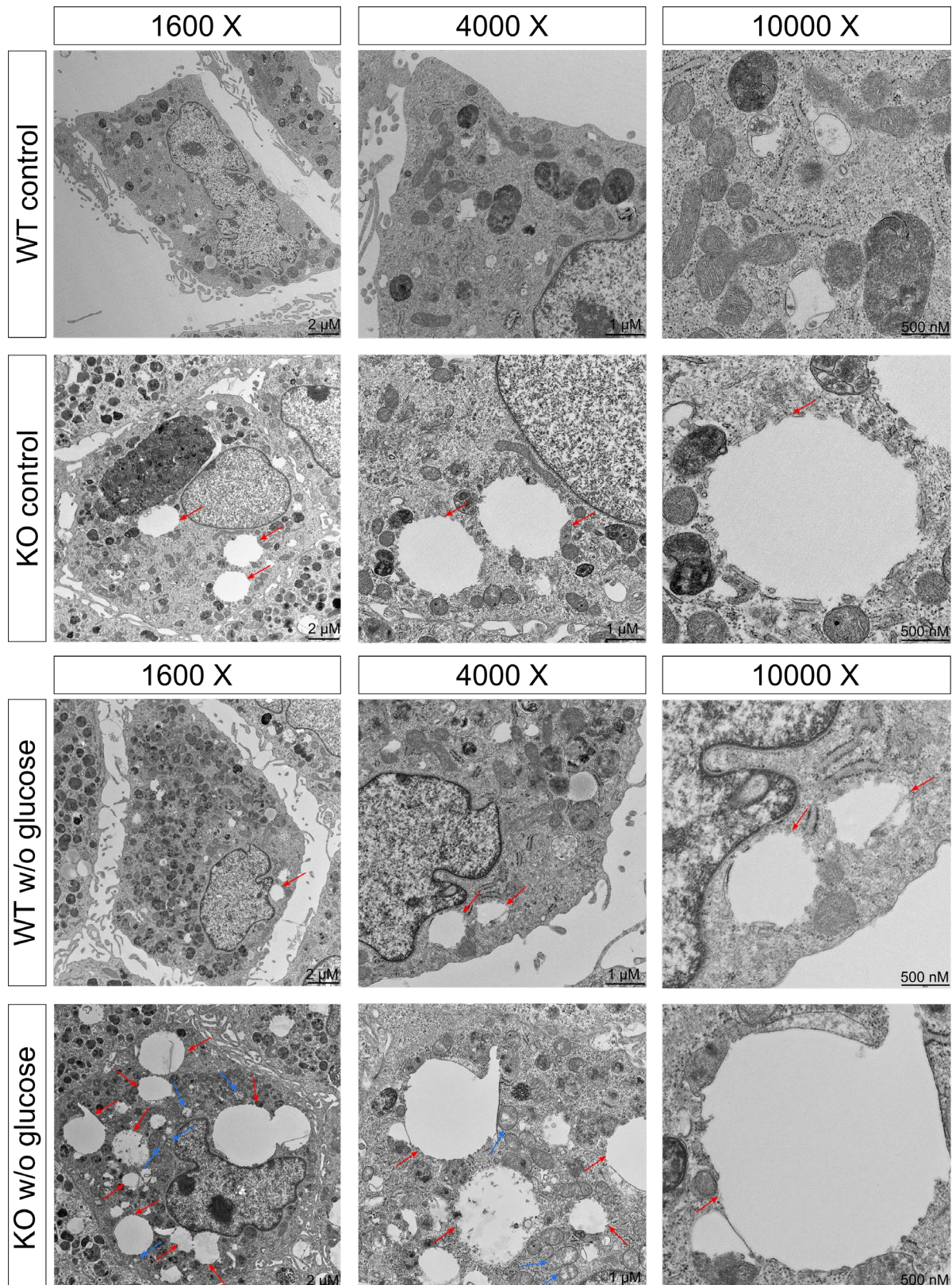


Figure 14 Transmission electron microscopy (TEM) pictures from GPX8 WT and KO MEFs

The upper panel ("control") shows the ultrastructure under normal cell culture conditions, while the pictures in the lower panels are of cells that were challenged with glucose starvation. The red arrows point to vesicles that were observed previously by bright-field microscopy. TEM pictures demonstrate remarkably large and partially double membrane surrounded "empty" structures in GPX8 KO MEFs

which accumulated under glucose starvation. Blue arrows display abnormal mitochondria that were present in GPX8 KO MEFs under glucose starvation. Electron microscopy micrographs were kindly provided by Dr. Michaela Aichler (Helmholtz Zentrum München).

Glucose starvation activates autophagy [215, 216], and preliminary data already demonstrated (Fig. 13A) that GPX8 KO clones exhibited a higher level of LC3-II, thus indicating a potential aberrant autophagic flux.

Thus, the aim of this experiment was to investigate whether the vesicles that were found upon high confluency are related to autophagic flux. The results indicated that under normal circumstances, MEFs lacking GPX8 exhibited a significantly higher amount and increased size of “premature autophagy-like” vesicles (Fig. 14, red arrows), which were partially surrounded by double membranes. In addition, the number of these yet unidentified structures increased upon glucose starvation, which suggests the association of these vesicles to autophagic flux. More importantly, glucose starvation also led to morphological changes of mitochondria in GPX8 KO MEFs (Fig. 14 blue).

Taken together, this evidence puts forward the idea of an inadequate- or early stage-arrested autophagic flux. In addition, the results point out that under glucose starvation the mitochondria will likely be affected by the genetic interruption of *Gpx8 in vitro*.

4.4.3. Absence of GPX8 sensitizes MEFs against saturated fatty acid-induced cell death

Since knockout of GPX8 in MEFs was viable *in vitro* and no difference was evident under basal circumstances compared to WT cells, two KO clones (Cl17, Cl28) were compared to WT MEFs using different compounds known to cause different cell death modalities.

For this purpose, cells were plated into a 96/well plate and the following day the drug treatment was performed. All drugs were incubated for 24 hours and AquaBluer was used to determine cell viability. Cell death was induced by triggering ferroptosis (RSL3, and erastin), and apoptosis (auranofin), as well as by blocking autophagy (chloroquine, AGK2). Rapamycin, a drug which is used to activate autophagy, had no effect on cell viability in the concentration range of 0-100 μ M. In addition, dynamin (endocytosis) inhibitors were

tested to determine whether there is a difference in cell viability between KO and WT cells in response to any of these stimuli. Indeed, using any of aforementioned drugs, no significant difference was observed in cell viability between the two genotypes (Fig. 15).

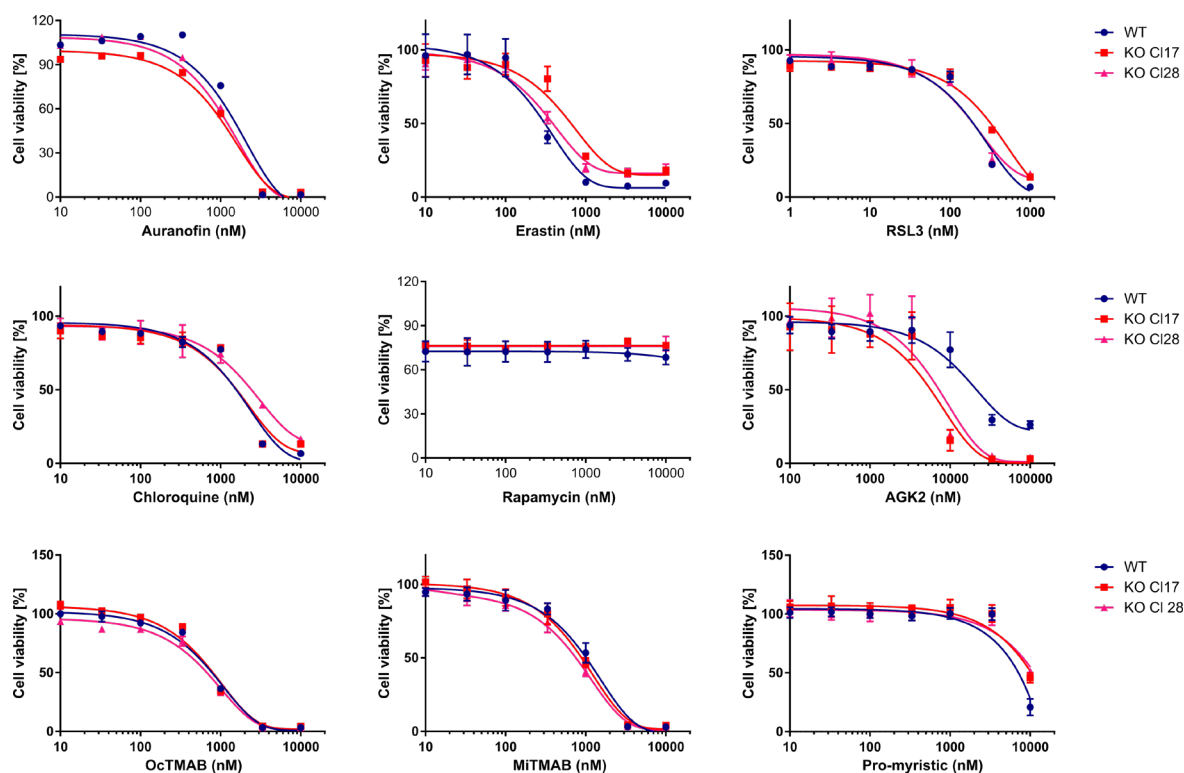


Figure 15 Cytotoxicity assay in response to various cell death inducing stimuli shows no difference between GPX8 WT and KO MEFs

Cell viability assays were performed using GPX8 WT cells and two KO clones (C117, C128). The cells were treated with several cell death inducing agent in a concentration-dependent manner for 24 hours and cell viability was assessed with AquaBluer method. Data represents the mean \pm s.d. $n=3$ from a representative experiment. GPX8 KO cells did not exhibit drug resistant or sensitive properties to any of these drugs. Data represents the mean \pm s.d. $n=3$ from a representative experiment. (Abbreviations: s.d.: standard deviation, n : sample size).

Despite these negative results, GPX8 KO MEFs exhibited an unforeseen sensitivity to palmitic acid (PA)-induced cell death, especially if $\Delta 9$ -desaturase (SCD1) was simultaneously inhibited. PA is one of the most abundant saturated fatty acids within the cells, and SCD1 is the key enzyme that catalyzes the desaturation of PA and stearic acid to monounsaturated fatty acids (MUFA). Low concentration of PA (25-50 μ M) already decreased cell viability in the two GPX8 KO clones, while WT MEFs were fully viable at the

same concentration of the drug. Even lower concentration of PA efficiently killed GPX8 KO MEF in the presence of the SCD1 inhibitor. In contrast, WT cells demonstrated reduced sensitivity to this cell death stimuli, and only the highest concentration of PA in combination with 10 μ M SCD1 inhibitor decreased the cell viability to \sim 50% (Fig. 16). Thus, either the accumulation of saturated long chain fatty acids, such as PA and stearic acid, or the absence of the final product of SCD1, namely palmitoleic acid and oleic acid, lead to cell death in GPX8 KO cells. These findings were confirmed using other GPX8 KO cell lines isolated from CRISPR targeted mice. The mechanism of PA and SCD1 inhibitor induced cell death was further investigated using these MEFs (4.8.3).

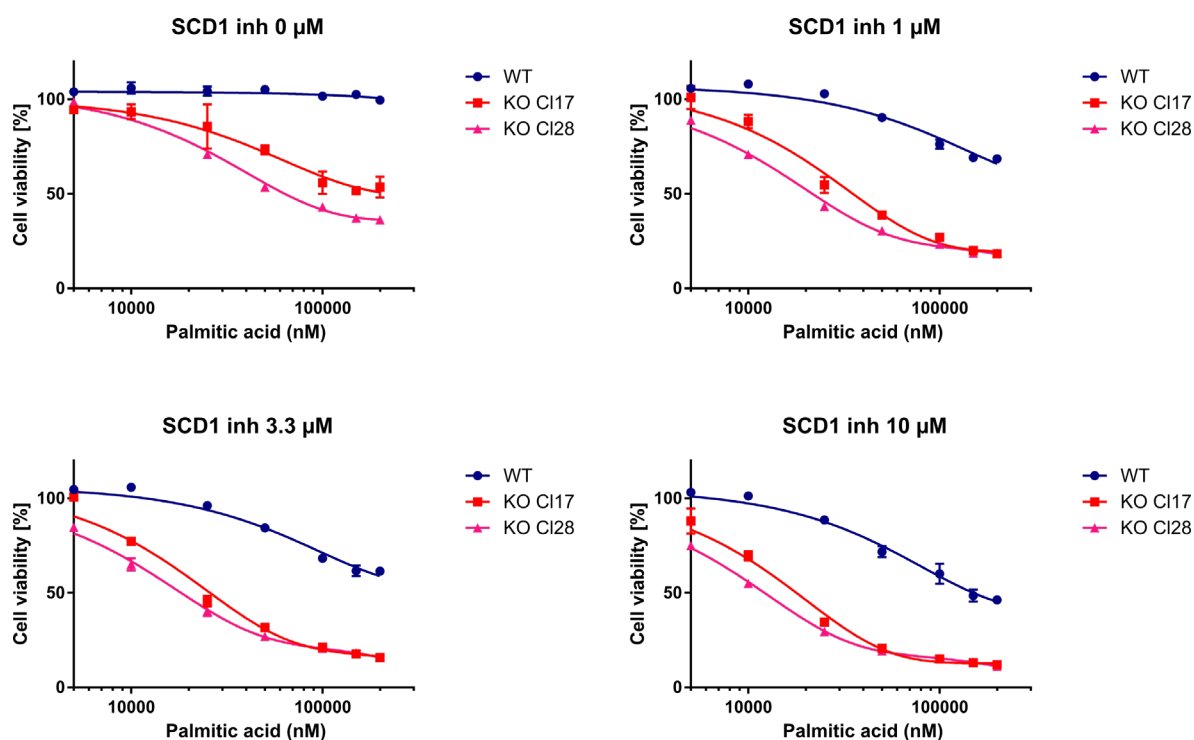


Figure 16 Deletion of GPX8 sensitizes MEFs towards palmitic acid induced cell death

Cell viability assay performed with GPX8 WT and GPX8 KO (C17, C128) MEFs. The cells were treated with palmitic acid along with SCD1 inhibitor in a concentration-dependent manner. The data shows a strong sensitivity of GPX8 KO clones in the response to the drug treatment. The sensitivity of GPX8 KO cells to palmitic acid was enhanced with increasing concentrations of the SCD1 inhibitor. Data represents the mean \pm s.d. $n=3$ from a representative experiment (Abbreviations: s.d.: standard deviation, n : sample size).

4.5. GPX8 response to ER stress by SERCA inhibition

4.5.1. SERCA inhibitors lead to GPX8 degradation, while KO of GPX8 does not influence ER stress response

Preliminary data indicated that GPX8 rapidly degrades upon thapsigargin treatment, while UPR is simultaneously activated. To further investigate these findings, two additional SERCA inhibitors were applied, i.e. cyclopiazonic acid (CPA) and 2,5-Di-*t*-butyl-1,4-benzohydroquinone (BHQ). All three SERCA inhibitors were used separately to treat WT and KO (Cl17 and Cl28) MEFs. Cell viability assay and immunoblot analysis were conducted as described in the foregoing (see 4.2.).

For cell viability assays, the cells were exposed to the compounds in a concentration-dependent manner and 24 hours after the treatment AquaBluer was used to assess cell viability (3.1.4). For immunoblot analysis, the cells were treated with the compounds in a time-dependent manner with the indicated concentrations.

The aim of the experiment was to investigate whether GPX8 KO cells show increased sensitivity to any of these agents and to see if GPX8 KO cells have increased UPR response and if GPX8 undergoes degradation using other SERCA inhibitors besides thapsigargin.

In response to any of the used SERCA inhibitors no significant difference was observed in cell viability of KO cells compared to WT (Fig. 17A). However, immunoblot blot analysis indicated that GPX8 degradation in WT cells occurred not only upon thapsigargin treatment but also when other SERCA inhibitors were used, including CPA and BHQ (Fig. 17B).

Moreover, the activation of UPR in response to the treatment was also confirmed based on the increased GRP78 expression level and the enhanced PERK phosphorylation. Unfortunately, upon thapsigargin treatment the signals for phosphorylated PERK (pPERK) were very weak and hardly detectable, although the enhanced level of GRP78 indicates the activation of the UPR signaling pathway in all cell lines. Nonetheless, BHQ and CPA were considered to induce ER stress based not only on GRP78 expression level but also on increased levels of PERK phosphorylation.

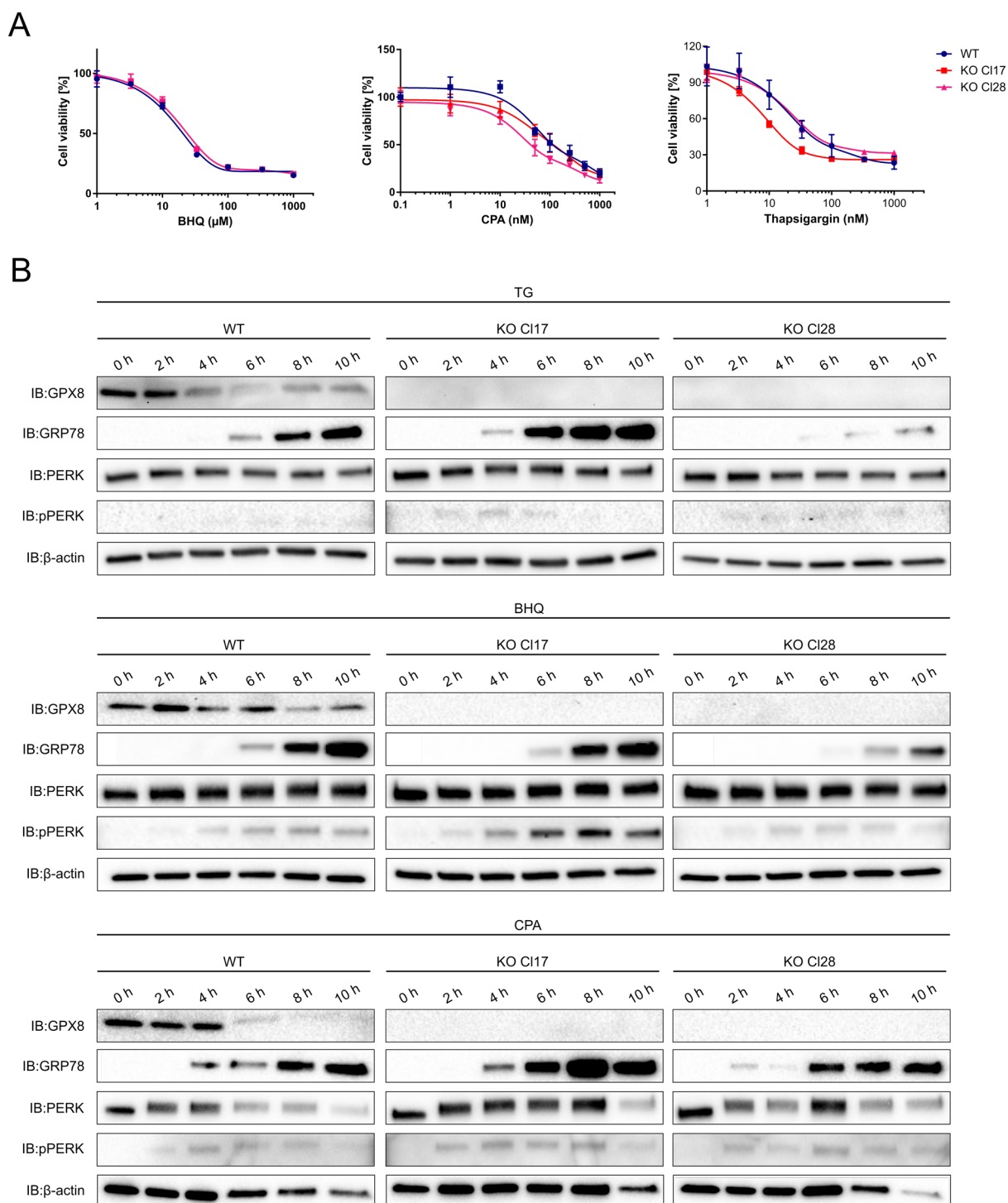


Figure 17 Analysis of UPR and GPX8 protein level in response to various SERCA inhibitors

(A) Cell viability assay performed on GPX8 KO and WT cells using three different SERCA inhibitors. AquaBluer was used to determine cell viability 24 hours after the treatment. Data represents the mean \pm s.d. $n=3$ from a representative experiment. (B) Immunoblot analysis of GPX8 KO and WT MEFs treated with either TG (20 nM), or BHQ (10 μ M) or CPA (10 μ M) in a time-dependent manner. All of these SERCA inhibitors decreased GPX8 levels, while ER stress was activated as indicated by enhanced GRP78 level and increased PERK phosphorylation. The autophagy marker LC3 did not show any evident changes in response to any of these compounds. Abbreviations: thapsigargin (TG); 2,5-di-*t*-butyl-1,4-benzohydroquinone (BHQ), cyclopiazonic acid (CPA).

Unfortunately, MEFs in response to CPA began to die after prolonged treatment, therefore the protein level was not suitable for Western blot analysis in the cases of WT 6-10 hours, KO Cl17 10 hours and KO Cl28 8-10 hours. Above all, ER stress response did not show significant differences between the two distinct genotype-based on GRP78 expression level and PERK phosphorylation.

4.5.2. Determination of Ca²⁺ level in GPX8 WT and KO MEFs using Fura-2 based Ca²⁺ sensors

In order to determine intracellular Ca²⁺ levels in GPX8 WT and KO MEFs, Fura-2 based store operated calcium entry (SOCE) measurement was performed in collaboration with Dr. Ivan Bogeski (Göttingen University). SOCE is a precisely regulated mechanism under which a dramatic depletion of Ca²⁺ in the ER is followed by an increased Ca²⁺ uptake. This process involves several “store operated channels” (SOCs) including SERCA, IP3R, calcium release-activated calcium channel 1 (Orai1), stromal interaction molecule (STIM), and phospholipase C (PLC) [217]. These proteins create a physical and functional connection between the ER and the plasma membrane to facilitate the refill of Ca²⁺. Orai proteins are located in the plasma membrane and are one of the major Ca²⁺ channels there. For instance, SOCE can be activated by using compounds that induce to the depletion of ER Ca²⁺ storage, such as thapsigargin. Consequently, Ca²⁺ depletion in the ER triggers the stimulation of Orai via its association with STIM which results in rapid Ca²⁺ uptake to restore the normal physiological Ca²⁺ concentration in the ER.

The data demonstrated no difference in basal Ca²⁺ level when comparing WT and GPX8 KO MEFs (Fig. 18A). However, following thapsigargin supplementation GPX8 KO cells exhibited significantly lower Ca²⁺ depletion in the ER than control cells (WT) (Fig. 18B), in addition to reduced Ca²⁺ reuptake in the ER (Fig. 18C). Conclusively, GPX8 KO led to a reduced Ca²⁺ uptake and consequently a decreased ER Ca²⁺ level following SOCE activation as compared to control (WT) MEFs.

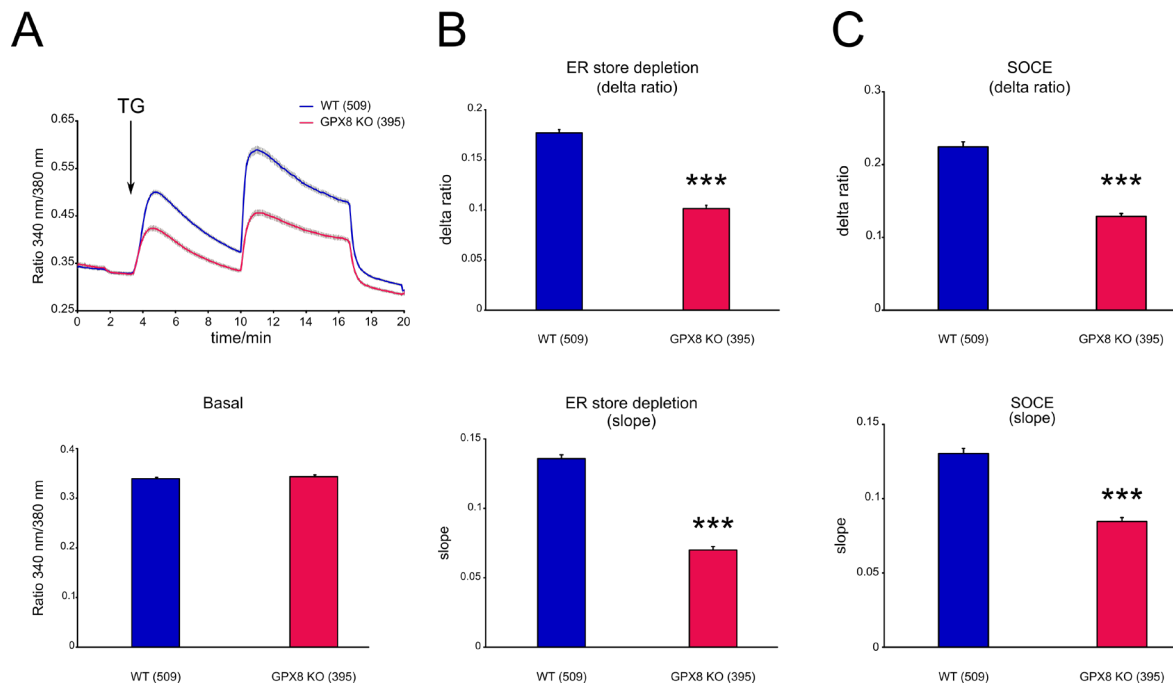


Figure 18 Assessment of intracellular Ca^{2+} levels using the Fura-2 Ca^{2+} sensor

(A) Fura-2-based store operated Ca^{2+} entry measurement demonstrated solid and highly reproducible differences between WT and KO cells. The lower scheme indicates the basal Ca^{2+} level, which showed no difference between the two cell lines. (B) The chart demonstrates that TG (10 μ M) induced ER Ca^{2+} depletion which was significantly lower in GPX8 KO cells compared to WT. (C) The results revealed decreased store operated Ca^{2+} entry after ER depletion in GPX8 KO cells. Data is represented as mean \pm SEM (n is indicated on each graph) and statistical significance was assessed by unpaired, two-sided standard Student's t test (*** p <0.005). Data was kindly provided by Dr. Ivan Bogeski (Göttingen University). (Abbreviations: SEM: standard error of the mean, n : sample size)

4.5.3. SERCA inhibition leads to subcellular translocalisation of GPX8

In order to be able to track GPX8 in living cells, mouse *Gpx8* cDNA was fused to yellow fluorescent protein (eYFP), a genetically modified version of green fluorescent protein (GFP). Due to some modifications, YFP is less sensitive to chloride and its maturation is faster than GFP.

Gpx8 cDNA originally contained a STREP(2X)/FLAG tag at the C-terminus which was replaced by eYFP. In addition, the START and STOP codons of eYFP were removed and the STOP codon of *Gpx8* was cloned at the C-terminal part of the fusion protein (Fig. 19A). These modifications were performed by overlap (OL) PCR in several steps using specific primers. In the first step (OL PCR I), GPX8 and YFP was amplified to generate fusion competent products, as described before. In the second PCR step (OL PCR II), the previously

amplified cDNAs of *Gpx8* and *eYFP* were used as template and fused to produce the final product with a size of 1500 bp (Fig. 19B). The amplified DNA was cloned into 442-PL1 vector and transformed into bacteria. After the subsequent plasmid DNA isolation, viruses were produced using HEK293T cells and the supernatant was applied to infect GPX8 KO MEFs. The transfected cells were selected with the corresponding antibiotics, and to increase the efficiency of selection, they were additionally sorted by FACS. The presence of the fusion proteins were confirmed by immunoblot analysis using anti-rat GPX8 and anti-chicken GFP antibodies (Fig. 19C).

GPX8-YFP expressing cells were used for treatments with the previously applied SERCA inhibitors, thapsigargin (TG), BHQ and CPA, and the localization of the protein was followed by fluorescent microscopy. Three hours after the treatment, the cells were fixed and pictures were taken by an Olympus confocal microscope IX81 (Olympus, Münster, Germany). Interestingly, based on the YFP signal, the localization of GPX8 was strongly affected by these drugs, although the results were not identical when comparing the three different SERCA inhibitors.

Remarkably, BHQ induced translocalization of GPX8-YFP into the nucleus, whereas TG and CPA had a less profound effect. Besides inhibiting SERCA, BHQ was presumed to increase intracellular superoxide level at higher concentrations [218]. In order to investigate whether this could explain the distinct effect of the inhibitors on GPX8 localization, NADPH oxidase 1 and 4 (NOX1, NOX4), two of the main sources of superoxide production, was inhibited (GKT 137831). Yet, the inhibitor did not prevent the translocalization of GPX8-YFP to the nucleus upon BHQ treatment (Fig. 19D).

In order to further explore subcellular changes of GPX8 localization, several co-staining experiments were performed with intracellular organelle-specific markers upon BHQ treatment. Golgi apparatus was labeled with Golgi-RFP, a Golgi-targeted protein fused to red fluorescent protein (RFP). Mitochondria and lysosome were stained with Mito-tracker and Lyso-tracker, respectively. GPX8-YFP cells were transiently transfected with Golgi-RFP expressing construct, incubated for 2 days and then treated with BHQ, while Mito-tracker and Lyso-tracker were given to the cells after the BHQ treatment and incubated for 20 min.

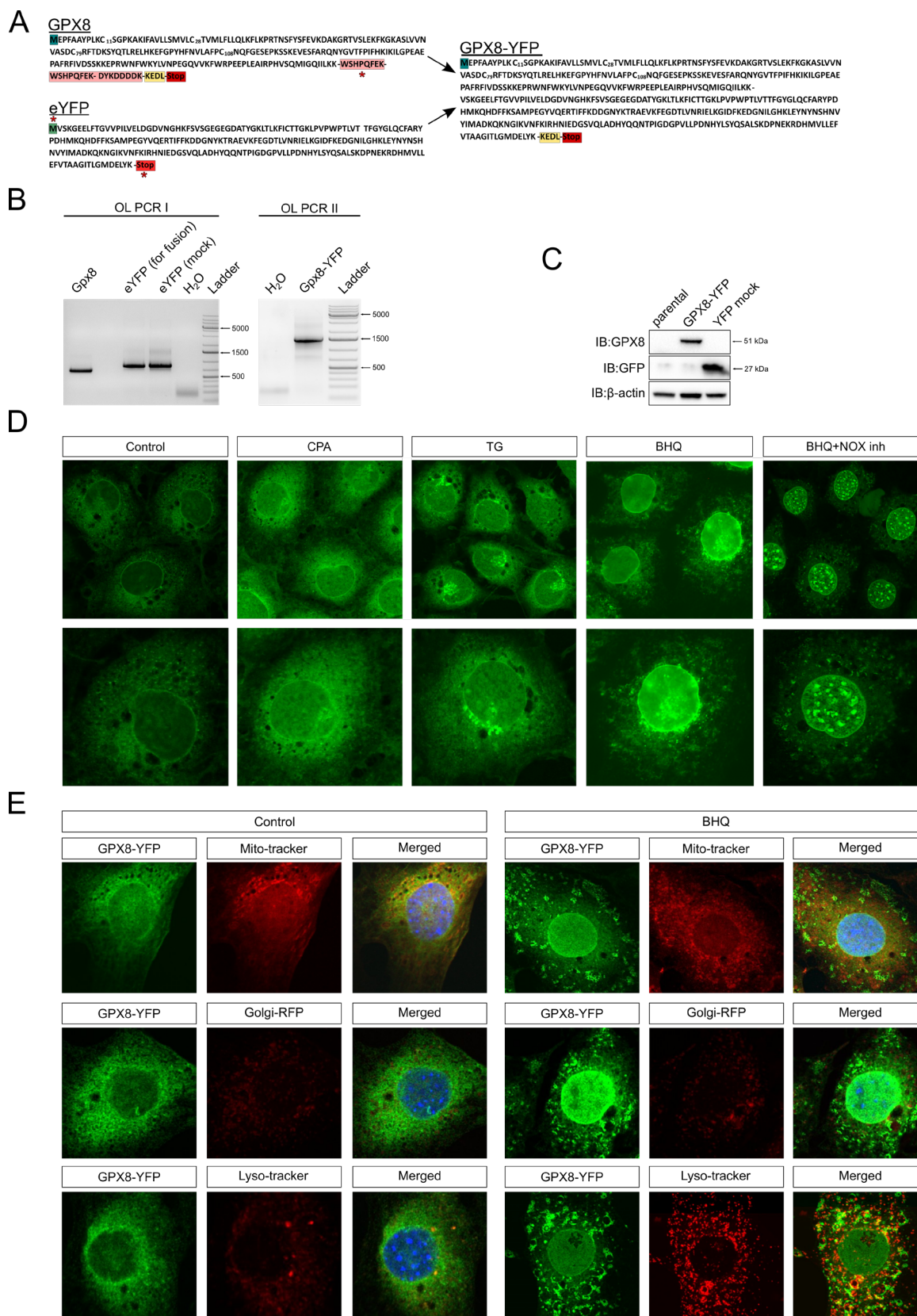


Figure 19 Generation of the GPX8-YFP fusion protein

(A) Scheme of generating the GPX8 and eYFP fusion protein. In the sequence of Gpx8 the additional STREP(2X)/FLAG tag, the ER retention signal (KEDL) and the stop codons are highlighted with pink, yellow and red, respectively. In eYFP the start codon and stop codon are highlighted with green and

red, respectively. The STREP(2X)/FLAG tag, and the start and stop codons of Gpx8 (marked with asterisks) were removed by applying several PCR steps. On the right side, GPX8-YFP represents the sequence of the fused protein with the KEDL and stop codon of Gpx8 at the C-terminal of the construct. **(B)** Individual PCR steps were performed to amplify the fusion-competent Gpx8 and eYFP and eYFP mock, which served as a control (OL PCR I). In the second PCR step (OL PCR II), the amplified sequences were fused using specific primers which generated a ~1500 bp length product. **(C)** Immunoblot analysis of GPX8 KO MEFs with or without stable expression of either GPX8-YFP or YFP mock. **(D)** Confocal microscopy pictures of GPX8-YFP expressing MEFs treated with different SERCA inhibitors for 3 hours. The cells were fixed with 4% PFA and mounted in Vectashield® mounting medium one day before the pictures were taken. **(E)** Confocal microscopy analysis of GPX8-YFP expressing MEFs treated with or without BHQ. The cells were co-stained with distinct intracellular markers such as Golgi-RFP, Mito-tracker, and Lyso-tracker. The pictures were taken with a magnification of 63 X.

After fixation, the cells were mounted with DAPI containing mounting medium (Vectashield®) to stain the nucleus and preserve the samples until the pictures were recorded. An Olympus confocal microscope was used to record the images with a magnification of 63 X.

The excitation and emission of fluorescent markers were the following: DAPI (358/461), YFP (514/527), Golgi-RFP (555/584), Mito-tracker (579/599) and Lyso-tracker (577/590). The results indicate no co-localization of GPX-YFP with any of used markers except for DAPI.

4.6. Investigation of transcriptional regulation of *Gpx8*

4.6.1. *In silico* promoter analysis

Gene expression is dependent on specific cell types and varies on different conditions due to the activation of alternative signaling pathways. Single strand RNA (ssRNA) synthesis is regulated by transcription factors and several other regulatory proteins which are activated or inactivated by upstream signaling mechanisms. The control of gene expression is indeed a very complex process which responds to relatively slight environmental changes. Activated transcription factors bind to a specific motif in promoter regions of particular genes and promote or repress their transcription. Therefore, identification of transcription factors can help to explain the function of particular genes through their regulation in different conditions. In order to identify lipid metabolism related transcription

factors in the promoter region of *Gpx8*, *in silico* promoter analysis was conducted in collaboration with Dr. Dietrich Trümbach (Helmholtz Zentrum München).

GO terms matching "lipid"		
GO term:	GO ID:	associated matrix families/transcription factors:
lipid metabolic process	GO:0006629	V\$NR2F (NR2F2), V\$PERO (PPARA Ppara PPARG), V\$PPAR (PPARG), V\$SREB (SREBF1, SREBF2), V\$ZF02 (ZNF202)
lipid homeostasis	GO:0055088	V\$PERO (PPARG), V\$PPAR (PPARG), V\$RXRF (Nr1h3)
lipid biosynthetic process	GO:0008610	V\$SREB (Srebf2)
lipid oxidation	GO:0034440	TFs not associated with a family: Hnf4
cellular lipid metabolic process	GO:0044255	V\$RXRF (Nr1h2, Nr1h3)
sphingolipid biosynthetic process	GO:0030148	TFs not associated with a family: Cers2 , Cers3 , Cers4 , Cers5
phospholipid biosynthetic process	GO:0008654	V\$PERO (Ppard)
regulation of lipid transport by positive regulation of transcription from RNA polymerase II promoter	GO:0072369	V\$PERO (PPARA)
positive regulation of phospholipid biosynthetic process	GO:0071073	TFs not associated with a family: scp1
positive regulation of lipid storage	GO:0010884	V\$NFKB (NFKB1)
response to lipid	GO:0033993	V\$PERO (Pparg), V\$PPAR (Pparg)
phospholipid metabolic process	GO:0006644	V\$GATA (Gata6), V\$NKXH (Nkx2-1)
regulation of lipid transport by negative regulation of transcription from RNA polymerase II promoter	GO:0072368	V\$SREB (SREBF2)
regulation of lipid kinase activity	GO:0043550	TFs not associated with a family: Rb1 , RbL1 , RbL2
regulation of lipid metabolic process	GO:0019216	V\$NR2F (HNF4A), V\$RXRF (Thrb) TFs not associated with a family: EDF1
lipid storage	GO:0019915	V\$STAT (Stat5a, Stat5b)
lipid catabolic process	GO:0016042	TFs not associated with a family: Hnf4

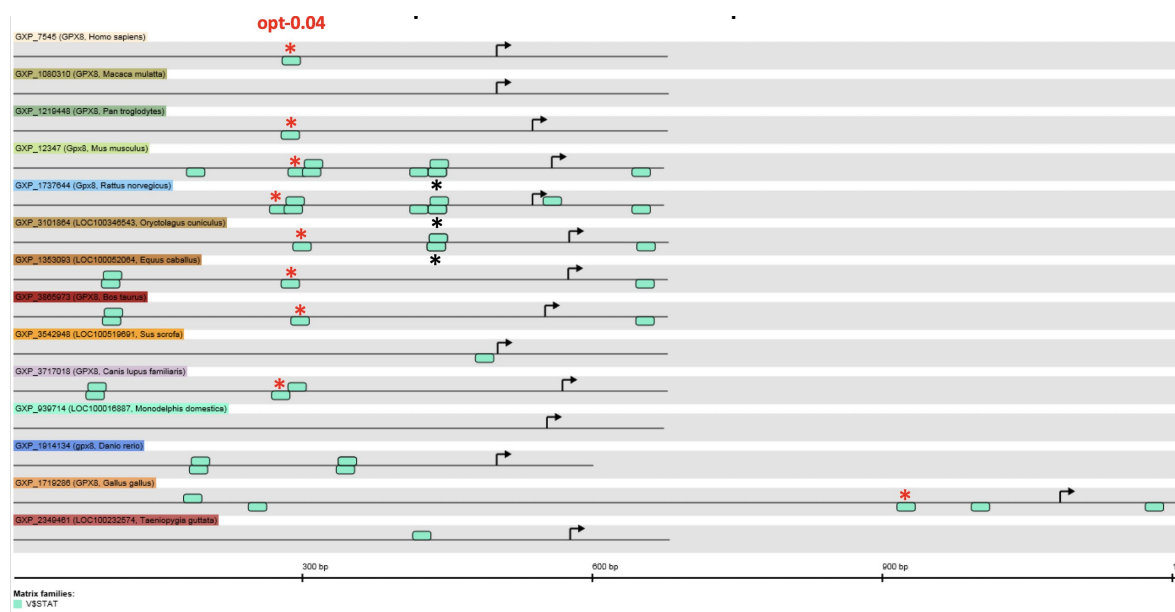


Figure 20 Identification of lipid homeostasis-related transcription binding sites in the promoter region of *Gpx8*

(A) The table shows the transcription factors that were identified with lipid metabolism-related functions according to Genomatix. (B) The results of the analysis of STAT5 indicate that the transcription factor binding site of STAT5b (red asterisk) and STAT5a (black asterisk) are conserved among several organism including human (only STAT5b), mouse rat and rabbit.

The upstream sequence relative to the *Gpx8* transcription start site has been investigated in numerous organisms to identify a conserved DNA motif, which can be involved in the regulation of the expression level of *Gpx8*. These specific DNA sequences are recognized by transcription factors which either repress or activate the transcription.

First, transcription factors that were assigned to “lipid” functional categories of Gene Ontology (GO) in MatBase (Genomatix) were annotated (Fig. 20). The typical motifs of these transcription factor binding sites were analyzed upstream of the *Gpx8* transcription start site. Three conserved transcription factor binding sites that are involved in lipid metabolism were identified: (I) peroxisome proliferator-activated receptor gamma, DR1 sites (PPAR γ), (II) signal transducer and activator of transcription 5 (STAT5A/B), and (III) liver X receptors/ retinoid X receptor (LXRb/RXR). PPAR γ plays a role in fatty acid storage, glucose metabolism and also regulates lipid uptake [219].

The PPAR γ binding site in the *Gpx8* promoter is conserved across mouse, human and chimp, while the binding site of the LXRb/RXR heterodimer is conserved across mouse, rat, human, chimp and horse. Among the three transcription factors, STAT5 was conserved among the most organisms including humans, chimps, mice, rats, and rabbits, thus it was further analyzed by ChipSeq. Upon the study, several Stat4/6 transcription binding sites from the CD4⁺ cells and Stat5b transcription binding sites from the T-lymphocyte cells were detected in the extended promoter region of *Gpx8* (Supplementary Fig 2). These transcription factors play a crucial role not only in the regulation of lipid mobilization and storage [220], but also in the response to a variety of cytokines [221, 222]. Yet, these candidates have to be validated using other techniques, such as chromatin immunoprecipitation (ChIP) assay, which is a useful tool to identify DNA-protein interactions in living cells.

4.6.2. Transcriptional analysis of GPX8 KO and WT mouse embryonic fibroblasts

Unlike GPX4 KO, which results in ferroptotic cell death [214], knockout of its closest homolog GPX8 in MEFs did not lead to cell death under normal cell culture conditions. In

order to validate a possible compensation of other genes and gain a deeper understanding of the function of GPX8 *in vitro*, gene expression profile of WT, GPX8 KO, addback (AB) and KO mock (KO mock) MEFs were compared by RNA microarray analysis. This approach should allow the identification of genes, whose transcriptional regulation is impacted by the expression level of GPX8.

One of the most important aspects of RNA microarray is the data quality. In order to ensure that the quality of the samples are suitable for the measurement, quality control (QC) metrics was carried out. Since RNA is unstable due to the ubiquitously present RNases, a measurement of RNA integrity number (RIN) was developed, which is a quantification method to validate the degradation degree of sample RNAs. RIN value of 8 or above is considered sufficient for transcriptome analysis. The results demonstrated that the RIN value of all samples were above 8 with the exception of No #89 (Fig. 21A), indicating that the quality of isolated RNAs was suitable for further applications. In addition, principal component analysis was performed (PCA) based on a linear combination of gene expression values in order to define unrelated variables (Fig. 21B). The similarities among the samples are correlated to the distance of space between their values on the plot. The data indicates that the RNA samples isolated from WT MEFs are very different in their gene expression profile as compared to GPX8 KO cells. However, the gene expression profile of GPX8 KO cells were more similar to both KO mock and addback cells than to WT cells. Moreover, the variability of the three replications were notable (#1, #2, #3). The replications represent three independent experiment sets, which could elucidate the observed variability between the same cell lines, as evidenced for instance by dynamically regulated expression of proliferation-related genes in different cell cycle stages.

The genome-wide study was conducted by applying the Affimetrix GeneChip WT Plus kit. The expression levels of individual genes were normalized to their expression level in WT MEFs. After calculation, the results of particular cell lines were ranked and the fold changes were compared. First, *Gpx8* RNA level was analyzed among different samples to confirm the efficiency of the genetic modification (Fig. 21C). The data indicates approximately 5-fold downregulation of *Gpx8* in KO and KO mock cells compared to WT MEFs, while GPX8 AB cells exhibited very high expression of the targeted gene, confirming the genetic modifications.

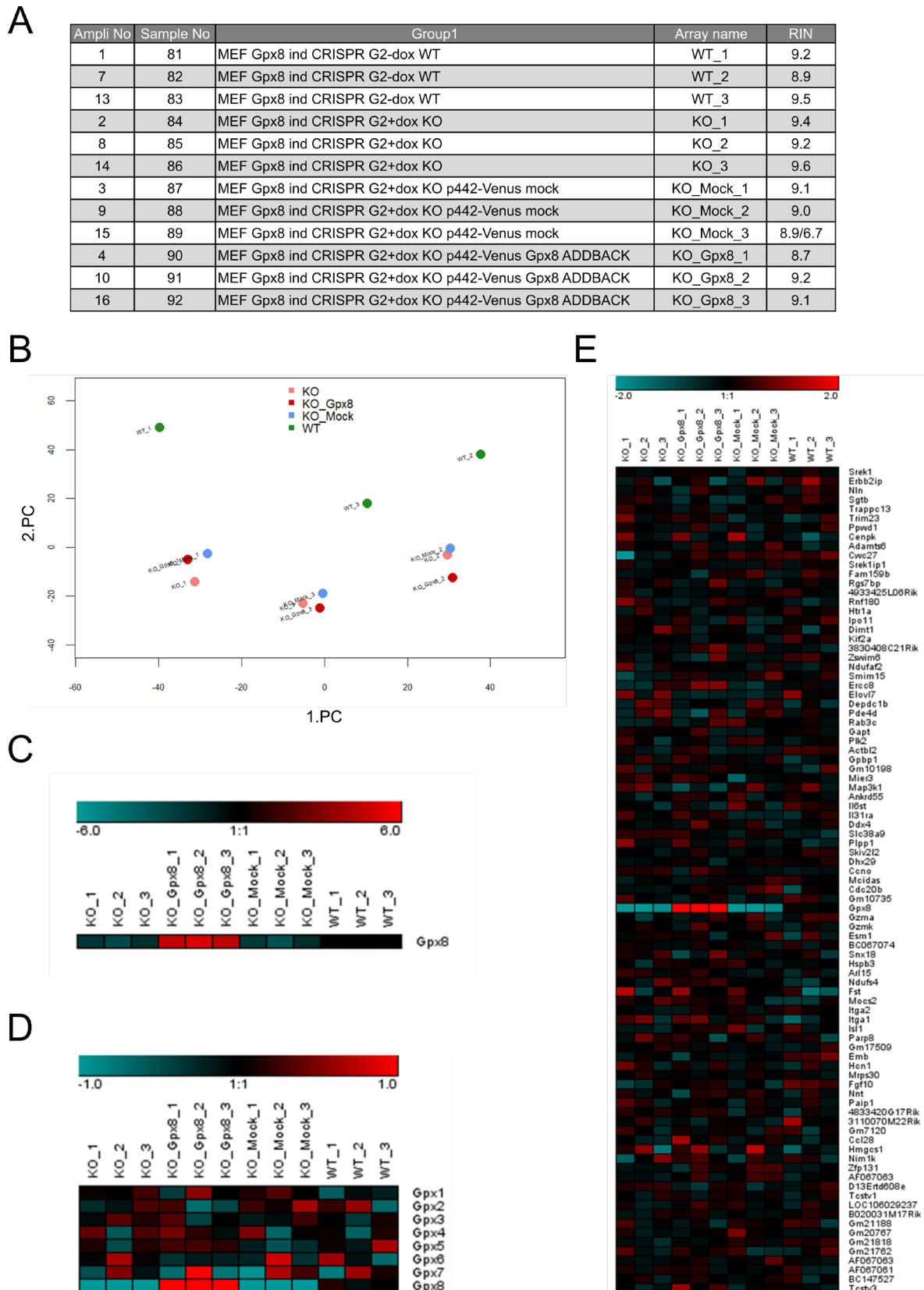


Figure 21 Microarray analysis of GPX8 WT, KO and AB MEFs

(A) Quality control (QC) metrics data demonstrates the RNA integrity number (RIN) of all individual samples. According to the analysis the RIN values indicated suitable RNA qualities for microarray

analysis. **(B)** Principal component analysis (PCA) was performed to validate the similarities in gene expression profile of different samples. The plot shows that the differences were not only significant between the distinct genotypes but also between the experimental repetitions. **(C)** *Gpx8* gene expression varies according to the genetic modifications. **(D)** Gene expression profile of all *Gpx* genes revealed no transcriptional regulation of any member of the enzyme family upon genetic loss of *Gpx8*. **(E)** Microarray analysis of the genes located on the same chromosome than *Gpx8* do not show any alterations of neighboring genes in response to *Gpx8* up- and downregulation.

Additionally, mRNA levels of other GPX family members were analyzed to investigate a possible compensatory mechanism of these genes, which could theoretically promote cell survival in the absence of GPX8. However, *Gpx8* expression level on did not affect the mRNA extent of other *glutathione peroxidases* (Fig. 21D).

Figure 21E demonstrates the expression level of genes that are located upstream and downstream of *Gpx8* on the same chromosome. Although the *Gpx8* level was strongly variable in the different cell lines, no regulation of neighboring genes could be observed.

Finally, genome-wide study was performed to identify any genes whose expression rely on *Gpx8* expression level. Unfortunately, only *Gpx8* RNA was proven to be regulated by the genetic modifications (Appendix Excel 1). Just as the PCA plot indicated, the expression of individual genes exhibited higher variability between GPX8 KO and WT cells than those between GPX8 addback and KO cells. Although, no regulation was found between WT and KO cells on mRNA level, it does not exclude that there is any substantial regulation on the translational or even posttranslational level, which was subject of studies as detailed in the following sections.

4.7. Identification of novel interaction partners of GPX8

4.7.1. Yeast two hybrid

Yeast two hybrid (Y2H) analysis was performed to identify possible interaction partners of GPX8. Although this approach has some advantages in contrast to co-immunoprecipitation, it also has some disadvantages. Y2H is a fast and feasible technique, but in some cases, it provides negative or false positive results since the experiment is performed in yeast using a cDNA library of other species. In fact, mammalian cells are more complex than yeast cells,

thus it is possible to detect an interaction in yeast which never occurs in mammalian cells due to the different subcellular localizations. Despite the aforementioned disadvantages, this method is still commonly used especially in cases if, for instance, the knowledge of a protein is very limited.

To this end, *Gpx8* cDNA was cloned into a 442-PL1 lentiviral expression plasmid and sent to the Hybrigenics service company. *Gpx8* expressing vector (bait) was simultaneously expressed along with a mouse pancreas cDNA library (prey). Fig. 22A illustrates the principle of the method, whereby the transcription factor of a reporter gene is split into two domains: the DNA-binding domain (DBD) and the transactivation domain (TAD). The bait is fused to the DBD while the prey is associated with the TAD of the transcription factor. The transcription of the reporter gene is initiated if the separated domains of the transcription factor are in a close proximity, which only occurs if an interaction between the bait and prey is present. In this case, the reporter gene was the imidazoleglycerol-phosphate dehydratase (HIS3) gene, which is required for histidine biosynthesis in yeast. Therefore, if the growing medium lacks histidine, the expression of HIS3 is essential for cell survival.

After the screening was carried out, the surviving clones were sequenced to identify which cDNA was expressed in the individual clones. Library sequences were then compared to reference sequences from GeneMatch to determine the genes that were represented by the unique sequences. For each interaction a predicted biological score (PBS) was assigned to estimate the reliability of the particular interaction. The PBS represents the probability of a non-specific interaction, accordingly the results were ranked from A to F where A indicated the highest confidence in interaction (Fig. 22B). Ranks B and C indicate high and good confidence in interaction, respectively. Score D represents moderate interactions of binding partners that were identified via one unique prey fragment, or several identical ones. PBS E demonstrates interactions that involve prey domains which bind to more than 10 mouse bait proteins. PBS F constitutes interactions which are experimentally proven to be artifacts of the Y2H technique, including proteins that bind to DNA upstream of the reporter gene.

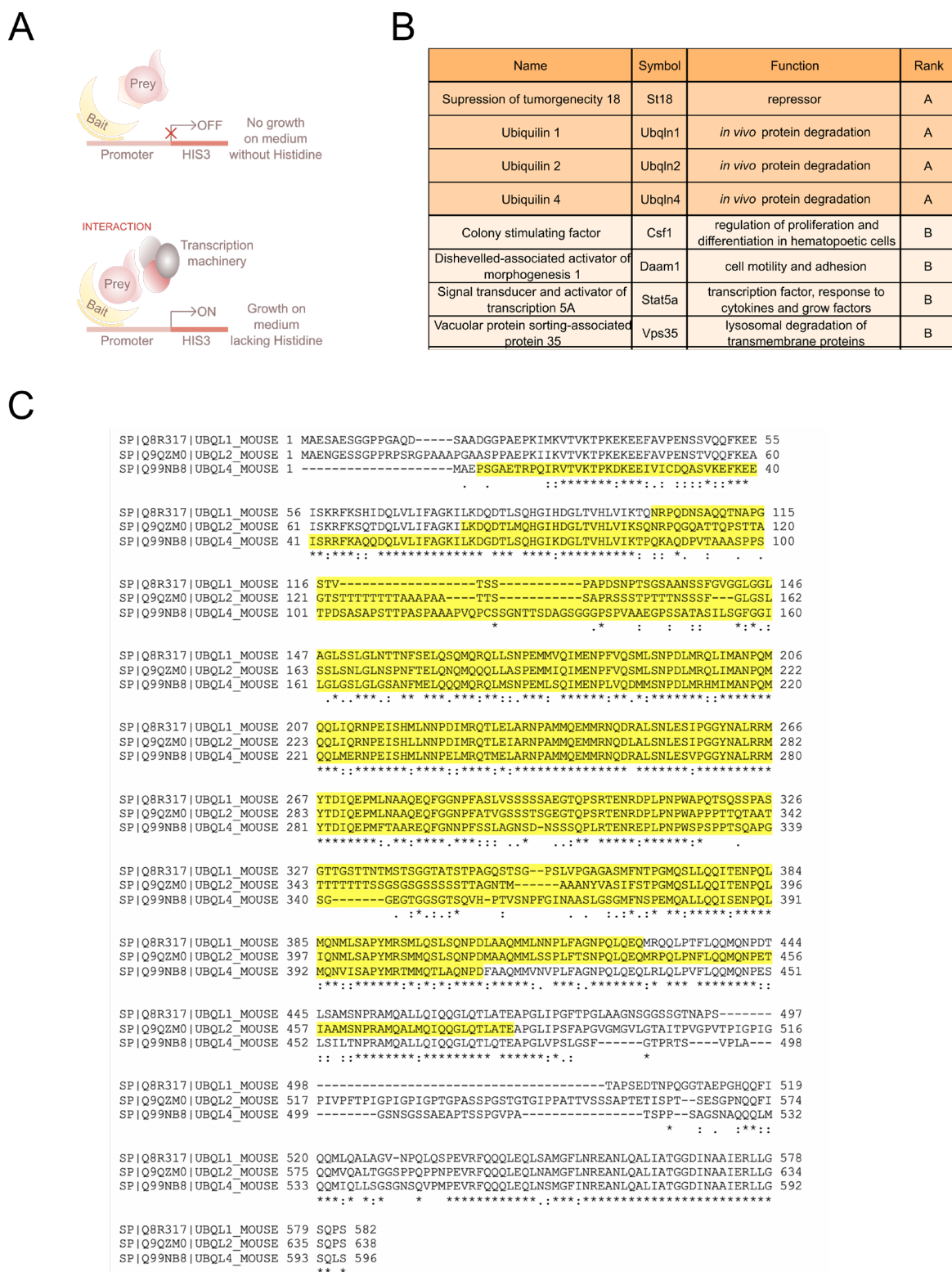


Figure 22 Yeast two hybrid analysis was performed to identify interaction partners of GPX8 in vitro

(A) Scheme of yeast two hybrid technology. If there is no interaction between the protein of interest (bait) and a protein of the library (prey), the cells die due to the transcriptional inhibition of HIS3, the gene which is crucial for cell survival in the histidine auxotrophic strain. However, if an interaction occurs, the transcription of HIS3 induced and the cell survive. (B) The table is a summary of the

yeast two hybrid screening. It demonstrates the best hits with the highest ranks (A and B) indicating the highest possibility of an interaction. (C) Alignment of the three ubiquitin proteins (ubiquitin 1,2 and 4) which were all in the highest rank A. The alignment indicates that these proteins show a high degree of homology, especially in the region which was identified in the screening (highlighted with yellow).

Only domains of four different proteins with the highest confidence (rank A) were identified: three of them belonged to the ubiquitin protein family (ubiquitin 1-2, 4), while the fourth was the suppression of tumorigenicity 18 (ST18). In fact, ubiquitins show a high degree of similarity (Fig. 22D), and were shown to be associated not only with proteasome but also with ubiquitin ligases, therefore their role in proteasomal degradation has been strongly suggested [221, 222]. Additionally, ubiquitins have been previously reported to be essential for macroautophagy, autophagosome formation and maturation by regulating LC3 maturation. They are also crucial for the fusion of autophagosome and lysosome [24]. ST18 is a repressor protein which binds to 5'-AAAGTTT-3' motifs in the DNA, which are separated by 2-9 bp in between the repeats [25].

In the second score group (B), proteins were identified, such as a colony stimulating factor (Csf1), disheveled-associated activator of morphogenesis 1 (Daam1), signal transducer and activator of transcription 5A (Stat5a), or vacuolar protein sorting associated protein 35 (Vsp35) as further possible binding partners with high confidence in the interaction. However, these interactions were not as representative as the ones in score A. In order to validate these results in MEFs and find further possible interaction partners, co-immunoprecipitation was performed as described in the following.

4.7.2. Identification of GPX8 interaction partners

One of the most common approaches employed to investigate the role of an unknown protein is the identification of novel interaction partners by co-immunoprecipitation. The proteomic-based technique involving the application of mass-spectrometry (MS) has been demonstrated to be a more reliable method for a protein-protein interaction screen than the previously used Y2H method. Unlike Y2H, in this case, the proteins are present in a fully processed form in their native environment. Furthermore, this method allows the

purification of multicomponent complexes in a single step. The MS-coupled co-immunoprecipitation serves as a rapid and reliable approach to identify previously unknown interactions that could be involved in biological processes but are difficult to detect with other methods such as the Y2H approach.

Since there is no commercial anti-GPX8 antibody available for this purpose and the in-house generated antibody is also not suitable for co-IP studies, STREP(2X)-FLAG tag was fused to GPX8 allowing the purification of the protein along with its covalently bound interaction partners (Fig. 23A). The tag was placed on the C-terminal part of GPX8, upstream of KEDL (Fig. 23B). The sequence of wild type (WT) and all-Cys mutant GPX8-STREP(2X)-FLAG-KEDL construct were purchased from Addgene, and the WT sequence was further used to introduce the mutations of each Cys separately. In all cases, Cys were replaced by serine (Ser) by using overlap PCR. All constructs were cloned into lentiviral expression plasmid (442-PL1) and WT MEFs were transfected with the virus to generate stable cell lines. The expression levels of the different constructs were verified by immunoblot analysis using GPX8 and FLAG antibodies. Interestingly, the expression levels were different among WT and the single Cys mutant forms of the protein, while the all-Cys mutant GPX8 was barely detectable (Fig. 23C).

In order to validate the localization of tagged GPX8, immunocytochemistry was performed on WT GPX8-STREP(2X)-FLAG tag expressing MEFs using a PDI-specific antibody as an ER marker and the FLAG antibody to monitor GPX8 expression (Fig. 23D). The results indicated co-localization of the ER marker and GPX8, proving that the tag did not cause any changes in the localization of the protein. Subsequently, co-immunoprecipitation was performed using biotinylated beads which efficiently bind to the STREP tag. WT GPX8-STREP(2X)-FLAG tag expressing cells were used for the isolation which were either left un-treated (control) or treated with thapsigargin (TG) in the presence or absence of MG132. Following protein purification, the samples were separated by polyacrylamide gelelectrophoresis and the entire protein content was visualized by silver staining (Fig. 23E). The data demonstrates the efficiency of the protein purification. Delta (Δ) indicates the bead control (GPX8 overexpression without the tag) and the detected bands in this sample reflect the unspecific interactors of the bead.

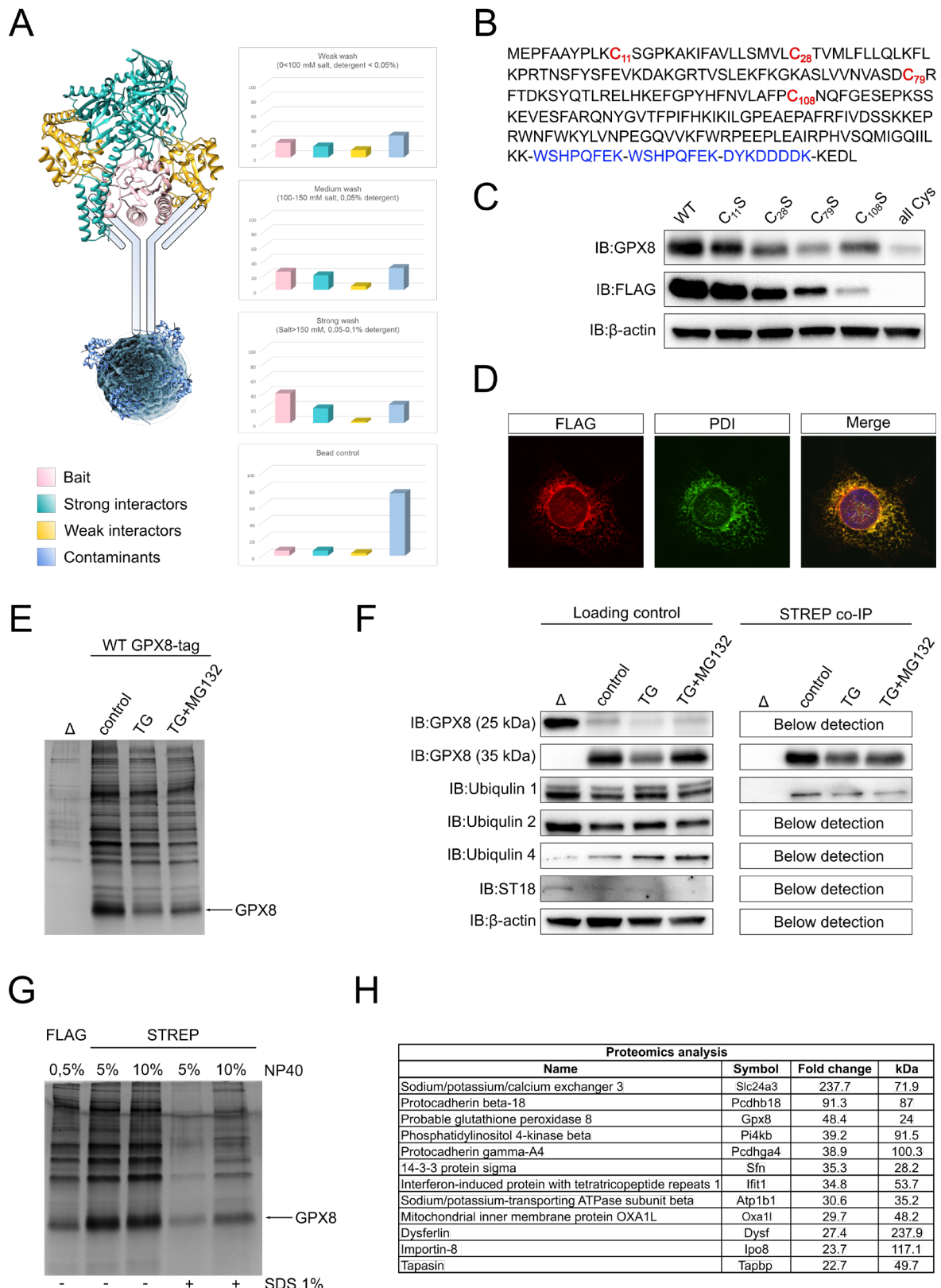


Figure 23 Tandem affinity purification was performed to identify possible GPX8 interaction partners

(A) The picture illustrates the principle of co-immunoprecipitation. The antibody-conjugated bead binds to the protein of interest which can be thereby isolated along with its strong and weak

interaction partners. However, as demonstrated here, a “strong” washing step can remove most of the weak interactors. Furthermore, some proteins bind unspecifically directly to the bead (contaminants) which can be identified and sorted out from the positive results by using a negative control (bead control). **(B)** Amino acid sequence of mouse GPX8 shows the position of STREP(2X)/FLAG tag (blue) and the position of each mutated cysteine (red) within the protein. **(C)** Immunoblot analysis demonstrates the expression level of each newly established construct. GPX8-STREP(2X)/FLAG tag fusion proteins with the individual cysteine mutations were expressed in WT MEFs. **(D)** The localization of the WT GPX8-STREP(2X)/FLAG protein was analyzed by immunocytochemistry using a PDI-specific antibody as an ER marker. The data shows that the tag at the C-terminus of GPX8 did not change the localization of the protein and is in line with previous reports that GPX8 was originally identified as an ER-associated protein. **(E)** Silver staining was performed after co-immunoprecipitation with biotin (STREP) coupled beads. Isolated protein samples of untreated (control) cells and thapsigargin (TG) treated cells with or without MG132 were separated by gel-electrophoresis and stained according to the silver-nitrate based method. As negative control (delta), cell line with the overexpression of non-tagged GPX8 was applied. Nonetheless, silver staining indicated that the co-immunoprecipitation resulted in the isolation of numerous other proteins, that were also present in the negative control. **(F)** Immunoblot analysis demonstrated the presence of GPX8-STREP(2X)/FLAG tag in the purified lysate following the co-immunoprecipitation by biotin (STREP) bead. Besides GPX8, Ubiquilin 1 but not the other investigated proteins were found in the lysate, only in the loading control. **(G)** As shown in Fig. 16E, the silver staining indicated several interactors of GPX8. To increase the specificity of the method, silver staining was conducted on lysates using different protocols. Considering these results, 10% NP40 and 1% SDS were applied to prepare samples for mass spectrometry analysis. **(H)** The table is a summary of the mass spectrometry analysis, demonstrating the most relevant hits with the highest fold change between the sample and bead control.

In the beads control GPX8 was undetectable, whereas in the other samples it was the most abundant protein, as expected. Besides GPX8, in the untreated (control) and treated (TG and TG+MG132) samples several proteins appeared with high intensity. However, the pattern of total proteins was comparable among these samples, revealing that the treatment did not result in any evident changes which could be detected by this method.

These purified samples were then applied for immunoblot analysis using antibodies against GPX8 and for other proteins that were identified in the Y2H screening in score A (Fig. 23F) such as Ubiquilin1, Ubiquilin2, Ubiquilin4, ST18 and finally β -actin as a loading control. Interestingly, Ubiquilin 1 and GPX8 were present in all conditions except for the negative control, but Ubiquilin 2, Ubiquilin 4 and ST18 were below detection level. To ensure that the detected proteins were expressed by the applied cell lines and conditions, immunoblot analysis was performed on cell lysates (loading control). Indeed, all studied proteins were present in the loading control, suggesting that they were not covalently associated to GPX8 and therefore could not be purified by STREP co-immunoprecipitation.

In order to optimize the condition for co-immunoprecipitation, different concentrations of detergent and other beads were tested (Fig. 23G). In fact, only the supplementation of 1% SDS resulted in decreased protein content, especially in combination with 5% NP-40, although the specificity of the purification was not improved. Therefore, for further application, STREP purification was performed in the presence of 5% NP-40 without SDS using control WT GPX8-STREP(2X)-FLAG expressing MEFs. Following the co-immunoprecipitation, mass spectrometry analysis was performed in collaboration with the core facility of Helmholtz Zentrum Munich.

Unfortunately, probably due to inappropriate purification, numerous proteins were detected in the lysate. Peptides from a total of 1263 proteins were identified in the screen. The enrichment of each protein was calculated based on their abundance in the GPX8-STREP(2X)-FLAG expressing cells, which was then divided by their amount in GPX8 AB cells. The top hits with the highest fold change gave an interesting insight into the possible function of the protein (Fig. 23H). Since the proteins were sorted according to their fold changes, GPX8 was the third in the list with fold change of 48,4. Besides GPX8, peptides were enriched of sodium/potassium/calcium exchanger 3 (Slc24a3), protocadherin-beta 18 (Pcdhb-18), phosphatidylinositol-4-kinase-beta (PI4Kb), protocadherin-gamma-A4 (Pcdhga4), 14-3-3 protein sigma (Sfn), interferon-induced protein with tetratricopeptide repeats-1 (Ifit-1), sodium/potassium-transporting ATPase subunit beta (Atp1b1), mitochondrial inner membrane protein OXA1L (Oxa1l), Dysferlin (Dysf), Importin-8 (Ipo-8), and TAP-associated glycoprotein/tapasins (Tapbp).

Tapasin and Ifit-1 are important in the case of infections and immune response [223-227], and Dysferlin was proven to contribute to membrane repair in skeletal muscle cells and cardiomyocytes in a Ca^{2+} -dependent manner [228-231]. Ipo-8 was shown to be required for nuclear transport of proteins [232-234], while protocadherins are members of cadherin superfamily which have been implicated to regulate Ca^{2+} -dependent cell-cell adhesion [235]. Slc24a3, a K^+ dependent Ca^{2+}/Na^+ exchanger is an important regulator of Ca^{2+} homeostasis [236], while Atp1b1 and PI4Kb have been shown to have multiple cellular functions via K^+/Na^+ and inositol signaling, respectively [237-242]. Finally, Oxa1l promotes the insertion of mitochondrial membrane proteins of the oxidative phosphorylation complexes [243, 244], while Sfn is an adaptor protein with several interaction partners. It

usually recognizes phosphoserine or phosphothreonine residues, and subsequent binding alters the activity of the target proteins. It has been shown that the members of this protein family serve as tumor suppressors [245-247].

4.8. Generation and characterisation of a *Gpx8*^{-/-} mouse line

4.8.1. Generation of *Gpx8*^{-/-} mouse line using CRISPR/Cas9

To examine the effect of the knockout of GPX8 *in vivo*, a mouse line was generated by targeting the critical second exon of *Gpx8* on a C57BL/6N mouse genetic background. Therefore, CRISPR/Cas9 technology was applied and the sgRNA was designed using an online tool and tested on MEFs (see 4.4.1.) before using them on single cell embryos. The mRNA of *Cas9* along with the sgRNA were injected into single cell embryos, which were subsequently implanted into a foster mother (Fig. 24A). After weaning, genotyping was performed by PCR amplification in order to confirm the absence or presence of the genetic modification. According to the genotyping PCR, only one female mouse carried a deletion in the *Gpx8* locus (Fig. 24B).

Subsequently, DNA of PCR products were isolated and sent for sequencing. The results confirmed that only one mouse was positive for the desired genetic alteration (Fig. 24D). The sequences were analyzed by using an online tool (<https://tide.nki.nl/>) which allowed the identification of the missing nucleotides in the two different alleles (Fig. 24E). The online tool identified a 16 bp deletion on one allele and a 1 bp deletion on the other allele of the positive female (#5). Since both deletions lead to an out of frame mutation, the mouse was considered to be a knockout. The modified gene was obtained by multiple backcross steps, first with wild type (*Gpx8*^{wt/wt}) and subsequently with heterozygous (*Gpx8*^{wt/-}) animals to generate knockout (*Gpx8*^{-/-}) mice. Unfortunately, the first *Gpx8*^{-/-} female (#5) had only one litter with 3 offspring and they all inherited the allele containing the 16 bp deletion. Therefore, the allele carrying the 1 bp deletion could not be further obtained.

The first observation was that knockout of GPX8 is viable in mice, and after several breedings, it was also concluded that the genotype of litter-mates followed the Mendelian model of inheritance (Fig. 24F,G).

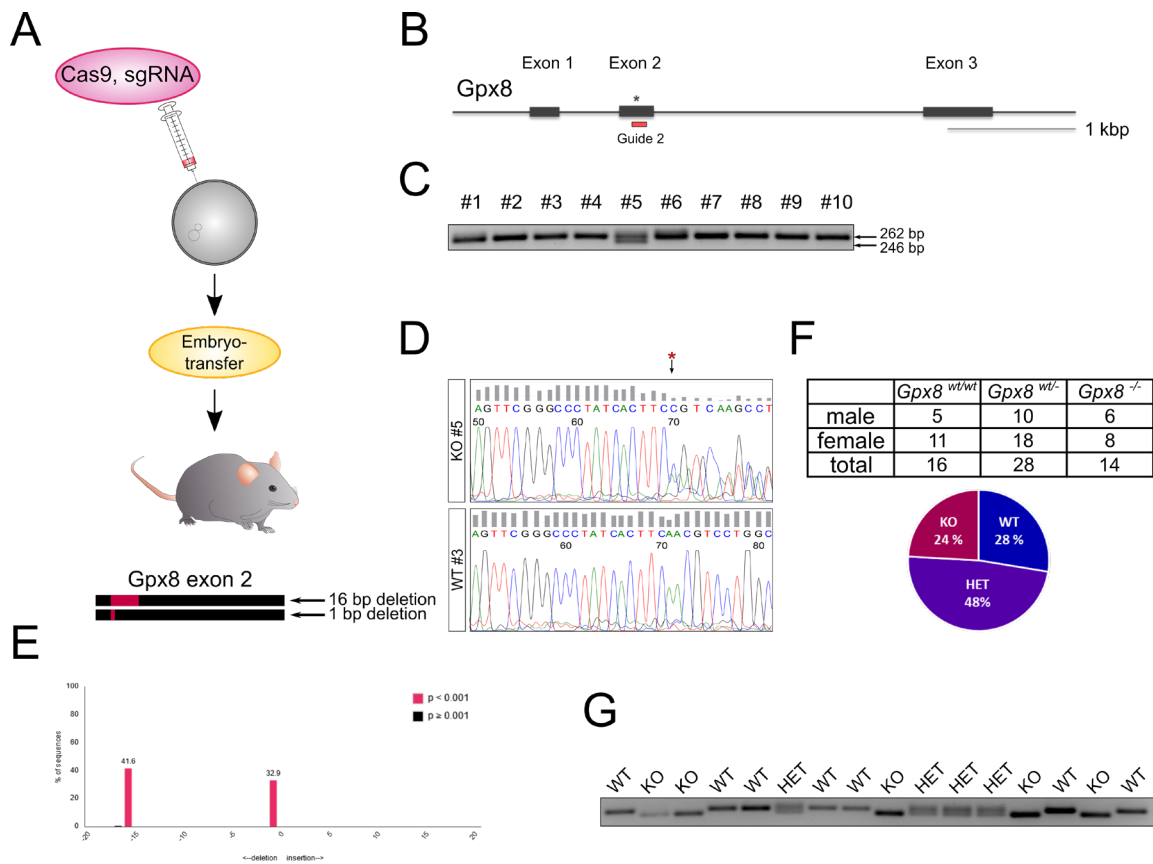


Figure 24 Generation of $Gpx8^{-/-}$ mouse line by CRISPR/Cas9 genome editing

(A) Workflow of the generation of CRISPR/Cas9 mediated knockout mouse line. (B) The scheme indicates the binding site of the CRISPR guide which was applied for in vivo gene editing. (C) PCR of the first genotyping by which the first knockout mouse was identified. The results demonstrate that the DNA of mouse #5 was cleaved in the CRISPR targeted region. (D) Sequencing data confirmed that Cas9 successfully cleaved both alleles in the second exon of Gpx8. (E) Online tool was used to identify the number of missing nucleotides on each allele of mouse #5. The analysis indicated a 1 bp deletion on one allele, while on the other allele a longer, 16 bp deletion was detected. Both deletions are “out of frame” mutations, therefore the translation of Gpx8 will be interrupted. (G) Genotyping PCR of the offspring which was obtained from mouse #5 through several breeding steps. Despite the small (16 bp) deletion, all genotypes can be unequivocally distinguished by using primer pairs binding up- and downstream of the targeted exon.

After an adequate number of mice was bred, the expression level of GPX8 in $Gpx8^{wt/wt}$ and $Gpx8^{-/-}$ animal tissues were analyzed by Western blot. In most of the tissues, the lack of

GPX8 protein was confirmed after CRISPR/Cas9 genome editing. However, in the kidney, liver and in some cases in the heart, GPX8-positive staining was detected (Fig. 25A). Therefore, DNA and RNA were isolated directly from the organs to confirm the genotype and to investigate a possible alternative splicing variant (Fig. 25B).

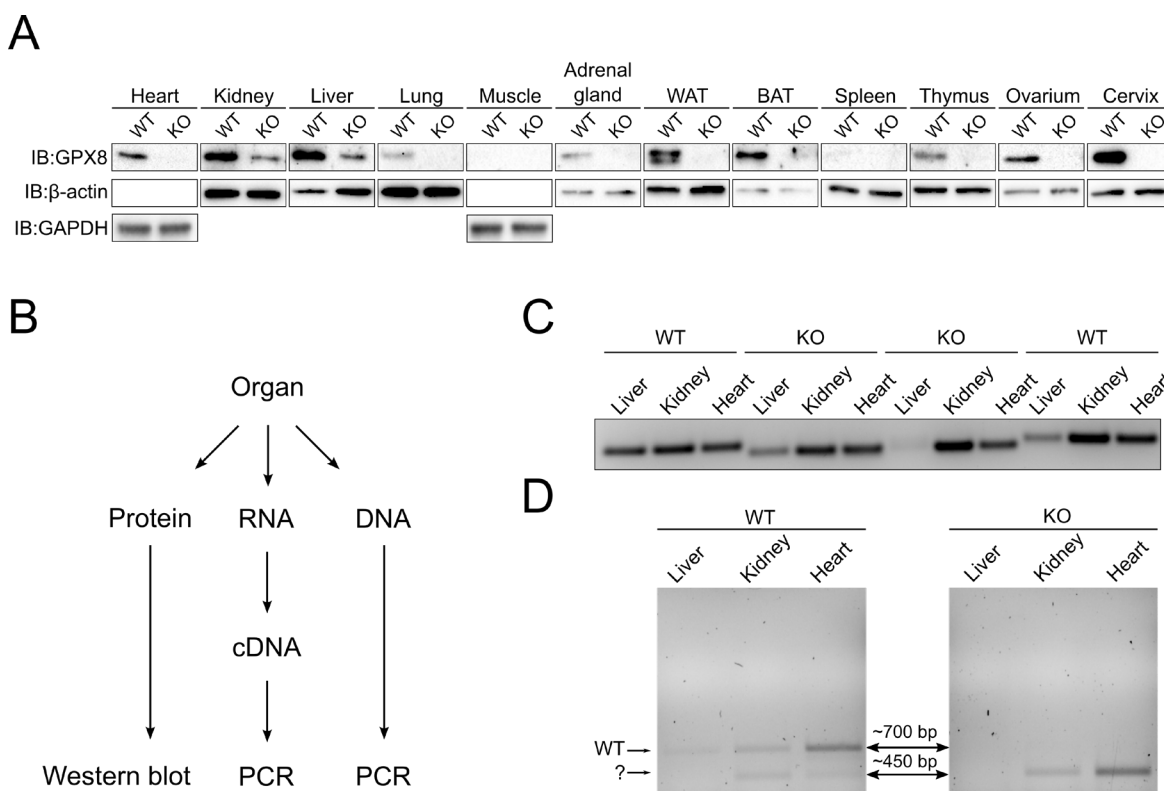


Figure 25 Analysis of GPX8 expression in mouse tissues from $Gpx8^{wt/wt}$ and $Gpx8^{-/-}$ animals

(A) Immunoblot analysis of mouse tissues from $Gpx8^{wt/wt}$ and $Gpx8^{-/-}$ animals. In $Gpx8^{wt/wt}$ animals most of the tissues exhibited expression of the protein to varying degrees, whereas tissues from $Gpx8^{-/-}$ animals showed no signal except in kidney, liver and in some cases in the heart (data not shown). **(B)** Scheme of the process of mouse tissue analysis. **(C)** Genotyping PCR of mouse tissues. Liver, heart and kidney were taken for DNA isolation of two $Gpx8^{wt/wt}$ and two $Gpx8^{-/-}$ animals to confirm the genotype in the respective tissues. **(D)** PCR of cDNA derived from mRNA of $Gpx8^{wt/wt}$ and $Gpx8^{-/-}$ mouse organs. The primers were designed to allow the amplification of all of the three exons of $Gpx8$. The data indicates a potential alternative gene product in kidney and heart which is about 450 bp. It could be an alternative splicing variant of the gene excluding the CRISPR targeted second exon. However, the sequencing of this product was unfortunately not yet successful, therefore this fragment has to be cloned into lentiviral vector to facilitate a suitable sequencing.

The PCR conducted on $Gpx8^{wt/wt}$ and $Gpx8^{-/-}$ mouse tissues confirmed the presence of deletion by CRISPR/Cas9. All DNA originating from tissues of $Gpx8^{-/-}$ mice were smaller

compared to *Gpx8*^{wt/wt} samples (Fig. 25C). The results of cDNA amplification indicated the presence of an alternative gene product, although the size of this variant was significantly smaller than the so far known splice variant of *Gpx8* (Fig. 25D). Therefore, it is rather unlikely that this product is responsible for the residual protein level which was seen on the Western blot. Following the PCR amplification, DNA was isolated from the samples and sent for sequencing, however the analysis failed. Thus, these DNA products first have to be cloned into lentiviral vector to allow the further investigation of a possible splicing variant.

4.8.2. Generation of MEFs from *Gpx8*^{-/-} and *Gpx8*^{wt/wt} mice

The advantage of this method, compared to the previously applied CRISPR/Cas9 genome editing in isolated MEFs (4.4.1.), is the lack of any virus residues including lentiviruses etc. For this purpose, *Gpx8*^{wt/wt} and *Gpx8*^{-/-} mice were mated separately to minimize the chance of possible cross-contamination between the embryos during the isolation procedure. The embryos were sacrificed at day of 13.5 of embryonic development and kept at least for 20 passages in an incubator with a controlled O₂ concentration (3 % O₂ and 5 % CO₂) to enhance immortalization of the cells (Fig. 26A) [248]. The genotypes of MEFs, originated from single embryos, were verified by both PCR amplification and immunoblot analysis (Fig. 26B,C).

Since my previous findings indicated an accumulation of LC3-II in GPX8 KO MEFs (Fig. 13A), LC3 conversion was also determined in primary MEFs by Western blot. Nevertheless, former observations could not be confirmed, as there was no accumulation of LC3-II in *Gpx8* KO MEFs as compared to control cells (Fig. 26C). Preliminary results exhibited morphological alterations in GPX8 KO cells upon glucose starvation (Fig. 14), therefore a cell viability assay was performed using different mediums: (1) high glucose standard DMEM, 10% FCS, (2) high glucose DMEM supplemented with 1% FCS, (3) DMEM without glucose, 5% FCS, (4) DMEM without glucose 10 % FCS. Thereby, GPX8 KO MEFs showed a significantly higher sensitivity to glucose starvation than WT cells (Fig. 26D). This could be the consequence of an aberrant metabolism, such as the KO cells, for a yet unidentified reason, preferentially utilize glucose as an energy source. Interestingly, under glucose starvation in the presence of 10% FCS, the GPX8 KO MEFs were more sensitive than when

kept on 5% FCS. This phenomenon can be explained by the higher concentration of growth factors in 10% FCS, which promote cell proliferation and growth, while the required energy for this purpose is not available.

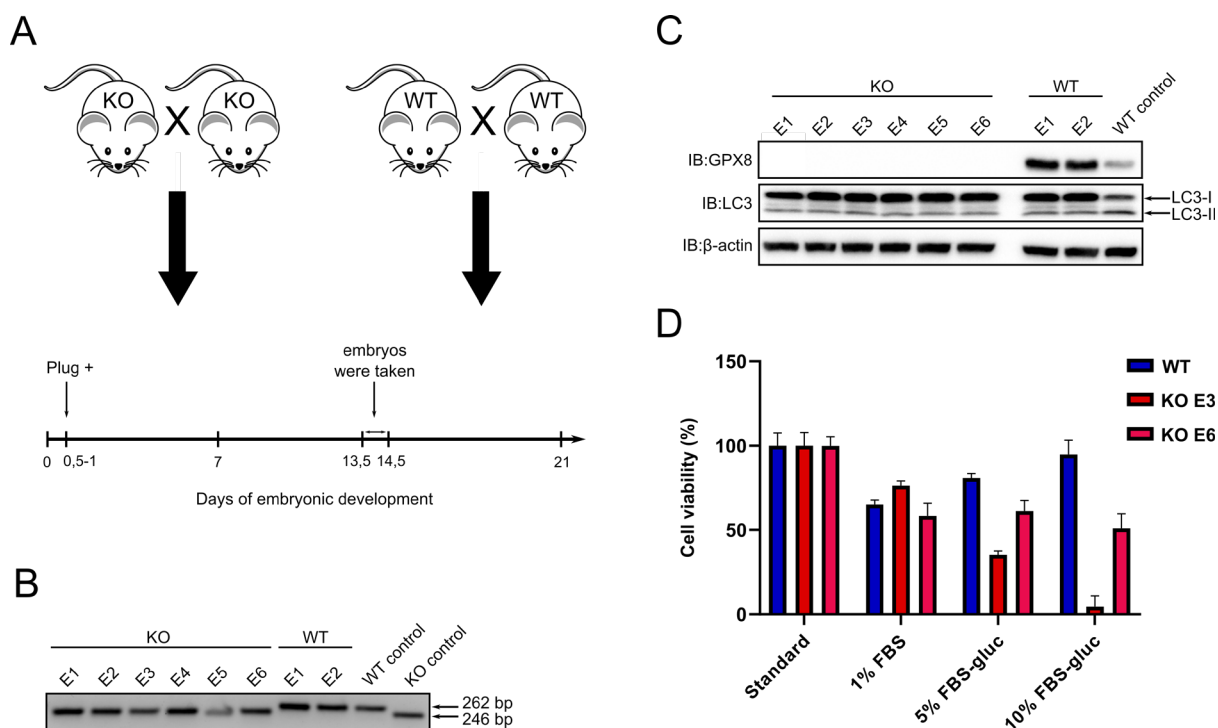


Figure 26 Isolation of primary MEFs from *Gpx8*^{-/-} and *Gpx8*^{wt/wt} animals

(A) Workflow of the procedure of generating MEFs from *Gpx8*^{wt/wt} and *Gpx8*^{-/-} mouse embryos. The scheme shows that homozygous wild type and knockout animals were taken for the breeding and the embryos were sacrificed between 13.5-14.5 days of the embryonic development. (B) MEFs isolated from the embryos were genotyped. The results confirmed that the cells, derived from the two offspring of *Gpx8*^{wt/wt} breeding, were also wild type (262 bp), while the cell lines originated from the embryos of *Gpx8*^{-/-} breeding were all knockout (246 bp). (C) Immunoblot analysis of the newly generated MEF cell lines. GPX8 protein level could not be detected in any of the GPX8 KO MEF lines, confirming the data of genotyping PCR. Since preliminary data indicated increased LC3-II level in CRISPR/Cas9 mediated *Gpx8* KO MEFs, LC3 levels were also investigated by Western blot. However, in this case there was no significant difference in LC3-I/II level between WT and KO MEFs. (D) Cell viability assay was performed on newly generated MEF cell lines. One WT cell line (WT E1) and two KO cell lines (KO E3, KO E6) were challenged to various starving conditions. Both KO cell lines were remarkably sensitive to glucose starvation, and interestingly it was more evident using 10% FBS than if the medium was completed with 5% FBS.

4.8.3. MUFA and PUFA prevent palmitic acid and SCD1 inhibitor induced cell death in GPX8 KO MEFs

To confirm the previous results (Fig. 16) on GPX8 KO MEFs isolated directly from *Gpx8*^{-/-} mouse embryos, the former cell viability assay was repeated using PA and SCD1 inhibitor in a concentration-dependent manner. For this purpose, two GPX8 KO cell lines (E3, E6) and one control WT cell line were used. 24 hours after the treatment, AquaBluer cell viability assay was assessed. The data demonstrated a similar outcome to the previously observed effect. GPX8 KO MEFs were remarkably sensitive to the lethal stimuli induced by PA, and the effect was more severe if PA was simultaneously used with a SCD1 inhibitor (Fig. 27A).

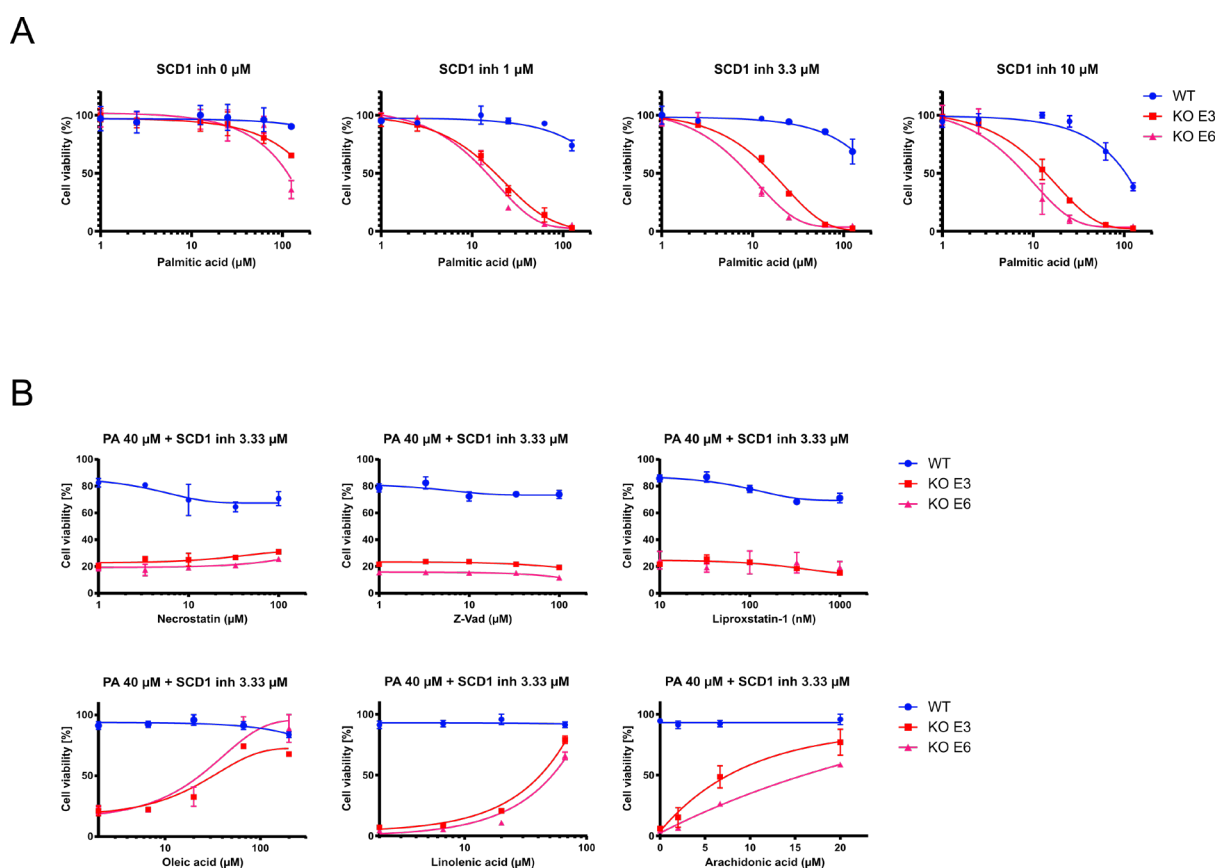


Figure 27 MUFA and PUFA prevent palmitic acid and SCD1 inhibitor induced cell death in *Gpx8* KO MEFs

(A) Cell viability assay demonstrates that *Gpx8* KO MEFs isolated from CRISPR/Cas9 edited knockout mouse embryos are also very sensitive to PA compared to WT cells. In addition, SCD1 inhibitor supplementation increased the observed sensitivity, which confirmed the previous results

of experiments which were conducted on MEFs, directly targeted with CRISPR/Cas9 (Fig. 16). **(B)** PA and SCD1 inhibitor induced cell death were prevented by oleic acid, one of the final products of enzymatic activity of SCD1, and also with linoleic acid and arachidonic acid supplementation.

In order to identify the cell death mechanism behind the observed phenomenon, different cell death inhibitors were used to investigate whether any of them could prevent PA and SCD1 inhibitor induced cell death in GPX8 null MEFs. To address this, the cells were preincubated for 2 hours with the particular inhibitor in a concentration-dependent manner and subsequently treated with the combination of 40 μ M PA and 3.3 μ M SCD1 inhibitor. Necroptosis, apoptosis and ferroptosis pathways were triggered by necrostatin-1, z-VAD-fmk and liproxstatin-1 respectively. In fact, none of these inhibitors were able to inhibit cell death, unlike oleic acid which could effectively prevent the lethal stimuli. Oleic acid, generated from stearic acid is one of the final products of SCD1. In addition, other unsaturated fatty acids were used including linolenic acid and arachidonic acid, as these polyunsaturated fatty acids (PUFA) were also able to increase cell viability and prevent PA and SCD1 inhibitor induced cell death.

4.8.4. Knockout of GPX8 decreases body weight gain on high fat diet mice

To gain a better understanding of the *in vivo* function of GPX8, the generated CRISPR knockout mouse model (see 4.8.1.) was used for further *in vivo* studies. ER stress has been indicated to be involved in the pathomechanisms of diet induced obesity [249, 250]. In addition, *in vitro* studies showed that lack of GPX8 sensitizes MEFs against saturated fatty acid induced cell death (4.4.3. and 4.8.3.), and that the protein is dynamically regulated upon ER stress. Considering these together, the high fat diet was chosen as a stress model to investigate the role of GPX8 *in vivo*.

Diet induced obesity is a commonly used stress model for mice to investigate pathomechanisms of obesity and obesity-related diseases including type 2 diabetes and cardiovascular diseases. To address this, 10 weeks old *Gpx8*^{-/-} and *Gpx8*^{wt/wt} mice were grouped in separated cages according to their gender and genotype. 9-11 male and female

animals were taken of each genotype and fed with a 45% high fat diet (3.7.3) for 20 weeks. The body weight and food intake were measured every week.

The results demonstrated that *Gpx8*^{-/-} males exhibited lower body weight from the beginning of the experiment (Fig. 28), a difference that remained evident for the duration of experiment (20 weeks). Body weight gain was also lower in *Gpx8*^{-/-} males; however, when body weight gain was normalized to body weight (body weight increase in percentage), the difference was much less significant, and after 15 weeks not evident anymore. While female mice did not exhibit significant differences in body weight at the start of the high fat diet (week 0), the body weight curves of *Gpx8*^{wt/wt} and *Gpx8*^{-/-} mice opened up with the progress of the experiment. Body weight, body weight increase, as well as body weight gain in percent, showed that *Gpx8*^{-/-} females were more resistant to fat accumulation under a high fat diet. After the experiment, half of the animals were taken for blood collection and organ withdrawal to further analyze the tissue by Western blot and immunohistochemical staining (3.6.5).

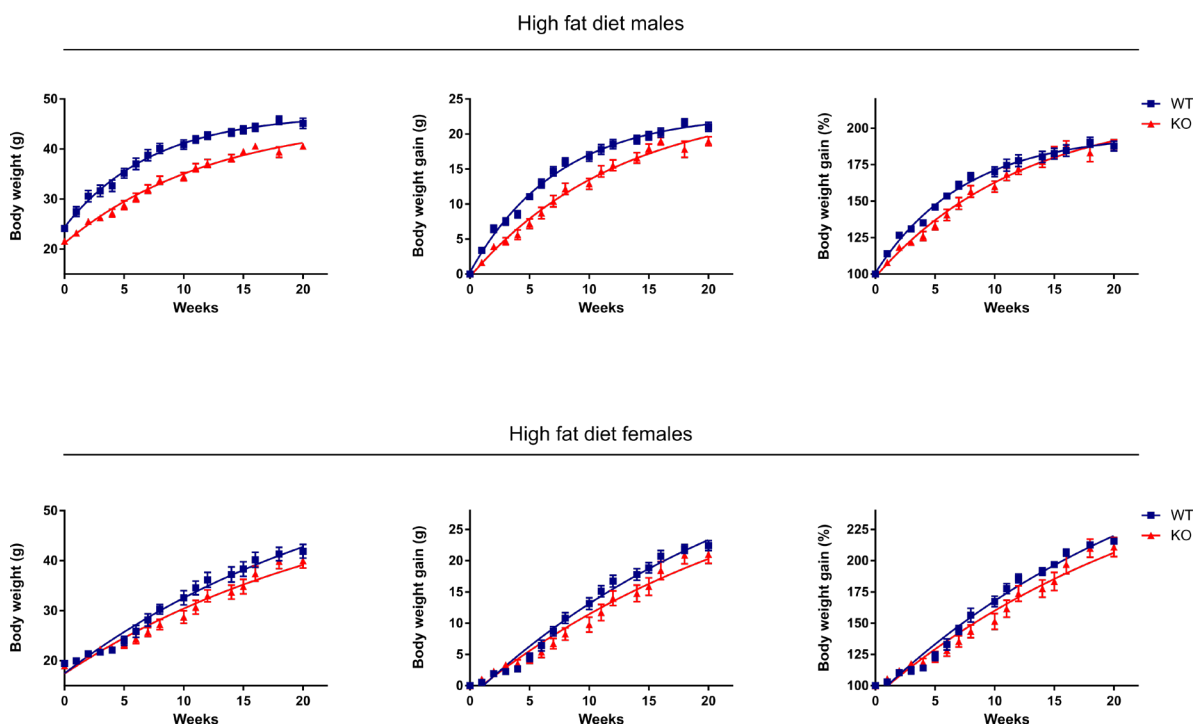


Figure 28 Monitoring body weight of *Gpx8*^{wt/wt} and *Gpx8*^{-/-} animals under high fat diet (45%)

Summary of the *in vivo* experiment in which *Gpx8*^{wt/wt} and *Gpx8*^{-/-} mice were challenged to 45% high fat diet for 20 weeks. Body weight was monitored every weeks during that period. Week 0

indicates the start of the high fat diet feeding, when the animals were 10 weeks old. The data represents the results of 10 $Gpx8^{wt/wt}$ and 11 $Gpx8^{-/-}$ males, and 9 $Gpx8^{wt/wt}$ and 9 $Gpx8^{-/-}$ females.

The other half of the animals were kept for two more weeks on the diet and subsequently taken to determinate body composition by EchoMRI™. This is a non-invasive monitoring method which provides valuable information of body composition including body fat (g), lean weight (g), total water (%) and free water (%).

EchoMRI™ is an approach that is very rapid, reliable and appropriate for living subjects, however it still requires animal protocol. Since we did not have one at the endpoint of the study, after the body weights were measured, the animals were sacrificed prior to place them into the instrument.

After the measurement was carried out, the results were analyzed by GraphPad Prism. $Gpx8^{-/-}$ males exhibited lower body weight (g), body fat, lean weight and total water, while free water was slightly increased. Female mice did not show significant differences in any of these parameters, as the standard deviation tended to be more variable than the difference itself.

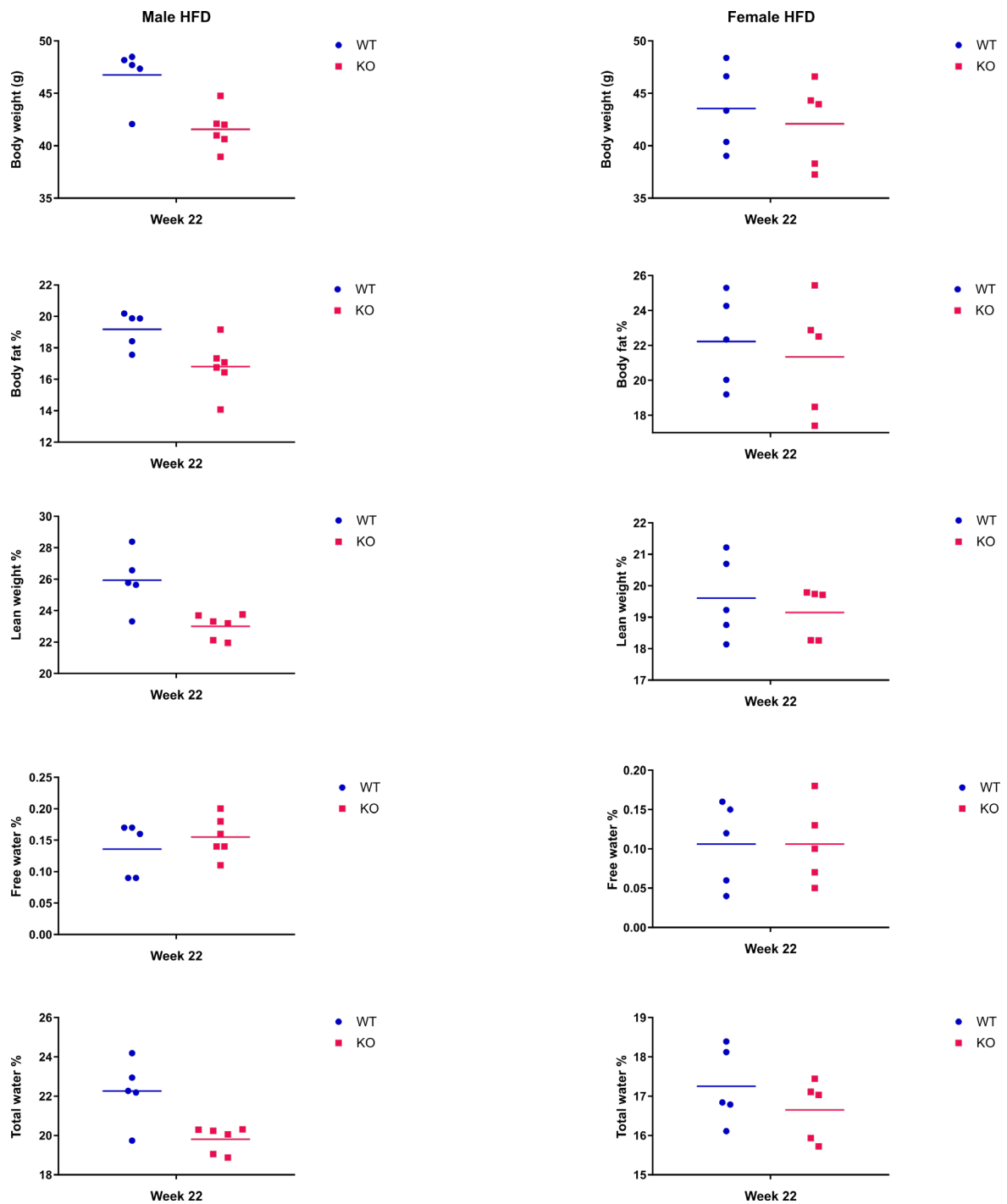


Figure 29 Body composition analysis by EchoMRI™

At the endpoint of the experiment, the body composition of the animals was analyzed by a non-invasive NMR-MRI based method (EchoMRI™). Body fat, lean mass, total water and free water were examined by the instrument, while body weights were measured before the analysis was conducted.

4.8.5. Structural analysis of *Gpx8*^{wt/wt} and *Gpx8*^{-/-} liver of HFD fed animals

It is known that a high fat diet not only affects adipose tissue but also induces dramatic changes in liver tissue [251, 252]. Therefore, the livers of *Gpx8*^{wt/wt} and *Gpx8*^{-/-} mice were analyzed after feeding them a high fat diet for 20 weeks as described before (3.6.6).

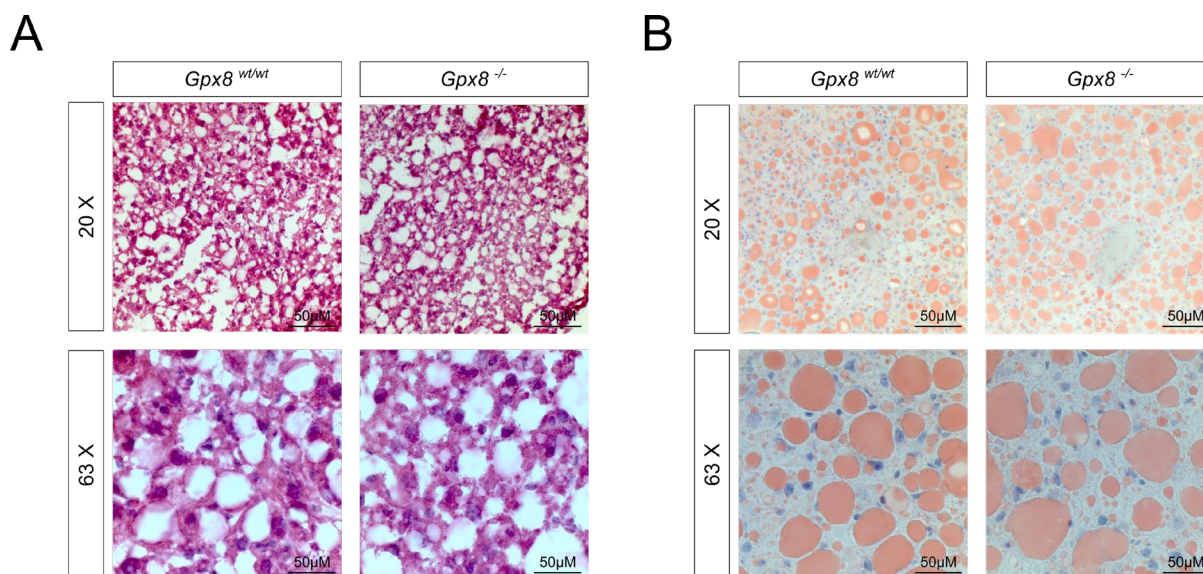


Figure 30 Analysis of liver tissue from *Gpx8*^{wt/wt} and *Gpx8*^{-/-} animals kept on high fat diet

(A) Histological analysis of liver tissues by H&E staining showed no evident difference in *Gpx8*^{wt/wt} animals compared to *Gpx8*^{-/-} (B) Neutral lipids were analyzed by Oil Red-O staining of liver of *Gpx8*^{wt/wt} and *Gpx8*^{-/-} mice kept on high fat diet (45%) for 20 weeks. The pictures were taken by Axioplan2 Imaging microscope (Zeiss). The magnification and scale bars are indicated on each pictures.

Hematoxylin&Eosin (H&E) staining and Oil red-O staining were conducted on frozen liver sections. Animals developed severe hepatic steatosis, which was already assumed based on H&E staining (Fig. 30A -white area-) and confirmed by Oil red-O staining (Fig. 30B). However, no evident difference was observed in the amount or size of accumulated lipid droplets in the liver tissue when *Gpx8*^{wt/wt} and *Gpx8*^{-/-} animals were compared.

4.8.6. Transmission electron microscopy indicates aberrant mitochondria in *Gpx8*^{-/-} animals

Transmission electron microscopy was performed with different mouse tissues to investigate the impact of the knockout of GPX8 on a cellular level *in vivo*. The tissues were prepared as described above (3.6.7) and analyzed in collaboration with Dr. Michaela Aichler (Core facility of Helmholtz Zentrum Munich). For this purpose, heart, liver, white adipose tissue (WAT), brown adipose tissue (BAT) and pancreas were dissected from *Gpx8*^{-/-} and *Gpx8*^{wt/wt} animals.

Under non-stressed circumstances, knockout of GPX8 showed an obvious phenotype affecting the mitochondria, which was especially severe in the heart and WAT (Fig. 31). However, pancreas did not show to be effected by the genetic loss of GPX8 expression. Tissues derived from GPX8^{-/-} animals exhibited damaged mitochondria with a tendency towards a decreased number of cristae (Fig. 14). However, the number and size of the mitochondria in different tissues were comparable between the two genotypes. In addition, after analyzing ER-mitochondria contact site, no evident difference was observed in tissues from *Gpx8*^{-/-} mice compared to *Gpx8*^{wt/wt} mice. Interestingly, the organs which prefer to use fatty acids to produce ATP, such as the heart and WAT, tended to be more affected by the absence of GPX8. This is in line with the previous findings, that GPX8 might be involved in lipid metabolism and that MEFs lacking GPX8 are more sensitive to glucose starvation (Fig. 26D) and lastly, that mitochondria of glucose starved GPX8 KO MEFs exhibited a similar phenotype (Fig. 14) which can be observed in the heart and WAT from *Gpx8*^{-/-} animals.

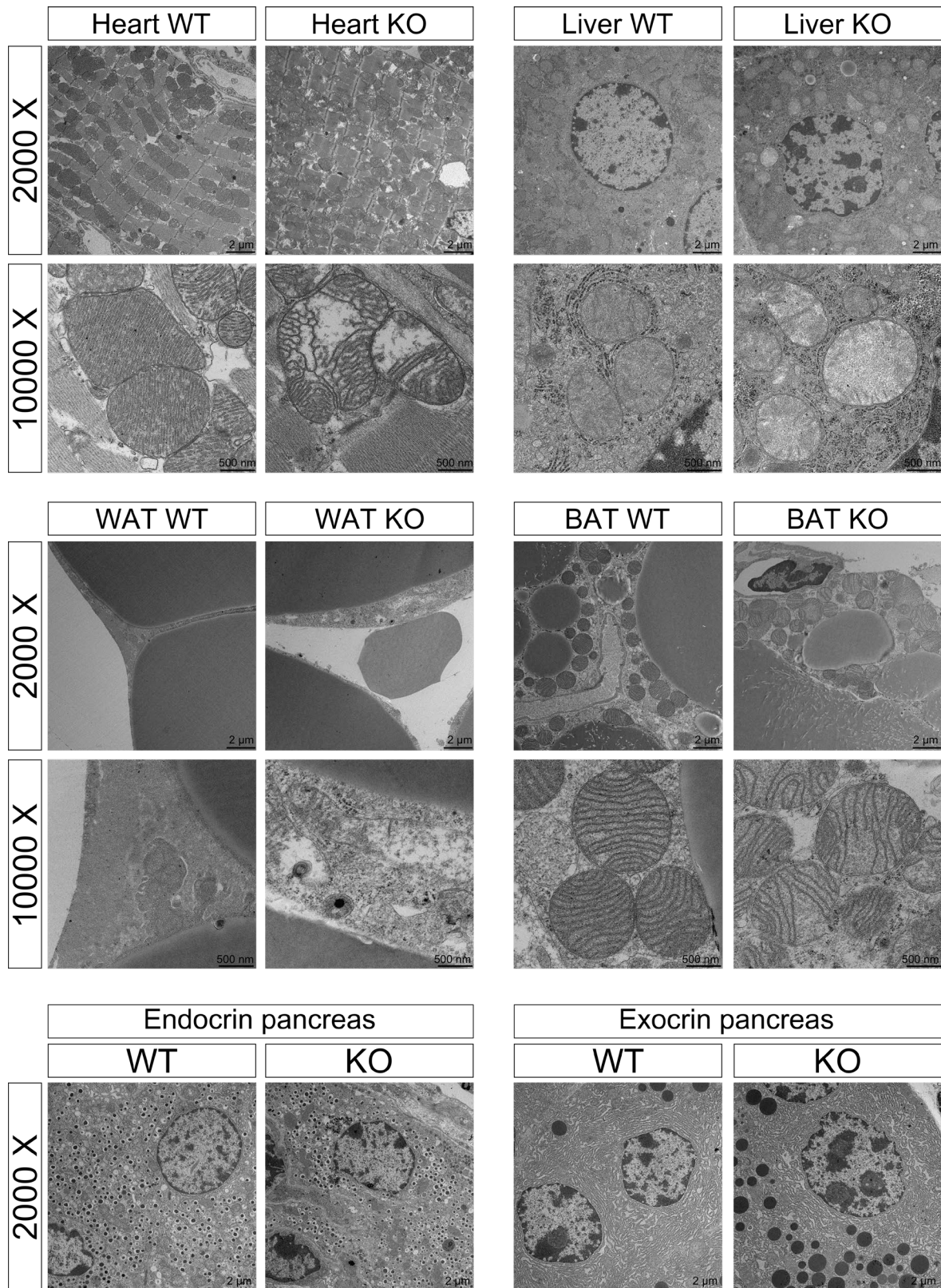


Figure 31 Transmission electron microscopy of tissues from CRISP/Cas9 edited *Gpx8*^{-/-} animals indicated aberrant cristae formation in the mitochondria

Ultrastructural analysis by transmission electron microscopy of *Gpx8*^{-/-} mouse tissues demonstrate abnormal mitochondrial structures in heart, liver, WAT and BAT. Lack of GPX8 lead to decreased

crisetae formation especially in the heart and WAT, which are known to prefer fatty acids as energy sources. However, in the pancreas no evident difference was observed. The data was kindly provided by Dr. Michaela Aichler, Helmholtz Zentrum München.

5. DISCUSSION

5.1. Monoclonal antibody production

Monoclonal antibodies are produced by identical cell clones, which are expanded from a single immune cell. Due to this property, they have monovalent affinity and bind to the same epitope of the antigen. Therefore, generally mABs are more specific to the particular protein and are better suited for immunoblot analysis or even for immunotherapy. However, for some applications, including immunohistochemical staining or co-immunoprecipitation, polyclonal antibodies are preferable.

Hybridoma technique was used to generate mouse and human GPX8 mABs, which were then tested by immunoblot analysis using cells that were stably infected with a virus expressing mouse or human GPX8, respectively. During the antibody screening, the selected mABs clones showed remarkable specificity and sensitivity for the antigen. However, cells with lentiviral overexpression of GPX8 are not comparable with its endogenous expression. Therefore, it is far easier to detect GPX8 in cells, which overexpress it. This was seen not only when mouse GPX8 AB was tested on wild type MEFs, but also when the human GPX8 AB was tested on other human cell lines (4.1).

```

GPX8_MOUSE  MEPFAAYPLKCSGPKAKIFAVLLSMVLCTVMLFLLQLKFLKPRTNSFYSSFYEVKDAKGRTV 60
GPX8_HUMAN  MEPLAAYPLKCSGPRAKVFAVLLSIVLCTVTLFLLQLKFLKPKINSFYAFYEVKDAKGRTV 60
          ***:*****:***:*****:***** *****: *****:*****

GPX8_MOUSE  SLEKFKGKASLVNVASDCRFTDKSYQTLRELHKEFGPYHFNVLAFPCNQFGESEPKSSK 120
GPX8_HUMAN  SLEKYKGVSLVNVASDCQLTDRNYLGLKELHKEFGPSHFSVLAFPCNQFGESEPRPSK 120
          ****:***.*****:***:.* *:****** **.******: **

GPX8_MOUSE  EVESFARQNYGVTFPIFHKIKILGPEAEPAFRFIVDSSKKEPRWNFWKYLVNPEGQVVKF 180
GPX8_HUMAN  EVESFARKNYGVTFPIFHKIKILGSEGEPAFRFLVDSSKKEPRWNFWKYLVNPEGQVVKF 180
          *****:***** *.******:*****

GPX8_MOUSE  WRPEEPLEAIRPHVSQMIGQIILKKKEDL 209
GPX8_HUMAN  WKPEEPIEVIRPDIAALVRQVIKKKEDL 209
          *:****:*.***.: : *:*:*****

```

Figure 32 Homology of mouse and human GPX8

Mouse and human GPX8 show a high degree of homology. The peptides, which were used to produce mouse and human monoclonal antibodies, are marked with blue and pink, respectively.

Indeed, on any tested human cell lines, the human GPX8 mAB failed to detect the endogenous protein. This could be due to the fact, that these cells do not express the protein, or that the GPX8 level is under the detection limit of the newly generated human-specific antibody. Yet, in two human cancer cell lines the mouse GPX8 AB could efficiently detect the presence of the antigen. On one hand, this indicates that the mouse and human GPX8 show a high degree of homology at the site where the antibody binds (Fig. 32), and on the other hand it suggests that the mouse GPX8 mABs are more sensitive than the human ones.

5.2. GPX8 stability upon ER stress

Based on previous findings, it was strongly suggested that GPX8 is involved in the oxidative protein folding in the ER [83, 111, 253]. This possibility was investigated by using cell lines with different genetic modifications of Gpx8. First, WT MEFs were compared to GPX8 addback (AB) MEFs in response to several ER stress inducing stimuli. Cell viability assay was performed following thapsigargin (TG), tunicamycin and dithiothreitol (DTT) treatment, which did not show any significant difference between the two cell lines. However, when the GPX8 protein level was analyzed by immunoblot, TG induced a remarkable and rapid decrease in the protein level in WT as well as in GPX8 AB cells (4.2). Since GPX8 was originally thought to contribute to oxidative protein folding in the ER, the opposite effect, that ER stress leads to increased GPX8 level, was actually expected.

It is well-known that TG induces ER-stress due to SERCA inhibition and consequently Ca^{2+} depletion in the ER [254]. Ca^{2+} is required for many biological processes including proper function of chaperons, which are involved in protein folding, introduction of post-translational modification in target proteins and also lipid biosynthesis [204]. Hence, the presence of ER stress was investigated in WT and GPX8 AB cells following TG treatment. The expression of unfolded protein response (UPR) markers such as GRP78, pPERK and Xbp1 splicing, were similar in their response to the treatment between the two cell lines. Interestingly, as the level of GRP78 and pPERK increased, the degradation of GPX8 exhibited a similar tendency. This experiment was repeated on Gpx8 KO MEFs using two additional SERCA inhibitors, 2,5-di-t-butyl-1,4-benzohydroquinone (BHQ) and

cyclopiazonic acid (CPA). Cell viability demonstrated no significant difference between GPX8 KO and WT cells, however GPX8 degradation was observed in WT MEFs using any of these structurally unrelated SERCA inhibitors. Moreover, PERK phosphorylation and GRP78 expression indicated the activation of UPR, which was comparable in GPX8 KO and WT cells.

Taken together, despite the fact that GPX8 is dynamically regulated upon ER stress induced by SERCA inhibitors, it is rather unlikely that GPX8 promotes protein folding under ER stress. If that were to be the case, overexpression of GPX8 would likely show a protective effect in cell viability against these drugs, and a possible involvement of GPX8 in protein folding would rather suggest an increased protein level in response to ER-stress, like in the case of other chaperones such as GRP78. In addition, if this hypothesis was true, GPX8 KO would lead to an increased ER stress response under SERCA inhibition, which was not the case. Indeed, a recent study also failed to show that GPX8 contributes to the oxidative protein folding process in INS-1E β -cells [115].

UPR triggers temporary inhibition of general translation by arresting the initial step of protein synthesis and, in parallel, enhances the clearance of defective proteins by proteasomal degradation and autophagy, thereby promoting cellular adaptation [255-257]. To mimic ER stress-induced inhibition of general protein synthesis, emetine, a drug that inhibits protein synthesis by binding to the 40S subunit of ribosome in eukaryotic cells [208], was applied. Translational inhibition led to GPX8 degradation, similar to TG treatment. In addition, when emetine was used in combination with TG, it exacerbated the effect of TG on GPX8 degradation. However, MG132 stabilized the protein, indicating the involvement of proteasome in GPX8 breakdown. These data also demonstrate that GPX8 is a dynamically regulated protein with a very short half-life. Therefore, there is a possibility that the previously seen degradation of GPX8 in response to TG is the consequence of the inhibition of general translation and the short half-life of GPX8.

The ER-associated protein degradation (ERAD), a precisely regulated process, is required for the clearance of misfolded/unfolded proteins via the proteasome. ERAD consists of three distinct ubiquitin ligase complexes (RNF5, MARCH6, SYVN/AMFR/HRD complex), which share several common motifs although some components differ among the

complexes as shown in Fig. 33. Taking advantage of these differences, the individual complexes were inhibited using siRNAs, in order to examine whether one or more of them may have an impact on GPX8 stability. Interestingly, under basal conditions, all of the siRNAs significantly increased the protein level of GPX8. However, under TG treatment, GPX8 degradation was observed in all cases and the protein level did not show that siRNAs significantly inhibited protein degradation. This data indicates that under non-stressed conditions, GPX8 stability is partially controlled by the ERAD quality control machinery with the highest impact of HRD complex, while under TG induced ER-stress, other protein degradation pathways are most likely involved. Moreover, it has to be mentioned, that due to the lack of antibodies, the efficiency of the siRNAs could not be confirmed so far. Alternatively, real-time RT-PCR would be an option to monitor mRNA level of these ERAD complex subunits.

In order to investigate whether GPX8 undergoes autophagic degradation in response to TG, an inhibitor study was conducted. This study showed that GPX8 degradation is partially inhibited not only by proteasome inhibitor but also by an autophagy inhibitor (chloroquine). However, the precise mechanism of action of chloroquine is not fully understood yet, as it has been shown that chloroquine targets other pathways besides inhibiting lysosomal degradation [211, 212]. Additionally, another explanation could be that the two clearance pathways in the cells are not completely distinct, and recent evidence actually suggests that autophagy and proteasomal degradation activity are precisely orchestrated via certain factors [258]. Therefore, it can be hypothesized that inhibiting one of these pathways could affect the activity of the other pathway, as it was previously demonstrated by other groups already [259, 260].

Since inhibitors frequently have multiple targets, lysine mutants of GPX8 were expressed in GPX8 KO MEFs and challenged to TG treatment to further investigate the mechanisms of GPX8 breakdown by proteasomal degradation process. The data indicated that GPX8 stability is strongly dependent on the presence of its cytosolic lysine (K10, K15 and K17). Among them, the mutation of K10 to arginine led to the most robust inhibitory effect of GPX8 breakdown upon SERCA inhibition. This is in line with previous findings, which demonstrated that GPX8 is important for HCV virus particle production.

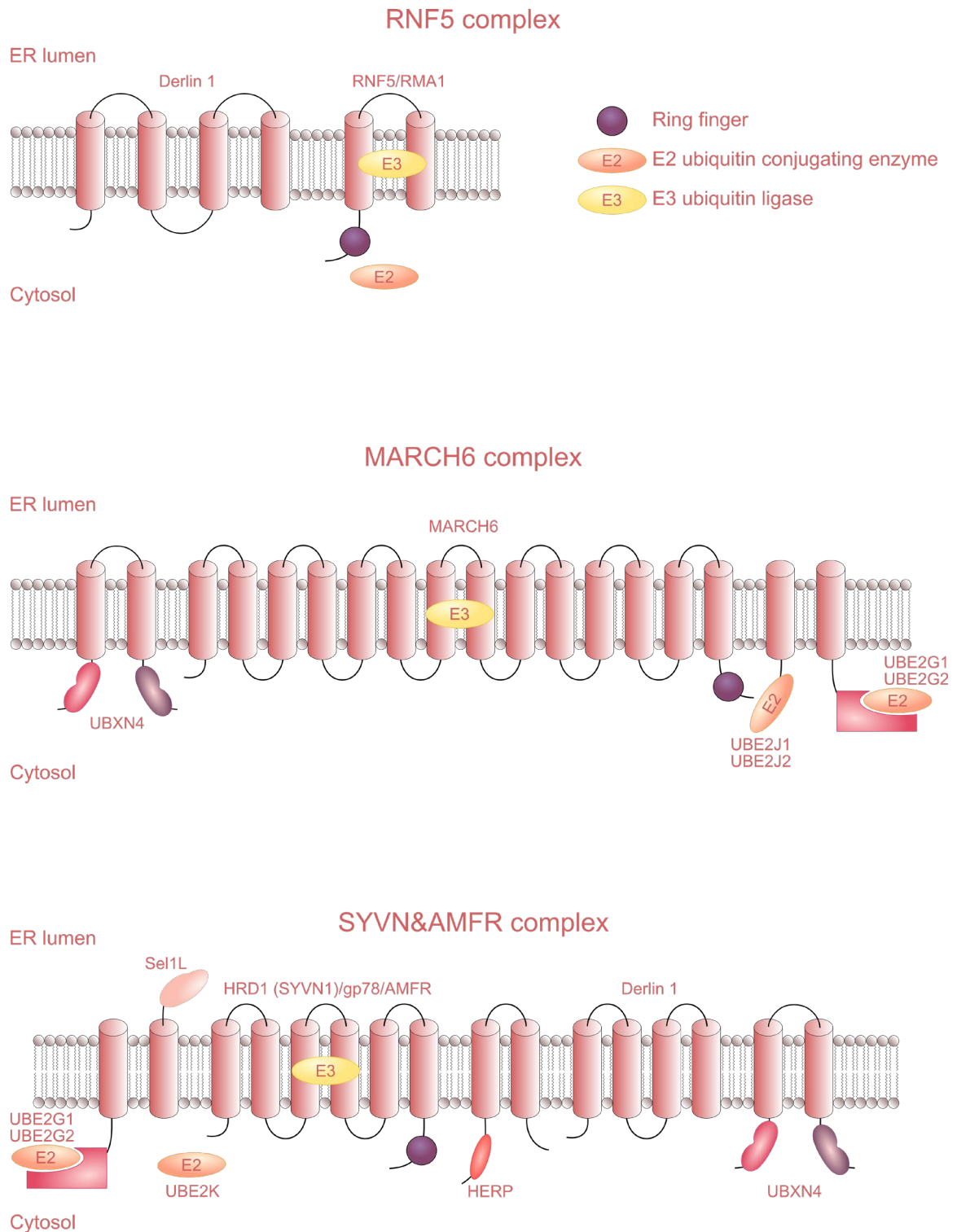


Figure 33 The scheme represents the three different ERAD complexes in the ER membrane.

Despite similar features, in all complexes unique subunits can be found. Taking the advantage of these differences, the individual complexes were inhibited using siRNA, specific for each complex. Figure adjusted from [261].

Also, the virus protease NS3-4A targets GPX8 and cleaves at C11, suggesting, that it might be necessary for the virus to stabilize the human GPX8 protein in order to ensure efficient virus particle production [109]. Yet, the proteasome and autophagy dependent GPX8 degradation process has to be investigated in more detail, although this might be challenging since it is hard to specifically inhibit GPX8 degradation via autophagy.

Equally important, as GPX8-YFP expressing cells allowed to monitor the subcellular localization of the protein, SERCA inhibitors were applied to identify possible changes in GPX8 subcellular localisation before its degradation occurred. The results revealed that despite the three chemicals used to inhibit SERCA, the effect on GPX8-YFP localisation was quite different. While treating MEFs with CPA and TG showed a more similar effect on GPX8 localisation, except for that among them only TG induced accumulation of GPX8 in a close proximity to nucleus, BHQ resulted in accumulation of GPX8 in the nucleus and in defined circular structures within the cytosol. Even when NOX1/NOX4 was inhibited, it did not lead to apparent changes in the effect of BHQ. The most obvious explanation would be that GPX8 serves as a co-transcriptional factor in response to BHQ treatment, however, this hypothesis has to be confirmed by for instance co-immunoprecipitation under BHQ treatment. It is tempting to speculate that upon SERCA inhibition, GPX8 binds to a yet to be identified transcription factor thereby localising to the nucleus. In addition, it would be also interesting to know whether the localization of GPX8 is dependent on the presence of its individual cysteines, therefore, ongoing experiments must attempt to address this question.

5.3. Characterization of CRISPR targeted GPX8 knockout in MEFs

Since the knowledge regarding the physiological function of GPX8 is scarce and there is no knockout models published yet, CRISPR/Cas9 technology was applied to introduce genetic interruption of *Gpx8* in MEFs, a model that should be used for further *in vitro* functional studies. The first strategy applied single guides and resulted in only one positive clone which was detected as a knockout according to immunoblot analysis. However, sequencing data indicated a bi-allelic modification, including a 10 bp deletion on one allele and a 6 bp deletion on the other allele. Unfortunately, the 6 bp deletion was an in-frame mutation,

consequently leading to the deletion of 2 amino acids in the protein. Nonetheless, the GPX8 protein could not be detected by immunoblot in this particular clone (4.4.1).

In order to improve the efficiency of CRISPR/Cas9 system, in the second attempt two guides were used simultaneously. Based on genotyping PCR and immunoblot analysis, several KO clones were identified that were generated by this approach. However, the exact deletion (191 bp) could be evaluated only in clone 28 (Cl28). The first evident phenotype of the KO clones were assessed, when cells reached high confluency, large vesicles developed within the cytosol. This phenomenon was observed in three out of four KO clones. The first consideration was that these structures might be a form of lipid droplets, therefore the cells were stained by lipid droplet specific dye (BODIPY 493/503). Unfortunately, the results could not confirm the hypothesis as the vesicles were not stained by the dye (Supplementary Fig. 1). Nevertheless, similar structures were noted when the cells were treated with chloroquine, which blocks the fusion of autophagosome and lysosome. Consequently, autophagosomes accumulated in the cell due to the lack of their clearance mechanism. To investigate the possibility of accumulation of degradation-incompetent autophagosomes, LC3-I/ LC3-II conversion was analyzed by immunoblot, which indicated accumulated LC3-II in the KO clones. The ratio between LC3-I and LC3-II is tightly regulated by different factors. In a proper autophagic flux LC3 is produced and cleaved by ATG proteins, thereby generating LC3-I which is subsequently fused to the membrane bounded PE and finally LC3-II is formed. LC3-II stays conjugated as long as the autophagosome fuses with the lysosome. Depending on which leaflet of the membrane LC3-II takes place, it is either degraded within the lysosome or converted back to LC3-I [53]. Accordingly, the accumulation of LC3-II is a sign of a decelerated or arrested autophagic flux [210, 211, 262]. This idea is supported by the electron microscopy data since the vesicles accumulated upon glucose starvation, which has been shown to induce autophagy via mTORc inhibition by AMP-activated protein kinase (AMPK) [263-265]. Additionally, the vesicles were partially surrounded by double membranes, which are also typical for autophagosomes, although in Gpx8 KO MEFs, these membranes were not closed around the vesicles, which is indeed atypical for a proper autophagosome. Taken together, it can be hypothesized, that a lack of GPX8 hinders the clearance of cell debris by lysosomal degradation. However, in contrast to these findings, GPX8 KO MEFs, isolated directly from CRISPR/Cas9 targeted mice, were

sensitive to glucose-starvation but did not show an increased level of LC3-II or an accumulation of “atypical autophagosome-like” vesicles. After discussing with Dr. Tadauki Tsujita (Saga University, Japan) sample preparation might be highly critical to reliably detect LC3-II levels in cells, thus a careful consideration is warranted. PE conjugation can be rapidly destroyed by a longer or stronger isolation step, therefore the experiment has to be repeated taking into account these considerations.

Moreover, lipid hydroperoxides were analyzed by FACS, which, unlike Gpx4 KO [71], demonstrated no accumulation of LPOOH/LOOH in Gpx8 KO MEFs compared to WT cells. Additionally, when the cells were challenged with RSL3, which is a well-known inducer of LOOH/PLOOH accumulation, no difference was observed when comparing GPX8 KO to WT MEFs. To exclude a possible compensation mechanism of GPX8 homologues, immunoblot analysis was performed, which indicated no effect of GPX8 level on GPX4 and GPX7 expression levels. This finding was confirmed by microarray analysis, which showed no transcriptional regulation of any GPX family members if Gpx8 expression was disrupted or promoted (4.6.2). Consequently, despite a high degree of homology between GPX8 and GPX4, knockout of GPX8 in MEFs does not present any well-known hallmarks of cells lacking GPX4 [67]. Unlike Gpx4, GPX8 KO MEFs are viable and do not exhibit increased level of LOOH/PLOOH compared to WT cells.

To investigate whether cells lacking GPX8 are more sensitive to any cell death inducing drugs, cell viability assay was performed using several cell death inducing stimuli. Indeed, GPX8 KO MEFs did not show sensitivity to any classical cell death inducing agents, including RSL3, erastin, chloroquine, AGK-2, auranofin, and endosome inhibitors (OcTMAB, MiTMAB, Pro-myristic). However, cells in lack of GPX8 were highly sensitive to saturated fatty acids, especially when SCD1 was inhibited.

Introducing CRISPR/Cas9 knockout in cultured cells is a convenient and reliable way to study the function of the protein of interest. However, taking the advantage of the *Gpx8*^{-/-} mouse, new cell lines were established. Since the mouse was generated by injecting CRISPR guide RNA and Cas9 mRNA into single cell embryo, the benefit of these cell lines is the lack of any residual viruses. Therefore, these primary MEFs were immortalized by culturing at low oxygen tension for more than 20 doubling times and used for further *in vitro* studies.

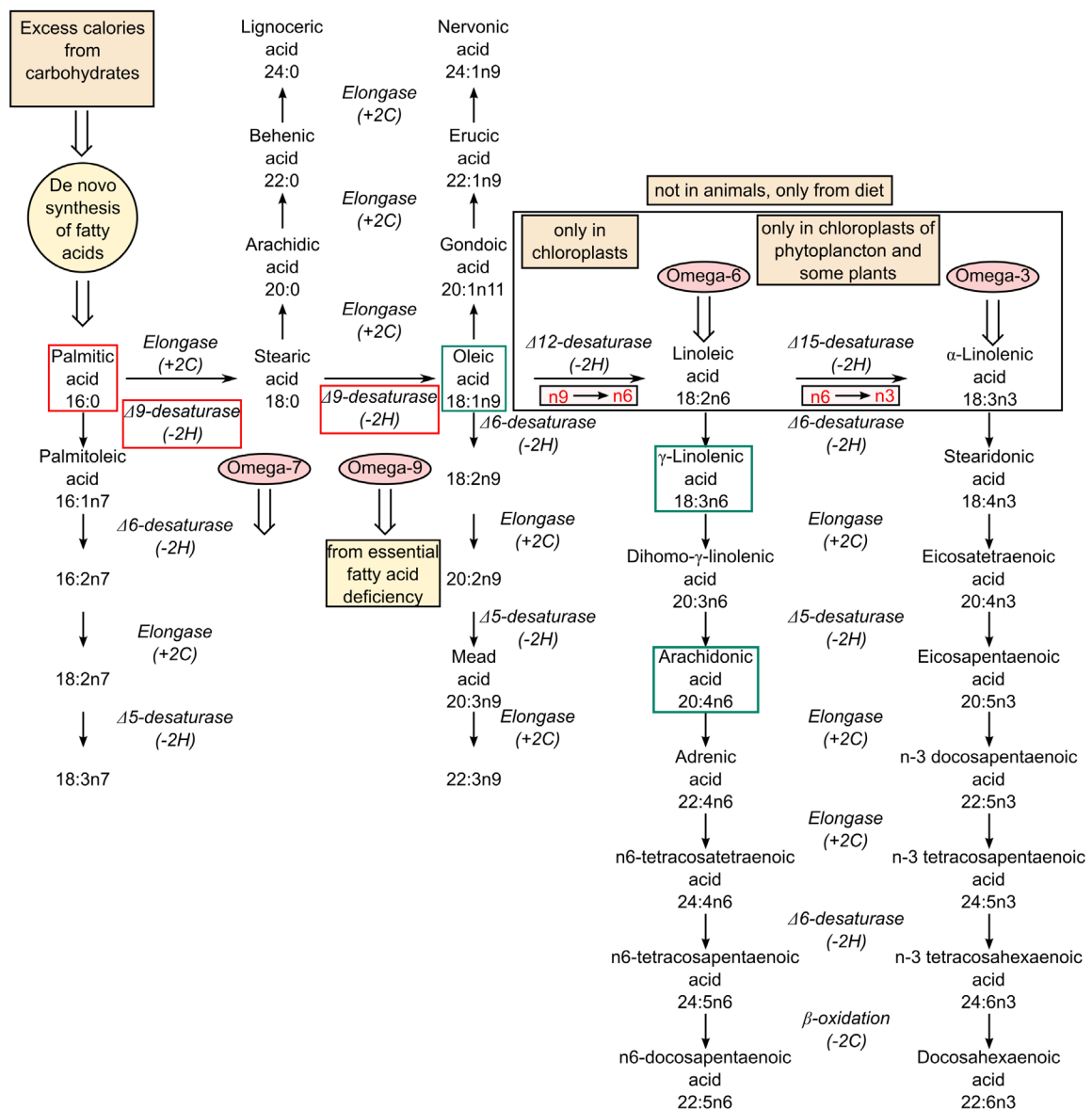


Figure 34 Biosynthesis of fatty acids in eukaryotic cells.

Steps that only take place in plants are marked with the black frame. Figure adopted and modified from <http://www.tuscany-diet.net/2013/02/03/long-chain-fatty-acid-synthesis/>.

The results of these experiments confirmed the sensitizing effect of GPX8 KO to co-treatment with PA and the SCD1 inhibitor (4-(2-Chlorophenoxy)-N-[3-[(methylamino)carbonyl]phenyl]-1-piperidinecarboxamide). Additionally, the underlying cell death mechanism was investigated using apoptosis, necroptosis and ferroptosis inhibitors. Interestingly, all of these cell death inhibitors failed to rescue GPX8 KO MEFs from PA/SCD1 inhibitor induced cell death, while oleic acid could successfully prevent this

kind of cell death. Indeed, oleic acid is one of the major products generated by SCD1, indicating the importance of SCD1 activity under conditions when GPX8 is not available and when cells are exposed to saturated fatty acids. In order to investigate whether oleic acid itself is the major contributor to the prevention of cell death or if other unsaturated fatty acids are also suitable for this purpose, γ -linolenic acid and arachidonic acid were tested. In fact, both unsaturated fatty acids could improve cell viability in GPX8 KO cells. As the mammalian cells are not able to produce any of these unsaturated fatty acids using oleic acid as a substrate (Fig. 34), it is rather unlikely that oleic acid prevented cell death due to serving as an intermediate for γ -linolenic acid and arachidonic acid biosynthesis. Moreover, since both γ -linolenic acid and arachidonic acid prevented the cell death, it can also be excluded that oleic acid supplementation substituted the importance of SCD1 catalytic activity and thereby prevented cell death. Consequently, it is more likely that GPX8 KO MEFs die due to the accumulation of saturated fatty acids and that this can be compensated by the supplementation of other unsaturated fatty acids. It has been previously reported that accumulation of saturated fatty acids impairs cellular viability due to their incorporation into the ER-membranes, leading to decreased membrane plasticity [266].

Other cell viability assays demonstrated that GPX8 KO cells are highly sensitive to glucose starvation and unexpectedly, higher concentrations of FBS even worsened the phenotype. As discussed above, preliminary data suggested that MEFs lacking GPX8 are not able to fulfill proper autophagic flux, and it is well-known that autophagy, induced by glucose starvation, is essential to cell survival. Conclusively, it can be hypothesized that GPX8 KO MEFs are sensitive to glucose starvation because GPX8 is necessary for proper autophagy, and under conditions where this mechanism is required, GPX8 KO cells fail to survive. Although MEFs isolated from CRISPR targeted mice did not exhibit vesicle formation, under basal conditions LC3-II was also not accumulated. However, when these cells were analyzed by immunoblot, they were still primary cells, making it difficult to compare with previously used MEFs (CI17, CI28). Indeed, for primary cells it is preferable to keep them on high confluence as long as immortalization takes place, while immortalized cells die at high density.

Finally, Fura-2 based Ca^{2+} measurement was assessed on GPX8 KO MEFs. TG was used to inhibit SERCA and to lower ER Ca^{2+} levels via Ca^{2+} leakage through IP3R. In response to ER Ca^{2+} deprivation, a protective mechanism, SOCE, is activated. SOCE activation is intended to restore basal Ca^{2+} levels in the ER. Classically, this occurs via the interaction of ER-membrane resident STIM and plasma membrane resident Orai1 [217]. Interestingly, under SERCA inhibition GPX8 KO MEFs exhibited decreased Ca^{2+} levels in the ER which was concluded from the decreased release and subsequent refill of Ca^{2+} into the ER under TG induced SOCE. This difference was leveled out, as basal Ca^{2+} did not show differences between GPX8 KO and WT cells (4.5.2). However, it was previously reported by Sitia and his co-workers that knockdown of GPX8 leads to increased Ca^{2+} in the ER in Hela cells [114]. Nevertheless, the cell line they used for the study and the method used to decrease GPX8 level was different from our approach. Previous data revealed that GPX8 rapidly degrades upon SERCA inhibition by various drugs, and before this degradation occurs, subcellular localization of GPX8 is also changed. Moreover, the interaction partner analysis showed the highest confidence in interaction with a plasma membrane resident Slc24a3 Ca^{2+} transporter (fold change of 237,7). Not only Slc24a3 but also SERCA, with a fold change of 9.8, and IP3R, with a fold change of 4.9 (Appendix Excel 2), were detected as possible binding partners of GPX8. Therefore, it is not surprising that knockout of GPX8 exhibited such a difference on store operated Ca^{2+} entry analysis. Taken together, these data strongly suggest the involvement of GPX8 in the regulation of intracellular Ca^{2+} homeostasis, while the underlying mechanisms remain to be explored in detail.

5.4. Interaction partners and promoter analysis

In order to evaluate novel functions of GPX8, different studies were performed regarding the transcriptional regulation and identification of interaction partners of GPX8. First, *in silico* promoter analysis was performed in collaboration with Dr. Dietrich Trümbach (Helmholtz Zentrum München). The promoter region of *Gpx8* was analyzed among various organisms to identify conserved transcription factor binding sites that are related to lipid metabolism. Three highly conserved transcription factors were identified in the *Gpx8* promoter region, including PPAR γ , STAT5b and LXRB/RXR. PPAR γ has two isoforms, PPAR γ 1

and PPAR γ 2. PPAR γ 1 is ubiquitously expressed, while PPAR γ 2 is mainly present in adipose tissues, in colon and macrophages. PPAR γ has been shown to be involved in lipid uptake in adipose tissues and to regulate glucose metabolism and fatty acid storage. Indeed, PPAR γ forms a heterodimer with RXR and thereby regulates the transcription of their target genes. It has been demonstrated that deletion of PPAR γ in adipose tissue in mice protected them from diet induced obesity and insulin resistance [219]. These findings are consistent with previously presented results, which indicated that GPX8 is highly expressed in metabolism related tissues, such as WAT and BAT. In addition, male *Gpx8*^{-/-} mice exhibited lower body weight and body fat mass under a high fat diet (4.8.4) similar to *Ppar γ* ^{-/-} animals.

In two different *in vitro* binding assays, several possible interaction partners of GPX8 were identified. For this purpose, a yeast two-hybrid technique and MS-coupled co-immunoprecipitation analysis were conducted and compared. Yeast two-hybrid analysis suggested interaction between GPX8 and several members of the ubiquitin enzyme family, including ubiquitin 1, ubiquitin 2 and ubiquitin 4. These enzymes have been shown to be important for protein degradation via proteasome, ER-stress and autophagy [267-269]. Despite this, immunoblot analysis performed after co-immunoprecipitation confirmed the interaction between GPX8-STREP(2X)/FLAG and ubiquitin 1, but unfortunately, MS analysis of the same lysate could not confirm these findings. Therefore, the detected bands are most likely due to the un-specificity of the antibody. Conclusively, either the expression level was not high enough to detect ubiquitins by co-immunoprecipitation, or the results of the yeast-two hybrid technique are not relevant in mammalian cell culture. However, MS data revealed other possible interaction partners, which gave new insight into a possible function of GPX8. One of the most abundant proteins was the phosphatidylinositol-4-kinase beta (PI4KB), which has been shown to be involved in HCV viral replication, just as seen before for GPX8 [242]. PI4KB is a soluble cytosolic protein, and generates PI4P by the phosphorylation of PI. PI4P is an essential lipid present in numerous membrane compartments including the “membranous web”, a compartment where also viral replication takes place. Several interactions of PI4KB that have an impact on the localization of PI4KB has been reported to date. For instance tethering of acyl-coenzyme A binding domain containing protein 3 (ACBD3) leads to membrane localization of PI4KB

[241]. Interestingly, the tumor suppressor 14-3-3 protein family members [246, 247] were also demonstrated to interact with PI4KB and stabilize its active conformation [270].

In line with this, tapasin and Ifit-1 have also been shown to interact with GPX8. Both are important in case of infections. Tapasin forms a complex with major histocompatibility complex I (MHC I), Erp57, antigen peptide transporter (TAP), and calreticulin and this complex is crucial for antigen presentation. In fact, tapasin is one of the most important components of this complex, as it regulates the peptide repertoire of presented antigens on the cell surface [224]. Additionally, Ifit-1 is also a key regulator of antiviral response due to its unique importance in inhibition of non-self RNA translation and replication [271]. Indeed, members of Ifit protein family are the earliest and most abundant genes expressed in antiviral immune response [272, 273]. Atp1B1 was shown to be a tumor suppressor in clear cell renal carcinoma (ccRCC) [238], while more recent studies demonstrated strong correlation between high expression of Atp1b1 and poor prognosis in cytogenetically normal acute myeloid leukemia (CN-MAL) [239].

More importantly, OXA1L has been previously shown to be involved in the insertion of proteins into the inner membrane of mitochondria, such as F1Fo-ATP synthase and NADH-ubiquinone oxidoreductase, by binding with its C-terminal tail to the mitochondrial ribosomes [243, 274, 275]. Recently, a case was published describing a patient having a bi-allelic variant of OXA1L (Ser170Gln and Cys620Phe) which led to mitochondrial complex IV and V deficiency and consequently severe hypotonia and encephalopathy. The patient died at the age of 5 years due to cardiorespiratory arrest [244]. In this study, affinity purification was carried out on HEK293T cells expressing OXA1L-FLAG, but GPX8 was not identified as interaction partner of OXA1L under these experimental circumstances. However, according to The Human Protein Atlas database, the mRNA expression of *Gpx8* in HEK293T cells is very low.

The plasma membrane associated dysferlin, another possible GPX8-interactor, was reported to be involved in membrane repair in a Ca²⁺-dependent manner. In addition, dysferlin deficiency results in the development of muscular dystrophy and cardiomyopathy in mice [228, 230]. Also, several studies confirm the involvement of dysferlin in limb-girdle dystrophy and myopathy in humans [276-282]. In addition, it has been recently

demonstrated that dysferlin is closely associated with lipid droplets, and dysferlin deficiency in mice and human patients results in lipid droplet accumulation in myocytes and also enhances the adipocyte level in between the myofibers [283, 284].

Based on fold change, Slc24a3/NCKX3 is a K⁺-dependent Na⁺/Ca²⁺ exchanger and was found to be a GPX8 interaction partner with the highest confidence. Slc24a3 localizes in the plasma membrane and regulates Ca²⁺ homeostasis. It is highly expressed in the kidney and uterus, and in the latter, Slc24a3 is regulated by steroid hormones, estrogen and progesterone [285-287]. Knockout of *Slc24a3* in mice lowered mineral content in the bone and increased parathyroid hormone levels in plasma, but it did not affect body weight under a high fat diet nor did it result in changed plasma ion levels [236].

Finally, the protocadherin family members, Pcdhb18 and Pcdhga4 are poorly characterized, but the members of cadherin enzyme family are highly expressed in central nervous system and have been shown to be involved in the formation of neuronal connectivity [288]. As demonstrated here, MS-coupled interaction partner analysis revealed several interactors of GPX8 which have been shown to have similar functions to what was found *in vitro* for GPX8. Therefore, it is a good overview which helps to define the direction of further *in vitro* and *in vivo* investigations.

5.5. Analyzation of *Gpx8*^{-/-} mouse line

In order to unravel novel functions of GPX8 *in vivo*, a knockout mouse line was generated using CRISPR/Cas9 genome editing. It was demonstrated for the very first time, that unlike that for *Gpx4* [67], the whole-body knockout of *Gpx8* does not lead to embryonic lethality at least and under non-stressed conditions. First, GPX8 expression levels were investigated in different mouse tissues which should help to plan future studies and to provide potential insights about the *in vivo* function of the protein. The data demonstrated remarkably strong expression in the heart, kidney, liver, white adipose tissue (WAT), brown adipose tissue (BAT) and ovaries.

Since previous *in vitro* studies indicated that GPX8 protects against palmitic acid induced lipotoxicity in NSF-β cells [115] and in MEFs (4.4.3 and 4.8.3), the animals were challenged

to a 45 % high fat diet. The data revealed lower body weight and body weight gain in *Gpx8*^{-/-} males, a difference that was apparent from the start point to the endpoint of the experiment. When the body weight gain of each mouse was normalized to their body weight, the effect was less significant. Indeed, the difference between *Gpx8*^{-/-} and *Gpx8*^{wt/wt} males leveled out after 15 weeks of a high fat diet. In contrast, *Gpx8*^{-/-} females responded very similar to the control group, however, a prolonged high fat diet led to a tendency of lower body weight of *Gpx8*^{-/-} females. This phenomenon is often discernible and this is the reason why usually female mice are excluded from experiments using high fat diet. It has been previously reported that female animals respond different to metabolic stress due to the higher estrogen levels in their body [289]. Despite the similar weight gain between male and female animals, the females tended to be more protected against visceral inflammation, glucose intolerance, insulin resistance and hyperinsulinemia [290]. The pro-inflammatory action of estrogen has been shown in humans as well. It has been proven that non-obese females have lower levels of circulating IL-6 in their blood than males [291]. However, the opposite was observed in obese individuals [292], and also after consuming a high fat meal [293]. In addition, estrogens were also shown to inhibit IL-6 production by Kupffer cells in mice [294]. Conclusively, these results reflect the importance of gender differences in animal studies, especially in high fat diet induced obesity model.

Besides, EchoMRI data revealed lower body fat mass, lean mass and total water content in *Gpx8*^{-/-} mice compared to control animals. Consequently, this phenomenon was also only evident in males. However, the Oil Red O staining, conducted after high fat diet, did not show any evident changes in lipid accumulation in the liver of *Gpx8*^{-/-} animals compared to *Gpx8*^{wt/wt}. However, in contrast to Oil Red O staining, ultrastructural analysis revealed dramatic alteration of mitochondria in *Gpx8*^{-/-} animals, which was most evident in the heart, BAT and WAT. Based on this data it can be concluded that these cells lacking GPX8 are not able to properly form mitochondrial cristae. Some studies reported a similar phenotype in mice expressing S2808D/A mutated ryanodine receptor 2 (RyR2). In cardiomyocytes Ca²⁺ mainly leaks from the sarcoplasmic reticulum via RyR2 and not via inositol phosphate 3 receptor type 2 (IP3R2). RyR2 has also been shown to regulate excitation-contraction of cardiomyocytes [295]. Increased release of Ca²⁺ from the sarcoplasmic reticulum leads to impaired mitochondrial function and ROS accumulation.

Therefore, RyR2 plays a crucial role in heart failure by regulating mitochondrial Ca^{2+} overload and dysfunction. In addition, it has been shown that Ca^{2+} supplementation, which leads to the accumulation of Ca^{2+} in cytoplasm, mitochondria and around the lipid droplets, increased the size of mitochondria and improved the cristae formation in rats BAT [296].

Taken together, GPX8 deficient mice exhibited a decreased number of mitochondrial cristae similar to animals which expressed a mutant form of RyR2, or Ca^{2+} deficient rats. In addition, MEFs lacking GPX8 showed a reduced Ca^{2+} level in the ER. In line with this, GPX8 has been found to interact with several proteins that are involved in Ca^{2+} transport in the plasma membrane, as well as in the ER membrane. Also, GPX8 was found to rapidly degrade when SERCA is inhibited. More importantly, GPX8 was shown to protect against saturated fatty acid induced cell death *in vitro*, and *in vivo* was also found to play a role in a high fat diet induced obesity model. Conclusively, these results strongly indicate the involvement of GPX8 in the regulation of Ca^{2+} levels and lipid metabolism *in vitro* and *in vivo*. Considering that GPX8 localizes in the ER membrane with a short cytosolic tail and as it was previously reported to accumulate in the mitochondria associated membrane [114], an important platform for Ca^{2+} signaling and lipid trafficking, these findings can be highly relevant to identify a new player in Ca^{2+} regulated lipid biosynthesis.

6. OUTLOOK

Since GPX8 was found to be highly expressed in BAT, WAT and cardiac tissue, and the absence of the protein led to a severe mitochondrial phenotype in these organs, it will be intriguing to investigate other stress models *in vivo*, in which heart and adipose tissues play a critical role to adapt to the particular stress conditions. Therefore, the animals will be challenged to cold exposure and starvation to investigate whether the lack of GPX8 leads to any changes in response to these stress models. The adaptation to both stress models requires proper mitochondrial activity of BAT to produce energy and heat which are critical to prevent cellular damage throughout the body. In addition, as *Gpx8*^{-/-} resulted in aberrant mitochondria in the heart, which is the major energy producing organ in the body, the animals will be also challenged to exercise, a condition under which the elevated ATP production of the heart is essential to maintain a rapid heartbeat. Since the high fat diet used here only contained 45% fat, another feeding experiment with 65% fat content is planned as this is mainly consisting of palmitic acid, which provoked strong phenotypes in the cell-based studies. Moreover, the animals will be analyzed in the German Mouse Clinic to unravel novel and rather subtle phenotypes in mice in the absence of GPX8.

In vitro studies will also be continued which will address the functional analysis of mitochondria from GPX8 KO MEFs and mouse tissues. Additionally, CRISPR screening will be performed using palmitic acid and a SCD1 inhibitor as lethal stimuli in GPX8 KO cells, after which selected clones will be analyzed to identify proteins which could be involved in the prevention mechanism in GPX8 deficient cells. Moreover, small molecule screens will be conducted to identify novel inhibitors that prevent from palmitic acid/SCD1 inhibitor induced cell death. Hence, all these studies aim to yield a better understanding of the role played by this last identified member of the glutathione peroxidase family, glutathione peroxidase 8.

7. REFERENCES

1. Salvador-Gallego, R., M.J. Hoyer, and G.K. Voeltz, *SnapShot: Functions of Endoplasmic Reticulum Membrane Contact Sites*. Cell, 2017. **171**(5): p. 1224-1224 e1.
2. Raiborg, C., E.M. Wenzel, and H. Stenmark, *ER-endosome contact sites: molecular compositions and functions*. EMBO J, 2015. **34**(14): p. 1848-58.
3. Jacquemyn, J., A. Cascalho, and R.E. Goodchild, *The ins and outs of endoplasmic reticulum-controlled lipid biosynthesis*. EMBO Rep, 2017. **18**(11): p. 1905-1921.
4. Tu, B.P. and J.S. Weissman, *Oxidative protein folding in eukaryotes: mechanisms and consequences*. J Cell Biol, 2004. **164**(3): p. 341-6.
5. Appenzeller-Herzog, C. and L. Ellgaard, *The human PDI family: versatility packed into a single fold*. Biochim Biophys Acta, 2008. **1783**(4): p. 535-48.
6. Zito, E., et al., *ERO1-beta, a pancreas-specific disulfide oxidase, promotes insulin biogenesis and glucose homeostasis*. J Cell Biol, 2010. **188**(6): p. 821-32.
7. Bulleid, N.J. and L. Ellgaard, *Multiple ways to make disulfides*. Trends Biochem Sci, 2011. **36**(9): p. 485-92.
8. Schulman, S., et al., *Vitamin K epoxide reductase prefers ER membrane-anchored thioredoxin-like redox partners*. Proc Natl Acad Sci U S A, 2010. **107**(34): p. 15027-32.
9. Morgan, B., et al., *Multiple glutathione disulfide removal pathways mediate cytosolic redox homeostasis*. Nat Chem Biol, 2013. **9**(2): p. 119-25.
10. Hwang, C., A.J. Sinskey, and H.F. Lodish, *Oxidized redox state of glutathione in the endoplasmic reticulum*. Science, 1992. **257**(5076): p. 1496-502.
11. Santos, C.X., et al., *Mechanisms and implications of reactive oxygen species generation during the unfolded protein response: roles of endoplasmic reticulum oxidoreductases, mitochondrial electron transport, and NADPH oxidase*. Antioxid Redox Signal, 2009. **11**(10): p. 2409-27.
12. Cao, S.S. and R.J. Kaufman, *Endoplasmic reticulum stress and oxidative stress in cell fate decision and human disease*. Antioxid Redox Signal, 2014. **21**(3): p. 396-413.
13. Castillero, E., et al., *Attenuation of the unfolded protein response and endoplasmic reticulum stress after mechanical unloading in dilated cardiomyopathy*. Am J Physiol Heart Circ Physiol, 2015. **309**(3): p. H459-70.
14. Lacaille, F., et al., *Intestinal failure-associated liver disease: a position paper of the ESPGHAN Working Group of Intestinal Failure and Intestinal Transplantation*. J Pediatr Gastroenterol Nutr, 2015. **60**(2): p. 272-83.
15. Grootjans, J., et al., *The unfolded protein response in immunity and inflammation*. Nat Rev Immunol, 2016. **16**(8): p. 469-84.
16. Walter, P. and D. Ron, *The unfolded protein response: from stress pathway to homeostatic regulation*. Science, 2011. **334**(6059): p. 1081-6.
17. Kaneko, M., Y. Niinuma, and Y. Nomura, *Activation signal of nuclear factor-kappa B in response to endoplasmic reticulum stress is transduced via IRE1 and tumor necrosis factor receptor-associated factor 2*. Biol Pharm Bull, 2003. **26**(7): p. 931-5.
18. McGuckin, M.A., et al., *ER stress and the unfolded protein response in intestinal inflammation*. Am J Physiol Gastrointest Liver Physiol, 2010. **298**(6): p. G820-32.

19. Yoshida, H., et al., *Identification of the cis-acting endoplasmic reticulum stress response element responsible for transcriptional induction of mammalian glucose-regulated proteins. Involvement of basic leucine zipper transcription factors.* J Biol Chem, 1998. **273**(50): p. 33741-9.
20. Rutkowski, D.T., et al., *Adaptation to ER stress is mediated by differential stabilities of pro-survival and pro-apoptotic mRNAs and proteins.* PLoS Biol, 2006. **4**(11): p. e374.
21. Yoshida, H., et al., *XBP1 mRNA is induced by ATF6 and spliced by IRE1 in response to ER stress to produce a highly active transcription factor.* Cell, 2001. **107**(7): p. 881-91.
22. Hampton, R.Y., R.G. Gardner, and J. Rine, *Role of 26S proteasome and HRD genes in the degradation of 3-hydroxy-3-methylglutaryl-CoA reductase, an integral endoplasmic reticulum membrane protein.* Mol Biol Cell, 1996. **7**(12): p. 2029-44.
23. Caramelo, J.J., et al., *UDP-Glc:glycoprotein glucosyltransferase recognizes structured and solvent accessible hydrophobic patches in molten globule-like folding intermediates.* Proc Natl Acad Sci U S A, 2003. **100**(1): p. 86-91.
24. Caramelo, J.J., et al., *The endoplasmic reticulum glucosyltransferase recognizes nearly native glycoprotein folding intermediates.* J Biol Chem, 2004. **279**(44): p. 46280-5.
25. Caramelo, J.J. and A.J. Parodi, *Getting in and out from calnexin/calreticulin cycles.* J Biol Chem, 2008. **283**(16): p. 10221-5.
26. Cormier, J.H., et al., *EDEM1 recognition and delivery of misfolded proteins to the SEL1L-containing ERAD complex.* Mol Cell, 2009. **34**(5): p. 627-33.
27. Molinari, M., et al., *Role of EDEM in the release of misfolded glycoproteins from the calnexin cycle.* Science, 2003. **299**(5611): p. 1397-400.
28. Oda, Y., et al., *EDEM as an acceptor of terminally misfolded glycoproteins released from calnexin.* Science, 2003. **299**(5611): p. 1394-7.
29. Plemper, R.K., et al., *Mutant analysis links the translocon and BiP to retrograde protein transport for ER degradation.* Nature, 1997. **388**(6645): p. 891-5.
30. Hatahet, F. and L.W. Ruddock, *Protein disulfide isomerase: a critical evaluation of its function in disulfide bond formation.* Antioxid Redox Signal, 2009. **11**(11): p. 2807-50.
31. Gardner, R.G., et al., *Endoplasmic reticulum degradation requires lumen to cytosol signaling. Transmembrane control of Hrd1p by Hrd3p.* J Cell Biol, 2000. **151**(1): p. 69-82.
32. Mueller, B., et al., *SEL1L nucleates a protein complex required for dislocation of misfolded glycoproteins.* Proc Natl Acad Sci U S A, 2008. **105**(34): p. 12325-30.
33. Mueller, B., B.N. Lilley, and H.L. Ploegh, *SEL1L, the homologue of yeast Hrd3p, is involved in protein dislocation from the mammalian ER.* J Cell Biol, 2006. **175**(2): p. 261-70.
34. Carvalho, P., A.M. Stanley, and T.A. Rapoport, *Retrotranslocation of a misfolded luminal ER protein by the ubiquitin-ligase Hrd1p.* Cell, 2010. **143**(4): p. 579-91.
35. Preston, G.M. and J.L. Brodsky, *The evolving role of ubiquitin modification in endoplasmic reticulum-associated degradation.* Biochem J, 2017. **474**(4): p. 445-469.

36. Francisco, A.B., et al., *Deficiency of suppressor enhancer Lin12 1 like (SEL1L) in mice leads to systemic endoplasmic reticulum stress and embryonic lethality*. J Biol Chem, 2010. **285**(18): p. 13694-703.
37. Yagishita, N., et al., *Essential role of synoviolin in embryogenesis*. J Biol Chem, 2005. **280**(9): p. 7909-16.
38. Bernales, S., K.L. McDonald, and P. Walter, *Autophagy counterbalances endoplasmic reticulum expansion during the unfolded protein response*. PLoS Biol, 2006. **4**(12): p. e423.
39. Fernandez, A., et al., *Melatonin and endoplasmic reticulum stress: relation to autophagy and apoptosis*. J Pineal Res, 2015. **59**(3): p. 292-307.
40. Katsiogiannis, S., R. Tenta, and F.N. Skopouli, *Endoplasmic reticulum stress causes autophagy and apoptosis leading to cellular redistribution of the autoantigens Ro/Sjogren's syndrome-related antigen A (SSA) and La/SSB in salivary gland epithelial cells*. Clin Exp Immunol, 2015. **181**(2): p. 244-52.
41. Klionsky, D.J., et al., *A comprehensive glossary of autophagy-related molecules and processes*. Autophagy, 2010. **6**(4): p. 438-48.
42. Kroemer, G. and B. Levine, *Autophagic cell death: the story of a misnomer*. Nat Rev Mol Cell Biol, 2008. **9**(12): p. 1004-10.
43. Das, G., B.V. Shrivage, and E.H. Baehrecke, *Regulation and function of autophagy during cell survival and cell death*. Cold Spring Harb Perspect Biol, 2012. **4**(6).
44. Kaushik, S. and A.M. Cuervo, *Chaperone-mediated autophagy: a unique way to enter the lysosome world*. Trends Cell Biol, 2012. **22**(8): p. 407-17.
45. Mijaljica, D., M. Prescott, and R.J. Devenish, *Microautophagy in mammalian cells: revisiting a 40-year-old conundrum*. Autophagy, 2011. **7**(7): p. 673-82.
46. Ravikumar, B., et al., *Regulation of mammalian autophagy in physiology and pathophysiology*. Physiol Rev, 2010. **90**(4): p. 1383-435.
47. Hayashi-Nishino, M., et al., *A subdomain of the endoplasmic reticulum forms a cradle for autophagosome formation*. Nat Cell Biol, 2009. **11**(12): p. 1433-7.
48. Hailey, D.W., et al., *Mitochondria supply membranes for autophagosome biogenesis during starvation*. Cell, 2010. **141**(4): p. 656-67.
49. Ravikumar, B., et al., *Plasma membrane contributes to the formation of pre-autophagosomal structures*. Nat Cell Biol, 2010. **12**(8): p. 747-57.
50. Hamasaki, M., et al., *Autophagosomes form at ER-mitochondria contact sites*. Nature, 2013. **495**(7441): p. 389-93.
51. Berg, T.O., et al., *Isolation and characterization of rat liver amphisomes. Evidence for fusion of autophagosomes with both early and late endosomes*. J Biol Chem, 1998. **273**(34): p. 21883-92.
52. Patel, K.K., et al., *Autophagy proteins control goblet cell function by potentiating reactive oxygen species production*. EMBO J, 2013. **32**(24): p. 3130-44.
53. Tanida, I., et al., *HsAtg4B/HsApg4B/autophagin-1 cleaves the carboxyl termini of three human Atg8 homologues and delipidates microtubule-associated protein light chain 3- and GABAA receptor-associated protein-phospholipid conjugates*. J Biol Chem, 2004. **279**(35): p. 36268-76.
54. Rouschop, K.M., et al., *The unfolded protein response protects human tumor cells during hypoxia through regulation of the autophagy genes MAP1LC3B and ATG5*. J Clin Invest, 2010. **120**(1): p. 127-41.

55. B'Chir, W., et al., *The eIF2alpha/ATF4 pathway is essential for stress-induced autophagy gene expression*. Nucleic Acids Res, 2013. **41**(16): p. 7683-99.
56. Heath-Engel, H.M., N.C. Chang, and G.C. Shore, *The endoplasmic reticulum in apoptosis and autophagy: role of the BCL-2 protein family*. Oncogene, 2008. **27**(50): p. 6419-33.
57. Wei, Y., S. Sinha, and B. Levine, *Dual role of JNK1-mediated phosphorylation of Bcl-2 in autophagy and apoptosis regulation*. Autophagy, 2008. **4**(7): p. 949-51.
58. Rashid, H.O., et al., *ER stress: Autophagy induction, inhibition and selection*. Autophagy, 2015. **11**(11): p. 1956-1977.
59. Kaneko, M., et al., *ER Stress and Disease: Toward Prevention and Treatment*. Biol Pharm Bull, 2017. **40**(9): p. 1337-1343.
60. Brigelius-Flohe, R. and L. Flohe, *Basic principles and emerging concepts in the redox control of transcription factors*. Antioxid Redox Signal, 2011. **15**(8): p. 2335-81.
61. Flohe, L., *Changing paradigms in thiology from antioxidant defense toward redox regulation*. Methods Enzymol, 2010. **473**: p. 1-39.
62. Forman, H.J., M. Maiorino, and F. Ursini, *Signaling functions of reactive oxygen species*. Biochemistry, 2010. **49**(5): p. 835-42.
63. Rhee, S.G., *Cell signaling. H2O2, a necessary evil for cell signaling*. Science, 2006. **312**(5782): p. 1882-3.
64. Brigelius-Flohe, R. and M. Maiorino, *Glutathione peroxidases*. Biochim Biophys Acta, 2013. **1830**(5): p. 3289-303.
65. Bosello-Travain, V., et al., *Glutathione peroxidase 8 is transcriptionally regulated by HIFalpha and modulates growth factor signaling in HeLa cells*. Free Radic Biol Med, 2015. **81**: p. 58-68.
66. Conrad, M., et al., *ROS, thiols and thiol-regulating systems in male gametogenesis*. Biochim Biophys Acta, 2015. **1850**(8): p. 1566-74.
67. Yant, L.J., et al., *The selenoprotein GPX4 is essential for mouse development and protects from radiation and oxidative damage insults*. Free Radic Biol Med, 2003. **34**(4): p. 496-502.
68. Shi, Z.Z., et al., *Glutathione synthesis is essential for mouse development but not for cell growth in culture*. Proc Natl Acad Sci U S A, 2000. **97**(10): p. 5101-6.
69. Conrad, M., et al., *The nuclear form of phospholipid hydroperoxide glutathione peroxidase is a protein thiol peroxidase contributing to sperm chromatin stability*. Mol Cell Biol, 2005. **25**(17): p. 7637-44.
70. Wirth, E.K., et al., *Neuronal selenoprotein expression is required for interneuron development and prevents seizures and neurodegeneration*. FASEB J, 2010. **24**(3): p. 844-52.
71. Seiler, A., et al., *Glutathione Peroxidase 4 Senses and Translates Oxidative Stress into 12/15-Lipoxygenase Dependent- and AIF-Mediated Cell Death*. Cell Metab, 2008. **8**(3): p. 237-48.
72. Wirth, E.K., et al., *Cerebellar hypoplasia in mice lacking selenoprotein biosynthesis in neurons*. Biol Trace Elem Res, 2014. **158**(2): p. 203-10.
73. Chen, L., et al., *Ablation of the Ferroptosis Inhibitor Glutathione Peroxidase 4 in Neurons Results in Rapid Motor Neuron Degeneration and Paralysis*. J Biol Chem, 2015. **290**(47): p. 28097-106.
74. Ueta, T., et al., *Glutathione peroxidase 4 is required for maturation of photoreceptor cells*. J Biol Chem, 2012. **287**(10): p. 7675-82.

75. Sengupta, A., et al., *Targeted Disruption of Glutathione Peroxidase 4 in Mouse Skin Epithelial Cells Impairs Postnatal Hair Follicle Morphogenesis that Is Partially Rescued through Inhibition of COX-2*. *J Invest Dermatol*, 2013. **133**(7): p. 1731-41.
76. Wortmann, M., et al., *Combined deficiency in glutathione peroxidase 4 and vitamin e causes multiorgan thrombus formation and early death in mice*. *Circ Res*, 2013. **113**(4): p. 408-17.
77. Matsushita, M., et al., *T cell lipid peroxidation induces ferroptosis and prevents immunity to infection*. *J Exp Med*, 2015. **212**(4): p. 555-68.
78. Canli, O., et al., *Glutathione peroxidase 4 prevents necroptosis in mouse erythroid precursors*. *Blood*, 2015.
79. Carlson, B.A., et al., *Glutathione peroxidase 4 and vitamin E cooperatively prevent hepatocellular degeneration*. *Redox Biol*, 2016. **9**: p. 22-31.
80. Dixon, S.J., et al., *Ferroptosis: an iron-dependent form of nonapoptotic cell death*. *Cell*, 2012. **149**(5): p. 1060-72.
81. Conrad, M., *Transgenic mouse models for the vital selenoenzymes cytosolic thioredoxin reductase, mitochondrial thioredoxin reductase and glutathione peroxidase 4*. *Biochim Biophys Acta*, 2009. **1790**(11): p. 1575-85.
82. Utomo, A., et al., *Identification of a novel putative non-selenocysteine containing phospholipid hydroperoxide glutathione peroxidase (NPGPx) essential for alleviating oxidative stress generated from polyunsaturated fatty acids in breast cancer cells*. *J Biol Chem*, 2004. **279**(42): p. 43522-9.
83. Nguyen, V.D., et al., *Two endoplasmic reticulum PDI peroxidases increase the efficiency of the use of peroxide during disulfide bond formation*. *J Mol Biol*, 2011. **406**(3): p. 503-15.
84. Wei, P.C., et al., *Loss of the oxidative stress sensor NPGPx compromises GRP78 chaperone activity and induces systemic disease*. *Mol Cell*, 2012. **48**(5): p. 747-59.
85. Chang, Y.C., et al., *Deficiency of NPGPx, an oxidative stress sensor, leads to obesity in mice and human*. *EMBO Mol Med*, 2013. **5**(8): p. 1165-79.
86. Flohe, L., W.A. Gunzler, and H.H. Schock, *Glutathione peroxidase: a selenoenzyme*. *FEBS Lett*, 1973. **32**(1): p. 132-4.
87. Rotruck, J.T., et al., *Selenium: biochemical role as a component of glutathione peroxidase*. *Science*, 1973. **179**(4073): p. 588-90.
88. de Haan, J.B., et al., *Mice with a homozygous null mutation for the most abundant glutathione peroxidase, Gpx1, show increased susceptibility to the oxidative stress-inducing agents paraquat and hydrogen peroxide*. *J Biol Chem*, 1998. **273**(35): p. 22528-36.
89. Ho, Y.S., et al., *Mice deficient in cellular glutathione peroxidase develop normally and show no increased sensitivity to hyperoxia*. *J Biol Chem*, 1997. **272**(26): p. 16644-51.
90. Thu, V.T., et al., *Glutathione peroxidase 1 protects mitochondria against hypoxia/reoxygenation damage in mouse hearts*. *Pflugers Arch*, 2010. **460**(1): p. 55-68.
91. Cheng, W.H., et al., *Cellular glutathione peroxidase is the mediator of body selenium to protect against paraquat lethality in transgenic mice*. *J Nutr*, 1998. **128**(7): p. 1070-6.

92. Chu, F.F., J.H. Doroshov, and R.S. Esworthy, *Expression, characterization, and tissue distribution of a new cellular selenium-dependent glutathione peroxidase, GSHPx-Gl*. J Biol Chem, 1993. **268**(4): p. 2571-6.
93. Esworthy, R.S., et al., *Low glutathione peroxidase activity in Gpx1 knockout mice protects jejunum crypts from gamma-irradiation damage*. Am J Physiol Gastrointest Liver Physiol, 2000. **279**(2): p. G426-36.
94. Naiki, T., et al., *GPX2 promotes development of bladder cancer with squamous cell differentiation through the control of apoptosis*. Oncotarget, 2018. **9**(22): p. 15847-15859.
95. Liu, T., et al., *GPX2 overexpression indicates poor prognosis in patients with hepatocellular carcinoma*. Tumour Biol, 2017. **39**(6): p. 1010428317700410.
96. Banning, A., et al., *GPx2 counteracts PGE2 production by dampening COX-2 and mPGES-1 expression in human colon cancer cells*. Antioxid Redox Signal, 2008. **10**(9): p. 1491-500.
97. Te Velde, A.A., et al., *Glutathione peroxidase 2 and aquaporin 8 as new markers for colonic inflammation in experimental colitis and inflammatory bowel diseases: an important role for H2O2?* Eur J Gastroenterol Hepatol, 2008. **20**(6): p. 555-60.
98. Avissar, N., et al., *Human kidney proximal tubules are the main source of plasma glutathione peroxidase*. Am J Physiol, 1994. **266**(2 Pt 1): p. C367-75.
99. Maeda, K., et al., *Analysis of an expression profile of genes in the human adipose tissue*. Gene, 1997. **190**(2): p. 227-35.
100. Olson, G.E., et al., *Extracellular glutathione peroxidase (Gpx3) binds specifically to basement membranes of mouse renal cortex tubule cells*. Am J Physiol Renal Physiol, 2010. **298**(5): p. F1244-53.
101. Whitin, J.C., et al., *Extracellular glutathione peroxidase is secreted basolaterally by human renal proximal tubule cells*. Am J Physiol Renal Physiol, 2002. **283**(1): p. F20-8.
102. An, B.C., et al., *GPx3-mediated redox signaling arrests the cell cycle and acts as a tumor suppressor in lung cancer cell lines*. PLoS One, 2018. **13**(9): p. e0204170.
103. Worley, B.L., et al., *GPx3 supports ovarian cancer progression by manipulating the extracellular redox environment*. Redox Biol, 2018.
104. Zhu, X., et al., *GPX3 suppresses tumor migration and invasion via the FAK/AKT pathway in esophageal squamous cell carcinoma*. Am J Transl Res, 2018. **10**(6): p. 1908-1920.
105. Rejraji, H., P. Vernet, and J.R. Drevet, *GPX5 is present in the mouse caput and cauda epididymidis lumen at three different locations*. Mol Reprod Dev, 2002. **63**(1): p. 96-103.
106. Chabory, E., et al., *Epididymis seleno-independent glutathione peroxidase 5 maintains sperm DNA integrity in mice*. J Clin Invest, 2009. **119**(7): p. 2074-85.
107. Kryukov, G.V., et al., *Characterization of mammalian selenoproteomes*. Science, 2003. **300**(5624): p. 1439-43.
108. Ramming, T. and C. Appenzeller-Herzog, *Destroy and exploit: catalyzed removal of hydroperoxides from the endoplasmic reticulum*. Int J Cell Biol, 2013. **2013**: p. 180906.
109. Morikawa, K., et al., *Quantitative proteomics identifies the membrane-associated peroxidase GPx8 as a cellular substrate of the hepatitis C virus NS3-4A protease*. Hepatology, 2014. **59**(2): p. 423-33.

110. Toppo, S., et al., *Evolutionary and structural insights into the multifaceted glutathione peroxidase (Gpx) superfamily*. *Antioxid Redox Signal*, 2008. **10**(9): p. 1501-14.
111. Ramming, T., et al., *GPx8 peroxidase prevents leakage of H₂O₂ from the endoplasmic reticulum*. *Free Radic Biol Med*, 2014. **70**: p. 106-16.
112. Salmeen, A., et al., *Redox regulation of protein tyrosine phosphatase 1B involves a sulphenyl-amide intermediate*. *Nature*, 2003. **423**(6941): p. 769-73.
113. Loh, K., et al., *Reactive oxygen species enhance insulin sensitivity*. *Cell Metab*, 2009. **10**(4): p. 260-72.
114. Yoboue, E.D., et al., *Regulation of Calcium Fluxes by GPX8, a Type-II Transmembrane Peroxidase Enriched at the Mitochondria-Associated Endoplasmic Reticulum Membrane*. *Antioxid Redox Signal*, 2017. **27**(9): p. 583-595.
115. Mehmeti, I., et al., *ER-resident antioxidative GPx7 and GPx8 enzyme isoforms protect insulin-secreting INS-1E beta-cells against lipotoxicity by improving the ER antioxidative capacity*. *Free Radic Biol Med*, 2017. **112**: p. 121-130.
116. Olzmann, J.A. and P. Carvalho, *Dynamics and functions of lipid droplets*. *Nat Rev Mol Cell Biol*, 2018.
117. Jain, A. and J.C.M. Holthuis, *Membrane contact sites, ancient and central hubs of cellular lipid logistics*. *Biochim Biophys Acta Mol Cell Res*, 2017. **1864**(9): p. 1450-1458.
118. Kannan, M., et al., *Phosphatidylserine synthesis at membrane contact sites promotes its transport out of the ER*. *J Lipid Res*, 2017. **58**(3): p. 553-562.
119. Stone, S.J. and J.E. Vance, *Phosphatidylserine synthase-1 and -2 are localized to mitochondria-associated membranes*. *J Biol Chem*, 2000. **275**(44): p. 34534-40.
120. Breslow, D.K. and J.S. Weissman, *Membranes in balance: mechanisms of sphingolipid homeostasis*. *Mol Cell*, 2010. **40**(2): p. 267-79.
121. Krahmer, N., et al., *Phosphatidylcholine synthesis for lipid droplet expansion is mediated by localized activation of CTP:phosphocholine cytidyltransferase*. *Cell Metab*, 2011. **14**(4): p. 504-15.
122. Vamparys, L., et al., *Conical lipids in flat bilayers induce packing defects similar to that induced by positive curvature*. *Biophys J*, 2013. **104**(3): p. 585-93.
123. Cornell, R.B., *Membrane lipid compositional sensing by the inducible amphipathic helix of CCT*. *Biochim Biophys Acta*, 2016. **1861**(8 Pt B): p. 847-861.
124. Olson, D.K., et al., *Taming the sphinx: Mechanisms of cellular sphingolipid homeostasis*. *Biochim Biophys Acta*, 2016. **1861**(8 Pt B): p. 784-792.
125. Fu, S., et al., *Aberrant lipid metabolism disrupts calcium homeostasis causing liver endoplasmic reticulum stress in obesity*. *Nature*, 2011. **473**(7348): p. 528-31.
126. Bi, J., et al., *Seipin promotes adipose tissue fat storage through the ER Ca²⁺(+)-ATPase SERCA*. *Cell Metab*, 2014. **19**(5): p. 861-71.
127. Schuck, S., et al., *Membrane expansion alleviates endoplasmic reticulum stress independently of the unfolded protein response*. *J Cell Biol*, 2009. **187**(4): p. 525-36.
128. Sriburi, R., et al., *XBP1: a link between the unfolded protein response, lipid biosynthesis, and biogenesis of the endoplasmic reticulum*. *J Cell Biol*, 2004. **167**(1): p. 35-41.
129. Lee, A.H., et al., *XBP-1 is required for biogenesis of cellular secretory machinery of exocrine glands*. *EMBO J*, 2005. **24**(24): p. 4368-80.

130. Sriburi, R., et al., *Coordinate regulation of phospholipid biosynthesis and secretory pathway gene expression in XBP-1(S)-induced endoplasmic reticulum biogenesis*. J Biol Chem, 2007. **282**(10): p. 7024-34.
131. Fagone, P., et al., *Phospholipid biosynthesis program underlying membrane expansion during B-lymphocyte differentiation*. J Biol Chem, 2007. **282**(10): p. 7591-605.
132. Maiuolo, J., et al., *Selective activation of the transcription factor ATF6 mediates endoplasmic reticulum proliferation triggered by a membrane protein*. Proc Natl Acad Sci U S A, 2011. **108**(19): p. 7832-7.
133. Yoshida, H., et al., *ATF6 activated by proteolysis binds in the presence of NF-Y (CBF) directly to the cis-acting element responsible for the mammalian unfolded protein response*. Mol Cell Biol, 2000. **20**(18): p. 6755-67.
134. Tsuru, A., et al., *Novel mechanism of enhancing IRE1alpha-XBP1 signalling via the PERK-ATF4 pathway*. Sci Rep, 2016. **6**: p. 24217.
135. Pineau, L., et al., *Lipid-induced ER stress: synergistic effects of sterols and saturated fatty acids*. Traffic, 2009. **10**(6): p. 673-90.
136. Ariyama, H., et al., *Decrease in membrane phospholipid unsaturation induces unfolded protein response*. J Biol Chem, 2010. **285**(29): p. 22027-35.
137. Hou, N.S., et al., *Activation of the endoplasmic reticulum unfolded protein response by lipid disequilibrium without disturbed proteostasis in vivo*. Proc Natl Acad Sci U S A, 2014. **111**(22): p. E2271-80.
138. Volmer, R., K. van der Ploeg, and D. Ron, *Membrane lipid saturation activates endoplasmic reticulum unfolded protein response transducers through their transmembrane domains*. Proc Natl Acad Sci U S A, 2013. **110**(12): p. 4628-33.
139. Aguilar, P.S. and D. de Mendoza, *Control of fatty acid desaturation: a mechanism conserved from bacteria to humans*. Mol Microbiol, 2006. **62**(6): p. 1507-14.
140. Ntambi, J.M., et al., *Loss of stearoyl-CoA desaturase-1 function protects mice against adiposity*. Proc Natl Acad Sci U S A, 2002. **99**(17): p. 11482-6.
141. Lau, D.H.W., et al., *Disruption of ER-mitochondria signalling in fronto-temporal dementia and related amyotrophic lateral sclerosis*. Cell Death Dis, 2018. **9**(3): p. 327.
142. Csordas, G., et al., *Structural and functional features and significance of the physical linkage between ER and mitochondria*. J Cell Biol, 2006. **174**(7): p. 915-21.
143. Goetz, J.G. and I.R. Nabi, *Interaction of the smooth endoplasmic reticulum and mitochondria*. Biochem Soc Trans, 2006. **34**(Pt 3): p. 370-3.
144. Area-Gomez, E., et al., *A key role for MAM in mediating mitochondrial dysfunction in Alzheimer disease*. Cell Death Dis, 2018. **9**(3): p. 335.
145. Gomez-Suaga, P., et al., *ER-mitochondria signaling in Parkinson's disease*. Cell Death Dis, 2018. **9**(3): p. 337.
146. Delprat, B., T. Maurice, and C. Delettre, *Wolfram syndrome: MAMs' connection?* Cell Death Dis, 2018. **9**(3): p. 364.
147. Rieusset, J., *The role of endoplasmic reticulum-mitochondria contact sites in the control of glucose homeostasis: an update*. Cell Death Dis, 2018. **9**(3): p. 388.
148. Annunziata, I., R. Sano, and A. d'Azzo, *Mitochondria-associated ER membranes (MAMs) and lysosomal storage diseases*. Cell Death Dis, 2018. **9**(3): p. 328.

149. Poston, C.N., S.C. Krishnan, and C.R. Bazemore-Walker, *In-depth proteomic analysis of mammalian mitochondria-associated membranes (MAM)*. J Proteomics, 2013. **79**: p. 219-30.
150. Bottinger, L., et al., *Phosphatidylethanolamine and cardiolipin differentially affect the stability of mitochondrial respiratory chain supercomplexes*. J Mol Biol, 2012. **423**(5): p. 677-86.
151. Rusinol, A.E., et al., *A unique mitochondria-associated membrane fraction from rat liver has a high capacity for lipid synthesis and contains pre-Golgi secretory proteins including nascent lipoproteins*. J Biol Chem, 1994. **269**(44): p. 27494-502.
152. Stone, S.J., et al., *The endoplasmic reticulum enzyme DGAT2 is found in mitochondria-associated membranes and has a mitochondrial targeting signal that promotes its association with mitochondria*. J Biol Chem, 2009. **284**(8): p. 5352-61.
153. Cui, Z., et al., *Cloning and expression of a novel phosphatidylethanolamine N-methyltransferase. A specific biochemical and cytological marker for a unique membrane fraction in rat liver*. J Biol Chem, 1993. **268**(22): p. 16655-63.
154. Lewin, T.M., et al., *Acyl-CoA synthetase isoforms 1, 4, and 5 are present in different subcellular membranes in rat liver and can be inhibited independently*. J Biol Chem, 2001. **276**(27): p. 24674-9.
155. Farese, R.V., Jr. and T.C. Walther, *Lipid droplets finally get a little R-E-S-P-E-C-T*. Cell, 2009. **139**(5): p. 855-60.
156. Bosanac, I., et al., *Structural insights into the regulatory mechanism of IP3 receptor*. Biochim Biophys Acta, 2004. **1742**(1-3): p. 89-102.
157. Irvine, R.F., *'Quantal' Ca²⁺ release and the control of Ca²⁺ entry by inositol phosphates--a possible mechanism*. FEBS Lett, 1990. **263**(1): p. 5-9.
158. Missiaen, L., et al., *Ca²⁺ release induced by inositol 1,4,5-trisphosphate is a steady-state phenomenon controlled by luminal Ca²⁺ in permeabilized cells*. Nature, 1992. **357**(6379): p. 599-602.
159. Berridge, M.J., *The endoplasmic reticulum: a multifunctional signaling organelle*. Cell Calcium, 2002. **32**(5-6): p. 235-49.
160. Papp, S., et al., *Is all of the endoplasmic reticulum created equal? The effects of the heterogeneous distribution of endoplasmic reticulum Ca²⁺-handling proteins*. J Cell Biol, 2003. **160**(4): p. 475-9.
161. Szabadkai, G., et al., *Chaperone-mediated coupling of endoplasmic reticulum and mitochondrial Ca²⁺ channels*. J Cell Biol, 2006. **175**(6): p. 901-11.
162. Bragadin, M., T. Pozzan, and G.F. Azzone, *Kinetics of Ca²⁺ carrier in rat liver mitochondria*. Biochemistry, 1979. **18**(26): p. 5972-8.
163. Giorgi, C., et al., *Ca²⁺ signaling, mitochondria and cell death*. Curr Mol Med, 2008. **8**(2): p. 119-30.
164. Verkhatsky, A. and P. Fernyhough, *Mitochondrial malfunction and Ca²⁺ dyshomeostasis drive neuronal pathology in diabetes*. Cell Calcium, 2008. **44**(1): p. 112-22.
165. Bers, D.M., D.A. Eisner, and H.H. Valdivia, *Sarcoplasmic reticulum Ca²⁺ and heart failure: roles of diastolic leak and Ca²⁺ transport*. Circ Res, 2003. **93**(6): p. 487-90.
166. Cooper, M.E., et al., *Mechanisms of diabetic vasculopathy: an overview*. Am J Hypertens, 2001. **14**(5 Pt 1): p. 475-86.

167. Dickhout, J.G., et al., *Peroxynitrite causes endoplasmic reticulum stress and apoptosis in human vascular endothelium: implications in atherogenesis*. *Arterioscler Thromb Vasc Biol*, 2005. **25**(12): p. 2623-9.
168. Tong, X., A. Evangelista, and R.A. Cohen, *Targeting the redox regulation of SERCA in vascular physiology and disease*. *Curr Opin Pharmacol*, 2010. **10**(2): p. 133-8.
169. Kanekura, K., et al., *ER stress and unfolded protein response in amyotrophic lateral sclerosis*. *Mol Neurobiol*, 2009. **39**(2): p. 81-9.
170. Lindholm, D., H. Wootz, and L. Korhonen, *ER stress and neurodegenerative diseases*. *Cell Death Differ*, 2006. **13**(3): p. 385-92.
171. Ryu, E.J., et al., *Endoplasmic reticulum stress and the unfolded protein response in cellular models of Parkinson's disease*. *J Neurosci*, 2002. **22**(24): p. 10690-8.
172. Benali-Furet, N.L., et al., *Hepatitis C virus core triggers apoptosis in liver cells by inducing ER stress and ER calcium depletion*. *Oncogene*, 2005. **24**(31): p. 4921-33.
173. Sharon-Friling, R., et al., *Human cytomegalovirus pUL37x1 induces the release of endoplasmic reticulum calcium stores*. *Proc Natl Acad Sci U S A*, 2006. **103**(50): p. 19117-22.
174. Cantero-Recasens, G., et al., *The asthma-associated ORMDL3 gene product regulates endoplasmic reticulum-mediated calcium signaling and cellular stress*. *Hum Mol Genet*, 2010. **19**(1): p. 111-21.
175. Sathish, V., et al., *Effect of proinflammatory cytokines on regulation of sarcoplasmic reticulum Ca²⁺ reuptake in human airway smooth muscle*. *Am J Physiol Lung Cell Mol Physiol*, 2009. **297**(1): p. L26-34.
176. Wei, Y., et al., *Reduced endoplasmic reticulum luminal calcium links saturated fatty acid-mediated endoplasmic reticulum stress and cell death in liver cells*. *Mol Cell Biochem*, 2009. **331**(1-2): p. 31-40.
177. Sakakura, C., et al., *Possible involvement of inositol 1,4,5-trisphosphate receptor type 3 (IP3R3) in the peritoneal dissemination of gastric cancers*. *Anticancer Res*, 2003. **23**(5A): p. 3691-7.
178. Patergnani, S., et al., *Calcium signaling around Mitochondria Associated Membranes (MAMs)*. *Cell Commun Signal*, 2011. **9**: p. 19.
179. Bhaya, D., M. Davison, and R. Barrangou, *CRISPR-Cas systems in bacteria and archaea: versatile small RNAs for adaptive defense and regulation*. *Annu Rev Genet*, 2011. **45**: p. 273-97.
180. Terns, M.P. and R.M. Terns, *CRISPR-based adaptive immune systems*. *Curr Opin Microbiol*, 2011. **14**(3): p. 321-7.
181. Wiedenheft, B., S.H. Sternberg, and J.A. Doudna, *RNA-guided genetic silencing systems in bacteria and archaea*. *Nature*, 2012. **482**(7385): p. 331-8.
182. Yosef, I., et al., *DNA motifs determining the efficiency of adaptation into the Escherichia coli CRISPR array*. *Proc Natl Acad Sci U S A*, 2013. **110**(35): p. 14396-401.
183. Mojica, F.J., et al., *Short motif sequences determine the targets of the prokaryotic CRISPR defence system*. *Microbiology*, 2009. **155**(Pt 3): p. 733-40.
184. Datsenko, K.A., et al., *Molecular memory of prior infections activates the CRISPR/Cas adaptive bacterial immunity system*. *Nat Commun*, 2012. **3**: p. 945.
185. Nunez, J.K., et al., *Integrase-mediated spacer acquisition during CRISPR-Cas adaptive immunity*. *Nature*, 2015. **519**(7542): p. 193-8.
186. Wang, J., et al., *Structural and Mechanistic Basis of PAM-Dependent Spacer Acquisition in CRISPR-Cas Systems*. *Cell*, 2015. **163**(4): p. 840-53.

187. Yosef, I., M.G. Goren, and U. Qimron, *Proteins and DNA elements essential for the CRISPR adaptation process in Escherichia coli*. Nucleic Acids Res, 2012. **40**(12): p. 5569-76.
188. Brouns, S.J., et al., *Small CRISPR RNAs guide antiviral defense in prokaryotes*. Science, 2008. **321**(5891): p. 960-4.
189. Garneau, J.E., et al., *The CRISPR/Cas bacterial immune system cleaves bacteriophage and plasmid DNA*. Nature, 2010. **468**(7320): p. 67-71.
190. Gupta, R.M. and K. Musunuru, *Expanding the genetic editing tool kit: ZFNs, TALENs, and CRISPR-Cas9*. J Clin Invest, 2014. **124**(10): p. 4154-61.
191. Kim, H. and J.S. Kim, *A guide to genome engineering with programmable nucleases*. Nat Rev Genet, 2014. **15**(5): p. 321-34.
192. Jiang, W. and L.A. Marraffini, *CRISPR-Cas: New Tools for Genetic Manipulations from Bacterial Immunity Systems*. Annu Rev Microbiol, 2015. **69**: p. 209-28.
193. Shinwari, Z.K., F. Tanveer, and A.T. Khalil, *Ethical Issues Regarding CRISPR Mediated Genome Editing*. Curr Issues Mol Biol, 2018. **26**: p. 103-110.
194. Wright, A.V., J.K. Nunez, and J.A. Doudna, *Biology and Applications of CRISPR Systems: Harnessing Nature's Toolbox for Genome Engineering*. Cell, 2016. **164**(1-2): p. 29-44.
195. Rouet, P., F. Smih, and M. Jasin, *Introduction of double-strand breaks into the genome of mouse cells by expression of a rare-cutting endonuclease*. Mol Cell Biol, 1994. **14**(12): p. 8096-106.
196. Doench, J.G., et al., *Rational design of highly active sgRNAs for CRISPR-Cas9-mediated gene inactivation*. Nat Biotechnol, 2014. **32**(12): p. 1262-7.
197. Shalem, O., N.E. Sanjana, and F. Zhang, *High-throughput functional genomics using CRISPR-Cas9*. Nat Rev Genet, 2015. **16**(5): p. 299-311.
198. Williams, A., J. Henao-Mejia, and R.A. Flavell, *Editing the Mouse Genome Using the CRISPR-Cas9 System*. Cold Spring Harb Protoc, 2016. **2016**(2): p. pdb top087536.
199. Burgio, G., *Redefining mouse transgenesis with CRISPR/Cas9 genome editing technology*. Genome Biol, 2018. **19**(1): p. 27.
200. Harms, D.W., et al., *Mouse Genome Editing Using the CRISPR/Cas System*. Curr Protoc Hum Genet, 2014. **83**: p. 15 7 1-27.
201. Gloeckner, C.J., et al., *A novel tandem affinity purification strategy for the efficient isolation and characterisation of native protein complexes*. Proteomics, 2007. **7**(23): p. 4228-34.
202. Zhang, C., *Hybridoma technology for the generation of monoclonal antibodies*. Methods Mol Biol, 2012. **901**: p. 117-35.
203. Sehgal, P., et al., *Inhibition of the sarco/endoplasmic reticulum (ER) Ca(2+)-ATPase by thapsigargin analogs induces cell death via ER Ca(2+) depletion and the unfolded protein response*. J Biol Chem, 2017. **292**(48): p. 19656-19673.
204. Michalak, M., J.M. Robert Parker, and M. Opas, *Ca²⁺ signaling and calcium binding chaperones of the endoplasmic reticulum*. Cell Calcium, 2002. **32**(5-6): p. 269-78.
205. Ding, W.X., et al., *Differential effects of endoplasmic reticulum stress-induced autophagy on cell survival*. J Biol Chem, 2007. **282**(7): p. 4702-10.
206. Duksin, D. and W.C. Mahoney, *Relationship of the structure and biological activity of the natural homologues of tunicamycin*. J Biol Chem, 1982. **257**(6): p. 3105-9.

207. Li, B., et al., *Differences in endoplasmic reticulum stress signalling kinetics determine cell survival outcome through activation of MKP-1*. Cell Signal, 2011. **23**(1): p. 35-45.
208. Gupta, R.S. and L. Siminovitch, *The molecular basis of emetine resistance in Chinese hamster ovary cells: alteration in the 40S ribosomal subunit*. Cell, 1977. **10**(1): p. 61-6.
209. Lee, D.H. and A.L. Goldberg, *Proteasome inhibitors: valuable new tools for cell biologists*. Trends Cell Biol, 1998. **8**(10): p. 397-403.
210. Redmann, M., et al., *Inhibition of autophagy with bafilomycin and chloroquine decreases mitochondrial quality and bioenergetic function in primary neurons*. Redox Biol, 2017. **11**: p. 73-81.
211. Geng, Y., et al., *Chloroquine-induced autophagic vacuole accumulation and cell death in glioma cells is p53 independent*. Neuro Oncol, 2010. **12**(5): p. 473-81.
212. Mauthe, M., et al., *Chloroquine inhibits autophagic flux by decreasing autophagosome-lysosome fusion*. Autophagy, 2018. **14**(8): p. 1435-1455.
213. Yang, W.S., et al., *Regulation of ferroptotic cancer cell death by GPX4*. Cell, 2014. **156**(1-2): p. 317-331.
214. Friedmann Angeli, J.P., et al., *Inactivation of the ferroptosis regulator Gpx4 triggers acute renal failure in mice*. Nat Cell Biol, 2014. **16**(12): p. 1180-91.
215. Mihaylova, M.M. and R.J. Shaw, *The AMPK signalling pathway coordinates cell growth, autophagy and metabolism*. Nat Cell Biol, 2011. **13**(9): p. 1016-23.
216. Ha, J., K.L. Guan, and J. Kim, *AMPK and autophagy in glucose/glycogen metabolism*. Mol Aspects Med, 2015. **46**: p. 46-62.
217. Prakriya, M. and R.S. Lewis, *Store-Operated Calcium Channels*. Physiol Rev, 2015. **95**(4): p. 1383-436.
218. Fusi, F., et al., *2,5-Di-t-butyl-1,4-benzohydroquinone (BHQ) inhibits vascular L-type Ca(2+) channel via superoxide anion generation*. Br J Pharmacol, 2001. **133**(7): p. 988-96.
219. Jones, J.R., et al., *Deletion of PPARgamma in adipose tissues of mice protects against high fat diet-induced obesity and insulin resistance*. Proc Natl Acad Sci U S A, 2005. **102**(17): p. 6207-12.
220. Kaltenecker, D., et al., *Adipocyte STAT5 deficiency promotes adiposity and impairs lipid mobilisation in mice*. Diabetologia, 2017. **60**(2): p. 296-305.
221. Wang, D., et al., *Naturally occurring dominant negative variants of Stat5*. Mol Cell Biol, 1996. **16**(11): p. 6141-8.
222. Good, S.R., et al., *Temporal induction pattern of STAT4 target genes defines potential for Th1 lineage-specific programming*. J Immunol, 2009. **183**(6): p. 3839-47.
223. Tan, P., et al., *Recruitment of MHC class I molecules by tapasin into the transporter associated with antigen processing-associated complex is essential for optimal peptide loading*. J Immunol, 2002. **168**(4): p. 1950-60.
224. Howarth, M., et al., *Tapasin enhances MHC class I peptide presentation according to peptide half-life*. Proc Natl Acad Sci U S A, 2004. **101**(32): p. 11737-42.
225. Daffis, S., et al., *2'-O methylation of the viral mRNA cap evades host restriction by IFIT family members*. Nature, 2010. **468**(7322): p. 452-6.

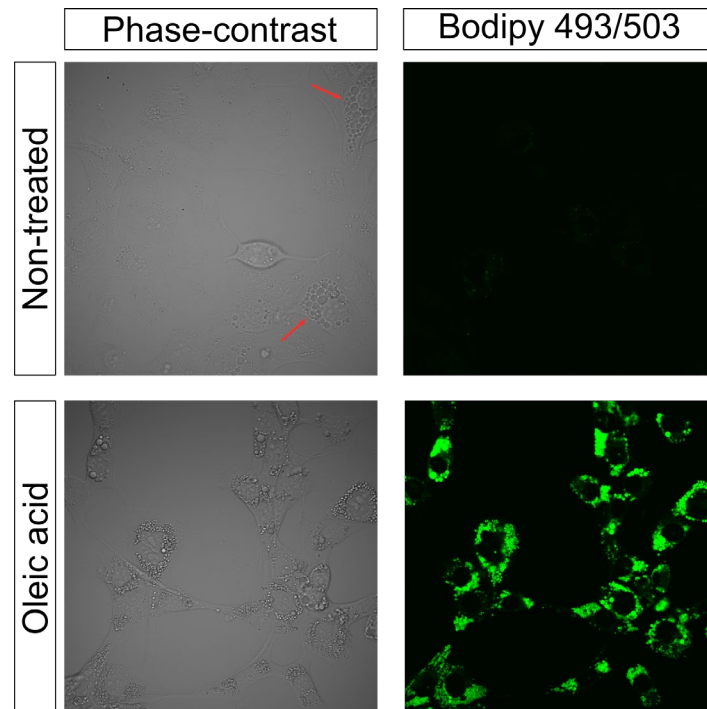
-
226. Szretter, K.J., et al., *2'-O methylation of the viral mRNA cap by West Nile virus evades ifit1-dependent and -independent mechanisms of host restriction in vivo*. PLoS Pathog, 2012. **8**(5): p. e1002698.
227. Mears, H.V. and T.R. Sweeney, *Better together: the role of IFIT protein-protein interactions in the antiviral response*. J Gen Virol, 2018. **99**(11): p. 1463-1477.
228. Bansal, D., et al., *Defective membrane repair in dysferlin-deficient muscular dystrophy*. Nature, 2003. **423**(6936): p. 168-72.
229. Lennon, N.J., et al., *Dysferlin interacts with annexins A1 and A2 and mediates sarcolemmal wound-healing*. J Biol Chem, 2003. **278**(50): p. 50466-73.
230. Han, R., et al., *Dysferlin-mediated membrane repair protects the heart from stress-induced left ventricular injury*. J Clin Invest, 2007. **117**(7): p. 1805-13.
231. Han, R. and K.P. Campbell, *Dysferlin and muscle membrane repair*. Curr Opin Cell Biol, 2007. **19**(4): p. 409-16.
232. Dean, K.A., et al., *Signal recognition particle protein 19 is imported into the nucleus by importin 8 (RanBP8) and transportin*. J Cell Sci, 2001. **114**(Pt 19): p. 3479-85.
233. Kimoto, C., et al., *Functional characterization of importin alpha8 as a classical nuclear localization signal receptor*. Biochim Biophys Acta, 2015. **1853**(10 Pt A): p. 2676-83.
234. Volpon, L., et al., *Importin 8 mediates m7G cap-sensitive nuclear import of the eukaryotic translation initiation factor eIF4E*. Proc Natl Acad Sci U S A, 2016. **113**(19): p. 5263-8.
235. Tsukasaki, Y., et al., *Giant cadherins Fat and Dachous self-bend to organize properly spaced intercellular junctions*. Proc Natl Acad Sci U S A, 2014. **111**(45): p. 16011-6.
236. Yang, H., et al., *NCKX3 was compensated by calcium transporting genes and bone resorption in a NCKX3 KO mouse model*. Mol Cell Endocrinol, 2017. **454**: p. 93-102.
237. Prasad, M.K., et al., *A polymorphic 3'UTR element in ATP1B1 regulates alternative polyadenylation and is associated with blood pressure*. PLoS One, 2013. **8**(10): p. e76290.
238. Selvakumar, P., et al., *Epigenetic silencing of Na,K-ATPase beta 1 subunit gene ATP1B1 by methylation in clear cell renal cell carcinoma*. Epigenetics, 2014. **9**(4): p. 579-86.
239. Shi, J.L., et al., *Overexpression of ATP1B1 predicts an adverse prognosis in cytogenetically normal acute myeloid leukemia*. Oncotarget, 2016. **7**(3): p. 2585-95.
240. Hong, Z., et al., *Hepatitis C virus NS5A competes with PI4KB for binding to ACBD3 in a genotype-dependent manner*. Antiviral Res, 2014. **107**: p. 50-5.
241. Klima, M., et al., *Structural insights and in vitro reconstitution of membrane targeting and activation of human PI4KB by the ACBD3 protein*. Sci Rep, 2016. **6**: p. 23641.
242. Tai, A.W. and S. Salloum, *The role of the phosphatidylinositol 4-kinase PI4KA in hepatitis C virus-induced host membrane rearrangement*. PLoS One, 2011. **6**(10): p. e26300.
243. Stiburek, L., et al., *Knockdown of human Oxa1l impairs the biogenesis of F1Fo-ATP synthase and NADH:ubiquinone oxidoreductase*. J Mol Biol, 2007. **374**(2): p. 506-16.
244. Thompson, K., et al., *OXA1L mutations cause mitochondrial encephalopathy and a combined oxidative phosphorylation defect*. EMBO Mol Med, 2018. **10**(11).
245. Yang, H.Y., et al., *14-3-3 sigma positively regulates p53 and suppresses tumor growth*. Mol Cell Biol, 2003. **23**(20): p. 7096-107.

246. Sun, N., et al., *Decreased expression of 14-3-3 sigma, an early event of malignant transformation of respiratory epithelium, also facilitates progression of squamous cell lung cancer*. Thorac Cancer, 2015. **6**(6): p. 715-21.
247. Young, G.M., et al., *Comparative analysis of 14-3-3 isoform expression and epigenetic alterations in colorectal cancer*. BMC Cancer, 2015. **15**: p. 826.
248. Parrinello, S., et al., *Oxygen sensitivity severely limits the replicative lifespan of murine fibroblasts*. Nat Cell Biol, 2003. **5**(8): p. 741-7.
249. Castro, G., et al., *Diet-induced obesity induces endoplasmic reticulum stress and insulin resistance in the amygdala of rats*. FEBS Open Bio, 2013. **3**: p. 443-9.
250. Kawasaki, N., et al., *Obesity-induced endoplasmic reticulum stress causes chronic inflammation in adipose tissue*. Sci Rep, 2012. **2**: p. 799.
251. Meli, R., et al., *High Fat Diet Induces Liver Steatosis and Early Dysregulation of Iron Metabolism in Rats*. PLoS One, 2013. **8**(6): p. e66570.
252. Wires, E.S., et al., *High fat diet disrupts endoplasmic reticulum calcium homeostasis in the rat liver*. J Hepatol, 2017. **67**(5): p. 1009-1017.
253. Ramming, T., et al., *Cysteines 208 and 241 in Ero1alpha are required for maximal catalytic turnover*. Redox Biol, 2016. **7**: p. 14-20.
254. Lytton, J., M. Westlin, and M.R. Hanley, *Thapsigargin inhibits the sarcoplasmic or endoplasmic reticulum Ca-ATPase family of calcium pumps*. J Biol Chem, 1991. **266**(26): p. 17067-71.
255. Hampton, R.Y., *ER-associated degradation in protein quality control and cellular regulation*. Curr Opin Cell Biol, 2002. **14**(4): p. 476-82.
256. Hong, M., et al., *Endoplasmic reticulum stress triggers an acute proteasome-dependent degradation of ATF6*. J Cell Biochem, 2004. **92**(4): p. 723-32.
257. Lee, W.S., W.H. Yoo, and H.J. Chae, *ER Stress and Autophagy*. Curr Mol Med, 2015. **15**(8): p. 735-45.
258. Lilienbaum, A., *Relationship between the proteasomal system and autophagy*. Int J Biochem Mol Biol, 2013. **4**(1): p. 1-26.
259. Bao, W., et al., *Induction of autophagy by the MG132 proteasome inhibitor is associated with endoplasmic reticulum stress in MCF7 cells*. Mol Med Rep, 2016. **13**(1): p. 796-804.
260. Wang, C. and X. Wang, *The interplay between autophagy and the ubiquitin-proteasome system in cardiac proteotoxicity*. Biochim Biophys Acta, 2015. **1852**(2): p. 188-94.
261. Hirsch, C., et al., *The ubiquitylation machinery of the endoplasmic reticulum*. Nature, 2009. **458**(7237): p. 453-60.
262. Pestana, C.R., et al., *Inhibition of autophagy by chloroquine stimulates nitric oxide production and protects endothelial function during serum deprivation*. Cell Physiol Biochem, 2015. **37**(3): p. 1168-77.
263. Moruno, F., E. Perez-Jimenez, and E. Knecht, *Regulation of autophagy by glucose in Mammalian cells*. Cells, 2012. **1**(3): p. 372-95.
264. Singh, R. and A.M. Cuervo, *Autophagy in the cellular energetic balance*. Cell Metab, 2011. **13**(5): p. 495-504.
265. Mitchener, J.S., et al., *Cellular autophagocytosis induced by deprivation of serum and amino acids in HeLa cells*. Am J Pathol, 1976. **83**(3): p. 485-92.
266. Shen, Y., et al., *Metabolic activity induces membrane phase separation in endoplasmic reticulum*. Proc Natl Acad Sci U S A, 2017. **114**(51): p. 13394-13399.

267. Senturk, M., et al., *Ubiquilins regulate autophagic flux through mTOR signalling and lysosomal acidification*. Nat Cell Biol, 2019. **21**(3): p. 384-396.
268. Rothenberg, C., et al., *Ubiquilin functions in autophagy and is degraded by chaperone-mediated autophagy*. Hum Mol Genet, 2010. **19**(16): p. 3219-32.
269. Lim, P.J., et al., *Ubiquilin and p97/VCP bind erasin, forming a complex involved in ERAD*. J Cell Biol, 2009. **187**(2): p. 201-17.
270. Hausser, A., et al., *Phospho-specific binding of 14-3-3 proteins to phosphatidylinositol 4-kinase III beta protects from dephosphorylation and stabilizes lipid kinase activity*. J Cell Sci, 2006. **119**(Pt 17): p. 3613-21.
271. Pichlmair, A., et al., *IFIT1 is an antiviral protein that recognizes 5'-triphosphate RNA*. Nat Immunol, 2011. **12**(7): p. 624-30.
272. Liu, Y., et al., *Lineage-specific expansion of IFIT gene family: an insight into coevolution with IFN gene family*. PLoS One, 2013. **8**(6): p. e66859.
273. Fensterl, V. and G.C. Sen, *Interferon-induced Ifit proteins: their role in viral pathogenesis*. J Virol, 2015. **89**(5): p. 2462-8.
274. Haque, M.E., et al., *Properties of the C-terminal tail of human mitochondrial inner membrane protein Oxa1L and its interactions with mammalian mitochondrial ribosomes*. J Biol Chem, 2010. **285**(36): p. 28353-62.
275. Haque, M.E., L.L. Spremulli, and C.J. Fecko, *Identification of protein-protein and protein-ribosome interacting regions of the C-terminal tail of human mitochondrial inner membrane protein Oxa1L*. J Biol Chem, 2010. **285**(45): p. 34991-8.
276. Liu, J., et al., *Dysferlin, a novel skeletal muscle gene, is mutated in Miyoshi myopathy and limb girdle muscular dystrophy*. Nat Genet, 1998. **20**(1): p. 31-6.
277. Matsuda, C., et al., *Dysferlin is a surface membrane-associated protein that is absent in Miyoshi myopathy*. Neurology, 1999. **53**(5): p. 1119-22.
278. Illarioshkin, S.N., et al., *Identical dysferlin mutation in limb-girdle muscular dystrophy type 2B and distal myopathy*. Neurology, 2000. **55**(12): p. 1931-3.
279. Piccolo, F., et al., *Intracellular accumulation and reduced sarcolemmal expression of dysferlin in limb-girdle muscular dystrophies*. Ann Neurol, 2000. **48**(6): p. 902-12.
280. Fanin, M., et al., *Calpain-3 and dysferlin protein screening in patients with limb-girdle dystrophy and myopathy*. Neurology, 2001. **56**(5): p. 660-5.
281. Ueyama, H., et al., *A new dysferlin gene mutation in two Japanese families with limb-girdle muscular dystrophy 2B and Miyoshi myopathy*. Neuromuscul Disord, 2001. **11**(2): p. 139-45.
282. Hu, Y.Y., et al., *Novel, de novo dysferlin gene mutations in a patient with Miyoshi myopathy*. Neurosci Lett, 2018. **664**: p. 107-109.
283. Grounds, M.D., et al., *Lipid accumulation in dysferlin-deficient muscles*. Am J Pathol, 2014. **184**(6): p. 1668-76.
284. Li, L., et al., *Comparative proteomics reveals abnormal binding of ATGL and dysferlin on lipid droplets from pressure overload-induced dysfunctional rat hearts*. Sci Rep, 2016. **6**: p. 19782.
285. Lee, G.S., K.C. Choi, and E.B. Jeung, *K⁺-dependent Na⁺/Ca²⁺ exchanger 3 is involved in renal active calcium transport and is differentially expressed in the mouse kidney*. Am J Physiol Renal Physiol, 2009. **297**(2): p. F371-9.

-
286. Yang, H., et al., *Sodium/potassium/calcium exchanger 3 is regulated by the steroid hormones estrogen and progesterone in the uterus of mice during the estrous cycle.* Biochem Biophys Res Commun, 2009. **385**(2): p. 279-83.
287. Ahn, C., J.S. Choi, and E.B. Jeung, *Organspecific expression of the divalent ion channel proteins NCKX3, TRPV2, CTR1, ATP7A, IREG1 and HEPH in various canine organs.* Mol Med Rep, 2018. **18**(2): p. 1773-1781.
288. Wang, X., H. Su, and A. Bradley, *Molecular mechanisms governing Pcdh-gamma gene expression: evidence for a multiple promoter and cis-alternative splicing model.* Genes Dev, 2002. **16**(15): p. 1890-905.
289. Louet, J.F., C. LeMay, and F. Mauvais-Jarvis, *Antidiabetic actions of estrogen: insight from human and genetic mouse models.* Curr Atheroscler Rep, 2004. **6**(3): p. 180-5.
290. Pettersson, U.S., et al., *Female mice are protected against high-fat diet induced metabolic syndrome and increase the regulatory T cell population in adipose tissue.* PLoS One, 2012. **7**(9): p. e46057.
291. Chan, J.C., et al., *The central roles of obesity-associated dyslipidaemia, endothelial activation and cytokines in the Metabolic Syndrome--an analysis by structural equation modelling.* Int J Obes Relat Metab Disord, 2002. **26**(7): p. 994-1008.
292. Kocak, H., et al., *Advanced oxidation protein products in obese women: its relation to insulin resistance and resistin.* Clin Exp Med, 2007. **7**(4): p. 173-8.
293. Payette, C., et al., *Sex differences in postprandial plasma tumor necrosis factor-alpha, interleukin-6, and C-reactive protein concentrations.* Metabolism, 2009. **58**(11): p. 1593-601.
294. Naugler, W.E., et al., *Gender disparity in liver cancer due to sex differences in MyD88-dependent IL-6 production.* Science, 2007. **317**(5834): p. 121-4.
295. Marks, A.R., *Calcium cycling proteins and heart failure: mechanisms and therapeutics.* J Clin Invest, 2013. **123**(1): p. 46-52.
296. Golic, I., et al., *Calcium-induced alteration of mitochondrial morphology and mitochondrial-endoplasmic reticulum contacts in rat brown adipocytes.* Eur J Histochem, 2014. **58**(3): p. 2377.

8. APPENDIX



Supplementary figure 1 Bodipy 493/503 staining on GPX8 KO MEFs

Bodipy 493/503 lipid droplet staining was negative on GPX8 KO MEFs under normal cell culture conditions. Red arrows point to accumulated vesicles in the cells. As positive control, the cells were treated with oleic acid, which is a well-known lipid droplet inducing compound.



Supplementary figure 2 ChipSeq analysis of the extended promoter region of mouse *Gpx8*

The analysis revealed several *Stat4/6* TFBS from CD4+ and *Stat5b* TFBS from T-lymphocyte cells

Description of accompanying files:

Excel file 1:

Results from microarray analysis of parental, GPX8 KO and GPX8 AB cell lines.

Excel file 2:

Mass spectrometry data from co-immunoprecipitation of GPX8-STREP(2X)/FLAG tag expressing MEFs.

9. CURRICULUM VITAE

Katalin Judit Buday

Title: Master of Science (M.Sc.)
Place of birth: Veszprém, Hungary
Date of birth: 05.03.1988
Nationality: Hungarian
Private address: Würmbachstraße 13, D-85716 Unterschleißheim
Mobil: +4915124705042
E-Mail: budaykatalin@gmail.com

Education

May 2014 - dato PhD student at the Institute of Developmental Genetics,
Helmholtz Zentrum München

2012 - 2014 Master degree course: Bioengineer
Faculty: Chemical Technology and Biotechnology at
Budapest University of Technology and Economics
Graduation M.Sc.

2006 - 2012 Bachelor degree course: Bioengineer
Faculty: Chemical Technology and Biotechnology at
Budapest University of Technology and Economics
Graduation: B.Sc.

2002 - 2006 Industrial Secondary Technical School and Gymnasium,
Veszprém
Graduation: Abitur

Work experience

May 2014 - dato	PhD student at the Institute of Developmental Genetics, Helmholtz Zentrum München under the supervision of Dr. Marcus Conrad
September 2013-November 2013	Internship at the Institute of Developmental Genetics, Helmholtz Zentrum München
2012 - 2013	Master thesis at Chemical Technology and Biotechnology at Budapest University of Technology and Economics under the supervision of Prof. Dr. András Szarka
February 2011- November 2011	Bachelor Thesis at Chemical Technology and Biotechnology at Budapest University of Technology and Economics under the supervision of Prof. Dr. András Szarka
June 2011 - July 2011	Internship at Drug Research Center, Balatonfüred

Publications

Rodriguez Camargo DC, Garg D, **Buday K**, Franko A, Rodriguez Camargo A, Schmidt F, Cox SJ, Suladze S, Haslbeck M, Mideksa YG, Gemmecker G, Aichler M, Mettenleiter G, Schulz M, Walch AK, Hrabě de Angelis M, Feige MJ, Sierra CA, Conrad M, Tripsianes K, Ramamoorthy A, Reif B.: hIAPP forms toxic oligomers in plasma. *Chem Commun (Camb)* 2018 May

Ingold I, Berndt C, Schmitt S, Doll S, Poschmann G, **Buday K**, Roveri A, Peng X, Porto Freitas F, Seibt T, Mehr L, Aichler M, Walch A, Lamp D, Jastroch M, Miyamoto S, Wurst W, Ursini F, Arnér ESJ, Fradejas-Villar N, Schweizer U, Zischka H, Friedmann Angeli JP, Conrad M.: Senelocysteine utilization in GPX4 was evolutionary preserved to prevent ferroptosis in vertebrates. *Cell* 2018 Jan

Rodriguez Camargo DC, Tripsianes K, **Buday K**, Franko A, Göbl C, Hartmüller C, Sarkar R, Aichler M, Mettenleiter G, Schulz M, Böddrich A, Erck C, Martens H, Walch AK, Madl T, Wanker EE, Conrad M, de Angelis MH, Reif B.: The redox environment triggers conformational changes and aggregation of hIAPP in Type II Diabetes. *Sci Rep.* 2017 Mar

Ingold I., Aichler M., Yefremova E., Roveri A., **Buday K.**, Doll S., Tasdemir A., Hoffard N., Wurst W., Walch A., Ursini F., Friedmann Angeli J.P., Conrad M.: Expression of catalytically inactive form of glutathione peroxidase (Gpx) 4 confers a dominant negative effect in male fertility. *J Biol Chem.* 2015 Jun

Conrad M., Ingold I., **Buday K.**, Kobayashi S., Angeli J.P.: ROS, thiols and thiol-regulating systems in male gametogenesis. *Biochim Biophys Acta*. 2015 Aug

Presentations

Selected speaker at the Plant and Human Sulfur Biology Conference, Balatonfüred (2017).
Titel: Functional evaluation of glutathione peroxidase 8 (GPX8) as a mammalian redox sensor in the endoplasmic reticulum

Buday K., Szabó E., Doll S., Lorenz S., Gibhardt C.S., Habich M., Aichler M., Bogeski I., Riemer J., Conrad M. (2019). Poster presentation at the 9th Symposium of the DFG Priority Program SPP 1710.

Buday K., Ingold I., Yefremova E., Mehr L., Doll S., Friedmann Angeli J.P., Habich M., Riemer J., Conrad M. (2017). Poster presentation at EMBO conference on Redox Biology

Buday K., Ingold I., Yefremova E., Flatley A., Doll S., Friedmann Angeli J.P., Habich M., Riemer J., Conrad M. (2016). Poster presentation at the 3th meeting of the study group redox biology of the German Society for Biochemistry and Molecular Biology (GBM).

Buday K., Ingold I., Yefremova E., Doll S., Friedmann Angeli J.P., Flatley A., Habich M., Riemer J., Conrad M. (2016). Poster presentation at the 6th Symposium of the DFG Priority Program SPP 1710.

10. ACKNOWLEDGEMENT

This PhD thesis has been a demanding and extensive work, but overall an excellent and instructive experience. The accomplishments of this work wouldn't have been done without the help, support and encouragement of many people.

First of all, I would like to thank my supervisor Dr. Marcus Conrad for giving me the opportunity to accomplish my PhD in his laboratory with his excellent guidance and support. I am very thankful to him for sharing his broad scientific knowledge and his passion for science through which he motivates and encourages his students and co-workers.

I want to thank my official supervisor Prof. Dr. Wolfgang Wurst, the head of the Institute of Developmental Genetics for giving me the opportunity to do my PhD in his institute and for his constructive comments and suggestions throughout my PhD.

I am thankful to Dr. Paul Pfluger for his great suggestions and discussions at my annual thesis committees and at our meetings.

I owe gratitude to Prof. Dr. Jan Riemer from University of Cologne for allowing me to do a lab-exchange in his laboratory and learn very useful methods from experts which helped me to fulfill this work. I also thank to him for sharing me his broad knowledge and experiments therefore helping me to avoid technical issues.

I am also very thankful to Dr. Markus Habich from University of Cologne who helped me with all the experiment I was doing in Prof. Dr. Jan Riemer's laboratory.

I would like to thank Prof. Dr. Ivan Bogeski and Dr. Christine Silvia Gibhardt from the University of Göttingen for their help to analyze intracellular Ca^{2+} level of GPX8 KO cells.

I am very thankful to Dr. Elisabeth Kremmer, Andrew Flatley and Dr. Regina Feederle for generating GPX8 monoclonal antibodies, which was essential to study GPX8 *in vivo* and *in vitro*.

I am very grateful to Dr. Uli Ohmayer and Dr. Stefanie Hauck who analyzed and provided me GPX8 mass spectrometry data presented in this work.

I would like to thank Dr. Michaela Aichler who provided me the transmission electron microscopy pictures.

I am thankful to Dr. Martin Irmler for helping me with the microarray experiments.

I thank Dr. Dietrich Trümbach for providing me the *in silico* promoter analysis of *Gpx8*.

I am very thankful for Elena Yefremova who was working on this project before I joined this laboratory and shared me her experience and helped me to learn all techniques which was necessary for *in vivo* experiments.

I am expressing my thankfulness to Szabó Eszter, my master student who's excellent work and efforts contributed significantly to the development of this project.

Most importantly, I owe great gratitude to our present and former lab members, Dr. Sebastian Doll, Dr. Irina Ingold, Dr. Jose Pedro Friedmann Angeli, Dr. Milene Soraia Costa da Silva, Svenja Lorenz, Lisa Mehr, Dr. Bettina Proneth, Dr. Marina Theodorou, Dr. Tobias Seibt, Dr. Florencio Porto Freitas, Muhammad Ismail, Heidi Förster, Nicole Fritz and Jonas Wanninger for sharing their experience, and for creating a great atmosphere in the lab and also for helping me whenever I needed their help.

Here, I want to express my thank to Dr. Lőrincz Tamás and Prof. Dr. Szarka András from Budapest University of Technology and Economics to share their knowledge and their passion for science with me. Working with them helped me to decide, science is something I am really interested about and I would like to continue working on this field and do my PhD.

Most importantly, I want to express my deepest gratitude to my family for their constant support and encourage. Your education taught me to never give up anything and to always do my best to achieve I really want. Thank you!

11. AFFIDAVIT

I hereby declare that the dissertation titled „ Functional characterization of glutathione peroxidase 8 (GPX8)” prepared under the guidance and supervision of Prof. Dr. Wolfgang Wurst, head of the chair of developmental genetics, and submitted to the degreeawarding institution Fakultät Wissenschaftszentrum Weihenstephan für Ernährung, Landnutzung und Umwelt of the Technical University of Munich is my own, original work undertaken in partial fulfillments of the requirements for the doctoral degree. I have made no use of sources, materials or assistance other than those specified in §6 (&) and (7), clause 2.

I have not employed the services of an organization that provides dissertations supervisors in return for paymaent or that fulfills, in whole or in part, the obligations incubement in me in connection with my dissertation.

I have not submitted the dissertation, either in the present or in a similar form, as part of another examination process.

The degree-awarding institution Fakultät Wissenschaftszentrum Weihenstephan für Ernährung, Landnutzung und Umwelt has approved prior publication oft he dissertation.

I have not yet been awarded the desired doctoral degree nor have I failed the last possible attempt to obtain the desired degree in a previous doctoral program.

I am familiar with the public available Regulations of the Award of Doctoral Degrees of the Technical University Munich, in particular §28 (invalidation of doctoral degree) and §29 (Revocation of doctoral degree). I am aware of the consequences of filling a false affidavit.

I agree, I do not agree

that my personal data is stored in the TUM alumni database.

Munich, _____

Katalin Judit Buday